

JOURNAL OF THE

# Electrochemical Society

Vol. 109, No. 6

June 1962



มหาวิทยาลัยเทคโนโลยีพระจอมเกล้า  
พระนครเหนือ



# THE GLC PROGRAM OF PROGRESS

You can start sharing the rewards of the GLC program of progress by putting custom made GLC anodes to work now in your electrolytic cells. Appreciable cost savings are being achieved by GLC anode customers through our past technical exchanges with them.

**will  
improve  
cell  
operations**

By working with you now, custom making anodes for your specific cell requirements, we can help accelerate your cost reduction program, and assist you in developing the technical information needed to improve the over-all efficiency of your chlor-alkali cells.



**GREAT LAKES CARBON CORPORATION**

18 EAST 48TH STREET, NEW YORK 17, N.Y. OFFICES IN PRINCIPAL CITIES

## EDITORIAL STAFF

C. L. Faust, Chairman, Publication Committee  
 Cecil V. King, Editor  
 Norman Hackerman, Technical Editor  
 Ruth G. Sterns, Managing Editor  
 U. B. Thomas, News Editor  
 H. W. Salzburg, Book Review Editor  
 Natalie Michalski, Assistant Editor

## DIVISIONAL EDITORS

W. C. Vosburgh, Battery  
 G. A. Marsh, Corrosion  
 A. C. Makrides, Corrosion  
 Harry C. Gatos, Corrosion—Semiconductors  
 Louis J. Frisco, Electric Insulation  
 Seymour Senderoff, Electrodeposition  
 H. C. Froelich, Electronics  
 Ephraim Banks, Electronics  
 Ernest Paskell, Electronics—Semiconductors  
 D. R. Frankl, Electronics—Semiconductors  
 Sherlock Swann, Jr., Electro-Organic  
 Stanley Wawzonek, Electro-Organic  
 John M. Blocher, Jr., Electrothermics and Metallurgy  
 J. H. Westbrook, Electrothermics and Metallurgy  
 N. J. Johnson, Industrial Electrolytic  
 C. W. Tobias, Theoretical Electrochemistry  
 A. J. deBethune, Theoretical Electrochemistry  
 R. M. Hurd, Theoretical Electrochemistry

## ADVERTISING OFFICE

### ECS

30 East 42 St., New York 17, N. Y.

### ECS OFFICERS

F. L. LaQue, President  
 International Nickel Co., Inc.,  
 New York, N. Y.  
 W. J. Hamer, Vice-President  
 National Bureau of Standards,  
 Washington, D. C.  
 Lyle I. Gilbertson, Vice-President  
 207 Dogwood Lane,  
 Berkeley Heights, N. J.  
 E. B. Yeager, Vice-President  
 Western Reserve University,  
 Cleveland, Ohio  
 Ernest G. Enck, Treasurer  
 Felicity Farm  
 Gwynedd Valley, Pa.  
 Ivor E. Campbell, Secretary  
 National Steel Corp., Weirton, W. Va.  
 Robert K. Shannon, Executive Secretary  
 National Headquarters, The ECS,  
 30 East 42 St., New York 17, N. Y.

Manuscripts submitted to the Journal should be sent, in triplicate, to the Editorial Office at 30 East 42 St., New York 17, N. Y. They should conform to the revised Instructions to Authors published on pp. 131C-132C of the May issue. Manuscripts so submitted become the property of The Electrochemical Society and may not be published elsewhere, in whole or in part, unless permission is requested and granted by the Editor.

The Electrochemical Society does not maintain a supply of reprints of papers appearing in its Journal. A photoprint copy of any particular paper, however, may be obtained by corresponding direct with the Engineering Societies Library, 345 E. 47 St., New York, N. Y.

Inquiries re positive microfilm copies of volumes should be addressed to University Microfilms, Inc., 313 N. First St., Ann Arbor, Mich.  
 Walter J. Johnson, Inc., 111 Fifth Ave, New York 3, N. Y., have reprint rights to out-of-print volumes of the Journal, and also have available for sale back volumes and single issues, with the exception of the current calendar year. Anyone interested in securing back copies should correspond direct with them.

# Journal of the Electrochemical Society

JUNE 1962

VOL. 109 • NO. 6

## CONTENTS

### Editorial

Diversified Interests. *F. L. LaQue* ..... 144C

### Technical Papers

Copper Corrosion. *D. J. G. Ives and A. E. Rawson*  
 I. Thermodynamic Aspects ..... 447  
 II. Kinetic Studies ..... 452  
 III. Electrochemical Theory of General Corrosion ..... 458  
 IV. The Effects of Saline Additions ..... 462  
 Electrochemical Dissolution of Single Crystalline Copper. *L. H. Jenkins and J. O. Stiegler* ..... 467  
 The Oxidation of Sputtered Tantalum Films. *H. Basseches* ..... 475  
 The Influence of Residual Stress on the Magnetic Characteristics of Electrodeposited Nickel and Cobalt. *R. D. Fisher* ..... 479  
 Preparation of Magnetic Characteristics of Chemically Deposited Cobalt for High-Density Storage. *R. D. Fisher and W. H. Chilton* ..... 485  
 Effect of Binary Alloy Plating on Delayed Brittle Failure of Ultrahigh Strength Steel. *W. Beck and E. J. Jankowsky* ..... 490  
 Rotating Disk Electrode Techniques for the Study of Addition Agents. I. Preliminary Studies with Cupric Sulfate Solutions. *S. E. Beacom and R. N. Hollyer, Jr.* ..... 495  
 A Flow Synthesis of Gallium Phosphide and Some Properties of Gallium Phosphide Powder Layers. *L. J. Bodi* ..... 497  
 Preparation and Properties of ZnO Phosphors. *A. Pfahnl* ..... 502  
 Dissolution of Germanium in Aqueous Hydrogen Peroxide Solution. *N. Cerniglia and P. Wang* ..... 508  
 Batch Evaporation or Crystallization at Constant Composition by a Two-Container Method. *W. G. Pfann, J. R. Patel, and H. C. Theuerer* ..... 512  
 Epitaxial Deposition of Silicon in a Hot-Tube Furnace. *B. E. Deal* ..... 514  
 Polarography of Mercaptoalkyl Compounds and Their Disulfides. *W. Stricks, J. K. Frischmann, and R. G. Mueller* ..... 518  
 Equilibrium Studies in the Reduction of Thorium Oxide by Aluminum. *D. O. Raleigh* ..... 521  
 Diagrammatic Representation of the Thermodynamics of Metal-Fused Chloride Systems. *R. Littlewood* ..... 525

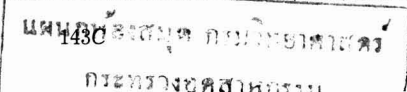
### Technical Notes

A Pulse Measurement of the Semiconductor-Electrolyte Space Charge Capacity. *P. T. Wrotenbery and A. W. Nolle* ..... 534  
 Electrolytic Etching of Germanium in Water. *W. Rindner and R. C. Ellis, Jr.* ..... 537

Discussion Section ..... 540-552

Current Affairs ..... 147C-156C

Published monthly by The Electrochemical Society, Inc., from Manchester, N.H.; Executive Offices, Editorial Office and Circulation Dept., and Advertising Office at 30 East 42 St., New York 17, N. Y., combining the JOURNAL and TRANSACTIONS OF THE ELECTROCHEMICAL SOCIETY. Statements and opinions given in articles and papers in the JOURNAL OF THE ELECTROCHEMICAL SOCIETY are those of the contributors, and The Electrochemical Society assumes no responsibility for them. Subscription to members as part of membership service; subscription to nonmembers \$24.00 plus \$1.50 for postage outside U.S. and Canada. Single copies \$1.70 to members, \$2.25 to nonmembers. Copyright 1962 by The Electrochemical Society, Inc. Entered as second-class matter at the Post Office at Manchester, N. H., under the act of August 24, 1912.





## Diversified Interests

*T*HE Electrochemical Society is a heterogeneous organization with its several Divisions having as a bonding influence concern with some effect of the passage of an electric current. From the engineering point of view there is very little common ground between, for example, the Electrothermics and Metallurgy Division and the Electro-Organic Division. Similarly, the effects of the passage of current that occupy the attention of the Corrosion Division are almost the reverse of what the Electrodeposition Division seeks to accomplish, if the formation of a metallic coating, rather than dissolution of an anode, is recognized as the major objective of electrodeposition.

However, the principal purposes of the Society, as such, do not require that all of its Divisions and all of its members have a common interest. Any one of the Divisions could serve as a nucleus around which a useful and effective organization could grow. The principal requirement is that the nucleus be alive and vigorous and capable of accommodating a pattern of growth that will serve the needs of the other associated groups having their own special interests.

Presumably, any one of the Divisions could be organized to function as a separate technical or scientific society. As a matter of fact, such a splintering process has become all too common recently with the formation of new technical societies by groups who have felt that their special interests were not being catered to sufficiently by existing organizations. This has resulted in a proliferation of societies each with its divisions, sections, committees, and administrative staff. All too often, a principal effect of this splintering process has been to require those working in a particular field to divide their interests among a number of groups with inevitable overlaps and wasteful duplications of effort.

It is much better for those who recognize a need for more intensive activity in a particular area to cultivate attention to this interest in some appropriate division of an existing organization.


It is evident that The Electrochemical Society provides ample scope for such specialized concern with the use, generation, and various effects of electricity. Through its administrative functions, its national and sectional meetings, and its publications, it serves as a most efficient agency for dealing with the interests and needs of its members. At the same time, it provides frequent opportunities for the cross-fertilization and stimulation that frequently result from bringing together scientists whose advances in one area may be used to accelerate progress in quite a different field.

It is evident, therefore, that The Electrochemical Society doesn't need to be homogeneous to be useful and that, with their very considerable autonomy, its several Divisions can serve the special needs of their members while taking advantage of those functions of the Society that benefit all Divisions and all members.

We hope that recent trends toward even more general use of over-all society facilities for meetings and publications will continue and that the several Divisions and Local Sections will take full advantage of what the Society as a whole has to offer.

—F. L. LAQUE<sup>1</sup>

<sup>1</sup> President of The Electrochemical Society, 1962-1963; Executive Dept., International Nickel Co., Inc., New York, N. Y.



... Greatly Reduced Clogging  
of Diaphragms

**NOW!**

... Lower  
Cell Maintenance Costs

... Longer Anode Life

Costly, troublesome clogging of diaphragms due to the oil impregnant in conventional anodes, is materially lessened by the new Stackpole "GraphAnodes." Cell maintenance costs are reduced accordingly.

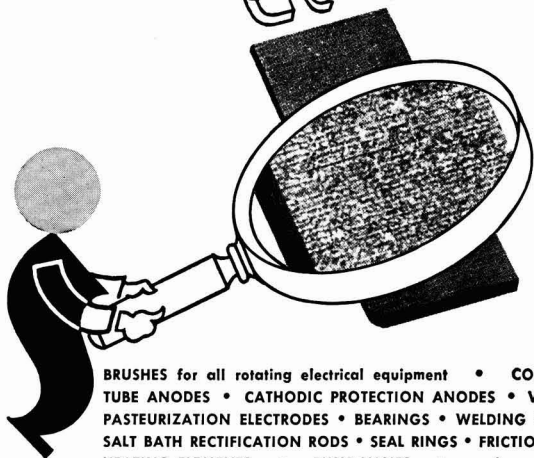
Better results are achieved because Stackpole *GraphAnodes* present a uniform, low-porosity surface to the electrolyte. The graphite is consumed slowly and evenly. It does not slough off to clog the diaphragm or contaminate the cell.

Let Stackpole arrange for a convincing demonstration of these new anodes on your own equipment. You be the judge—and, by way of convincing proof we suggest that you pay particular attention to the reduced frequency of diaphragm renewals.

**STACKPOLE CARBON COMPANY**  
St. Marys, Pa.

**STACKPOLE**

**GraphAnodes**



MAGNIFIED, UNRETOUCHED PHOTO . . . shows uniform structure of Stackpole *GraphAnodes*. The low-porosity surface assures that electrolyte will act on the surface, not below to cause premature anode deterioration and cell contamination by droppings of unconsumed graphite particles.

BRUSHES for all rotating electrical equipment • CONTACTS (carbon-graphite and metal powder types)  
TUBE ANODES • CATHODIC PROTECTION ANODES • VOLTAGE REGULATOR DISCS • WATER HEATER and  
PASTEURIZATION ELECTRODES • BEARINGS • WELDING CARBONS • MOLDS AND DIES • POROUS CARBON  
SALT BATH RECTIFICATION RODS • SEAL RINGS • FRICTION SEGMENTS • CLUTCH RINGS • ELECTRIC FURNACE  
HEATING ELEMENTS • PUMP VANES • and many other carbon, graphite, and electronic components.

choose the  
**SARGENT**  
 MODEL XV  
**RECORDING**  
**POLAROGRAPH**<sup>®</sup>  
 4 important advantages!



1. Full 10" Chart
2. 1/10% Accuracy of Measurement
3. 10 Standardized Polarizing Ranges
4. Low Cost

This Sargent POLAROGRAPH gives you a large 250 mm (10 inches) chart and the highest accuracy and current sensitivity at the lowest price of any pen writing polarographic instrument meeting these specifications.

It offers you optimum specifications based on over twenty years of leadership in design, manufacture and service in this specialized field of analysis.

The polarographic method is capable of reproducibility to 1/10% and analytical accuracy to 1/2%. To make use of this facility, the instrument must be accurate to 1/10% and chart space must be provided for recording large steps to achieve measuring precision. We strongly advise against the purchase of any polarographic instrument using miniature (5 inch) charts and low gain balancing systems in the 1% order of precision.

This Model XV is adaptable to 10<sup>-6</sup>M determinations with the S-29315 Micro Range Extender.

#### SPECIFICATIONS

**Current Ranges:** 19, from .003 to 1.0  $\mu$ A/mm.

**Polarizing Ranges, volts:** 0 to -1; -1 to -2; -2 to -3; -3 to -4; +.5 to -5; 0 to -2; -2 to -4; +1 to -1; 0 to -3; +1.5 to -1.5.

**Balancing Speed:** standard, 10 seconds; 1 second or 4 seconds optional.

**Bridge Drive:** synchronous, continuous repeating, reversible; rotation time, 10 minutes.

**Chart Scale:** current axis, 250 mm; voltage axis, 10 inches equals one bridge revolution.

**Current Accuracy:** 1/10%

**Voltage Accuracy:** 1/4%

**Chart Drive:** synchronous, 1 inch per minute standard; other speeds optional.

**Writing Plate:** 10 1/2 x 12 1/2 inches; angle of slope, 30°.

**Standardization:** manual against internal cadmium sulfate standard cell for both current and voltage.

**Damping:** RC, four stage.

**Pen:** ball point; Leroy type optional.

**Suppression:** zero displacement control, mercury cell powered, 6 times chart width, upscale or downscale.

**Potentiometric Range:** 2.5 millivolts, usable as general potentiometric recorder.

**Finish:** case, enameled steel; panels, anodized aluminum; writing plate, polished stainless steel; knobs and dials, chromium plated and buffed.

**Dimensions:** 23 x 17 x 10 inches.

**Net Weight:** 65 pounds.

S-29310 Sargent Model XV Recording Polarograph with accessories and supplies.....\$1585.00

For complete information write for Sargent Bulletin P.

E. H. SARGENT & CO., 4647 W. FOSTER AVE., CHICAGO 30, ILLINOIS  
 Detroit 4, Mich. - Dallas 35, Texas - Birmingham 4, Ala.  
 Springfield, New Jersey - Anaheim, California



**SARGENT**

Scientific Laboratory Instruments  
 Apparatus · Supplies · Chemicals

# Copper Corrosion

## I. Thermodynamic Aspects

D. J. G. Ives

Department of Chemistry, Birkbeck College, London, England

and A. E. Rawson

Colne Valley Water Company, Watford, Hertfordshire, England

### ABSTRACT

Thermodynamic data for reactions concerned in the corrosion of copper in waters containing dissolved oxygen and carbon dioxide are assembled and are used to demonstrate certain features of the corrosion processes. These include the extreme vulnerability of copper to attack, the critical effects of oxygen, and the inadequately protective properties of films of solid corrosion products. Confirmation and extension of these conclusions are obtained by experimental studies of systems derived from copper, cuprous oxide, cupric oxide, malachite, and azurite in water kept in equilibrium with gaseous atmospheres containing known partial pressures of oxygen and carbon dioxide. It is shown, *inter alia*, that cuprous oxide is highly susceptible to dissolution, both by disproportionation and oxidation, and that metallic copper dissolves in such media at a constant rate, despite the accompanying film growth, accumulation of cupric bicarbonate in solution, and rise of pH. The maximum rate of dissolution is attained at a molar ratio of  $O_2/CO_2 = 7/3$  in the gas phase, when a substantial oxide film is formed on the metal.

The general (nonpitting) corrosion of copper by waters containing oxygen and carbon dioxide produces cupric bicarbonate in solution and an inadequately protective film of cuprous oxide on the metal. This action, which may be indefinitely prolonged, is an insidious industrial hazard, because the copper in solution may initiate acute corrosion elsewhere by setting up local cell action. Yet little effort has been made to study it systematically, even to discover whether the reactions producing soluble and insoluble corrosion products are functionally inter-related. There is thus a need for thermodynamic and kinetic studies of the Cu, H<sub>2</sub>O, O<sub>2</sub>, CO<sub>2</sub> system (both without and with saline additions), which the present series of papers is intended to initiate.

In attempting to correlate laboratory experiments with practical corrosion problems, a difficulty arises in the disparity of time scales; some adjustment of conditions must be made to hasten the experiments, with unavoidable introduction of an element of artificiality. In the present work, this adjustment has been confined to an increase above normal of the partial pressures of oxygen and of carbon dioxide with which the experimental systems have been kept in equilibrium. It is believed that this is a better compromise than some others which have been adopted.

### Application of Thermodynamic Data

The thermodynamic data in Table I were derived from entries in the N.B.S. Circular 500 (1), except for the case of reactions involving the basic carbonates. For these substances, only heats of formation could be found (2), and an attempt to obtain the required Gibbs free energies of formation on the basis

of entropy estimates [using approximate figures quoted by Latimer (3) for carbonate and hydroxide] was unsuccessful, giving results widely at variance with experiment. The entries in Table I for reactions involving malachite (5) and azurite (6) are therefore derived from our own experimental work and are of correspondingly limited accuracy.

Each reaction in Table I produces one mole of cupric bicarbonate in solution, so that subtraction of one equation from another (with the appropriate free energy changes) provides information about a third reaction in which cupric bicarbonate is not involved. The table thus summarizes data for 28 re-

Table I. Standard free energies,  $\Delta G^\circ$ , and equilibrium ionic products,  $K' = (Cu^{2+})(HCO_3^-)^2$ , for copper corrosion reactions at 25°C

Reaction	$\Delta G^\circ$ , kcal	$\log K'$
[1] $Cu + H_2O + 2CO_2 + \frac{1}{2}O_2 = Cu(HCO_3)_2$	-19.88	$14.57 + 2 \log P_{CO_2} + \frac{1}{2} \log P_{O_2}$
[2] $\frac{1}{2}Cu_2O + H_2O + 2CO_2 + \frac{1}{4}O_2 = Cu(HCO_3)_2$	-2.39	$1.75 + 2 \log P_{CO_2} + \frac{1}{4} \log P_{O_2}$
[3] $Cu(OH)_2 + 2CO_2 = Cu(HCO_3)_2$	8.73	$-6.40 + 2 \log P_{CO_2}$
[4] $CuO + H_2O + 2CO_2 = Cu(HCO_3)_2$	10.52	$-7.71 + 2 \log P_{CO_2}$
[5] $\frac{1}{2}[CuCO_3 \cdot Cu(OH)_2] + \frac{1}{2}H_2O + 1\frac{1}{2}CO_2 = Cu(HCO_3)_2$	11.9	$-8.69 + 1\frac{1}{2} \log P_{CO_2}$
[6] $\frac{1}{3}[2CuCO_3 \cdot Cu(OH)_2] + 2\frac{1}{3}H_2O + 1\frac{1}{3}CO_2 = Cu(HCO_3)_2$	12.1	$-8.84 + 1\frac{1}{3} \log P_{CO_2}$
[7] $Cu_2O - Cu + H_2O + 2CO_2 = Cu(HCO_3)_2$	15.10	$-11.07 + 2 \log P_{CO_2}$

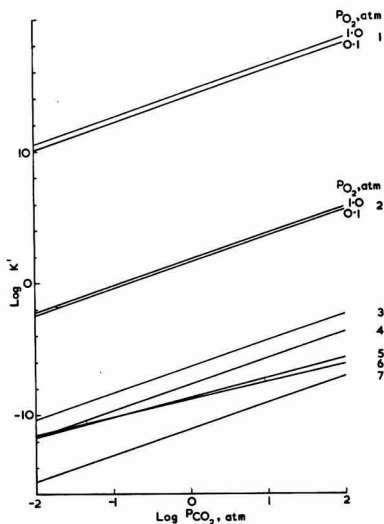


Fig. 1.  $\log K' = \log (\text{Cu}^{2+})(\text{HCO}_3^-)^2$  as function of  $\log P_{\text{CO}_2}$  at 25°C for reactions [1] to [7] of Table I. Plots relating to  $P_{\text{O}_2} = 1.0$  atm and 0.1 atm are shown for reactions [1] and [2].

actions which may be concerned in the corrosion of copper in the Cu,  $\text{H}_2\text{O}$ ,  $\text{O}_2$ ,  $\text{CO}_2$  system. The last column contains values of  $\log K'$ , where  $K' = (\text{Cu}^{2+})(\text{HCO}_3^-)^2$ , the ionic activity product, which would be attained in solution if each reaction proceeded to equilibrium. Figure 1 shows the dependence of the  $\log K'$  values on appropriate gas pressures.

Certain inferences may be drawn from this thermodynamic survey.

Reaction [1] is accompanied by a free energy loss of nearly 20 kcal, indicating that copper has a considerable tendency to dissolve in water containing oxygen and carbon dioxide. Since it is this dissolution which constitutes the main problem, it is reasonable to regard this quantity as an over-all "corrosion potential" of copper in this connection. It is, however, unlikely to be fully effective because the system can decrease its free energy still further by undergoing any of the reactions [3] to [7] in reverse. All of these produce solid compounds, which are likely to deposit on the metal and exert some protective action.

The same inference may be drawn by inspection of Fig. 1. Thus, it can be seen that for  $P_{\text{O}_2} = P_{\text{CO}_2} = 0.1$  atm,  $\log K'$  for reaction [1] has a value of around 12. This corresponds with cupric bicarbonate in solution at molality  $\sim 6000$  mole  $\text{kg}^{-1}$ . This striking result is absurd only because it expresses the corrosion potential of copper on an unsuitable scale. It correctly indicates that copper, far from being noble, is extremely vulnerable and is protected from rapid destruction only by the solid films which form on it. Thermodynamic information about these secondary film forming processes can be obtained from Fig. 1. Thus, a concentration of cupric bicarbonate defined by a point on this diagram will exceed the equilibrium concentration for a reaction represented by a line passing below the point. Such a concentration of cupric bicarbonate will therefore have a thermody-

amic tendency to drive this reaction backwards. It is emphasized that these thermodynamic arguments are unlikely to be related to mechanisms of reaction and certainly carry no implication that all solid corrosion products arise from consecutive dissolution and deposition steps. Such arguments should, on the other hand, give the true sequence of stabilities of the solid corrosion products under defined  $P_{\text{O}_2}$  and  $P_{\text{CO}_2}$  conditions.

Reaction [7] is a disproportionation reaction occurring anaerobically. The data indicate that, by this reaction, cuprous oxide in presence of metallic copper can send appreciable concentrations of cupric ion into solution. Thus, for  $P_{\text{CO}_2} = 1$  atm, the equilibrium concentration of cupric ion is 8 ppm,<sup>1</sup> indicating that cuprous oxide is unlikely to form a protective film of any permanence unless it is constantly regenerated; such regeneration, however, implies continued attack on the copper substrate.

The waters in which copper corrosion normally occurs contain oxygen as well as carbon dioxide; this greatly worsens the situation because reaction [2], which is much more favored thermodynamically, comes into play. Even if the effects of this should be largely nullified by deposition of hydroxide, oxide, or basic carbonate (reactions [3] to [6] in reverse), the damage is not entirely repaired, for all these substances provide far from negligible concentrations of cupric ions in solution. This provides an additional reason why it is unlikely that copper will, in course of time, provide its own adequately protective film.

The critical effects of oxygen are well illustrated by calculating equilibrium molalities of cupric bicarbonate in solution for reactions [1] and [2] over a complete range of oxygen-carbon dioxide mixtures at a total pressure of 1 atm. The results are shown in Fig. 2. The very steep rise of the curves as the oxygen partial pressure increases from zero is obvious; the tendency of copper to dissolve increases rapidly, and the protective action of a cuprous oxide film decreases even more rapidly.

#### Exploratory Experiments and Results

Although not all the equilibria of interest could be accessible, experiments were carried out to check the inferences made from the available thermodynamic data and to serve as a guide for further work. Pow-

<sup>1</sup> The convenient notation of parts per million ( $\text{mg l}^{-1}$ ) is used for very low concentrations of solutes.

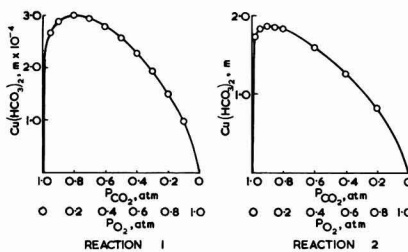


Fig. 2. Calculated molalities of  $\text{Cu}(\text{HCO}_3)_2$  for reaction [1],  $\text{Cu} + \text{H}_2\text{O} + 2\text{CO}_2 + \frac{1}{2}\text{O}_2 = \text{Cu}(\text{HCO}_3)_2$  and reaction [2],  $\frac{1}{2}\text{Cu}_2\text{O} + \text{H}_2\text{O} + 2\text{CO}_2 + \frac{1}{4}\text{O}_2 = \text{Cu}(\text{HCO}_3)_2$  for systems in equilibrium with mixtures of  $\text{O}_2$  and  $\text{CO}_2$  at a total pressure of 1 atm.



dered (100 mesh) solid phases, carefully freed from electrolytic impurities, were maintained in contact with circulating water continuously equilibrated with known gas mixtures ( $O_2$ ,  $CO_2$ ,  $N_2$ ) at a total pressure slightly greater than barometric. Samples of aqueous phase were periodically withdrawn for estimation of copper content, and records were kept of conductance and pH. Accuracy in these experiments, conducted in a thermostatically controlled room at  $24^\circ \pm 1^\circ C$ , was not better than  $\pm 5\%$ , but the following useful indications were obtained.

Dissolution of cupric compounds, or of cuprous oxide, or copper in oxygenated media, led to increase in pH and (sometimes after an initial decrease) conductance. In conjunction with copper analyses and  $P_{CO_2}$  values, such results were invariably consistent with the existence of copper in solution solely as fully dissociated cupric bicarbonate, and with pH determined by the bicarbonate/carbonic acid buffer ratio. To establish this, use was made of the electroneutrality requirement, of data for the solubility of carbon dioxide in water (4) and its dependence on partial pressure (5), of the ionic product of water (6), the dissociation constants of carbonic acid (6), and ion conductances of hydrogen (7), cupric (8) and bicarbonate (9) ions.

Cupric oxide, prepared from cuprous oxide (see below) by heating in oxygen at  $400^\circ C$ , was used in studies of equilibria in  $CuO$ ,  $H_2O$ ,  $N_2$ ,  $CO_2$  and  $CuO$ ,  $H_2O$ ,  $O_2$ ,  $CO_2$  systems. The results, shown in Fig. 3(a), agreed reasonably well with some earlier determinations (10) and with those calculated thermodynamically for reaction [4], from which the curve in Fig. 3(a) was constructed.

The thermodynamic data indicate, however, that cupric oxide is not the most stable solid phase except at very low partial pressures of carbon dioxide. This

was confirmed by the occasional appearance of green-blue solids at  $P_{CO_2} \sim 1$  atm. In two cases these were identified by x-rays as malachite, or a mixture of malachite and azurite.

Malachite (Burra Burra, Australia) and azurite (MacAlder Mine, Kenya), hand-picked, ground, and extracted with water to constant conductance of the aqueous phase, were used in similar equilibrium studies. The results are shown in Fig. 3(b) and 3(c), in which the curves represent the requirements of the data in Table I for reactions [5] and [6]; these data were, however, derived from these same experiments, so the agreement is not significant. Agreement with some earlier data (10, 11) is not good, but it is believed that the present results slightly improve an unsatisfactory situation, even though they are derived from rough, exploratory experiments quite inadequate for setting up new standards (thus, the experimental values, for reactions [4], [5], and [6], respectively, of  $\partial \log K' / \partial \log P_{CO_2}$  were 1.84, 1.40, and 1.20).

There is some subsidiary evidence relating to the placing of the lines in Fig. 1. If, by some means (possibly reaction [1]), a concentration of cupric bicarbonate has been set up in solution, then, in the presence of metallic copper, reaction [7] in reverse is thermodynamically preferred, and there is no doubt that cuprous oxide is the first solid corrosion product to appear under these circumstances. In long-term experiments in which copper strips were allowed to corrode for many months in aerated solutions the second product was malachite. Azurite, cupric oxide, or hydroxide were not found. This is in agreement with expectations from Fig. 1. On the other hand, in experiments in which cuprous oxide has been subjected to prolonged treatment with water in equilibrium with  $P_{CO_2} = 0.3$  atm, malachite, not azurite, has been identified by x-rays as the final product. This suggests that the malachite line in Fig. 1 should be slightly dropped relative to the azurite line. Such adjustments, however, must await the provision of more satisfactory data. It must also be remarked that purely thermodynamic arguments of this kind cannot be taken as an infallible guide to the sequence in which corrosion products may appear and can certainly not be taken as evidence on the mechanisms of their formation.

Cuprous oxide, prepared by glucose reduction of cupric acetate solution, was extracted with water in absence of air to constant conductance of the aqueous phase, dried, graded (100 mesh), and used in studies of  $Cu_2O$ ,  $H_2O$ ,  $N_2$ ,  $CO_2$  and  $Cu_2O$ ,  $H_2O$ ,  $O_2$ ,  $CO_2$  systems. The results for the first of these are shown in Fig. 4(a) and are seen to be erratic, corresponding with observations of instability and deposition of green-blue solid phases. Copper in solution was undoubtedly predominantly, if not exclusively, in the form of cupric bicarbonate (basic cupric carbonate was recovered on displacement of dissolved carbon dioxide by nitrogen), which must have been formed by the disproportionation reaction [7]. Yet at  $P_{CO_2} = 1$  atm, the concentration of cupric ion in solution, 83 ppm, was ten times that expected from the thermodynamic data. This result could not have been due to imperfect deoxygenation of the system (residual

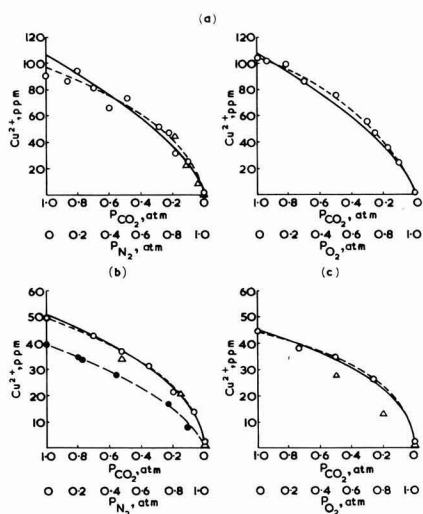


Fig. 3. Experimental concentrations of  $Cu^{2+}$ , ppm, for (a)  $CuO$ , (b) malachite, and (c) azurite equilibrated with water and with  $N_2$  and  $CO_2$  mixtures (left-hand diagrams) or with  $O_2$  and  $CO_2$  mixtures (right-hand diagrams) at a total pressure of 1 atm. — Thermodynamic curve; ---○--- experimental, present work; △ Tronstad and Veimo; ---●--- free.

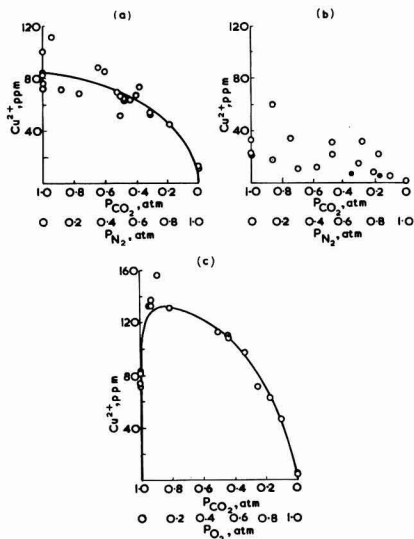


Fig. 4. Experimental studies of systems (a)  $\text{Cu}_2\text{O}$ ,  $\text{H}_2\text{O}$ ,  $\text{N}_2$ ,  $\text{CO}_2$ , (b)  $\text{Cu}$ ,  $\text{Cu}_2\text{O}$ ,  $\text{H}_2\text{O}$ ,  $\text{N}_2$ ,  $\text{CO}_2$ , and (c)  $\text{Cu}_2\text{O}$ ,  $\text{H}_2\text{O}$ ,  $\text{O}_2$ ,  $\text{CO}_2$  for binary gaseous mixtures to a total pressure of 1 atm.  $\circ$  Present work;  $\bullet$  Tronstad and Veimo.

oxygen 0.0 – 0.7 ppm) and must be attributed to nonstoichiometry of the oxide and to the absence of metallic copper, except for that produced in the reaction itself, from the system. Such copper could, perhaps, be accommodated in lattice defects and certainly fell short of attaining the standard state for the metal. This point was checked by carrying out a set of experiments in which copper powder was included with the cuprous oxide. The results, shown in Fig. 4(b), were even more erratic, but appreciably lower. Instability was very marked, and some of the copper in solution must have been in the cuprous valency state.

Although these results have no absolute, quantitative significance, they underline the extreme vulnerability of cuprous oxide to dissolution, both by disproportionation and oxidation, and indicate the necessity of giving separate consideration to  $\text{Cu}_2\text{O}$  and  $\text{Cu}$ ,  $\text{Cu}_2\text{O}$  systems. In the latter case it seems that the copper may have some difficulty in controlling its somewhat thermodynamically undisciplined lower oxide. This general point seems to have escaped Tronstad and Veimo (10), who set out to determine the solubility of cuprite in water containing dissolved carbon dioxide. Their results (in presence of added copper) are included in Fig. 4(b) and fall within the scatter of the present determinations, but their conclusion that cuprous oxide is only 1/5 to 1/10 as "soluble" as cupric oxide in water containing carbon dioxide is untenable; their subsequent discussion of copper corrosion, hinging on this conclusion, consequently loses significance.

Inspection of Fig. 1 indicates that there could be no hope of realizing equilibria in the  $\text{Cu}_2\text{O}$ ,  $\text{H}_2\text{O}$ ,  $\text{O}_2$ ,  $\text{CO}_2$  system, for molalities of cupric bicarbonate up to nearly 2 mole  $\text{kg}^{-1}$  would have to be attained. In spite of this, an attempt was made to study this system.

Instability was encountered, but the highest attainable concentrations of copper in solution were recorded and appear as functions of gas composition in Fig. 4(c). Surprisingly enough, a curve can be placed through the somewhat scattered results (orders of magnitude lower than those corresponding with equilibrium) identical in shape with the thermodynamic curve of Fig. 2. Coincidental though this may be, the extreme vulnerability of cuprous oxide in such systems, containing even traces of oxygen, is demonstrated.

Since the limit of thermodynamic studies had been reached, and since in practical problems kinetic and thermodynamic factors are often not easily disentangled, experiments were made in order to follow the course of all the solid phase dissolution reactions over an initial period of 3 hr. In general, the results served only to confirm conclusions already reached, with the following exceptions.

For the cupric compounds, a fast initial reaction decreased smoothly in rate, giving a copper concentration curve concave to the time axis, a form not unexpected and easily explained. In the case of cuprous oxide, however, these features were accentuated; thus for the conditions  $P_{\text{O}_2} = 0.2$  atm and  $P_{\text{CO}_2} = 0.8$  atm, the aqueous phase contained 15 ppm of dissolved copper within 5 min, but required 3 hr to attain 30 ppm. This behavior could be due to a change in that part of the solid phase accessible to the aqueous medium, impoverishment in oxygen, or enrichment in copper of nonstoichiometric surface layers. But perhaps the most important aspect is again the high reactivity of cuprous oxide, now demonstrated kinetically as well as thermodynamically, when not under the restraining control of metallic copper in its standard state. Again, remarkably, the extent of copper uptake after 1, 2, or 3 hr of dissolution reproduced approximately the shape of the thermodynamic curve.

Copper powder, formed by reduction in hydrogen at 200°C of the same cuprous oxide (in the hope of preserving some correspondence of specific surface areas), was used to study the  $\text{Cu}$ ,  $\text{H}_2\text{O}$ ,  $\text{O}_2$ ,  $\text{CO}_2$  system. Attention was necessarily confined in this case to kinetic aspects, which were later studied in more detail by modified methods, but the following preliminary results of some significance were obtained.

The dissolution of metallic copper, often delayed by an induction period, took place at a constant rate. This is illustrated in Fig. 5(a) and stands in marked contrast to the behavior found for the four copper compounds examined in this way. This remarkable constancy of rate, later shown to be preserved for prolonged periods, suggested some sort of automatic self-regulation, the nature of which was not clear at this stage.

The extent of dissolution in a fixed time, as a function of gas composition, did not reproduce the shape of the thermodynamic curve in Fig. 2. The maximum copper uptake was found in the range 20–30 mole % of carbon dioxide, 80–70 mole % of oxygen. For gas mixtures containing less than 20 mole % of oxygen, the copper retained its pristine pink color, but for mixtures richer in oxygen, it rapidly became brown or black. This may be related to the peak in the solu-

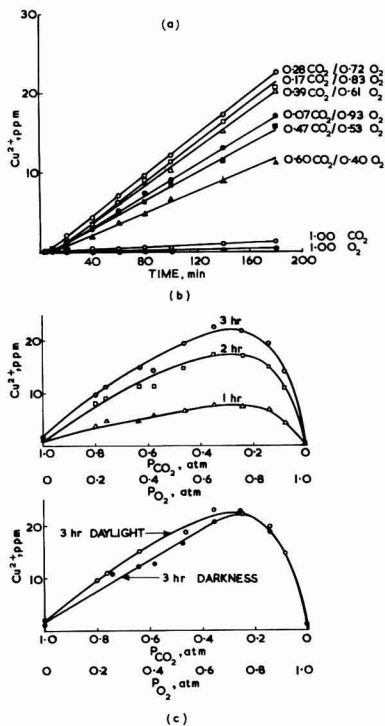


Fig. 5. Dissolution of Cu powder in water equilibrated with mixtures of  $\text{O}_2$  and  $\text{CO}_2$  to a total pressure of 1 atm (a) as a function of time for various gas mixtures, (b) as a function of gas composition for various times, and (c) as a function of gas composition for constant time, in daylight and in darkness.

bility of cuprous oxide at around 10 mole % of oxygen (Fig. 2 and 4(c)), which perhaps gives a film little chance to thicken. It was certainly the case that the maximum rate of dissolution was attained when the copper powder, as indicated by its color, was covered with a substantial oxide film. Although it was clear from the present and previous (12, 13) work that neither cuprous oxide nor cupric oxide can

be very protective in an aqueous medium, this conclusion does not imply an accelerated rate of dissolution as a consequence of progressive oxide formation. The idea that a film, far from giving increased protection with increasing thickness, might be active in promoting dissolution was novel.

In these experiments, previous observations (12, 14-16) that light accelerates chemical attack on copper was confirmed; steps were subsequently taken to eliminate this photo effect. Features of these experiments are illustrated in Fig. 5(b) and 5(c) and confirm that neither carbon dioxide nor oxygen is particularly aggressive toward copper in the absence of the other.

Manuscript received Oct. 2, 1961; revised manuscript received Jan. 23, 1962. This paper was prepared for delivery before the Ottawa Meeting, Sept. 28-Oct. 2, 1958.

Any discussion of this paper will appear in a Discussion Section to be published in the December 1962 JOURNAL.

#### REFERENCES

1. Selected Values of Chemical Thermodynamic Properties, Nat. Bur. Stand. Circular 500 (1952).
2. W. A. Roth, *J. prakt. Chem.*, **158**, 117 (1941).
3. W. M. Latimer, "Oxidation Potentials," 2nd. ed., Prentice-Hall, Inc., New York (1952).
4. Landolt-Börnstein, "Tabellen," **1**, 768 (1923).
5. International Critical Tables, **3**, 260 (1928).
6. R. A. Robinson and R. H. Stokes, "Electrolytic Solutions," p. 496, Butterworths, London (1955).
7. B. B. Owen and F. H. Sweeton, *J. Am. Chem. Soc.*, **63**, 2811 (1941).
8. B. B. Owen and R. W. Gurry, *ibid.*, **60**, 3074 (1938).
9. T. Shedlovsky and D. A. MacInnes, *ibid.*, **70**, 3281 (1948).
10. L. Tronstad and R. Veimo, *J. Inst. Metals*, **66**, 17 (1940).
11. E. E. Free, *J. Am. Chem. Soc.*, **30**, 1366 (1908).
12. G. D. Bengough and O. F. Hudson, *J. Inst. Metals*, **21**, 37 (1919).
13. W. H. J. Vernon, *Trans. Faraday Soc.*, **27**, 255 (1931).
14. T. W. Case, *Trans. Am. Electrochem. Soc.*, **31**, 351 (1917).
15. R. Audubert, *Compt. rend.*, **177**, 818 (1923).
16. O. Gatty and E. C. R. Spooner, "Electrode Potential Behavior of Corroding Metals," p. 184, Oxford (1938).

# Copper Corrosion

## II. Kinetic Studies

D. J. G. Ives

*Department of Chemistry, Birkbeck College, London, England*

and A. E. Rawson

*Colne Valley Water Company, Watford, Hertfordshire, England*

### ABSTRACT

Experimental methods are described for studying rates of formation of soluble and insoluble corrosion products of copper exposed to water containing dissolved oxygen and carbon dioxide. Coulometric reduction indicates that the films formed on copper under these conditions are predominantly of cuprous oxide. Generation of cupric bicarbonate in solution and film growth are constant in rate over long periods, and both are kinetically of first order with respect to dissolved oxygen. Dependence of these rates on the concentration of dissolved carbon dioxide follows no obvious kinetic law, but is such as to suggest that the initial pH of solution is a major factor. Experiments in which either solution or metallic phase is replaced during kinetic measurements demonstrate that a cuprous oxide film on copper may have either an activating or a passivating effect, depending on its mode of generation. The evidence indicates the existence of an electrochemical mechanism for general corrosion of copper by which dissolution and film growth are kinetically linked processes.

Preliminary work (Part I; preceding paper) indicated the need for concurrent measurements of rates of formation of soluble and insoluble corrosion products in the Cu, H<sub>2</sub>O, O<sub>2</sub>, CO<sub>2</sub> system. The technique developed for this purpose was designed to break a wide area of new ground, rather than to obtain precise kinetic data.

### Experimental Methods

#### *Corrosion Apparatus*

Units of the kind illustrated in Fig. 1, which is largely self-explanatory, were used to circulate glass-distilled water (initial  $\kappa \sim 3 \mu\text{mho cm}^{-1}$ , free NH<sub>3</sub> < 0.1 ppm) at a constant rate of 4-5 l hr<sup>-1</sup> through vessels containing copper electrodes, each of 15 cm<sup>2</sup> apparent surface area. The water was kept in equilibrium with gas mixtures of known composition (Orsat) by means of a diaphragm pump, which continuously circulated the gas through the main water reservoir. The apparatus, of silicone-treated Pyrex, was assembled with glass-to-glass junctions inside PVC sleeves, and neoprene stoppers were used for mounting electrodes and a dipping conductance cell. The electrodes were screened from light by shields round the electrode vessels.

Before use, the apparatus was repeatedly flushed out with batches of water to remove residual traces of copper and until the conductance of the water fell to about 3  $\mu\text{mho cm}^{-1}$  (residual CO<sub>2</sub>; glass-derived solutes). It was then charged with a standard volume (3.1 l) of water, which was brought into equilibrium with a prepared gas mixture; conductance and pH determinations were made and showed reasonably good correlation with the CO<sub>2</sub> contents of the mixtures concerned. The electrodes, prepared as described below, were then inserted and the run commenced.

The electrodes were made from electrolytic copper foil, 0.01 cm thick, initially degreased with acetone and polished to a mirror finish by use successively of "3/50 slow cutting Microid" alumina and " $\gamma$ -Microid" alumina. The foil was then cut into strips 2 cm wide and annealed in hydrogen ( $\sim 700^\circ\text{C}$ ). Shortly before use, these strips were cut to form electrodes, each provided with a tang which was gripped by a claw formed at the end of a heavy copper wire (1.6 mm diameter), sealed into a glass mounting tube with vacuum wax. Uncovered portions of the wire and tang were coated with beeswax, applied to leave only the desired area of foil exposed. The electrodes were stored in hydrogen and, immediately before use, were immersed for 1 min, with gentle agitation,

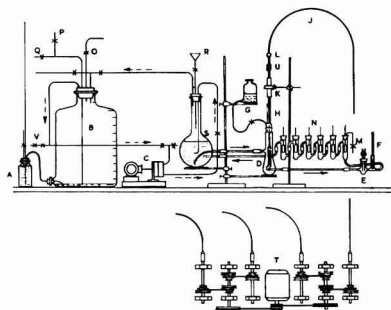


Fig. 1. Diagrammatic section of modified corrosion apparatus: A, gas seal and manometer; B, aspirator (22 l); C, gas circulating pump; D, solution circulating pump; E, conductance cell; F, thermometer; G, gas release; H, gas seal; J, flexible drive; K, bearing; L, drive connection; M, solution sampling point; N, electrodes and cells; O, gas sampling and filling point; P, water filling point; Q, water outlet; R, funnel for solution replacement; S, solution reservoir (2 l); T, 3-speed drive unit; U, worm drive; V, connection to second section.

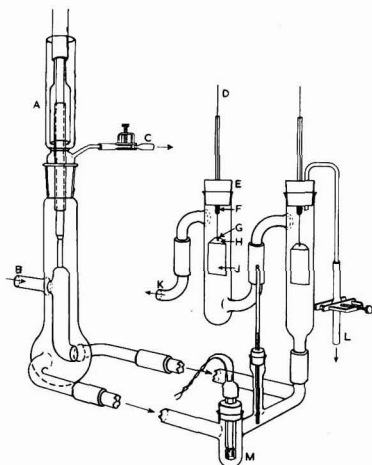


Fig. 2. Modified corrosion apparatus: solution circulating system: A, gas seal; B, from solution reservoir; C, gas release; D, 16 SWG hard copper wire; E, neoprene bung; F, picin wax seal; G, wire attached to foil; H, beeswax insulation; I, exposed copper foil; K, to solution reservoir; L, solution sampling point; M, conductance cell.

in 10% ammonium persulfate solution (1), washed rapidly in air-free water and inserted directly into the corrosion apparatus. This procedure removed any coulometrically measurable oxide film and gave a lightly etched surface hoped to be of reasonably reproducible properties. Details of electrode mounting and of part of the water-circulating system are shown in Fig. 2.

The progress of the kinetic runs, normally conducted for 100 hr at  $21^\circ \pm 2^\circ\text{C}$  was followed by conductance measurements, determinations of dissolved copper, and coulometric analyses of solid films formed on the electrodes.

#### Solution Analysis

Copper in solution (as cupric bicarbonate; cf. Part I) was determined colorimetrically (Hilger "Spekker"), using sodium diethyldithiocarbamate, bis-cyclohexanone oxalyldihydrazone, or rubeanic acid (preferred), against reference standards prepared from "Specpure" copper. Sampling reduced the volume of water in the corrosion apparatus progressively to 2.9 l, but a mean volume of 3.0 l was assumed, without appreciable error.

Electrodes were removed at intervals for examination, and correction was applied to the observed rates of change of cupric ion concentration (and of conductance) for the step-wise reduction of total area of metal-solution interface; all the results reported relate to a total apparent surface area of exposed copper of  $90\text{ cm}^2$ . At the conclusion of each run, pH was redetermined. Checks on gas composition by analysis indicated a maximum variation of about 0.01 atm in partial pressures.

#### Examination of Solid Films

Solid films on the electrodes were estimated coulometrically by galvanostatic cathodization in nitrogen-saturated, 0.2N ammonium chloride solution.

The apparatus was designed to secure reasonable uniformity of current density over the whole surface of an electrode undergoing cathodic reduction and was provided with Luggin capillaries leading to a saturated calomel electrode. The ammonium chloride electrolyte was recommended by Miley (2), but, because of its appreciable film-stripping action under open-circuit conditions (3), it has been replaced in some later work of this kind (1, 3-5) by 0.1N or 1.0N potassium chloride solutions. We have found, however, that ammonium chloride is preferable because it tends to reduce electrode polarization (reduction potentials less negative) and gives more sharply defined arrests on the potential-time curves. No serious discrepancies were found in estimates of film thickness due to this variation in the electrolyte, and 1.0N or 0.1N potassium chloride solution was frequently employed in confirmatory or duplicated measurements.

Although this coulometric method is unique in its suitability for a long series of routine measurements, it is, unfortunately, limited in accuracy and unsatisfactory in its powers of discrimination between alternative reducible copper compounds. Observed reduction potentials are not related to reversible potentials calculated for various copper-copper compound couples and vary considerably according to the current density within a practicable range. They also vary quite widely according to the physical nature and distribution of a given film substance, i.e., with the "topography" of the film (5). It is not surprising that films deposited in various ways, many of them conferring appreciable passivity, do not conform to the conditions required for electrode reversibility, nor that properties such as film conductance, permeability, and solubility should control irreversible reduction potentials, which are consequently thermodynamically unpredictable. In any case, no electrode carrying a composite deposit can be at equilibrium, and no reversible basic copper carbonate electrode exists.

The method therefore had to be used empirically, with calibration using films of known constitution. For this purpose, electrodes were subjected to the following treatments: (a) anodization for 15 min at  $4.0\text{ ma cm}^{-2}$  in 4N NaOH solution. Halliday (6) has shown that this provides a composite film, in which he identified  $\text{Cu}(\text{OH})_2$ ,  $\text{CuO}$ , and  $\text{Cu}_2\text{O}$  by electron diffraction; (b) exposure to moist oxygen at room temperature for 22 hr to produce a film consisting mainly of  $\text{Cu}_2\text{O}$ ; (c) ignition ( $\sim 300^\circ\text{C}$ ) for 1 min in air, then for 1 min in oxygen, to ensure the presence of  $\text{CuO}$ ; (d) long-term spontaneous corrosion in very dilute salt solutions [ $\sim 200$  ppm of  $\text{NaCl}$ ,  $\text{Na}_2\text{SO}_4$ ,  $\text{NaNO}_3$ ,  $\text{Ca}(\text{HCO}_3)_2$ ] in equilibrium with air, to produce basic salts. In all cases the films consisted of cuprous oxide overlaid with malachite, identified by x-rays.

Coulometric reduction curves of these electrodes are shown in Fig. 3. It is seen that cupric hydroxide and oxide, and cuprous oxide, are reduced at well-separated potentials, which differ from reversible potentials appropriate to the experimental conditions [ $\text{Cu}(\text{OH})_2 \rightarrow \text{Cu}_2\text{O}$ , 0.268v;  $\text{CuO} \rightarrow \text{Cu}_2\text{O}$ , 0.190v;  $\text{Cu}(\text{OH})_2 \rightarrow \text{Cu}$ , 0.130v;  $\text{CuO} \rightarrow \text{Cu}$ , 0.091v;  $\text{Cu}_2\text{O} \rightarrow \text{Cu}$ ,

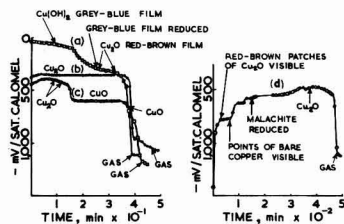


Fig. 3. Coulometric reduction of films on copper; control experiments, (a) to (d), details as in text [c.d.: (a) 0.2 ma/cm<sup>2</sup>; (b) 0.3 ma/cm<sup>2</sup>; (c) 0.5 ma/cm<sup>2</sup>; (d) 1.0 ma/cm<sup>2</sup>].

—0.008v).<sup>1</sup> Even the sequence of the reduction potentials is not the same, but is identical with that found by Halliday (6), although his cathodizations were performed in 4N NaOH solutions. The latter fact suggests that the irreversible reduction potentials are determined largely by the properties of the solid phases.

It is also seen that the malachite-bearing film initially was very resistant to cathodic reduction, and that no characteristic reduction potential could be identified. This was the case for all the electrodes of this kind. Fortunately malachite seems invariably to be a very long-term corrosion product which appears as an easily distinguishable, bright green phase. Neither malachite nor gray-blue cupric hydroxide has appeared in any of the kinetic corrosion experiments, so that attention may be confined to cuprous and cupric oxides.

The calibration experiments lead to typical reduction potentials for Cu<sub>2</sub>O and CuO of —390 ± 30 mv and —660 ± 60 mv, in 0.2N NH<sub>4</sub>Cl solution, with respect to the saturated calomel electrode. This agrees tolerably with Miley's (2) results of about —360 to —390 mv and —670 to —710 mv for these two oxides, and with —370 mv for Cu<sub>2</sub>O obtained by Price and Thomas (7). Although Lambert and Trevoy (5) were unable to confirm that CuO is reduced at a potential some 300 mv more negative than is Cu<sub>2</sub>O, this fact is now substantiated and is supported by Halliday's findings (6). In the present work, it was expedient to arrange for all the corrosion films to be cathodically reduced in a period not exceeding 40 min, and current densities were adjusted accordingly within the range 0.1–1.0 ma cm<sup>-2</sup>. Under these conditions, the films were generally reduced at potentials between —350 and —450 mv with respect to the saturated calomel electrode. Occasionally it was necessary to use higher current densities, with a corresponding negative displacement of potential. It was concluded that all the films were composed of cuprous oxide, and mean film thicknesses were calculated throughout on this assumption. At first sight somewhat questionable, this conclusion is strongly supported by the fact that, apart from initial eccentricities assigned to elimination of tendencies to passivity, or gentle gradients attributed to variation in physical nature, all the potential-time curves at constant current showed but a single plateau. Since it is undoubted that in all cases cuprous oxide was a major film constituent, the inference may be drawn

<sup>1</sup> The Stockholm sign convention, 1953, is used throughout.

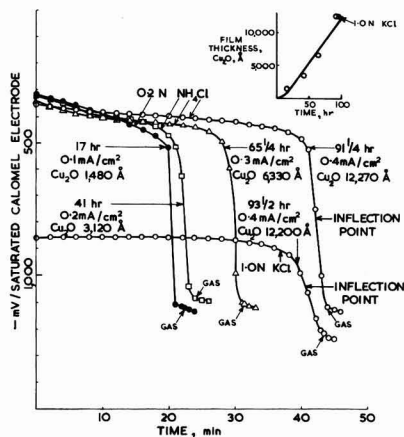


Fig. 4. Typical set of coulometric reduction curves used to follow growth of cuprous oxide film (inset).

that it was essentially the only constituent. It must be mentioned, however, that in a few isolated cases a second, ill-defined arrest occurred at —500 to —550 mv, the source of which was not identified. A typical set of coulometric reduction curves, illustrating the course of film growth on electrodes successively removed from the corrosion apparatus during a kinetic run, is shown in Fig. 4.

## Results

Since a complete survey of the effects on corrosion rates of two independent variables (i.e. partial pressures of oxygen and of carbon dioxide) was impracticable, one of these pressures was fixed in turn at 0.30 atm while the effect of variation in the other was studied. This choice was made in the light of the results of the preliminary experiments with copper powder described in the preceding paper, and led to the following sets of results.

*Experiments at constant pressure of carbon dioxide:  $P_{CO_2} = 0.30$  atm;  $P_{O_2} = 0.10 - 0.70$  atm.*—In these experiments, rates of copper dissolution and of film growth were measured as a function of the partial pressure of oxygen, total gas pressure being maintained slightly in excess of atmospheric by the required addition of nitrogen.

Difficulty was experienced in obtaining reproducible results, only partly due to the occurrence of an induction period in the dissolution reaction. This trouble, which appears to be common in this field of work, is no doubt to be associated with difficulty in reproducing the surface states of polycrystalline metal specimens and was reflected in the uneven early stages of film growth, particularly at low  $P_{O_2}$  values. As corrosion proceeded, however, the films became more uniform and were light brown or red-brown in color, except that blue, green, or purple patches were sometimes formed. Even in these cases subsequent coulometric reduction gave rise only to the single plateau assumed to be characteristic of cuprous oxide.

Considerable scatter had therefore to be tolerated in the results, a typical selection of which is pre-

sented graphically in Fig. 5(a) and 5(b), and establish beyond reasonable doubt that there is a constant rate of copper dissolution for each value of  $P_{O_2}$ , confirming the results of the earlier experiments with copper powder. It is also shown, with somewhat less certainty, that there is a constant rate of film growth which is a function of  $P_{O_2}$ . It is noteworthy that a film of cuprous oxide about 25,000 Å thick seems to confer no additional protection to the metal, for dissolution continues at the same constant rate when such a film has been formed.

The erraticity of these results has been countered to some extent by replication of experiments. In later studies of the effects of saline additions (Part IV), each experiment was accompanied by a control, identical in all respects except that no salt was added. Many such control experimental results were combined by interpolation and averaging and gave rise to the plots shown in Fig. 6(a) and 6(b). These give the average concentrations of dissolved copper and the average thicknesses of cuprous oxide films, attained at 20, 50, and 100 hr of corrosion time, as a function of  $P_{O_2}$  at constant  $P_{CO_2}$  (0.30 atm).

In these plots, the lines are those predicted by the equations  $d[Cu^{2+}]/dt = 0.00645 P_{O_2}$  ppm hr<sup>-1</sup> for dissolution and  $d(\text{Å})/dt = 390 P_{O_2}$  Å hr<sup>-1</sup> for film growth. It is justifiable to conclude that, after an induction period, both of these processes follow first order kinetics with respect to oxygen; at least, first order kinetics fit the results better than any other. It is perhaps more important to observe that dissolution and film growth may be linked together kinetically, or both may be controlled by the same rate-limiting process. This seems all the more probable in the light of the fact that, in this set of experiments, the ratio of film thickness to cupric ion concentration in solution was constant to  $\pm 7\%$  over the range of  $P_{O_2} = 0.25$  to 0.70 atm for 60 determinations. It

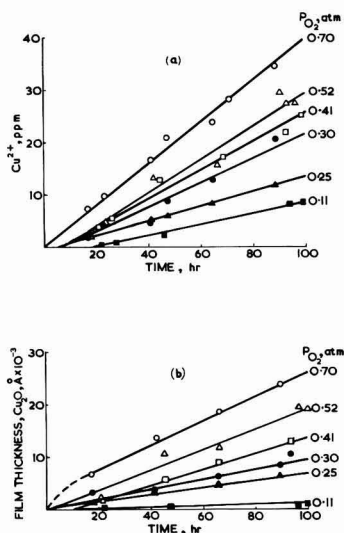


Fig. 5. Typical selection of corrosion experiments;  $P_{CO_2} = 0.30$  atm (const.),  $P_{O_2} = 0.11$  to 0.70 atm,  $P_{N_2} = (1.00 - P_{O_2} - P_{CO_2})$  atm; (a)  $Cu^{2+}$ , ppm, as function of time, (b)  $Cu_2O$ , film thickness, Å  $\times 10^{-3}$ , as function of time.

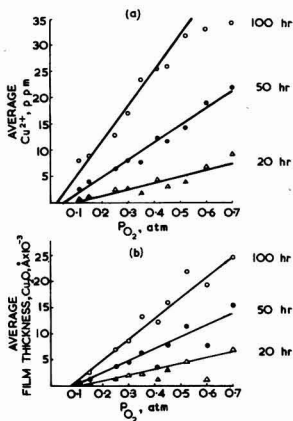


Fig. 6. Average results of corrosion experiments;  $P_{CO_2} = 0.30$  atm (const.),  $P_{O_2} = 0.10$  to 0.70 atm,  $P_{N_2} = (1.00 - P_{O_2} - P_{CO_2})$  atm; (a) dissolution, (b) film growth, for periods of 20, 50, and 100 hr.

was shown that diffusion of oxygen in solution ( $P_{O_2} = 0.70$  atm;  $C \sim 9 \times 10^{-4}$  mole l<sup>-1</sup>;  $D \sim 2 \times 10^{-5}$  cm<sup>2</sup> sec<sup>-1</sup>;  $\delta \sim 0.05$  cm) could cope with a dissolution rate more than tenfold that observed and could be excluded from rate control. Some confirmation of this point came from two corrosion runs ( $P_{O_2} = 0.20$  and 0.40 atm) with 250 ppm of EDTA (sodium salt) added to the aqueous phase, with the idea of suppressing back reaction (disproportionation of  $Cu_2O$  in reverse). Dissolution rates were increased by factors of about 3 and 2, respectively, and were independent of  $P_{O_2}$ . Film growth was largely inhibited.

*Experiments at constant pressure of oxygen:*  $P_{O_2} = 0.30$  atm;  $P_{CO_2} = 0.10$ -0.70 atm. Reproducibility was even less satisfactory, but was adequate, within each kinetic run, to establish that rates of dissolution and film growth were constant for periods up to 100 hr. Averaged results are displayed in Fig. 7(a) and 7(b), which are to be compared with Fig. 6(a) and 6(b). The dependence of the corrosion rates on  $P_{CO_2}$  at constant  $P_{O_2}$  is seen to be quite different from the dependence on  $P_{O_2}$  at constant  $P_{CO_2}$ . Nevertheless, although some imagination was required in drawing the representative curves, similarity of shape is retained between those relating to dissolution and those relating to film growth. This adds a little weight to the idea that these two processes may be functionally related.

The two sets of experiments differ in an important respect. In the first set ( $P_{CO_2}$  constant) the initial pH was the same for all the kinetic runs, but in the second ( $P_{CO_2}$  variable), this was not the case. Attention must therefore be given to the variation of pH with  $P_{CO_2}$ , and this is shown in Fig. 7(c), for the initial waters (calculated values) and for the solutions produced after 100 hr corrosion time (observed values). In the latter case, the expected flattening of the curve due to the accumulation of bicarbonate ion in solution is discernible. If the corrosion rates increase with falling pH, and it can hardly be otherwise, it therefore seems that the dependences of pH on  $P_{CO_2}$  and on concentration of

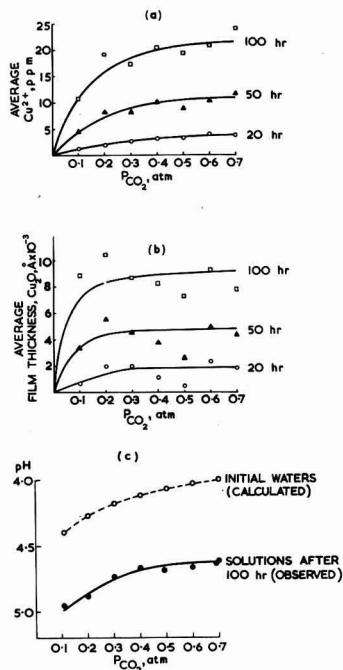


Fig. 7. Average results of corrosion experiments;  $P_{\text{O}_2} = 0.30$  atm (const.),  $P_{\text{CO}_2} = 0.10$  to  $0.70$  atm,  $P_{\text{N}_2} = (1.00 - P_{\text{O}_2} - P_{\text{CO}_2})$  atm; (a) dissolution, (b) film growth, for periods of 20, 50, and 100 hr, and (c) pH values at 0 and 100 hr.

cupric bicarbonate in solution might be the factors principally concerned in determining the shapes of the curves in Fig. 7(a) and 7(b). This assumption, however, leads to a paradox, for during a kinetic run pH continuously rises and this should cause the corrosion rates to fall, which they do not. On any grounds, the constancy of these rates is remarkable; there is no indication of a falling away by reason of an approach to an equilibrium state and no sign of the increasing incidence of a back reaction, which might favor the production of cuprous oxide at the expense of cupric ion in solution.

This paradox can be resolved by assuming that the thickening film of cuprous oxide progressively promotes both dissolution and its own continued growth, so compensating the increasing effects of factors adverse to these processes. It was recollected that, in the preliminary experiments (Part I), the maximum rate of dissolution of copper powder was attained when the latter was discolored by the presence of a substantial oxide film.

The possible functional properties of oxide films were investigated accordingly by means of two kinds of "replacement experiments," as follows.

#### Replacement Experiments

**Solution replacement.**—The course of an experiment of this kind is recorded in detail in Fig. 8. A normal kinetic run was carried out, with  $P_{\text{O}_2} = P_{\text{CO}_2} = 0.30$  atm, for 92 hr; the increasing concentration of cupric ion in solution is shown in curve (a) of Fig. 8. One electrode was then removed for coulo-

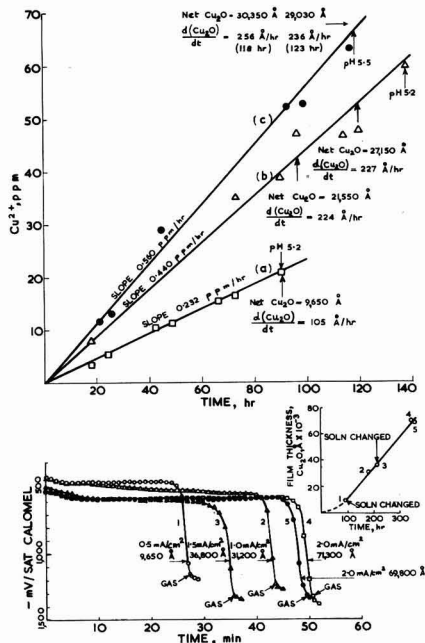


Fig. 8. Solution replacement experiments

metric estimation of film thickness (these estimations are represented in the lower part of Fig. 8). The entire solution in the apparatus was then removed and replaced by a fresh charge of water, already equilibrated with the same gaseous mixture. A similar run was at once started with the remaining five electrodes, carrying the films deposited on them in the first run. It is seen from curve (b) of Fig. 8 that dissolution proceeded at about twice the original rate and continued constantly at this higher rate for a further 140 hr. This increase in dissolution rate did not occur at the expense of the existing oxide film on the copper, for tests on two of the electrodes showed that the rate of film growth had also been approximately doubled. A further replacement of the solution led to another increment in dissolution rate, curve (c) in Fig. 8, but not in rate of film growth.

**Copper replacement.**—Under the same standard conditions of  $P_{\text{O}_2} = P_{\text{CO}_2} = 0.30$  atm, a kinetic run was followed for 110 hr. Dissolution and film growth are represented by the rectilinear curves (a) in Fig. 9. The remaining electrodes were discarded and six new ones, prepared by the standard method, were introduced. The kinetic run was then continued, with the solution unchanged. It is understandable that the dissolution reaction was temporarily reversed, and that a film grew rapidly upon the fresh copper surfaces, as shown by curves (b) in Fig. 9. But it can be seen that, after the initial spurt, film growth practically ceased and a normal rate of dissolution was reached only after a delay of 60–80 hr. A second replacement of the same kind produced even more marked effects on dissolution and film growth, curves (c) in Fig. 9.



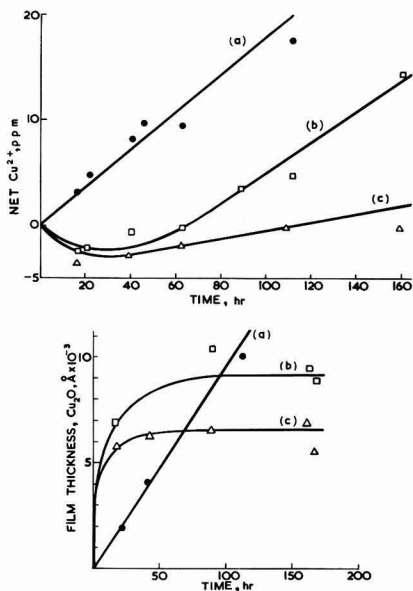
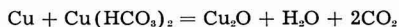


Fig. 9. Copper replacement experiments

#### Conclusions from Replacement Experiments

At first sight, the results of these experiments seem to be explicable in terms of a back reaction



eliminated when the solution is changed, and facilitated when oxide coated copper is replaced by fresh metal. Although such a reaction must play its part in the latter case, it is inadequate to explain all the facts. This can be seen from the data collected in Table I, which shows the state of affairs toward the end of experiments lasting approximately two weeks, in each of which two replacements had been made.

If, for a given total rate of corrosion, the much lower concentration of cupric ion attained in solution were due to the back reaction, the deficit should appear as an excess of cuprous oxide. This is not the case, and it is obvious that the total corrosion rates are quite different after the two kinds of replacement. It is quite remarkable that in one case copper bearing a film about 73,000 Å thick should be growing more film and dissolving (at a less favorable pH) enormously faster than in the other case, where the copper is carrying a film less than one tenth as thick. The conclusion is inescapable

Table I

	Replacement of Solution	Copper
Cu converted to $\text{Cu}^{2+}$ , g	0.35	0.09
Cu converted to $\text{Cu}_2\text{O}$ , g	0.13	0.12
Total Cu metal lost by corrosion, g	0.48	0.21
Total area of Cu exposed for corrosion, $\text{cm}^2$	90	270
Total area of Cu $\times$ period of exposure, $\text{cm}^2 \text{ hr} \times 10^{-3}$	21	39
Final concentration of $\text{Cu}^{2+}$ in solution, ppm	60	21
attained in hr	117	440
Final rate of dissolution, ppm $\text{hr}^{-1}$ (per 90 $\text{cm}^2$ )	0.56	$\sim 0$
Final film thickness, Å	73,000	6,500
attained in, hr	350	160
Final rate of film growth, Å $\text{hr}^{-1}$	236	$\sim 0$
Final pH of solution	5.5	5.2

that the "naturally grown" film, generated in the course of corrosion, is catalytically active for dissolution and autocatalytic for film growth. On the other hand, the "unnaturally deposited" film is appreciably protective.

These results have some bearing on practical corrosion problems. The effects of the intermittent flow of water in copper pipes and over other types of copper surfaces are likely to be similar to those observed in the solution-replacement experiments. It is seen that these are adverse, and films with activating rather than passivating properties are likely to be formed. Perhaps the copper replacement experiments give a pointer to one method by which this undesirable effect could be countered. It is, however, clear that a rather complex electrochemical mechanism for the linked corrosion processes remains to be identified; one possible mechanism is presented in the following paper.

Manuscript received Oct. 2, 1961; revised manuscript received Jan. 23, 1962. This paper was prepared for delivery before the Ottawa Meeting, Sept. 28-Oct. 2, 1958.

Any discussion of this paper will appear in a Discussion Section to be published in the December 1962 JOURNAL.

#### REFERENCES

1. G. R. Hill, *This Journal*, **100**, 345 (1953).
2. H. A. Miley, *J. Am. Chem. Soc.*, **59**, 2626 (1937).
3. W. E. Campbell and U. B. Thomas, *Trans. Electrochem. Soc.*, **76**, 303 (1939).
4. J. A. Allen, *Trans. Faraday Soc.*, **48**, 273 (1952).
5. R. H. Lambert and D. J. Trevo, *This Journal*, **105**, 18 (1958).
6. J. S. Halliday, *Trans. Faraday Soc.*, **50**, 171 (1954).
7. L. E. Price and G. J. Thomas, *Trans. Electrochem. Soc.*, **76**, 329 (1939).

# Copper Corrosion

## III. Electrochemical Theory of General Corrosion

D. J. G. Ives

*Department of Chemistry, Birkbeck College, London, England*

and A. E. Rawson

*Colne Valley Water Company, Watford, Hertfordshire, England*

### ABSTRACT

The oxidative dissolution of copper in acidic, aqueous media is limited in rate by the presence at the metal-solution interface of a growing film of cuprous oxide. A brief survey of what is known about the nature and modes of growth of such films provides the basis for a "duplex film" model of the corroding copper system. This leads to an interpretation of some features of the observed kinetics of the corrosion reactions reported in the preceding paper, including the constancy of rates of dissolution and film growth following induction periods, the kinetic link between them, the absence of effects due to concentration polarization of dissolved oxygen, and the results of "replacement experiments." The interpretation is made in terms of the operation of a hypothetical double electrochemical cell, corresponding with the duplex film model, and leaves unresolved problems associated with possible special functions of carbon dioxide and the mechanism of oxygen reduction.

The oxidative dissolution of copper in an acidic, aqueous medium,  $\text{Cu} + 2\text{H}^+ + \frac{1}{2}\text{O}_2 = \text{Cu}^{2+} + \text{H}_2\text{O}$ , has a standard free energy change of  $-41.16$  kcal, comparable with that of the reaction of sodium with water, but does not in practice occur as a vigorous, exothermic reaction because of the restraining influence of, *inter alia*, the cuprous oxide film which forms on the metal, at least at pH values greater than 3.5. In the absence of control by diffusion of hydrogen ions or dissolved oxygen, it is clear that this film, itself undergoing growth, must determine reaction rate, and this certainly seems to be the case for the corrosion experiments reported in the preceding paper. The kinetics of corrosion must therefore be intimately related to the nature and mode of growth of cuprous oxide films on copper, which accordingly require consideration.

#### *Oxidation of Copper in Gaseous Media*

Attention has hitherto been largely confined to the oxidation of copper in gaseous media, and the reaction has been discussed in terms of the properties of cuprous oxide as a metal-deficient, p-type semiconductor containing vacant cation sites and positive holes. At high temperatures, thick films of cuprous oxide grow at a rate inversely proportional to their thickness (1-4), following the so-called parabolic law first interpreted by Wagner (5) in terms of rate limitation by transport of ions across the film. Discussions of parabolic film growth by Hoar and Price (6) and, more recently, by Grimley (7) provide the following representation of reaction mechanism.

For the  $\text{Cu}$ ,  $\text{Cu}_2\text{O}$ ,  $\text{O}_2$  system at equilibrium, with  $P_{\text{O}_2}$  equal to the oxygen dissociation pressure of the  $\text{Cu}$ ,  $\text{Cu}_2\text{O}$  couple, vacant cation sites and positive holes are distributed uniformly throughout the oxide film. For greater oxygen pressures, however, a gradient of these defects is established in the film. They

are generated at the oxide-oxygen interface, where reduction of oxygen and generation of cuprous oxide occur, and are destroyed at the copper-oxide interface, where oxidation of copper takes place, with provision of cuprous ions and electrons. The system is analogous to a nearly reversible, working galvanic cell in which the outer surface of the film is the cathode and the inner surface the anode. The film itself serves both as electrolyte, transporting cuprous ions by diffusion *via* vacant cation sites, and as "external" resistive circuit, conducting electrons. The rate of film growth can be expressed in terms of a current conforming to Ohm's law, a function of appropriate film resistivities and a potential difference calculable from the free energy of the net oxidation process.

This model serves as a satisfactory basis for the more comprehensive theory of Mott (8), which deals with lower temperature, thin film oxidations which follow different kinetic growth laws, such as cubic (9, 10) or logarithmic (11). It is envisaged that electrons can penetrate an oxide layer by thermionic emission from the metal into conduction levels of the oxide or, for thin films, by quantum mechanical tunnelling, and cooperate in dissociative adsorption of oxygen at the oxide-gas interface. There is evidence (12) that singly charged oxygen ions and oxygen atoms are formed in this process, but the essential result is the establishment of a layer of negative charge, which gives rise to an electrical field in the oxide layer. This field may be strong enough to enforce an outward movement of cations at temperatures too low for normal diffusional mobility to sustain an adequate supply of them. In the general case, various kinetic consequences follow the dependence of cationic drift velocity on field strength. On scales of decreasing temperature and film thickness, there is a change from zero, through linear, to exponential

dependence, and this sequence corresponds with observed growth laws.

At low temperatures, many metals show asymptotic film growth, leading to the formation of very thin, limiting films which increase in thickness as the temperature is raised to a critical value, when continuous growth supervenes. This behavior, possibly due to rate limitation by release of cations from the metal to the film (13), is familiar in the case of self-passivating metals such as aluminum and is also shown by copper (14, 15). Such protective films must clearly be coherent and adherent, and this is no doubt associated with the tendency of the first formed layers of the oxide film to adopt the lattice parameters of the parent metal on which they are growing. This can occur if the dimensions of the cation lattice in the oxide do not exceed 109-114% of those in the metal lattice (16); this condition is satisfied for cuprous oxide on copper. It is to be expected, and is found, that rates of growth and limiting thicknesses should vary widely from one crystallographic plane of the metal to another (14, 17) so that some irregularity of behavior must be anticipated for polycrystalline metal samples. Films formed in this way must become increasingly metastable as they thicken because of lateral compressional strains, which ultimately will lead to breaking up. Lattice distortion in very thin films and absence of preferred orientation in thicker films of cuprous oxide on copper have been observed (18), but it has also been reported that cuprous oxide formed on a polished surface of polycrystalline copper has a unique orientation (19), no doubt through operation of other factors.

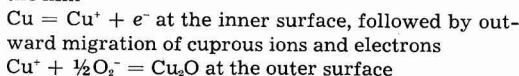
The stages through which oxygen must pass as it is transformed into its final "lattice ion" state are interesting and complex. It seems that p-type semiconductors are able to chemisorb oxygen "externally to the lattice" and can provide electrons for the process  $\frac{1}{2}O_2 + e^- \rightarrow O_{ads}^-$  at room temperature (20). The participation of the singly charged ion-radical  $O^-$  is supported by magnetic measurements (21) and has important implications, discussion of which is reserved. It has already been indicated that the initial uptake of oxygen by copper is extremely rapid, and the initial heat of reaction, 109 kcal mole<sup>-1</sup>, is so great that hydrogen cannot completely reduce the surface oxide so formed (22). This super-normal stability of "elementary" cuprous oxide films, no doubt due to strong adhesive forces, is supported by electrochemical evidence (23). After the formation of 3-4 layers of oxide, however, heat of reaction has fallen to about 55 kcal mole<sup>-1</sup> and remains sensibly constant for film thicknesses up to at least 170Å (22). Although the dissociation of oxygen molecules normally requires 117 kcal mole<sup>-1</sup>, dissociative adsorption at a cuprous oxide surface proceeds by a first order reaction (24) to provide oxygen atoms in two situations (25). One of these atoms is incorporated into the cuprous oxide film, generating vacant cation sites and positive holes (associated with cupric ions), and the other remains in a mobile adsorbed state until trapped at a surface discontinuity. In this state, it retains an exceptional chemical reactivity (as in the oxidation of carbon monoxide at room tempera-

ture) which decays with time (21). Discussions of the oxidation of copper, however, are not always conducted in terms of a mechanism involving the  $O^-$  radical ion.

This introductory survey provides the minimum background for the theory of copper corrosion in aqueous media which follows.

#### *Oxidation of Copper in Aqueous Media*

It is assumed that copper, immersed in an oxygenated aqueous medium, almost instantaneously forms a very thin film of cuprous oxide with a compressed structure fitted to that of the metal. Adherent, self-healing, and complete, it cannot grow in thickness beyond perhaps 20Å before mechanical strains break up its outer regions, and this is thought to occur before an asymptotic stage of growth can be reached. The film therefore never becomes fully protective and oxidation continues, leading at quite an early stage to a porous film of disorganized structure, somewhat loosely adherent to the compact, underlying layer, which is imagined to be constantly regenerated. It is further assumed that film growth is based primarily on dissociative adsorption of dissolved oxygen and passage outward through the film of cuprous ions and electrons. Without any implications as to detailed mechanism, and purely for the sake of simplicity, this may be represented



#### *Thermodynamic Treatment*

Taking a thermodynamic view of the corroding system, it is seen that between the extremes of the fully reduced substrate, metallic copper, and the fully-oxidized, aggressive reactant, oxygen, there is the possibility of various redox systems, one or another of which may be close to equilibrium. The least oxidized of these is the Cu, Cu<sub>2</sub>O couple, which, in aqueous solution free from dissolved copper, would confer on the metal phase a potential of

$$E_{Cu, Cu_2O, H^+} = 0.471 - 0.0592 \text{ pH} \quad \text{abs. V}$$

at 25°C. The most oxidized is the oxygen electrode equilibrium which, for a gaseous mixture typically used in the corrosion experiments described in the preceding paper (0.30, 0.30, and 0.40 atm, respectively, of O<sub>2</sub>, CO<sub>2</sub>, and N<sub>2</sub>), has a potential of

$$E_{O_2(0.30 \text{ atm}), H^+} = 1.222 - 0.0592 \text{ pH} \quad \text{abs. V}$$

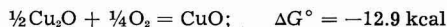
This is much more positive than any potential encountered in the Cu, H<sub>2</sub>O, O<sub>2</sub> system within the relevant pH range, corresponding with the fact that completion of corrosion would oxidize all the copper to the cupric state. There must therefore be a considerable oxidation gradient within the corroding system, no doubt mainly, if not exclusively, confined to a number of oxidation jumps, at the biggest of which rate limitation is likely to occur.

Oxidation beyond the cuprous state probably begins in the film itself, in virtue of the capacity of cuprous oxide to take up excess of oxygen. This is

unlikely to proceed far, as long as electrical contact with the copper substrate is preserved and, because the conductance of the oxide increases with its departure from stoichiometry, there may be a kind of automatic regulation of the state of oxidation of the film; the more it becomes oxidized, the better able is the copper substrate to keep it reduced. But the electrical resistance of the film is bound to increase as it grows, particularly when it begins to break up. This may allow the potential of the copper to deviate somewhat toward that of the Cu, CuO couple, namely

$$E_{\text{Cu, CuO, H}^+} = 0.570 - 0.0592 \text{ pH} \quad \text{abs. V}$$

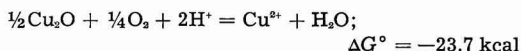
Certainly, oxidation of the film is thermodynamically favored, since



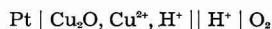
and so is subsequent dissolution



There is no reason why cupric oxide should be formed as an intermediate between these reactions occurring consecutively. Combined, they give



This is regarded as the primary dissolution reaction, which could occur reversibly in the cell



The potential of the left-hand electrode would be

$$E_{\text{Cu}_2\text{O, Cu}^{2+}, \text{H}^+} = 0.203 + 0.0592 \text{ pH} + 0.0592 \log (\text{Cu}^{2+}) \quad \text{abs. V}$$

For relevance to the Cu, H<sub>2</sub>O, O<sub>2</sub>, CO<sub>2</sub> system, the last two reactions should be combined with



to give the corrosion reactions, with their much less negative standard free energy changes, previously discussed (Part I).

These electrochemical considerations may be applied to the model of the corroding system, illustrated in Fig. 1, arising out of the preceding discussion.

#### Duplex Film Corrosion Model

The copper substrate is covered by a compact, adherent film of cuprous oxide, in good electrical contact with it. Superimposed on this is a porous film, formed in the corrosion process by the disruption of the growing film underneath it. This disruption would be accompanied by a large increase in the resistance

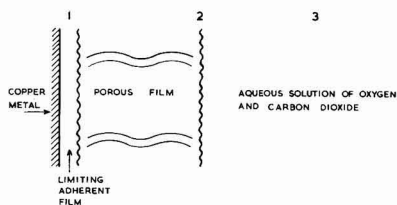


Fig. 1. "Duplex film" model of the copper corrosion system

of the electrical path between the metal and the partially broken away oxide. It is unlikely, however, that this resistance will become infinite, for any oxide which became insulated from the metal would either fall off, or dissolve quite rapidly, as free cuprous oxide has been shown to do (Part I). Thus, even the porous film remains to some extent under the influence of the copper substrate because of a significant electrical conductance of the film, over and above that of the aqueous phase which permeates it.

Attention is directed to the potentials at the three "zones," or locations, indicated in Fig. 1. The first of these is to be identified with that of the copper phase, acting as part of a copper-cuprous oxide couple. The second and third may be regarded as the potentials which would be recorded by hypothetical redox probes, appropriately situated. In so far as it is electronically conducting, the substance of the porous oxide film can assume a potential related to electrochemical reactions which may occur at its surface. The "probes" and the separation of zones 2 and 3 in space are devices introduced in the interests of clarity.

Ideally, these potentials would be

$$\left. \begin{aligned} E_1 &= 0.471 - 0.0592 \text{ pH at zone 1} \\ E_2 &= 0.203 + 0.0592 \text{ pH} \\ &\quad + 0.0592 \log (\text{Cu}^{2+}) \text{ at zone 2} \\ E_3 &= 1.222 - 0.0592 \text{ pH at zone 3} \end{aligned} \right\} \begin{array}{l} \text{abs. V} \\ \text{at} \\ 25^\circ\text{C} \end{array}$$

as previously enumerated. In the very early stages of corrosion when only the thin, compact film has been formed, zone 2 coincides with zone 1, and  $E_2$  must be identical with  $E_1$ . Under these conditions, it can be shown that at  $\text{pH} = 4$ , the equilibrium concentration of cupric ions in solution is 21 ppm, but is diminished by a factor of two powers of ten for each unit rise of  $\text{pH}$ . This indicates that there will be little tendency for dissolution to occur, except at quite low  $\text{pH}$  values. The development of an appreciable rate of dissolution must wait upon the growth of sufficient resistance between the copper and the surface of the dissolving film. This provides an interpretation of the induction periods reported in both preceding papers, and the behavior of "new" electrodes placed in "old" solution in the second kind of replacement experiment described in Part II.

Consideration may next be given to the case in which extensive corrosion has proceeded, with formation of cupric ions in solution and establishment of the suggested "duplex film." If it is supposed, by way of example, that the solution is at  $\text{pH} = 5$  and contains 20 ppm of cupric ions, the potentials at the three zones will be

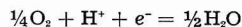
$$E_1 = 0.175; \quad E_2 = 0.292; \quad E_3 = 0.926 \text{ abs V at } 25^\circ\text{C}$$

except that  $E_2$  may be somewhat depressed toward  $E_1$ .

The primary dissolution process, which is imagined to occur at the hypothetical electrode at zone 2, is

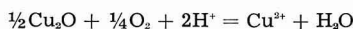


while

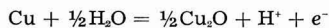


occurs at the imaginary oxygen electrode at zone 3.

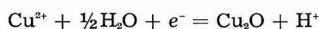
These two, added together, give the complete dissolution reaction



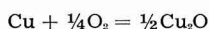
But zones 1 and 2 together constitute a cell which is, moreover, a working cell because the electronic conductance of the film is equivalent to an external, resistive connection between the electrodes. At 1 an anodic reaction proceeds



which will supply electrons to 2 and bring about the reverse of the dissolution reaction, i.e., the cathodic process



The electrode process at zone 1 may be regarded as the normal, primary film growth mechanism as it occurs in an aqueous medium, for, added to the cathodic process at zone 3, it gives



It is, however, no longer directly depolarized by elementary oxygen, but by cupric ion acting as an intermediary. This is no doubt why no sign of concentration polarization of dissolved oxygen has been found in any of the corrosion experiments, even when thick, porous films have been formed.

The cathodic reaction at zone 2 has the effect merely of diminishing the net anodic dissolution which occurs there, for electrode 2 is the anode with respect to 3 as cathode. At the same time, however, it provides more cuprous oxide at the expense of cupric ion and thus ensures that dissolution and film growth reactions remain in step with each other. It may also be regarded as a secondary film forming reaction, which generates cuprous oxide elsewhere than at the outer boundary of the compact film. Such a process is required to explain why even the thickest films are essentially composed of nothing but cuprous oxide. It may also be important that the rise in pH which accompanies the net anodic dissolution at zone 2 will facilitate the generation of cuprous oxide at zone 1 in the close vicinity. This reaction scheme may be clarified by the formal illustration of the hypothetical double cell given in Fig. 2.

The rise in pH and cupric ion concentration, which accompanies corrosion, might be expected to cause a decrease in dissolution rate with time, but this is observed not to be the case. This is because film growth proceeds in step with dissolution, and film thickening allows the potential at zone 2 to become

more positive, thus counteracting any tendency for the rate to fall away. When, however, the film becomes very thick, its worsening electrical conductance favors dissolution rather than film growth; this trend was observed in the first kind of "replacement experiment" described in the preceding paper. Ultimately, with a runaway dissolution reaction, the pH may rise so high close to the outer surface of a thick film that basic carbonate is formed. If the corroding medium is a natural water containing calcium bicarbonate in solution, calcium carbonate may be deposited. It is to be noted, however, that this is likely to occur only on a cuprous oxide film that is already thick, porous, and rather loosely attached to its substrate; a calcium carbonate film laid down on such a foundation is unlikely to have the adhesion and cohesion necessary to confer good protection. This may be associated with the fact that copper pipes, even when conveying such hard waters, often continue for years to send copper into solution; nevertheless calcium carbonate films, consolidated by traces of organic material, can afford a marked degree of protection, even if not complete protection.

#### Rate Limitation of the Corrosion Reaction

The final contribution to this theory of copper corrosion is concerned with over-all rate limitation. It has already been shown that this does not reside in oxygen diffusion, even through the pores of a thick film. The suggestion is made that it is due to hindrance of the oxygen electrode reaction, which must occur at some solid-solution interface at a rate proportional to the exponential factor familiar in electrode kinetics,  $\exp -(\omega - \alpha VF)/RT$ , where  $\omega$  is an activation energy,  $\alpha$  is a transfer coefficient probably much less than 0.5, and  $V$  is a potential difference effective in promoting reaction. If  $V$  can be identified with the difference between the oxygen and copper-cuprous oxide potentials

$$E_{\text{O}_2, \text{H}^+} - E_{\text{Cu}_2\text{O}, \text{H}^+} = 0.759 + 0.0148 \log P_{\text{O}_2} \quad \text{abs. V at } 25^\circ\text{C}$$

a possible basis is obtained for the observed first order kinetics with respect to oxygen, although this is likely to be a gross oversimplification.

Even if the theory of general corrosion of copper which has been proposed is along the right lines and uniquely explains some otherwise puzzling features, it cannot at present be extended without unwarrantable speculation, because it is obviously incomplete. Two outstanding defects may be mentioned.

Carbon dioxide has been treated merely as a component of a buffer system controlling pH, whereas it is quite strongly adsorbed from aqueous solution by cuprous oxide (cf. Part IV) and may play a far more intimate part. This is all the more likely in view of the observation (26) that cuprous oxide adsorbs carbon dioxide from the gas phase only if oxygen is simultaneously, or has been previously, adsorbed. This cooperative process leads to the formation of a reactive  $\text{CO}_2$  complex.

It is highly probable that the reduction of oxygen proceeds *via* the formation of hydrogen peroxide or its derivatives, for this is almost invariably the case (27) and is a tolerable certainty if the radical

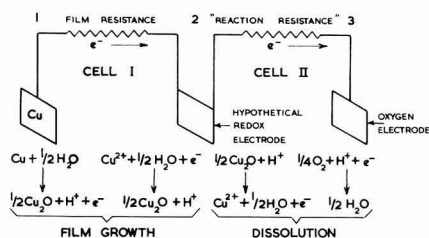


Fig. 2. Hypothetical double cell involved in copper corrosion

ion  $O^-$  is involved. Delahay (28) has shown that hydrogen peroxide is almost always formed when oxygen is cathodically reduced, even at copper electrodes; the yield is small in this case because of catalytic decomposition, but this might in itself indicate functional participation in oxidation mechanism. The Russell effect (29) has been re-investigated and has been shown to be due to the formation of hydrogen peroxide by the action of moist air on abraded metals (30, 31); it is attributed to the abnormal availability of electrons trapped in anion vacancies in freshly formed or disrupted oxide films (32). It is claimed that hydrogen peroxide has been detected in the vicinity of, *inter alia*, atmospherically corroding copper (33). The case for the formation and probable participation of hydrogen peroxide in the corrosion of copper is therefore quite strong, and there is also evidence (34) that it could cooperate with carbonic acid in a special way. The possible significance of this to corrosion problems has been noted (35).

Manuscript received Oct. 2, 1961; revised manuscript received Jan. 23, 1962. This paper was prepared for delivery before the Ottawa Meeting, Sept. 28-Oct. 2, 1958.

Any discussion of this paper will appear in a Discussion Section to be published in the December 1962 JOURNAL.

#### REFERENCES

1. G. Tammann, *Z. anorg. Chem.*, **111**, 78 (1920).
2. N. B. Pilling and R. E. Bedworth, *J. Inst. Metals*, **29**, 529 (1923).
3. H. Dünwald and C. Wagner, *Z. phys. Chem.*, **B**, **22**, 212 (1933).
4. C. Wagner and K. Grunewald, *ibid.*, **B**, **40**, 455 (1938).
5. C. Wagner, *ibid.*, **B**, **21**, 25 (1933); **B**, **32**, 447 (1936).
6. T. P. Hoar and L. E. Price, *Trans. Faraday Soc.*, **34**, 867 (1938).
7. T. B. Grimley, "Chemistry of the Solid State," W. E. Garner, Editor, p. 336, Butterworths, London (1955).
8. N. Cabrera and N. F. Mott, *Repts. Progr. Phys.*, **12**, 163 (1948-49).

9. N. Cabrera, *Phil. Mag.*, **40**, 175 (1949).
10. W. E. Campbell and U. B. Thomas, *Trans. Electrochem. Soc.*, **91**, 623 (1947).
11. A. L. Dighton and H. A. Miley, *ibid.*, **81**, 321 (1942).
12. T. J. Gray, "Chemistry of the Solid State," W. E. Garner, Editor, p. 140, Butterworths, London (1955).
13. N. F. Mott, *Trans. Faraday Soc.*, **43**, 429 (1947).
14. T. N. Rhodin, *J. Am. Chem. Soc.*, **72**, 5102 (1950).
15. J. A. Allen and J. W. Mitchell, *Discussions Faraday Soc.*, **8**, 309 (1950).
16. J. H. van der Merwe, *ibid.*, **5**, 201 (1949).
17. A. T. Gwathmey and F. W. Young, *Rev. mét.*, **48**, 434 (1951).
18. R. F. Mehl, E. L. McCandless, and F. N. Rhines, *Nature*, **134**, 1009 (1934).
19. G. D. Preston and L. L. Bircumshaw, *Phil. Mag.*, **20**, 706 (1935).
20. F. S. Stone, "Chemistry of the Solid State," W. E. Garner, Editor, pp. 396, 398, Butterworths, London (1955).
21. P. J. Fensham, "Magnetochemical Studies of Oxides of Copper and Nickel," Thesis, Bristol University (1955).
22. W. E. Garner, F. S. Stone, and P. F. Tiley, *Proc. Roy. Soc.*, **A211**, 472 (1952).
23. A. R. Tourky and S. E. S. El Wakkad, *J. Chem. Soc.*, **1948**, 740.
24. W. E. Garner, T. J. Gray, and F. S. Stone, *Discussions Faraday Soc.*, **8**, 246 (1950).
25. W. E. Garner and F. J. Veal, *J. Chem. Soc.*, **1935**, 1437.
26. F. S. Stone and P. F. Tiley, *Discussions Faraday Soc.*, **8**, 254 (1950).
27. D. J. G. Ives, "Reference Electrodes," Ives and Janz, Editors, p. 365, Academic Press, New York (1961).
28. P. Delahay, *This Journal*, **97**, 198 (1950).
29. W. J. Russell, *Proc. Roy. Soc.*, **61**, 424 (1897).
30. L. Grunberg and K. H. R. Wright, *Nature*, **170**, 456 (1952).
31. L. Grunberg, *Proc. Phys. Soc.*, **B66**, 153 (1953).
32. L. Grunberg, *Research*, **8**, 210, (1955); *Brit. J. Appl. Phys.*, **9**, 95 (1958).
33. I. L. Roykh, *Zhur. Fiz. Khim.*, **32**, 1136 (1958).
34. P. Van Rysselberghe, *et al.*, *J. Phys. Coll. Chem.*, **54**, 754 (1950).
35. R. B. Hoxeng and C. F. Prutton, *Corrosion*, **5**, 330 (1949).

## Copper Corrosion

### IV. The Effects of Saline Additions

D. J. G. Ives

*Department of Chemistry, Birkbeck College, London, England*

and A. E. Rawson

*Colne Valley Water Company, Watford, Hertfordshire, England*

#### ABSTRACT

The effects on the corrosion of copper, under the influence of dissolved oxygen and carbon dioxide, of trace additions of salts have been studied. In the case of chloride ion, radical changes in the kinetics of dissolution and film growth processes have been observed and have been interpreted in terms of a transition from general to local action corrosion. The effects of sulfate, nitrate, and bicarbonate ions are also reported. The influence of calcium bicarbonate, under conditions which preclude the deposition of calcium carbonate, in retarding corrosion is particularly noteworthy.

A study has been made of the effects on corrosion reactions in the Cu,  $H_2O$ ,  $O_2$ ,  $CO_2$  system of the ions  $Cl^-$ ,  $SO_4^{2-}$ ,  $NO_3^-$ , and  $HCO_3^-$  (as the sodium salts) and of  $HCO_3^-$  (as the calcium salt) at concentrations in

which they may occur in natural waters. The "powder method" of Part I was first used to explore the influence of these ions on rates of dissolution of cuprous oxide and of copper. This was followed by

kinetic studies of concurrent dissolution and film growth reactions by the method of Part II. In all cases, experiments were accompanied by salt-free controls in which all other conditions were identical.

**Results**

*Preliminary Powder Experiments*

Dissolution was followed in each case for 3 hr in solutions (or water in the controls), at  $24^\circ \pm 2^\circ\text{C}$ , kept in equilibrium with analyzed mixtures of oxygen and carbon dioxide at a total pressure slightly in excess of atmospheric.

*Cuprous oxide dissolution.*—For cuprous oxide, a qualitative report is adequate. Sodium chloride (100 ppm of  $\text{Cl}^-$ ) produced a marked acceleration of dissolution; the rate was approximately doubled near the mid-point of the gas composition range. Even 50 ppm of chloride ion produced about 30% increase in rate under these conditions. That this remarkable effect was specific to chloride ion was shown by the complete lack of influence of 100 ppm of sulfate or nitrate ion on dissolution rate. Both sodium and calcium bicarbonates depressed the rate of dissolution markedly, but to an extent commensurate with the rise in pH which they produced. Although in no case was equilibrium approached, it may be recalled that the equilibrium concentration of cupric ion is decreased by two powers of ten for each unit rise of pH (cf. Part III). It may be noted that, for the case of calcium bicarbonate, the Langelier (1) saturation index varied between  $-1.6$  and  $-2.0$ , which ostensibly precluded the deposition of calcium carbonate.

*Metallic copper dissolution.*—The results of the copper powder experiments are summarized in Fig. 1, in which each small-scale plot of the course of a

dissolution run is disposed along a gas-composition axis to define the conditions under which it was carried out. The broken curves, which are all approximately rectilinear, represent the parallel control runs. Each curve was characterized by a minimum of seven analytical determinations of dissolved copper.

It is evident that these very low concentrations of salts ( $\sim 0.001 - 0.002 \text{ g equiv l}^{-1}$ ) have surprisingly marked and variable effects on the dissolution of copper under the influence of dissolved oxygen and carbon dioxide. Perhaps the most outstanding effect is that of chloride ion in destroying constancy of dissolution rate; comparison with the appropriate controls indicates an initial acceleration of attack on the metal (particularly in darkness), followed by retardation, the latter making its appearance at an earlier stage in the more oxygenated systems. Conversely, the acceleration effect tends to be more prolonged, and perhaps more marked, in the least oxygenated systems. The other additions seem generally to depress dissolution rate (except that nitrate ion increases it at low  $P_{\text{O}_2}$  values) while usually maintaining its constancy. A very marked degree of passivation is attained in the presence of calcium bicarbonate in the least oxygenated solutions, but again a negative Langelier index suggests that this cannot be due to calcium carbonate deposition. The effects of illumination have not been systematically studied, but are in some cases seen to be considerable. It is suggested that the powder technique by which these results were assembled may be valuable for the rapid assessment of the corrosive or inhibitory properties of aqueous solutions on metals, for the indications obtained were generally confirmed subsequently. Nevertheless, significant color changes of the copper

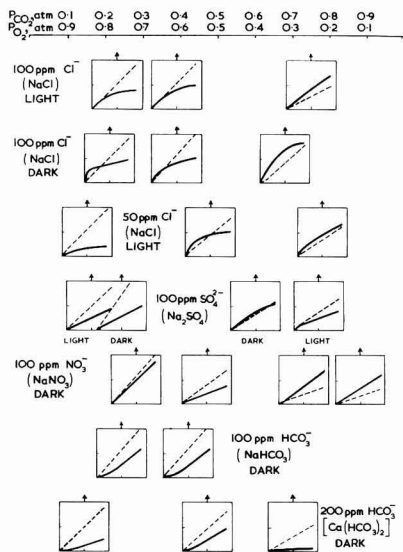


Fig. 1. Dissolution of Cu powder in water containing added salts, approximately at the concentration (ppm) indicated, equilibrated with mixtures of  $\text{O}_2$  and  $\text{CO}_2$  to a total pressure of 1 atm. Each plot is appropriately placed along the common gas composition axis, and has the same scales of abscissas (0-200 min) and ordinates (0-20 ppm of  $\text{Cu}^{2+}$ ). Broken lines indicate salt-free control experiments.

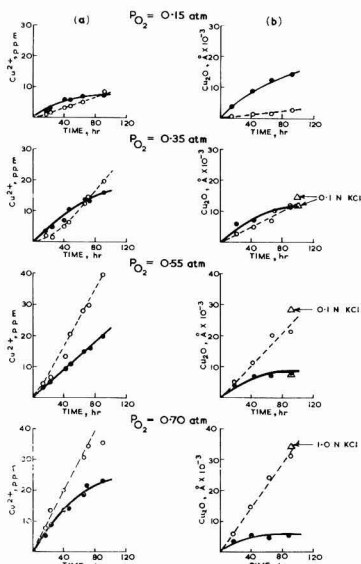


Fig. 2. Corrosion experiments showing influence of approximately 100 ppm  $\text{Cl}^-$  ( $\text{NaCl}$ );  $P_{\text{CO}_2} = 0.30 \text{ atm (const.)}$ ,  $P_{\text{O}_2} = 0.15-0.70 \text{ atm}$ ,  $P_{\text{N}_2} = (1.00 - P_{\text{O}_2} - P_{\text{CO}_2}) \text{ atm}$ , (a) dissolution, (b) film growth. Broken lines indicate salt-free control experiments.

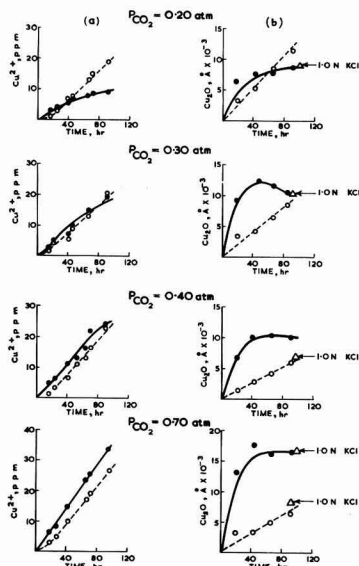


Fig. 3. Corrosion experiments showing influence of approximately 100 ppm  $Cl^-$  (NaCl);  $P_{O_2} = 0.30$  atm (const.),  $P_{CO_2} = 0.20-0.70$  atm,  $P_{N_2} = (1.00 - P_{O_2} - P_{CO_2})$  atm, (a) dissolution, (b) film growth. Broken lines indicate salt-free control experiments.

powder during the course of dissolution indicated the need for film formation studies.

#### Rates of Dissolution and Film Growth

The same two sets of conditions were used as in the studies of salt-free systems described in Part II;  $P_{CO_2}$  then  $P_{O_2}$  were successively fixed at a value of 0.30 atm while the other was varied, the total pressure being made up to 1 atm with nitrogen when necessary. Each kinetic run was continued for 100 hr at  $21^\circ \pm 2^\circ C$ .

**Sodium chloride additions.**—The results for systems containing 100 ppm of chloride ion as sodium chloride are shown in Fig. 2 and 3, the simultaneous controls being represented by broken lines. Three observations can be made immediately. Chloride ion does not always promote corrosion; on the contrary, it sometimes retards it. Rates of dissolution and film growth are no longer constant, but show a tendency to decrease with time, so that sometimes an initial activation of corrosion passes sooner or later to inhibition. There is obviously no longer a general relation between the kinetics of dissolution and film growth, except the tenuous one that the highest rate of dissolution was observed for the system in which the thickest film was developed. The main features of the results are summarized in Fig. 4, which contains plots of the copper concentrations in solution and the film thicknesses attained after 20, 50, and 100 hr of corrosion time, together with similar data for the controls, shown by broken lines. Although, even in these averaged data, the scatter is very large, it is clear that the almost dramatic effects of only 100 ppm of chloride ion are not obscured; the kinetics of the corrosion reactions are greatly changed, and the only regularity previously observed (first order kinetics with respect to  $P_{O_2}$ ) has gone.

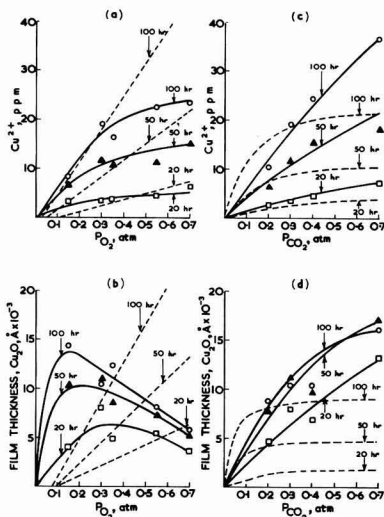


Fig. 4. Collected results of corrosion experiments involving the presence of approximately 100 ppm  $Cl^-$  (NaCl); (a) and (b) dissolution and film growth, respectively, for  $P_{CO_2} = 0.30$  atm (const.); (c) and (d), the same for  $P_{O_2} = 0.30$  atm (const.). Broken lines indicate salt-free control experiments.

Comparison of Fig. 4(a) and 4(c) suggests a reversal of the kinetic roles of oxygen and carbon dioxide, i.e., that in presence of 100 ppm of chloride ion, first order kinetics of dissolution with respect to oxygen has been replaced by first order kinetics with respect to carbon dioxide. A similar trend is less convincingly shown by comparison of Fig. 4(b) and 4(d) relating to film growth. It is not known if anything can be made of this, promising as it may appear in elucidating the role of carbon dioxide. The case for giving significance to this observation is weakened by the lack of relation between rates of dissolution and film growth, by the evidence which follows for a transition of corrosion mechanism, and by the great deterioration in reproducibility of physical conformation of the corroding system. It is felt that very careful and detailed studies would be needed to arrive at a decision on this point.

The main effects of chloride ion can perhaps best be seen by a formal tabulation, where acceleration or retardation of dissolution and film growth are indicated by + and - signs.

Acceleration (+) or retardation (-) of dissolution (D) and film growth (F) produced by 100 ppm of  $Cl^-$

	D	F
$P_{CO_2}$ const.	low $P_{O_2}$	++
	high $P_{O_2}$	--
$P_{O_2}$ const.	low $P_{CO_2}$	-
	high $P_{CO_2}$	+

Still more generally, increase of  $P_{O_2}$  has a relatively depressing effect on both dissolution and film formation; increase of  $P_{CO_2}$  has a relatively stim-



ulating effect. Perhaps the most significant observation of all is the complete breakdown of the kinetic relationship between dissolution and film growth.

Other diagnostic observations which were made may be enumerated.

The films, mainly red or red-brown in color, with sometimes greenish or purple areas, were less uniformly deposited. They were flocculent and loosely adherent, suggesting an enhanced degree of structural disorder. In some cases loss of film substance unavoidably occurred before coulombic estimation could be effected, and this is thought to be the reason for the apparent decrease in film thickness with time which was sometimes observed for the thickest films (cf. Fig. 3). This effect may be associated with the enhanced rate of dissolution of cuprous oxide in presence of chloride ion (already noted), with the effect of this ion upon a bed of cuprous oxide (reported below), and with the peptizing action reported by Gatty and Spooner (2) and the general facility of chloride ions in penetrating oxide films noted by Evans (3).

The coulometric film analysis method was insensitive to cuprous chloride in a film consisting essentially of cuprous oxide, but chemical analysis indicated the presence in the film substance of 0.7-1.5% of chloride. Although it has been shown (4) that atacamite may be present in films formed on copper in chloride solutions, it is unlikely that this was the case in films formed from solutions so dilute in chloride ion as ours. This basic cupric chloride would almost certainly have to appear as a discernible, separate phase, and the evidence is that when this does occur under our experimental conditions it is malachite which appears, not atacamite. These conditions were also outside the range of those required for stability of cuprous chloride as a solid phase (5), and it is therefore regarded as justified to regard the films as consisting of cuprous oxide, perhaps somewhat contaminated.

"Chromatographic" experiments with cuprous oxide columns, using solutions kept in equilibrium with standard pressures of oxygen and carbon dioxide ( $P_{O_2} = P_{CO_2} = 0.30$  atm) indicated strong chloride ion adsorption, which also considerably reduced the adsorption of carbon dioxide, observed to take place from salt-free aqueous solution. Further, the chloride ion had a marked effect on the cuprous oxide column, causing a lightening of color, with a loosening and disruption of the bed, which led to channelling. In long-term experiments of this kind, the upper regions of the column were converted to malachite, identified by x-rays. Chloride ion caused this conversion to extend to a much lower level in the column.

Films formed on copper in chloride-containing solutions were punctured by tiny holes, revealing bright spots of apparently bare metal. This was not observed in any salt-free control experiment.

These results, taken as a whole, seem to justify the following tentative interpretation of the influence of chloride ion on copper corrosion.

It is suggested that chloride ion is incorporated to a limited extent into the growing cuprous oxide film. If  $Cl^-$  is substituted for  $O^{2-}$ , the deficiency of

negative charge is likely to promote the formation of a vacant cation site. This may initially increase the ionic conductance of the film and accelerate the general corrosion reactions, both dissolution and film growth. It is also likely to lead to a more disrupted and porous film in which cracks and fissures may more readily develop, exposing the lower layers to easy access of the solution phase. This opening up process may have several consequences, as follows.

There may be a switch from general to local action corrosion and, perhaps, eventually to pitting corrosion. Local anodic dissolution,  $Cu \rightarrow Cu^{2+} + 2e^-$  supervenes, at exposed bare sites, from the anodic process which previously could only occur at the metal-oxide interface. The existing film in the vicinity has a much higher electronic than ionic conductance (all the more if the cuprous oxide has acquired n-type characteristics), and assumes a predominately cathodic function,  $\frac{1}{2}O_2 + H_2O + 2e^- \rightarrow 2OH^-$  occurring at its outer surface. This short-circuits the normal film growth mechanism, so that film growth practically stops. At the same time, the considerable increase in pH which now takes place at areas of film surrounding the anodic cavities, which are exuding cupric ions, favors the deposition of basic carbonate. This view is supported by the behavior of copper strips left corroding in very dilute, aerated salt solutions for many months. A uniform and often very beautiful red layer of cu-

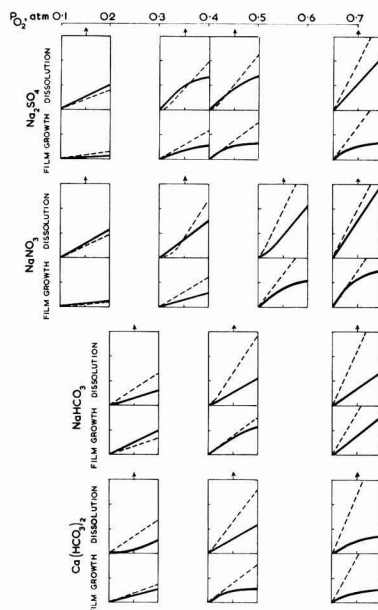


Fig. 5. Graphical summary of corrosion experiments involving the presence of approximately 100 ppm of  $SO_4^{2-}$ ,  $NO_3^-$ ,  $HCO_3^-$  as  $Na^+$  salts and of approximately 200 ppm of  $HCO_3^-$  as  $Ca^{2+}$  salt,  $P_{CO_2} = 0.30$  atm (const.),  $P_{O_2} = 0.15-0.70$  atm, etc. The pairs of plots (upper, dissolution; lower, film growth) are appropriately placed along the common gas composition axis and have the same scales of abscissas (0-100 hr) and of ordinates (0-30 ppm of  $Cu^{2+}$  or  $0.20\text{Å} \times 10^{-3}$  thickness of  $Cu_2O$  film). Broken lines indicate salt-free control experiments.

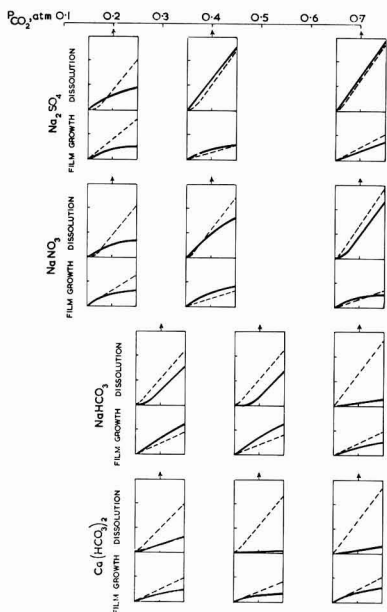


Fig. 6. As for Fig. 5 except that  $P_{O_2} = 0.30$  atm (const.),  $P_{CO_2} = 0.20-0.70$  atm, etc.

prite is overlaid by brilliant green islands of malachite. These have the appearance of having grown outward, over the cuprous oxide, from centers at which anodic pits may well have been located.

The effect of penetration of the aqueous phase into the porous film may be critically dependent on their respective conductances; if the solution is well-conducting, this will again have a short-circuiting effect and promote the switch to local action. On the other hand, if the solution is highly oxygenated, this may lead to a recrudescence of the primary film-forming process, with a corresponding tendency toward passivation by the sealing up of cracks and pores. Examples of the promotion of passivity by a sufficiently high concentration of dissolved oxygen are available (6). This is no doubt why a generally depressing effect of increasing oxygen partial pressure on corrosion is found in these particular systems.

In review, it is suggested that the main effects which have been observed are intelligible in terms of a rather delicate balance between general and local action corrosion, the latter taking over from the former sooner or later under the influence of added chloride with, however, a tendency to reversion in the more highly oxygenated systems.

*Other saline solutions.*—The effects of the addition of salts other than sodium chloride are summarized in Fig. 5 and 6, which are arranged similarly to Fig. 1. The information they contain may be supplemented by the observations that sulfate ion is strongly adsorbed from solution by cuprous oxide, but that nitrate and bicarbonate ions are not. Surprisingly, however, calcium bicarbonate shows strong adsorption. It may also be relevant to note that copper corrosion in the presence of 100 ppm of nitrate ion as sodium nitrate is accompanied by formation of traces of nitrite (Griess-Ilosvay reaction; 0.006-0.024 ppm).

Detailed interpretation of these results is not practicable at the present stage, and the main purpose must be to place them on record, for they demonstrate further the very large effects which trace concentrations of added salts may have on corrosion processes. The very remarkable passivating effect of calcium bicarbonate under certain conditions is worthy of special attention. Only partly due to a pH effect (largely shared by sodium bicarbonate), it cannot be due to deposition of calcium carbonate. Attention is also drawn to the possibility of establishing a criterion for the existence of general corrosion, as opposed to local action corrosion, of copper. It is the retention of constancy of rates of dissolution and of film growth.

#### Acknowledgments

Thanks are due to the Chairman and Directors of the Colne Valley Water Company for facilities and permission to publish. The authors also record their indebtedness to Professor J. D. Bernal, F.R.S., for x-ray analyses.

Manuscript received Oct. 2, 1961; revised manuscript received Jan. 23, 1962. This paper was prepared for delivery before the Ottawa Meeting, Sept. 28-Oct. 2, 1958.

Any discussion of this paper will appear in a Discussion Section to be published in the December 1962 JOURNAL.

#### REFERENCES

1. W. F. Langelier, *J. Am. Waterworks Assoc.*, **28**, 1500 (1936).
2. O. Gatty and E. C. R. Spooner, "The Electrode Potential Behaviour of Corroding Metals," p. 188, Oxford (1938).
3. U. R. Evans, "Metallic Corrosion, Passivity and Protection," pp. 21-23, Arnold (1948).
4. H. P. Rooksby and R. C. Chirnside, *J. Soc. Chem. Ind.*, **53**, 33T (1934).
5. M. J. N. Pourbaix, "Thermodynamics of Dilute Aqueous Solutions," p. 72, Arnold (1949).
6. U. R. Evans and D. E. Davies, *J. Chem. Soc.*, **1951**, 2607.

# Electrochemical Dissolution of Single Crystalline Copper

Leslie H. Jenkins and James O. Stiegler

*Solid State Division, Oak Ridge National Laboratory, Oak Ridge, Tennessee<sup>1</sup>*

## ABSTRACT

Galvanostatic studies of single crystal copper anodes in oxygen-free, 0.2M copper sulfate solutions revealed discontinuities in the curves resulting from a plot of electrode overpotentials vs. current density. Using observations of changes in electrode surface topography as supporting evidence, the discontinuities were explained on the basis of dissolution processes which were related to the defect structure of the electrode.

Since the early work of Glauner and Glocker (1) on the difference in chemical dissolution rates of the different crystallographic faces of copper crystals, similar effects have been noted for electrochemical dissolution. Early in his studies of anodic polishing of metals, Jacquet (2) established that, under certain conditions of current density and voltage, a difference in the reactivity of grain boundaries and other surfaces of copper polycrystals undergoing anodic dissolution in phosphoric acid could be demonstrated, and Bakish and Robertson (3) observed a potential difference between grains and grain boundaries in polycrystalline copper.

An orientation dependence of electrochemical dissolution of single crystalline copper in acidic copper sulfate was demonstrated by Leidheiser and Gwathmey (4), who also determined that the potential differences between different crystalline faces in their systems were changed by the presence of dissolved oxygen in the solution. The variation of equilibrium potential with crystallographic orientation of single crystalline copper in acidic copper sulfate was studied by Tragert and Robertson (5). They concluded that the (111) was the only truly stable surface in the system investigated. Faizullin and co-workers (6) observed a difference in the current density-potential relationships of anodes containing oriented and nonoriented copper deposits. More recently Piontelli's group has collected current-potential data for the low index faces of copper anodes (7) as well as hydrogen overvoltages on the same orientations (8).

The use of single crystals to study dissolution processes generally has two advantages: (i) the effect, if any, of crystallographic orientation of the reacting surface can be observed; (ii) if the defect structure of the metal affects the dissolution process, the effect is often more easily observed on single crystalline surfaces. It is generally assumed that anodic processes involving the dissolution of an ion from a metallic single crystal into a solution containing the metal ions of interest is most difficult at a theoretical, atomically smooth, close-packed surface. The most reactive site is assumed to be at a kink in a step on the surface, and the next most reactive site is at the straight step edge. Screw dislocations intersecting the surface may be considered sources of steps, but since it is very rare that a

difference in reactivity between edge and screw dislocations can be observed on metal surfaces (9), it is reasonable to consider the points where all line defects intersect the surface as reaction sites which are less active than step edges but more active than the idealized flat surface. This paper demonstrates that under certain conditions these assumptions are reasonable for (100) oriented surfaces of copper single crystals undergoing galvanostatic dissolution in acidic solutions of copper sulfate.

## Experimental

**Materials.**—Copper single crystals, 0.1 x 1 x 7 cm, of (100) orientation on the 7 x 1 cm area were grown from 99.999% metal, supplied by American Smelting and Refining Company, by seeding from the melt in graphite crucibles. From these crystals two samples, 0.1 x 1 x 3 cm, were carefully cut with a jeweler's saw and a 1/16 in. diameter hole drilled in one end of the crystal. The specimens were then chemically polished on a polishing wheel with a  $\text{CuCl}_2\text{-HCl}$  solution. Details of this operation have been discussed by Young and Wilson (10). Finally, the crystals were electropolished (usually ~ 40 min) to a smooth, bright finish in a phosphoric acid bath. Then in the manner recommended by Young and Gwathmey (11), they were rinsed in dilute  $\text{H}_3\text{PO}_4$ , washed in running distilled water, and dried in a jet of oxygen. Chemical polishing was necessary only to remove minor grown-in topographic irregularities (due to the graphite molds) in the surface of interest or to obtain a flatter surface over the entire crystal after the edges of the sample had become excessively rounded from repeated electropolishing. Usually, a crystal could be electropolished and used to obtain data about three times before another chemical polish was judged to be necessary.

With the one exception noted below, all the water used in these studies, both for preparation of solutions and for washing crystals, was prepared by distilling demineralized water through a tin-lined still. The storage reservoir for water was of seasoned polyethylene.

Hydrogen was purified by passing commercial tank gas over hot copper, then through magnesium perchlorate drying towers. Oxygen-free hydrogen saturated with water vapor was obtained by bypassing the drying towers and bubbling the gas through a series of three fritted glass disks in gas washing bottles.

<sup>1</sup>Oak Ridge National Laboratory is operated by Union Carbide Corporation for the United States Atomic Energy Commission.

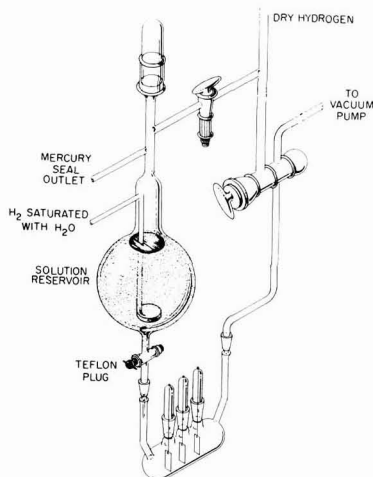


Fig. 1. Portion of filling rack with reaction cell

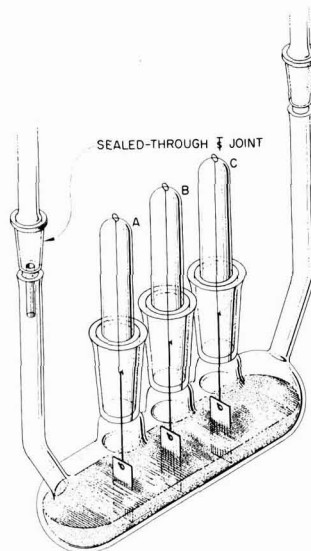
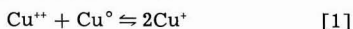


Fig. 2. Reaction cell with electrodes

Two types of copper sulfate solutions were prepared. One was made from material obtained by dissolving a weighed sample of 99.999% copper in excess reagent grade nitric acid. The resulting mixture was then evaporated in excess reagent grade sulfuric acid until free of nitric acid. Water for these solutions was prepared by triply distilling water from the polyethylene reservoir in an all-quartz apparatus. One distillation was from alkaline permanganate solution. Other solutions were prepared from reagent grade  $\text{CuSO}_4 \cdot 5\text{H}_2\text{O}$ . All the solutions used in this study were 0.2M in  $\text{CuSO}_4$ , with pH adjusted to 1.0 with  $\text{H}_2\text{SO}_4$ . Approximately half the data presented here were obtained from solutions of the first type. However, identical results were obtained both for surface effects and current-potential relationships regardless of which solutions were used.

After introducing the solutions into the 2-liter storage reservoir shown in Fig. 1 they were freed of dissolved oxygen in the following manner: After about 20 ft<sup>3</sup> of water saturated hydrogen had been bubbled through a fritted disk in the solution, the reservoir cover cap was momentarily removed, and a polycrystalline bar of ASR copper which had been cleaned in nitric acid and washed for 2 min in running distilled water was quickly immersed in the solution. The cover cap was replaced and about 80 ft<sup>3</sup> of moist hydrogen was passed through the solution at a rate of 10 ft<sup>3</sup> day<sup>-1</sup>. In this manner, not only was the resulting oxygen-free solution at equilibrium with a hydrogen atmosphere, but also the presence of metallic copper (surface area  $\sim 15 \text{ cm}^2$ ) allowed the equilibrium requirements of the following reaction to be satisfied



The previous precautions were taken to prevent changes in surface topography of the electrodes resulting from the oxidation and dissolution of the metal by oxygen and/or ions in solution.

*Experimental procedure.*—The reaction cell was attached to the filling rack as shown in Fig. 1. Three

polished samples of (100) orientation were then suspended from copper hooks which were fabricated from ASR metal. Prior to use, the hooks were cleaned in nitric acid, washed in running distilled water for 2 min, and then air dried. The hooks were attached to platinum wires sealed through the male standard taper joints which were then positioned in the cell as shown in Fig. 2. All joints on the cell were mechanically clamped to help guard against leaks in the system. The cell was alternately evacuated and filled with hydrogen for about 20 cycles, and then the samples were annealed in the dry hydrogen atmosphere overnight at 450°C. During annealing, jets of cooling air were blown over the sample port joints so that their outside temperature never exceeded 50°C. After the 16-20 hr anneal the furnace was removed and the system cooled to room temperature under positive hydrogen pressure. Solution from the rack reservoir was then admitted to the reaction cell until the copper crystals were immersed to a depth of 2 cm. The bottoms of the holes which had been drilled in the crystal were about 5 mm above the solution level. A portable constant temperature bath was then placed about the cell. This procedure permitted data to be gathered from oxide-free, electropolished metal surfaces in chemical equilibrium with oxygen-free, hydrogen-saturated solutions.

All the data reported here were gathered at 25°  $\pm 0.1^\circ \text{C}$  under galvanostatic conditions using a 6v dry cell with in-line, fixed resistors as a source of constant current. One copper crystal served as the anode, another as the cathode, and the third as a reference electrode. Potential differences of the working electrodes were measured *vs.* that of the third crystal in the system with a "master-slave" matched pair of vibrating reed electrometers,<sup>2</sup> outputs of which were coupled to Brown recorders so that potential-

<sup>2</sup> The model 31-31 VMS electrometers manufactured by the Applied Physics Corporation of Monrovia, California, permits synchronous reed drive in the two units by the oscillator in the "master" unit.

time relationships were recorded. The small currents used were measured with Weston model 301 DC microammeters which were accurate within 2%. Currents were constant within the accuracy of the meters under all experimental conditions. Although both anodic and cathodic overpotentials were measured, only anodic data are discussed here.

All the tapered joints on the cell were greased with silicone vacuum stopcock grease. The male through joint attaching the solution arm of the filling rack to the cell, as well as the joint on the vacuum side, was lightly greased prior to attaching the cell to the rack. Also, the male joints serving as sample holders were greased near the top just before the samples and joints were inserted in the female entry ports. At the completion of an experiment the apparatus was cleaned of grease by repeated scrubbing with benzene, then acetone. Next the apparatus was scrubbed with alcoholic potassium hydroxide, rinsed with alcohol, and then water. Finally, after soaking in hot nitric acid it was thoroughly rinsed with distilled water. Frequently the alcoholic potassium hydroxide treatment was eliminated without observable effect on the ensuing determinations.

### Experimental Results

**Anodic current-potential relationships.**—The sample ports of the reaction cell were approximately on 3 cm centers making it possible to vary the separation between working electrodes. Data were taken with the electrode surfaces parallel to each other, but at right angles to the long axis of the cell, and with the crystals at ports A and B (Fig. 2) serving as working electrodes. The polarity of the samples at each port was varied each time new assemblies were used. At other times the crystals at ports A and C, again at right angles to the long axis of the cell, served as working electrodes. In the latter series the reference electrode at port B was parallel to the long axis of the cell. Also, other cells of different design which allowed working electrode separations of 1 and 2 cm were used. These cells are discussed more fully below. No differences in potential-current ( $\eta$  vs.  $i$ ) relationships or surface effects due to changes in cell geometry could be found.

At equilibrium, the potential differences of the three electrodes were almost always zero. Occasionally, immediately after exposure to the solution, a difference which never exceeded 0.1 mv and which rapidly decayed to zero was observed. To demonstrate that these systems were at chemical equilibrium and that, therefore, there were no changes in electrode surface topography due to reaction [1], and also to determine if there were similar effects resulting from the reasonably large exchange current densities reported for systems such as these (12), several different assemblies were allowed to stand for various periods up to 8 days. During these times, in which no current was passed through the system, no potential differences were observed, nor were any changes in surface topography such as faceting, etc., detected when the samples were removed from the solutions and surface replicas ob-

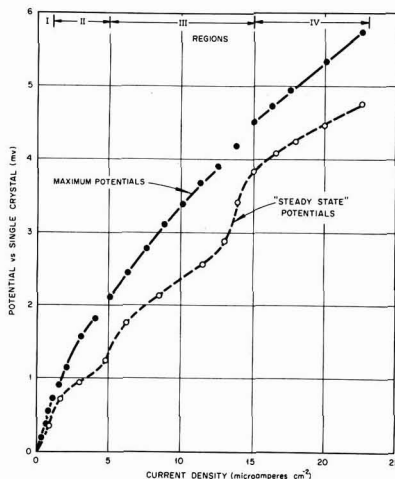


Fig. 3. Experimental current-potential data at 25°C in 0.2M  $\text{CuSO}_4$ , pH adjusted to 1.0 with  $\text{H}_2\text{SO}_4$ .

served with the electron microscope. It was concluded that, from the standpoint of surface topography, the system was in a state of at least metastable equilibrium.

Anodic overvoltages, resulting from the passage of current through the system, were characterized by initial maxima, the build-up times of which were functions of the current densities applied. At the lower current densities studied,  $\sim 0.5 \mu\text{a cm}^{-2}$ , the build-up times were 2-3 min while at the relatively high current density of  $\sim 20 \mu\text{a cm}^{-2}$  the time was 6-8 sec. After the maxima were established, anodic potentials rapidly decayed to about 70-80% of the peak values. They then decreased very slowly with time as long as current was passed through the system. A typical plot of these quasi-steady-state, post-maxima potentials are shown as a function of applied current density in Fig. 3. The inflections in the curves always occurred at the same current densities, but the values of the corresponding potentials varied widely from one assembly to another.

In most assemblies the applied current was interrupted as soon as possible after the maxima had been established so as to minimize surface changes due to pitting and faceting. The anodic potentials then decayed slowly to the initial zero value. At current densities of approximately  $7 \mu\text{a cm}^{-2}$  this usually required 15-20 min. At higher current densities, and correspondingly higher potentials, the decay, in addition to being slower, was characterized by a minimum value which was more negative than the reference crystal. The minima were never observed to be more than  $-0.7$  mv and may have been present, although too small to be observed, at lower current densities. This behavior led to decay times of as much as 2 hr at the highest current densities studied before the anode regained equilibrium potential.

In any one assembly the maximum anodic potential values were reproducible within 3% if the current was quickly interrupted after the maxima were attained, and if true equilibrium had been es-

established before current was again applied. However, at a given current density, maximum potential values varied as much as 20% from system to system, but in all cases discontinuities in the  $\eta_{\max}$  vs.  $i$  curves occurred at the same current densities. The maximum potentials shown in Fig. 3 as a function of anodic current density are experimental values obtained from one assembly. Coincidentally, they are near the average values obtained from determinations in more than thirty different assemblies. Smoother curves could have been drawn, but it was desired to emphasize the incoherent nature of the data. Inflections in the  $\eta_{\max}$  vs.  $i$  curves ordinarily could be attributed to experimental error. However, the reproducibility of the shapes of the curves from one assembly to another as well as their obvious relationship to the post maxima potentials vs. current curves and the topographic changes of electrode surfaces, which are discussed later, suggest that the discontinuities were real and significant.

By normalizing the maximum potentials observed at 15 and 20  $\mu\text{A cm}^{-2}$  to values arbitrarily selected as standard for these current densities, conversion factors were obtained which permitted all  $\eta_{\max}$  vs.  $i$  curves to be fitted to each other very well indeed. This fact suggested that the discontinuities in the curves were a function of the apparent current densities rather than the anodic overvoltages.

**Surface effects.**—In the presentation of the data below and in the discussions which follow, it is assumed *ipse dixit* that dissolution occurs from monatomic steps on the metal surface. Since, in systems such as these, it is possible to observe only the net effect of many single atom processes, the arguments advanced can in a sense be regarded as speculative at best. However, the data presented are capable of explanation and understanding on the self-consistent atomistic basis adopted.

The inflected nature of the anodic  $\eta$  vs.  $i$  curves suggested that possibly four different dissolution phenomena, each associated with a definite range of current densities as shown in Fig. 3, were occurring on the metal surfaces. Galvanostatic studies in which currents were passed for long periods of time were, therefore, conducted. After attaining the initial maxima, anodic potentials rapidly fell to about 80% of the maximum values. Thereafter, they decreased monotonically with time, although at a very slow rate, as long as current was passed through the system. Since the topography and area of an anode surface changed with time and rate of dissolution, and since the post-maxima potentials were reproducible only to  $\sim \pm 10\text{--}15\%$ , their utility was limited. However, they were useful in determining which areas of current density should be investigated for electrode surface effects as well as lending credence to the much less pronounced inflections in the  $\eta_{\max}$  vs.  $i$  curves. Although the times required to establish the potential maxima were longer than would be expected to be required to charge the double layer, the reproducibility of any one series of such potentials, as well as the coincidence of different  $\eta_{\max}$  vs.  $i$  curves when normalized to an arbitrary standard, suggest that these poten-

tials reflect a real property of the system. Their true significance is not clear at this time.

After interrupting the current, the anode was removed from the cell, washed in distilled water, and dried in a jet of oxygen. Crystal surfaces were then examined by optical and/or electron microscopy. Surface replicas for the electron microscope were platinum preshadowed carbon replicas which were chemically stripped from the metal (13). The results discussed below, obtained from observations on more than twenty anodic surfaces, strengthened the belief that different removal processes were operative at certain current densities. Changes in surface topography were the net result of both deposition and dissolution processes at the anode. To facilitate presentation, the surface effects are discussed solely in terms of the dissolution process. This problem is explored more completely in the discussion section.

**Region I ( $0\text{--}1 \mu\text{A cm}^{-2}$ ).**—Figure 4 illustrates that, in this region of current density, removal of material from the anode apparently occurred at atomic steps<sup>3</sup> on the crystal surface. The movement of steps across the surface was restricted in some manner for with time, facets, which must have resulted from the coincidence of steps, were developed. The electron micrograph seen in Fig. 5 shows the facets in detail. Large areas which protruded above the remainder of the surface, and which were therefore less reactive than steps, were also seen (Fig. 4). These areas, which seemed to serve as obstacles to restrict step motion, produced surface patterns of the type usually associated with subgrain bound-

<sup>3</sup> In this presentation the term "step" is used in the monatomic sense. Steps higher than  $\sim 50\text{\AA}$  (approximately the limit of resolution of the carbon replica technique used) are arbitrarily termed facets. Step facet signifies a facet formed by growth of steps, as opposed to facets developed from pits.

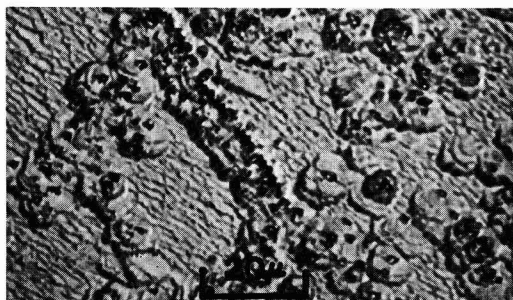


Fig. 4. Facets developed from step motion after 96 hr at  $1 \mu\text{A cm}^{-2}$

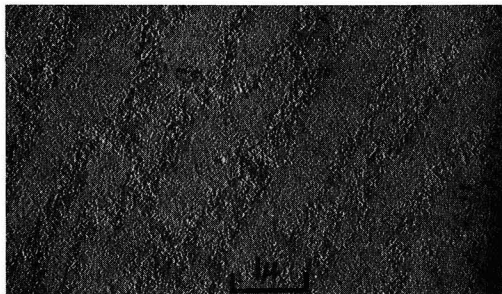


Fig. 5. Electron micrograph of facets on same surface seen in Fig. 4

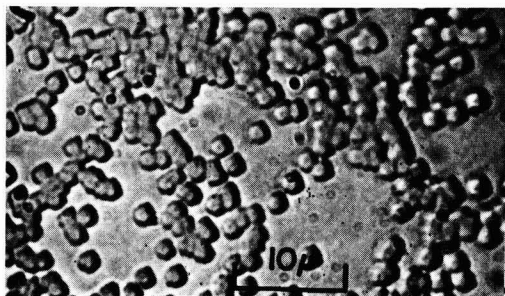


Fig. 6. Pits developed after 5 hr at  $10 \mu a \text{ cm}^{-2}$



Fig. 8. Surface just before pits obscured by facet development after 72 hr at  $9 \mu a \text{ cm}^{-2}$ .

aries and points where line defects intersect crystal surfaces. It has previously been observed that crystals of (100) surface orientation undergoing chemical dissolution were less reactive at subgrain boundaries (14).

*Region II ( $1-5 \mu a \text{ cm}^{-2}$ ).*—The inactive areas of Region I became active in this region. At current densities  $\sim 2 \mu a \text{ cm}^{-2}$  some tendency to form step facets was still observed, but no large, protruding unreacted areas were seen. As the current density approached  $\sim 5 \mu a \text{ cm}^{-2}$  no tendency to facet was observed nor were any differences in reactivity observed at areas corresponding to subgrain boundaries. Rather, surface replicas revealed a smooth surface much like that of the unpitted area shown in Fig. 9 and only slightly more roughened than the original surface.

*Region III ( $5-15 \mu a \text{ cm}^{-2}$ ).*—A further increase in dissolution rates resulted in pit formation as shown in Fig. 6. In the lower portions of Region III the less stringent removal demands resulted in pits which were very shallow, broad, and difficult to detect. The pits grew into each other and, in one experiment conducted at  $5 \mu a \text{ cm}^{-2}$ , formed a surface completely covered with very shallow facets after four days of such treatment. As the current density increased the area:depth ratio of pits decreased, and the pits were more easily discerned. However, the increased rate of removal also increased the rate at which pits grew together and consequently shortened the time before pits disappeared as facets developed from them.

Figure 6 shows pits in the earlier stages of development. After prolonged reaction at the same current density, the pits grew into each other and started facet formation as shown in Fig. 7. Even

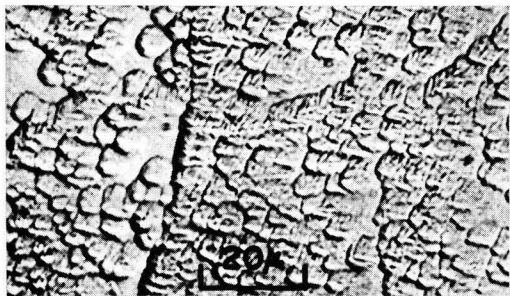


Fig. 7. Beginning of facet formation from large pits which were formed from union of smaller pits after 40 hr at  $10 \mu a \text{ cm}^{-2}$ .

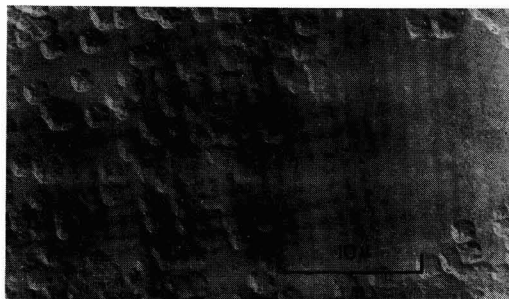


Fig. 9. Electron micrograph showing detail of pits developed after 5 hr at  $10 \mu a \text{ cm}^{-2}$ .

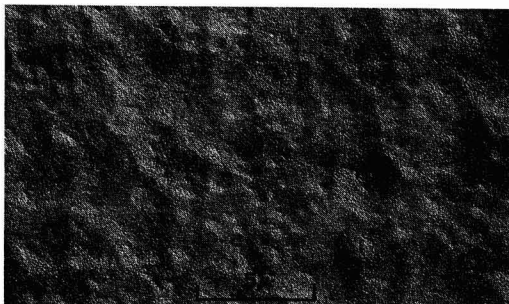


Fig. 10. Initial stages of facets developed from growth of pits after 40 hr at  $10 \mu a \text{ cm}^{-2}$ .

more material could be removed at slightly lower current densities, as is illustrated in Fig. 8, before the pits completely lost their identity. An electron micrograph of the same surface seen in Fig. 6 is shown in Fig. 9. The relative smoothness (lack of faceting) of the area between pits was typical of all surfaces in this region, as well as the nonpitted surfaces obtained at higher current densities in Region II. The electron micrograph of Fig. 10 illustrates the initial stages of facet development from pit growth. The faceted structure seen in Fig. 11 was initially developed by pit growth, for in the early stages of reaction this surface was pitted like that shown in Fig. 9. These facets are completely developed while the surface of Fig. 8 still shows distinguishable pits, even though approximately the same amount of material had been removed from each surface.

*Region IV ( $15-20 \mu a \text{ cm}^{-2}$ ).*—In this region the rates of dissolution were such that facet formation did

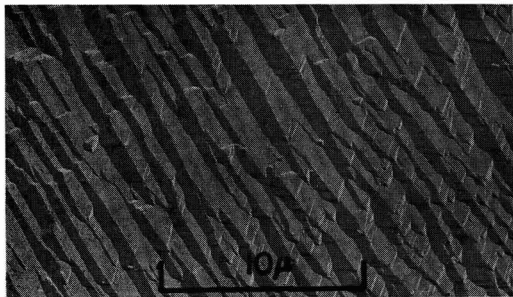


Fig. 11. Facets developed from pits after 47 hr at  $14 \mu\text{A cm}^{-2}$

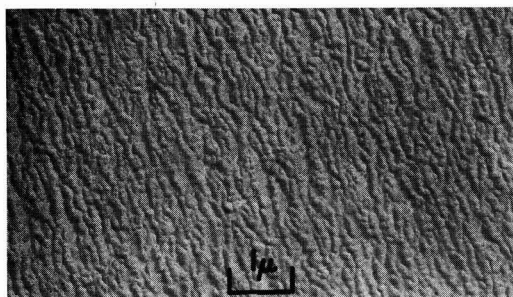


Fig. 12. Initial development of facets not resulting from pit growth after 2 hr at  $20 \mu\text{A cm}^{-2}$ .

not result from the growth of pits, but rather small facets immediately developed as material was removed. Figure 12 shows a surface with facet development well started even though less material has been removed than from the pitted surface of Region III shown in Fig. 9. With time the small facets grew together to form a surface indistinguishable from the surface with pit-developed facets shown in Fig. 11.

The preceding data and comments do not refer to observations made at equivalent microcoulomb values, but rather to the values indicated on the relevant figures. The values were chosen to best represent the cumulative changes in surface topography occurring at typical current densities within the various regions.

### Discussion

**Experimental method.**—Initially data were gathered using an adaptation of a previously described cell (14) designed for chemical dissolution studies. All stopcocks in this apparatus, which allowed anode-cathode separation of 1-2 cm, were of Teflon. Unfortunately, the mechanical pressure required to make the stopcocks vacuum tight resulted in a high rate of failure of the Teflon plugs, with the subsequent loss of samples and contamination of solutions in the reservoir by air. For this reason the cell design was changed to that shown in Fig. 2. Some weeks later the reservoir Teflon stopcock failed and was replaced with a glass stopcock lightly greased with silicone vacuum grease. Fortunately, no differences in  $\eta$  vs.  $i$  characteristics or surface effects resulted from these changes. It would, of course, have been ideal had no grease been used. However, the final experimental conditions seemed to be the best

available choice between compromises involving vacuum requirements, annealing conditions, etc. Apparently the cleaning method used was effective, and the major source of contamination was probably from the stopcock at the solution reservoir.

**Surface effects and current-potential data.**—Additional experiments were conducted to test further the hypothesis that discontinuities in the current vs. potential curves were governed by applied current densities rather than the corresponding overvoltages exhibited by the anode. Since the sides and ends of the electrodes were not of the desired orientation they were obviously a source of error. Therefore, data were gathered from crystals 0.2 cm thick so that the misoriented area of the electrode was increased to about 20%. Also, 0.1 cm thick crystals were electropolished for long periods so that the edges of the area of desired orientation were rounded. In both cases the current-potential data produced curves with less pronounced discontinuities, but with wide variations in potential values. However, the entire surface of proper orientation of the thick crystals, as well as the center of the corresponding area of the thin, rounded-edge crystals, did pit and/or facet at the same current densities previously observed. These observations—when considered with the previously discussed variations of potentials in different assemblies at a given current density, as well as the reproducibility of the shape of the  $\eta$  vs.  $i$  curves from one assembly to another, and the fact that the observed potentials in any one assembly could be normalized to an arbitrary standard—certainly indicate that the hypothesis is not an untenable one. Furthermore, the surface effects observed on typical crystals, as well as those crystals with a higher percentage of misoriented areas, were almost certainly a function of current densities. It was not unusual to observe pit development on a crystal which exhibited, at a low Region III current density, both a maximum and a “steady-state” potential lower than the corresponding potentials developed by another nonpitting anode at a high Region II current density in another assembly. Therefore, it is reasonable to assume that changes in current densities, rather than overvoltage changes, were responsible not only for discontinuities in  $\eta$  vs.  $i$  curves, but also for the different surface structures developed in the current density Regions defined by these discontinuities.

The following discussions of the different methods of facet formation in Regions I, III, and IV, as well as the lack of facet development in Region II and the development of pits in Region III, are based on the previous hypothesis.

**Region I.**—The development of step facets on anodic surfaces in Region I and the presence of less reactive areas which were compatible with a typical line defect structure suggested that material was removed by the motion of steps across the surface. Decreased reactivity at sites similar to subgrain boundaries and points where line defects intersect the surface could have been due to a “Cottrell atmosphere” of impurities at such imperfections. These sites could have served as pinning points to retard step motion and eventually would result in facets developed from the pile-ups of steps. The total number of steps present



on a surface before the passage of any current was surely not a reproducible number. Also, the pile-up of steps to form facets must have decreased the number of steps available. Therefore, it is not unreasonable to conclude that new steps were being nucleated, and that it was the maximum rate at which such steps could be nucleated which determined where this region ended. When the apparent current density reached  $1 \mu\text{a cm}^{-2}$  this rate was apparently at a maximum. If the areas where line defects intersected the surface did not act as step sources, then crystal edges and point defects must have served as nucleation sites for steps.

**Region II.**—The faster rate of removal in Region II apparently required nucleation of reaction sites more numerous than could be supplied by the sources active in Region I. The tendency to produce only step facets in lower portions of the region and the lack of faceting or pitting observed near the top of the region indicate that removal of material was still proceeding *via* a step motion mechanism. The smooth surfaces obtained at the higher current densities in the Region suggest that both line and point defects were acting as sources for step formation, and that at these current densities, steps were being removed at a rate at least equal to the rate at which they were created. Furthermore, it would appear that just before the onset of pitting at current densities greater than  $5 \mu\text{a cm}^{-2}$ , steps were being generated at the maximum rate possible. It seems that, as in Region I, it was the maximum rate at which steps could be nucleated which determined the end of this region.

**Region III.**—Having reached a maximum rate at which dissolution could proceed *via* step motion, pitting began to occur at current densities greater than  $5 \mu\text{a cm}^{-2}$ . The pits shown in Fig. 6, 7, and 8 reveal patterns which are typically associated with the defect structure of crystals such as these. Also, it was determined that the number of pits ( $5 \times 10^6 \text{ cm}^{-2}$ ) agreed with the measured number of dislocations in these crystals.\* Pits then are believed to have formed at subgrain boundaries and at areas surrounding points where line defects intersected the surface of the crystals. It is probable that these areas were active as step sources in Region II, but the lower removal rates did not require more material than could be supplied by the immediate surface. When dissolution rates increased, the additional material was more easily removed at these defect areas.

**Region IV.**—If removal rates exceeded the maximum amounts of material which could be supplied both by steps nucleated at areas surrounding defects and by pitting, nucleation of reaction sites apparently occurred at random on the crystal surface. This change marked the boundary between Regions III and IV. It is a reasonable assumption that in Region IV removal was by step motion. If so, the large number of steps nucleated and their rapid interaction resulted in such rapid development of facets (Fig. 12) that the mechanism of their early formation and growth could not be determined.

**Exchange current.**—By evaluating the slope of the overvoltage *vs.* current density curve at the lowest

current densities the exchange current density for the system was estimated to be  $\sim 5 \times 10^{-10} \text{ amp cm}^{-2}$ . This value agrees well enough with that anticipated from results on similar systems (12). Therefore, even the measurements obtained at the highest current densities studied represented relatively minor deviations from the equilibrium state. It is then reasonable to assume that deposition at the anode, as well as dissolution, contributed to changes in surface topography. However, it should be recalled that: (A) After eight days at equilibrium, surface replicas showed there had been no changes in electrode surface topography. (B) At higher current densities in Region II the anode surface remained relatively smooth after prolonged dissolution. (C) Even after pitting had been well developed in Region III the nonpitted area of the surface remained smooth.

Pitting in Region III obviously did not result directly from deposition, but it can be argued that the maintenance of smooth surfaces in non-pitted areas was aided by the simultaneous deposition reaction. The latter argument could also be applied to the upper portions of Region II. Thus it would be expected that as equilibrium was approached in the lower portions of Region II and in Region I, the deposition reaction became more important and contributed greatly to the development of facets. Finally, it should follow that at equilibrium, topographic changes, much like those seen in Region I, would be expected to occur. Such was not the case. Therefore, it is not unreasonable to conclude that the observed anodic topographic changes were due primarily to the dissolution reaction.

**Structural aspects.**—Assuming previously postulated processes of dissolution to be correct, some interesting calculations can be made. For the Region III surface illustrated in Fig. 9 only  $5 \mu\text{a cm}^{-2}$  of the total of  $10 \mu\text{a cm}^{-2}$  contributed to the formation of pits since half the material was being removed by the step mechanisms postulated for Region I and II. Using the measured dislocation density value of  $5 \times 10^6 \text{ cm}^{-2}$  and the coulombs of material removed by  $5 \mu\text{a cm}^{-2}$  after 5 hr, it was possible to calculate the average volume of material removed from each pit. Surface replicas showed the pits to be approximately  $2 \times 10^{-4} \text{ cm}^3$ . To accommodate the volume of material calculated to have been removed at each pit, the pits should have been an order of magnitude wider than they were deep. This was approximately the value observed, and since there was some slope to the sides of the pits, the agreement between calculated and observed results was considered good.

The operation of two sources of dissolution in Region III is illustrated by the surfaces shown in Fig. 6 and 7. Although almost an order of magnitude more material had been removed from the latter surface, faceting was not well developed since half the total material removed was supplied by steps which had also been active in Region II. This point is augmented by the surfaces seen in Fig. 8 and 11. Although approximately the same amount of material had been removed from both surfaces, the latter was well faceted due to the growth of pits since about 65% of the total material removed had been supplied by pitted areas, the remainder of the metal

\*Dislocation densities were determined by the persulfate etch method [see ref. (9) for details].

dissolving by step motion. Only 45% of all metal removed from the surface shown in Fig. 8 came from pits.

Just before the onset of pitting at  $5 \mu\text{a cm}^{-2}$  it has been postulated that  $1 \mu\text{a cm}^{-2}$  was removing material at sites which had been active in Region I and which were not related to line defects. The remaining  $4 \mu\text{a cm}^{-2}$  were associated with a dislocation density of  $5 \times 10^6 \text{ cm}^{-2}$ . Therefore, assuming the maximum rate of step removal to be constant regardless of the origin of the step, there would have been  $\sim 10^6$  sites  $\text{cm}^{-2}$  in Region I which acted as sources for nucleation of steps. The maximum dissolution rate in both Region I and II would then be  $\sim 3 \times 10^6$  atoms  $\text{site}^{-1} \text{ sec}^{-1}$ . The maximum rate of removal at a pit would be about twice as great.

It should be pointed out that an alternative explanation exists for the mechanism of removal in Region I. The approximately  $10^6 \text{ cm}^{-2}$  sources of step sites calculated above may have been associated with screw dislocations. Even if the presence of impurities prohibited dissolution near the core of the dislocation, a permanent step on the surface would emerge from the screw dislocation. The calculated number of step sources is probably of the proper magnitude for a correspondence to screw dislocations, and since all crystals were grown and handled in a similar manner, this number should have been reasonably constant from crystal to crystal. Therefore, if removal in Region I occurred at steps resulting from screw dislocations, it would be reasonable to expect the surface effects observed in this Region, as well as the reproducible ending of the Region, when removal rates exceeded those allowed at screw dislocation steps. However, it can be shown that for every  $\frac{1}{2}^\circ$  variation from the (100) orientation,  $\sim 5 \times 10^6$  monatomic steps  $\text{cm}^{-1}$  result on a copper surface. It is difficult to believe that the electropolishing techniques used in this study produced exact (100) surfaces, or that the degree of variation from the desired orientation, and consequently the total number of steps resulting from orientation changes and screw dislocations, was reproduced on every crystal. Also, the results obtained with rounded-edge, thin crystals, which must have contained more steps per unit area than crystals with flatter surfaces, cannot be ignored. Therefore, the argument that the end of Region I was determined by the rate at which new steps could be nucleated, regardless of their origin, seems preferable to the authors.

*Overpotential and kinetics.*—In all assemblies an interesting relationship was observed between the potential maxima at current densities corresponding to discontinuities in the  $\eta$  vs.  $i$  curves. In any one system the ratio of the potential at the Region II—Region III boundary to that at Region I—Region II was always  $\sim 3$ , and that of the Region III—Region IV discontinuity to the Region I—Region II value was always  $\sim 5$ . These potential ratios were reasonably constant even though, as previously noted, the measured potential maxima varied as much as 20% from one assembly to another. Perhaps if  $\epsilon$  was the energy required to nucleate steps at dislocations, then  $3\epsilon$  was required to remove material at points where dislocations with a "Cottrell atmosphere" of impurities

intersected the surface, and  $5\epsilon$  was necessary for removal from smooth surfaces of (100) orientation.

Since different anodic sites were reactive at distinct current densities, a distribution of reaction rates must have occurred over the surface. It would be a difficult, and not a particularly rewarding, task to adapt electrode kinetics, as well as to approximate the time dependence of surface structure and  $\eta$  vs.  $i$  data, in order to interpret the observed data kinetically. In systems of the type studied it is possible that the simpler equations of electrode kinetics should apply only at current densities as large as, or greater than, those of Region IV where nucleation of reactive sites apparently occurred in a random manner; that is, the metal surface acted homogeneously. For these reasons, and also since their solutions were more concentrated in both copper sulfate and sulfuric acid, these results could not be compared with those of Piontelli *et al.* (7) whose lowest current densities correspond to those of Region IV reported here.

### Conclusions

It should be emphasized that the discussions and interpretations of the data presented here were based on the reasonable assumption that dissolution occurred from monatomic steps on the anode surface. Obviously it is impossible to prove absolutely the validity of this assumption in a system of the type investigated. The following conclusions should be regarded solely as deductions arising from a self-consistent explanation of experimental observations:

1. It is believed that galvanostatic dissolution from (100) oriented surfaces of copper single crystals occurred initially at steps on the surface. These steps were not nucleated at areas where line defects intersected the crystal surface. The rate at which new steps could be nucleated determined the rate at which material could be removed in this manner.
2. An increase in dissolution rates demanded the formation of additional reaction sites. These sites were supplied by the nucleation of additional steps at areas where line defects intersected the crystal surface. The subsequent motion of steps across the surface provided a means of removing the metal from the anode.
3. After the maximum rate of step formation was reached, further increases in the rate of dissolution resulted in pit formation at points where line defects intersected the surface and at subgrain boundaries. As dissolution continued the pits grew together to form facets.
4. When removal demands exceeded the rate at which material could be supplied by the previous sources, reaction sites were apparently nucleated at random on the metal surface. A faceted structure, which was not formed by the growth of pits, developed rapidly.
5. The nucleation of reaction sites was probably governed by the rate of anodic dissolution, *i.e.*, impressed current density, rather than by the overpotential exhibited by the electrode.
6. The relative energies required to nucleate steps at dislocations, remove material from points where line defects intersected the surface and from the

idealized flat surface were apparently in the ratios of 1:3:5.

7. The applicability of simple kinetic electrode theory to the system studied could not be demonstrated. This was thought to be due to the heterogeneous nature of the anodic surface.

#### Acknowledgment

Dr. F. A. Posey made many helpful suggestions both while the work was in progress and during the preparation of this manuscript. The authors also acknowledge helpful discussions with Drs. F. W. Young, Jr. and D. K. Holmes.

Manuscript received Aug. 24, 1961; revised manuscript received Jan. 30, 1962.

Any discussion of this paper will appear in a Discussion Section to be published in the December 1962 JOURNAL.

#### REFERENCES

1. R. Glauner and R. Glocker, *Z. Krist.*, **80**, 377 (1931).
2. P. A. Jacquet, *This Journal*, **69**, 629 (1936).

3. R. Bakish and W. D. Robertson, *ibid.*, **103**, 320 (1956).
4. H. Leidheiser, Jr., and A. T. Gwathmey, *ibid.*, **91**, 97 (1947).
5. W. Tragert and W. D. Robertson, *ibid.*, **102**, 86 (1955).
6. F. F. Faizullin *et al.*, *Uchen. Zap. Kazan. Univ.*, **115**, 123 (1955).
7. R. Piontelli *et al.*, *Inst. Lombardo Rend. Sci.*, **91**, 355 (1957).
8. R. Piontelli *et al.*, *ibid.*, **91**, 378 (1957).
9. F. W. Young, Jr., *J. Appl. Phys.*, **32**, 192 (1961).
10. F. W. Young, Jr. and T. Wilson, *Rev. Sci. Inst.*, **32**, 559 (1961).
11. F. W. Young, Jr. and A. T. Gwathmey, *Acta Met.*, **4**, 145 (1956).
12. B. E. Conway and J. O'M. Bockris, *Plating Mag.*, April (1959).
13. J. O. Stiegler and T. S. Noggle, *J. Appl. Phys.*, **31**, 1827 (1960).
14. L. H. Jenkins, *This Journal*, **107**, 371 (1960).

## The Oxidation of Sputtered Tantalum Films

Harold Basseches

*Bell Telephone Laboratories, Incorporated, Allentown, Pennsylvania*

#### ABSTRACT

The oxidation of sputtered tantalum films has been studied over a temperature range of 100°-600°C in oxygen at a gas pressure of 7.6 cm of Hg. The results obtained by means of a vacuum microbalance are compared with data on bulk tantalum, and it is found the rate of oxidation and amount of oxidation is considerably smaller than the bulk. A logarithmic relation was found to represent the data best in the range 400°-600°C. The factors which may give rise to the differences found between the film and the bulk are discussed.

In the course of an investigation of the stability of the electrical resistance of thin sputtered tantalum films (1), the oxidation of these films has been studied as a function of temperature.

The oxidation of sputtered tantalum films was carried out using a vacuum microbalance to obtain weight gain over a range of temperatures from 100° to 600°C in pure oxygen at a pressure of 7.6 cm of Hg. A logarithmic relation of the form  $y = a \ln(1 + bt)$  was found to give a slightly better fit of the data over the range of temperatures 400°-600°C than a parabolic one.  $y$  is the weight gain of tantalum in  $\mu\text{g}/\text{cm}^2$ ,  $t$  is the time in minutes,  $a$  and  $b$  are constants at any given temperature and have the dimensions  $\mu\text{g}/\text{cm}^2$  and  $\text{min}^{-1}$ , respectively. The results indicate that the amount and rate of oxidation of the film are considerably smaller (by about an order of magnitude) than that reported for bulk tantalum. Vermilyea's (2) results are in somewhat closer agreement.

Although quantitative correlations are not yet possible, the factors which may affect the weight gain measurements and may explain the differences in oxidation between film and bulk tantalum are discussed.

#### Experimental Procedure and Results

The details of the sputtering technique and the sample preparation have been described elsewhere

(1). The samples consisted of tantalum films (600-2500Å in thickness) sputtered on quartz substrates  $\frac{1}{2}$  in. x 2 in. x 30 mils in thickness. The oxidation was performed in a vacuum microbalance (3-5) by Gulbransen. The oxidation was carried out over a range of temperatures from 100° to 600°C in a pure oxygen atmosphere at a pressure of 7.6 cm of mercury. The total oxidation time was 2 hr. The graphs of the results are shown in Fig. 1 and 2 in which the weight gain per unit area is plotted as a function of time. The sensitivity of the apparatus is between 0.1-0.2  $\mu\text{g}/\text{cm}^2$  and indicates that films of the order of 7-15Å of tantalum oxide could be detected (69 Å/ $\mu\text{g}/\text{cm}^2$  based on  $\text{Ta}_2\text{O}_5$ ) (6).

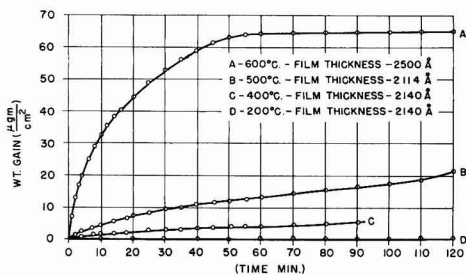


Fig. 1. Effect of temperature on oxidation of sputtered tantalum films ( $\text{O}_2$  pressure, 7.6 cm of Hg).

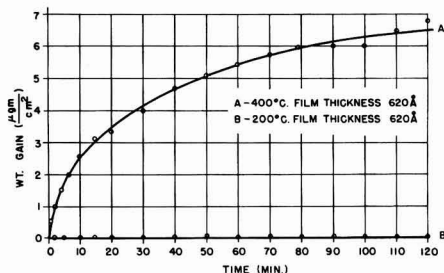


Fig. 2. Effect of temperature on oxidation of sputtered tantalum film ( $O_2$  pressure 7.6 cm of Hg).

There are several points that can be noted on these curves. The flat portion of curve A on Fig. 2 after the 60-min mark may result from the consumption of all the tantalum. Oxidation at a temperature of 200°C produced no measurable change, nor was there a visible color change. This is confirmed on two samples of different thicknesses, namely, curve D of Fig. 1 and curve B of Fig. 2. There appears to be no thickness effect in the oxidation since the value at 90 min for the total weight gain of curve C, Fig. 1 and curve A, Fig. 2 agree quite well.

It should be noted that the same samples were used for the 400°C tests as in the 200°C tests. Electron diffraction studies were made on the oxidized deposits on the quartz by Gulbransen. The results of this work are reported in Table I. In only one

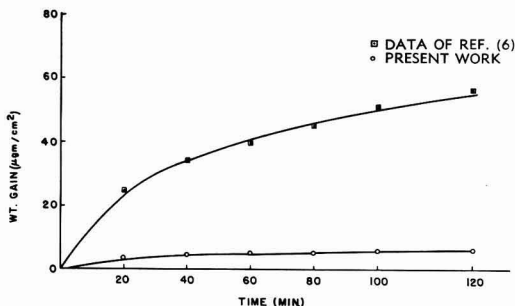


Fig. 3. Comparison of weight gain of sputtered tantalum film and bulk tantalum (400°C,  $O_2$  pressure, 7.6 cm of Hg).

case does there seem to be an indication of the tantalum oxide structure. The patterns in the other cases were very diffuse and difficult to interpret.

#### Comparison of Oxidation Data on Thin Tantalum Films with That of Bulk Tantalum

In Fig. 3 the data of the present work are compared to earlier work of Gulbransen and Andrew (6). The data for both bulk and sputtered tantalum were obtained in the same apparatus. The total amount of oxidation, as well as the rate of oxidation, is much less on the sputtered film than on the bulk material. Further comparisons are also available in Table II. The difference between Vermilyea's work and others may be related to differences in surface preparation; however, his

Table I. Oxidation of sputtered tantalum films, electron diffraction data

Sample thickness, Å	Oxidation temp, °C	Oxidation time, min	Weight gain, $\mu\text{g}/\text{cm}^2$	Color	Crystal structure	Physical characteristics
2140	400	90	5.17	Tarnished silver	Diffuse pattern	
620	400	120	6.76	Purple-orange	Diffuse pattern	
2500	600	120	65.0	—	Diffuse pattern	Film spalled off of quartz
2115	500	120	21.1	Green-blue	Probably $\text{Ta}_2\text{O}_5$	

Table II. Comparison of weight gain data in oxidation of tantalum in various investigation

Temp, °C	Length of oxid. run, hr	Pressure of oxygen, cm	Weight gain ( $\mu\text{g}/\text{cm}^2$ ) at end of run	Reference and remarks
1. 400	2	7.6	6.5	Present work
2. 400	2	7.6	57.2	Gulbransen and Andrew (6)
3. 600	1	7.6	63	Present work
4. 450	1	7.6	85	Gulbransen and Andrew (6)
5. 200	2	7.6	~0.1	Present work
6. 250	2	7.6	3.25	Gulbransen and Andrew (6)
7. 250	2	air ~15.2	~0.362*	Vermilyea (2)
8. 300	2	air ~15.2	~0.58*	Vermilyea (2)
9. 300	2	7.6	10	Gulbransen and Andrew (6)
10. 220	913	air ~15.2	20.5	Waber <i>et al.</i> (13)
11. 250	1400	air ~15.2	66	Waber <i>et al.</i> (13)
12. 216	2	air ~15.2	~3	Waber (14); value extrapolated from data given
13. 320	913	air ~15.2	227	Waber (7)
14. 500	1½	76 cm	~130	Cathcart, Bakish, & Norton (23)
15. 500	1½ hr	7.6 cm	16	Present work

\* Represent values obtained by conversion of Vermilyea's thickness data of 25 and 40 Å at the respective temperatures, utilizing a factor of  $69 \text{ Å}/\mu\text{g}/\text{cm}^2$  based on an oxide formula of  $\text{Ta}_2\text{O}_5$  (6).

comes closest to agreeing with the data of the present work.

It will be helpful to get some idea of what kind of reproducibility one can expect in oxidation studies of the type reported by Gulbransen. Although data are not available on tantalum, Gulbransen has worked on two other materials, columbium and zirconium, at several different times. In the case of columbium (6,7) and zirconium (6,8,9) differences of a factor of from 2 to 4 have been observed among samples studied at different times. The comparisons have been made at similar temperatures, but other conditions such as surface preparation and pressure of oxygen have not necessarily been the same. There is some risk in trying to compare sputtered films with bulk material since purity of samples, differences in surface treatment prior to oxidation, etc., could have strong influences on the result. It might have been expected that the conditions existent in films would tend to increase the rate over that of bulk rather than decrease it, as has been found.

It is also possible to make a comparison with bulk results and the present study as far as rate of oxide formation is concerned. From Gulbransen and Andrew's data (6) at 300°C for tantalum, an estimate can be made of the rate of oxide formation over the time interval of 1-2 hr to be of the order of 0.04 Å/sec. On the basis of Vermilyea's work (2), assuming that an oxide film of the order of 600Å has built up after oxidation of between 1 and 2 hr, one can estimate that at 300°C the rate of oxide formation would be of the order of 0.0001 Å/sec. This value is obtained from Fig. 4 which is a plot made from calculations of McLean (10) who used Vermilyea's data. However, this graph extends the calculations up to higher temperatures.

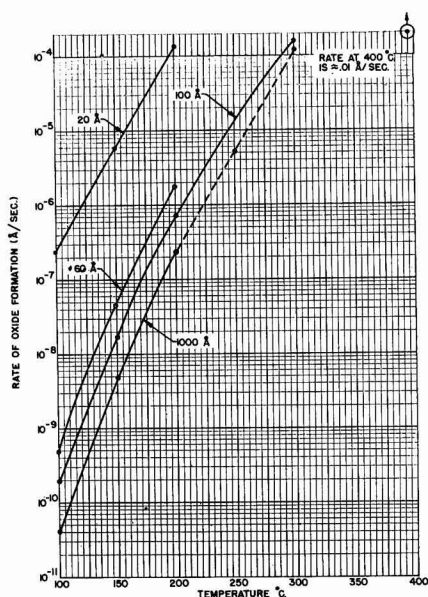


Fig. 4. Rate of oxidation of tantalum as a function of temperature and oxide thickness [data from Vermilyea (2)].

Table III. Constants for logarithmic rate law

Temp, °C	a	b
600	20.985	0.3820
500	7.029	0.0901
400 (2140Å)	2.399	0.0836
400 (620Å)	1.828	0.293

Unit of a is  $\mu\text{g}/\text{cm}^2$ ; unit of b is  $\text{min}^{-1}$ .

In an effort to make some comparisons with the present work, Vermilyea's data (2) have been extrapolated to 400°. Assuming a thickness of oxide of somewhere between 100-1000Å, extrapolation gives an oxidation rate of 0.01 Å/sec. as noted in Fig. 4. The data in the present study which can be used to best advantage to make a comparison are that of Fig. 2 at 400°C. The tangent to the 2-hr point gives the rate of 0.015 Å/sec. The rate calculated from a logarithmic relation deduced from the present study, as given below, is  $(dy/dt) = ab/(1 + bt)$ . Utilizing the values of a and b derived at 400°C for the 620Å film (see Table III) the rate is 0.017 Å/sec. Although it is dangerous to carry out the extrapolation of Vermilyea's data, the agreement may be noted.

A number of different equations has been proposed to account for the observed oxidation behavior of metals (11,12). In comparing parabolic with logarithmic behavior, on the basis of a least squares criterion, a logarithmic equation of the form  $y = a \ln(1 + bt)$  was found to fit the data slightly better than a parabolic one in the temperature range 400°-600°C. The various values of a and b are listed in Table III for data in the range of 400°-600°C. The units for t are in minutes. No theoretical significance is attached to this logarithmic behavior at the present time.

It appears that the amount of oxidation of sputtered tantalum is less, by about an order of magnitude, than that of bulk tantalum. Variations obtained over periods of time using the same apparatus suggest factors of somewhere between two and four could arise. Therefore, the factor of nearly ten obtained as the difference between the bulk material and the present thin film material does indeed suggest it to be a significant difference. A consideration of those factors which could affect this variability all tend to substantiate that differences exist between the bulk material and the sputtered film.

### Discussion

Previous studies of the oxidation of tantalum over various temperature and pressure ranges have characterized the behavior in various ways either as parabolic (6) logarithmic (2,13), cubic (14), and linear (15,16). In most of these studies the products of reaction were not completely identified so detailed discussion of the mechanism is not possible. In most cases the formation of tantalum pentoxide has been assumed. Recent studies of Kofstad *et al.* (17), however, give considerable detail on the products in the temperature range 500°-700°C.

X-ray diffraction and electron diffraction studies indicate that in the early stages, described as an incubation period, (for example, extending to 150-250 min at 500°C) oxygen dissolution occurs along with the formation of  $Ta_2O_5$  and a compound characterized by  $TaO_x$ . During the transition from the incubation period to the linear oxidation region,  $Ta_2O_5$  is formed as traces on the surface, and in the linear region there is heavy formation of  $\beta$ - $Ta_2O_5$ . The present electron diffraction studies have not characterized the products adequately. There was some suggestion that  $Ta_2O_5$  formed. However, if it is assumed from curve A in Fig. 1 that all of the tantalum is consumed at the point where the curve flattens out, then from the weight gain data it is shown that 65  $\mu\text{g}/\text{cm}^2$  of oxygen react with 415  $\mu\text{g}/\text{cm}^2$  of tantalum. On an atom basis this corresponds to a compound  $TaO_{1.75}$  which is one of the types of product indicated by Kofstad.

Although the evidence found in the present study indicates only a slight preference for a logarithmic over a parabolic behavior over the time periods studied, there seems to be no indication of linear behavior. This region may well correspond to the incubation period described by Kofstad (17). This incubation period, before the linear region, varied with the temperature and became shorter as the temperature and pressure increased. At 600°C and above it became too short to observe experimentally. The data of Albrecht *et al.* (16) still show an incubation period at 600°C. Kofstad (17) concluded that the oxidation during the incubation period was difficult to interpret in terms of any definite rate law although it was most closely approximated by a parabolic function.

Kofstad found oxygen dissolution to be an important step in the initial oxidation of tantalum. At 500°C the weight gain due to oxygen dissolution could amount to more than 75% of the weight gain found experimentally. Computations of the time necessary for oxygen to diffuse through a 2500Å thick tantalum film (18) using diffusion data of Gebhardt (19) were made. At 600°C this is 0.1 sec, at 400°C it is 10 sec, but at 300°C it is 6 min. It would appear therefore that in range of 400°-600°C oxygen dissolution is of minor importance in the rate measurements, although at lower temperatures it could become a major factor. Thus as far as measurements with thin films are concerned the relative importance of oxygen dissolution could change with temperature. The diffusion data used are those available for bulk tantalum, and it is conceivable that they are not strictly applicable to thin films.

The reasons for the difference between the behavior of the thin film and the bulk are not obvious. It may be due to differences in the oxides formed on the bulk as compared to that on the film. There is some evidence from studies on the anodization of sputtered tantalum films (20) made in connection with work on sputtered tantalum capacitors (21) that the oxide is different and does not crystallize as readily as on bulk tantalum. A strip of bulk tantalum was anodized in the same solution with a film of tantalum sputtered on a microscope slide.

The solutions used were those reported to promote crystallization (22). The strips were pulled out after a given time and examined microscopically. The bulk piece showed crystals, the sputtered film did not. The sputtered film was reimmersed for a period ten times longer and removed and examined. There were still no signs of crystallization.

The electron diffraction obtained on the present study suggests an amorphous structure at the elevated temperature. Vermilyea (2) showed on bulk tantalum, however, that at 350°C oxide films began to crystallize. His other work on tantalum (22) has shown that where crystalline oxide exists the rate of oxidation is more rapid than where the oxide film is amorphous. This may be the basis for the differences observed between the present study and bulk material.

The difference may arise because the surfaces of the films are in some way very different from most of the bulk samples studied. The oxidation data of Kofstad showed a profound effect of surface treatment on the oxidation behavior during the incubation period. Although no careful studies were made, chemical etching and high-vacuum annealing increased the incubation period. Albrecht's data at 600°C using vacuum annealed tantalum did indicate an incubation period (16). The structural results of Cathcart (23) on tantalum indicated a relationship between the state of perfection of the metal surface and its oxidation characteristics.

One perhaps may view the present work as giving a picture of what happens at the surface of the tantalum by greatly enhancing the surface to bulk relationship and hence the surface effects. Further kinetic and structural work using longer time periods, more intermediate temperatures, and a variety of thicknesses is necessary to get further understanding of the factors which appear to cause a difference between the oxidation results with thin film and bulk tantalum.

#### Acknowledgment

The author is indebted to Mr. E. A. Gulbransen of the Westinghouse Electric Corporation for carrying out the oxidation studies with his microbalance. Mr. S. S. Gupta and Miss Phyllis Groll contributed to the statistical analyses and data testing. He wishes to thank Mr. U. B. Thomas and Mr. N. Schwartz for helpful comments and discussion and Mr. P. Kofstad for detailed comments on the manuscript and the opportunity to discuss his work prior to publication.

Manuscript received May 8, 1961; revised manuscript received Jan. 30, 1962.

Any discussion of this paper will appear in a Discussion Section to be published in the December 1962 JOURNAL.

#### REFERENCES

1. H. Basseches, *IRE Trans. on Comp. Parts*, **CP-8**, 51 (1961).
2. D. A. Vermilyea, *Acta Met.*, **6**, 166 (1958).
3. E. A. Gulbransen, *Trans. Electrochem. Soc.*, **81**, 187 (1942).
4. E. A. Gulbransen, *Rev. Sci. Instr.*, **15**, 201 (1944).
5. E. A. Gulbransen and K. A. Andrew, *J. Phys. and Colloidal Chem.*, **53**, 690 (1949).

6. E. A. Gulbransen and K. A. Andrew, *J. Metals, Trans. AIME*, **188**, 586 (1950); *This Journal*, **96**, 364 (1949).
7. E. A. Gulbransen and K. A. Andrew, *This Journal*, **105**, 4 (1958).
8. E. A. Gulbransen and K. A. Andrew, *Trans. AIME*, **209**, 394 (1957).
9. R. G. Charles, S. Barnartt, and E. A. Gulbransen, *ibid.*, **212**, 101 (1958).
10. D. A. McLean, Private communication.
11. T. Mills, Corrosion Symposium held at University of Melbourne Nov. 28, 1955, p. 204, Wilke and Company Ltd., Melbourne, Australia (1955).
12. U. R. Evans, "The Corrosion and Oxidation of Metals," p. 819 ff, Edward Arnold, Ltd., London (1960).
13. J. T. Waber, G. E. Sturdy, E. M. Wise, and C. R. Topton, *Journal (and Trans.) Electrochem. Soc.*, **99**, 121 (1949).
14. J. T. Waber, *J. Chem. Phys.*, **20**, 734 (1952).
15. R. C. Petersen, W. M. Fassell, and M. E. Wadsworth, *J. Metals, Trans. AIME*, 1038 (1954).
16. W. M. Albrecht, W. D. Kloppe, B. G. Koehl, and R. I. Jaffee, *ibid.*, **221**, 110 (1961).
17. P. Kofstad, Central Institute for Industrial Research, Oslo-Blindern, Norway, Technical Note #4, April 1961, for Contract #AF61 (052)-90, Air Research and Development Command, European Office, Brussels, Belgium.
18. L. S. Darken and R. W. Gurry, "Physical Chemistry of Metals," p. 446, McGraw Hill Book Co. Inc., New York, N. Y. (1953).
19. E. Gebhardt, H. D. Seghezzi, and A. Stegherr, *Z. Metallkunde*, **48**, 624 (1957).
20. R. W. Berry, Private communication.
21. R. W. Berry and D. J. Sloan, *Proc. IRE*, **47**, 1070 (1959).
22. D. A. Vermilyea, *This Journal*, **102**, 207 (1955); **104**, 542 (1957).
23. J. V. Cathcart, R. Bakish, and D. R. Norton, *ibid.*, **107**, 668 (1960).

## The Influence of Residual Stress on the Magnetic Characteristics of Electrodeposited Nickel and Cobalt

Robert D. Fisher

*Physical Research Department, The National Cash Register Company, Dayton, Ohio*

### ABSTRACT

Cobalt and nickel were electrodeposited from aqueous solutions at a current density of 16 ma/cm<sup>2</sup>. The influence of the metal chloride salt and saccharin concentrations on the residual stress and microstructure of the cobalt and nickel electrodeposits was investigated in conjunction with measurements of their magnetic characteristics. In all cases the residual stress in the deposits as measured with a stressometer was found to be tensile in nature, *i.e.*, the deposits tend to contract. The coercive force of the cobalt and nickel deposits was determined as a function of the residual or internal stress at a thickness of approximately 7 $\mu$ . This coercive force was compared with a theoretical coercive force obtained from the relation  $H_c = \sigma\lambda/Is$  as proposed by Kersten where  $\sigma$  is the experimentally determined internal stress,  $\lambda$  is the magnetostriction value, and  $Is$  is the saturation magnetization. It is shown that the coercive force of nickel deposits is directly proportional to the internal stress. However, the coercive force of cobalt deposits appears to be dependent on the crystal structure as well as the internal stress. Heat treatment of the cobalt deposits for 2 hr at 440°C in nitrogen results in a decrease in the squareness and an increase in the coercive force while nickel deposits increased in squareness and decreased in coercive force. The former results are explained on a crystal structure basis while the latter results can be explained on a stress relief basis.

The magnetic characteristics of most ferromagnetic materials change with the application of stress. For example, the effect of a macroscopic unidirectional stress on the remanence and permeability of positive and negative magnetostrictive materials is well known (1). Electrolytic and vacuum deposited ferromagnetic materials possess an inherent residual or internal stress. Numerous investigators have determined this stress in both electro and vacuum deposited metals, but very little attention has been given to the effects of the internal stress on the magnetic characteristics of electrodeposits. In this investigation the internal stress and surface characteristics of electrodeposited cobalt and nickel were determined in conjunction with measurements of their magnetic properties at the same thickness. Deposits were prepared at a thickness of 7 $\mu$  in order to: (a)

minimize any effect of the substrate on the magnetic properties through epitaxial growth, and (b) obviate any changes in the coercive force of the deposit due to thickness. Cobalt and nickel were electrodeposited from aqueous solution containing primarily their metal salts. The influence of the metal salt concentration and small additions of saccharin to the solution was investigated as to their effects on the magnetic properties, internal stress, orientation, and surface characteristics of the deposited cobalt and/or nickel.

### Experimental

*Deposit preparation and stress measurements.*—Deposits for magnetic studies and stress measurements were made using a stressometer developed by J. B. Kushner. Its use and operation are described in detail elsewhere (2) and consequently will not be

discussed in this paper. The cathodes used in the stressometer were brass disks, 9 cm in diameter and 0.052 cm in thickness. All cathodes were cleaned in an identical manner and cut from the same sheet. The cleaning procedure was as follows: (a) alkaline cathodic cleaning, (b) distilled water rinse, (c) acid dip in 6N hydrochloric acid, and (d) distilled water rinse. The cathodes were then dried, weighed, and placed directly into the stressometer. The anode used with the stressometer was a platinum disk with the same diameter and area as the cathode, but the thickness was 0.21 cm. The stressometer was then calibrated and placed in the metal salt solution. Reagent grade metal salts of nickel chloride and cobalt chloride hexahydrate were dissolved in distilled water, and the single metals were independently deposited on the cathode of the stressometer at a current density of 16 ma/cm<sup>2</sup>. The total volume of solution in which the stressometer was immersed was approximately 7 liters. Agitation was not used in any of the solutions. Temperature of all solutions was 25°C, and the pH was adjusted with hydrochloric acid to a value of 2.0 ± 0.1.

**Magnetic measurements.**—B-H loops of the deposits were obtained from a low frequency (60 cycle) hysteresis loop tracer. The drive field was supplied by a pair of Helmholtz coils in series consisting of 400 turns each which permitted drive fields up to 400 oersteds without overheating. A Type 53/54B Tektronix preamplifier was used on the horizontal drive oscilloscope input. The sensing circuit consisted of a 5000-turn sense coil, a corresponding canceling coil wound in opposition, an R-C integrator and a Type 53/54E Tektronix preamplifier on the vertical oscilloscope input. The oscilloscope was a Tektronix 536.

**Thickness measurements.**—The thickness of all the deposits was determined by weight-density calculations. The thickness was then checked utilizing an x-ray diffraction technique. The integrated intensity of a diffraction peak of the brass substrate and the integrated intensity of the same peak with the magnetic coating over the substrate were obtained and related to the thickness. Agreement between the two methods was ±5%.

**Electron microscopy and x-ray diffraction.**—Samples examined with the electron microscope were replicated by applying a collodion-platinum replica followed by shadowing with carbon. The magnification in all instances was 20,000 diameters. The x-ray diffraction patterns were obtained using a Norelco x-ray diffractometer. Copper K $\alpha$  radiation and iron K $\alpha$  radiation were used on the nickel and cobalt deposits, respectively.

**Errors and reproducibility.**—The standard deviation of the stress measurements for electrodeposited cobalt was calculated as 140 kg/cm<sup>2</sup>. A value of 14 kg/cm<sup>2</sup> was determined for nickel electrodeposits. The average stress value of nickel deposits was 780 kg/cm<sup>2</sup>, and for cobalt deposits the average value was 1,660 kg/cm<sup>2</sup>. The stress measurements in each given system were reproducible within twice the standard deviation. Magnetic measurements were reproducible within the error of reading the oscilloscope which was ±3%.

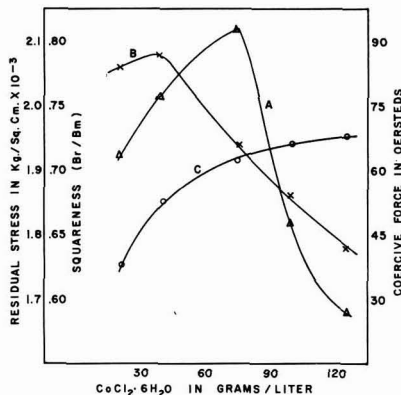


Fig. 1. Effect of cobalt chloride concentration on the residual stress and magnetic properties of electrodeposited cobalt; (A) residual stress; (B) squareness (Br/Bm); and (C) coercive force vs.  $\text{CoCl}_2 \cdot 6\text{H}_2\text{O}$  concentration.

### Experimental Results

**Cobalt deposits.**—The internal stress was determined in cobalt deposits from solutions containing 0.084M (20 g/l), 0.168M (40 g/l), 0.315M (75 g/l), 0.42M (100 g/l) and 0.525M (125 g/l) cobalt chloride hexahydrate. The current density was 16 ma/cm<sup>2</sup>. The internal stress gradually increases as the cobalt chloride concentration increases up to 75 g/l. Further increase in the cobalt chloride concentration (100-125 g/l) decreases the residual stress. Thus a maximum stress occurs at 75 g/l cobalt chloride hexahydrate (see Fig. 1A).

The magnetic characteristics of the deposits were obtained by observation of the hysteresis loop of the deposits. The squareness (Br/Bm) of the cobalt deposits tends to decrease (0.78-0.64) with increasing salt concentration (Fig. 1B). The coercive force varies from 38 to 68 oersteds and increases as the salt concentration increases. The coercive force increases rapidly with a small increase in metal salt concentration, but further additions results in smaller changes of the coercive force (Fig. 1C). The coercive force as a function of the internal stress is shown in Fig. 2A. The coercive force appears to be directly

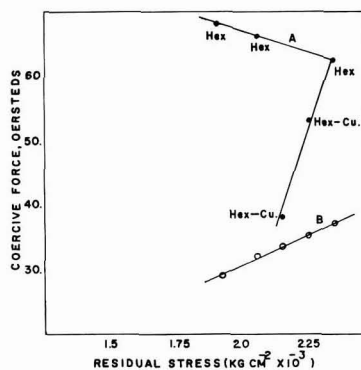


Fig. 2. Experimental and theoretical coercive force of cobalt as a function of the residual stress produced by varying salt concentration: (A) experimental coercive force vs. residual stress; (B) theoretical coercive force ( $H_c = \sigma_i/l_s$ ) vs. residual stress.



proportional to the internal stress up to 75 g/l cobalt chloride and then increases with a decrease in the internal stress. The increase in coercive force with a decrease in stress is similar to the results of Polukarov (3).

X-ray diffraction patterns of the deposits prepared from the low salt (20 and 40 g/l) concentrations have a hexagonal-cubic structure, but the other deposits at high salt concentrations have only a hexagonal structure with no discernible cubic peaks. Deposits which are hexagonal have the  $(11\bar{2}0)$  plane parallel to the substrate while deposits with the mixed structure have the  $(11\bar{2}0)$  and in addition the  $(220)$  cubic plane parallel to the substrate. There appears to be more cubic phase in the 20 g/l deposit than in the 40 g/l deposit based on the relative diffraction peak areas.

Electron micrographs (20,000X) of the cobalt deposits obtained at 20, 75, and 125 g/l of cobalt chloride hexahydrate were examined to determine the surface characteristics. A series (12 areas) of micrographs was obtained to assure a representative picture of the surface of each deposit. The 20 g/l deposit is relatively smooth with a fine texture in the range of 50-100 m $\mu$ . Approximately 15-20% of the surface shows a grain or crystallite development in the size range of 0.3 $\mu$ . The 75 g/l deposit displays the same fine texture as the 20 g/l deposit but the surface has become very rough (on the 1 $\mu$  scale) with little evidence of a characteristic grain structure. The 125 g/l deposit is also extremely rough, but there is better evidence of the development of grains similar to those observed in the 20 g/l deposit.

Heat treatment of these deposits at 440°C in nitrogen for 2 hr resulted in a decrease in the squareness and an increase in the coercive force of the deposits (Table I). X-ray diffraction patterns indicate that the percentage cubic phase present in the deposits prepared at 20 and 40 g/l cobalt chloride hexahydrate has decreased, especially in the case of the 40 g/l deposit. Also the diffraction peak heights increase and are sharper in nature, indicating an increased particle size and/or stress relief. No cobalt oxide phase was discernible from the diffraction peaks prior to or after the heat treatment. The deposit prepared at 20 g/l cobalt chloride showed the least increase in the coercive force after heat treatment and the 40 g/l cobalt chloride deposit showed the greatest increase in the coercive force after heat treatment. The other deposits increased in coercive force by approximately the same amount after heat treatment.

The influence of saccharin (Na salt O-benzoic sulfimide) on the internal stress of cobalt deposits was

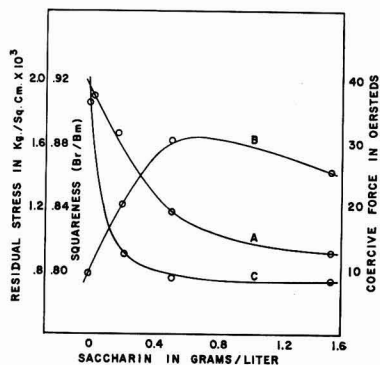


Fig. 3. Effect of saccharin on the residual stress and magnetic properties of electrodeposited cobalt: (A) residual stress; (B) squareness (Br/Bm); and (C) coercive force vs. saccharin concentration.

determined by depositing cobalt from a 20 g/l cobalt chloride hexahydrate solution containing 0.2 g/l ( $0.83 \times 10^{-3}M$ ), 0.5 g/l ( $2.07 \times 10^{-3}M$ ), and 1.5 g/l ( $6.22 \times 10^{-3}M$ ) of saccharin. The current density was 16 ma/cm<sup>2</sup>. The internal stress decreases with increasing saccharin concentration. Initial concentrations of saccharin (0 g/l, 0.2 g/l, and 0.5 g/l) decrease the stress linearly, but the 1.5 g/l addition decreases the stress less rapidly, i.e., it is less effective in reducing the stress (Fig. 3A)

The magnetic characteristics of the deposits were obtained as before by observation of the hysteresis loop of the deposits. The squareness of the deposits tends to increase slightly from approximately 0.8 Br/Bm to approximately 0.9 Br/Bm (Fig. 3B). Since the magnetostriction of the cobalt deposits is negative the increase in squareness may be partially attributed to a tensile stress relief. The coercive force of the deposits decreases with increasing saccharin concentration but not in a linear manner (Fig. 3C). Additions of small amounts of saccharin (0.2 and 0.5 g/l) decreases the coercive force from 38 oersteds to 8.5 oersteds at 0.5 g/l of saccharin. However, the coercive force remains constant with further additions of saccharin up to 1.5 g/l, although the internal stress continues to decrease. Deposits at high saccharin concentrations (0.5 and 1.5 g/l) have a coercive force which is the same as normal bulk deposits, namely, 8 oersteds (4). The coercive force of the deposits as a function of the internal stress is shown in Fig. 4A.

X-ray diffraction patterns of the deposits indicate a mixed hexagonal-cubic structure. Saccharin alters the orientation of the deposits from a hexagonal  $(11\bar{2}0)$ , cubic  $(220)$  planes parallel to the substrate to a hexagonal  $(10\bar{1}0)$ , cubic  $(111)$ . In addition saccharin increases the amount of cubic phase in the deposit as based on the relative peak heights.

Electron micrographs of the surface characteristics of each deposit were obtained at a magnification of 20,000 diameters (Fig. 5A-D). The surface characteristics of the 0.5 and 1.5 g/l saccharin deposits are nearly identical as far as can be estimated from the electron micrographs (Fig. 5C and D). Both

Table I. Cobalt deposits

g/l CoCl <sub>2</sub>	Magnetic properties after heat treatment, 440°C		Magnetic properties prior to heat treatment	
	Coercive force	Squareness Br/Bm	Coercive force, oersteds	Squareness Br/Bm
20	46.5	0.54	38.0	0.78
40	76.5	0.68	53.0	0.79
75	80.5	0.64	62.5	0.72
100	84.5	0.64	66.0	0.66
125	80.5	0.66	68.0	0.64

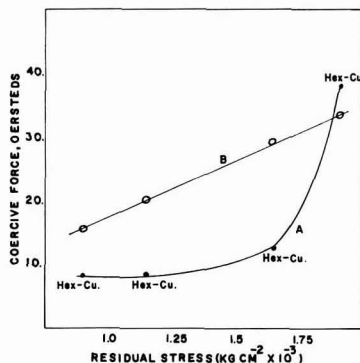


Fig. 4. Experimental and theoretical coercive force of cobalt as a function of the residual stress produced by additions of saccharin: (A) experimental coercive force vs. residual stress; (B) theoretical coercive force ( $H_c = \sigma\lambda/l_s$ ) vs. residual stress.

possess rounded surface projections which appear to be polycrystalline aggregates in the range of 3–5 $\mu$ . The remainder of the surface (background) has an extremely fine texture in the range of 10–50 m $\mu$ . Similar projections or aggregates in the 0.2 g/l saccharin deposit have dimensions in the range of 0.3–1.0 $\mu$  region. The background appears fine grained, but is more coarse than in the case of the 0.5 and 1.5 g/l saccharin deposits (Fig. 5B). The deposit without saccharin (20 g/l  $\text{CoCl}_2 \cdot 6\text{H}_2\text{O}$ ) is relatively smooth with a fine texture in the range of 50–100 m $\mu$  (Fig. 5A). A few projections or grains in the size

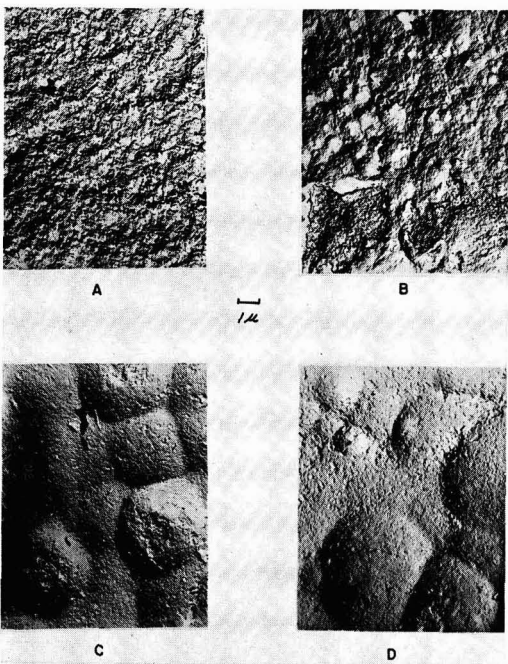


Fig. 5. Electron micrograph (magnification approximately 10,000 X) of the surface of cobalt deposits prepared in the presence of: (A) 0 g/l; (B) 0.2 g/l; (C) 0.5 g/l; and (D) 1.5 g/l of saccharin and 20 g/l of  $\text{CoCl}_2 \cdot 6\text{H}_2\text{O}$ .

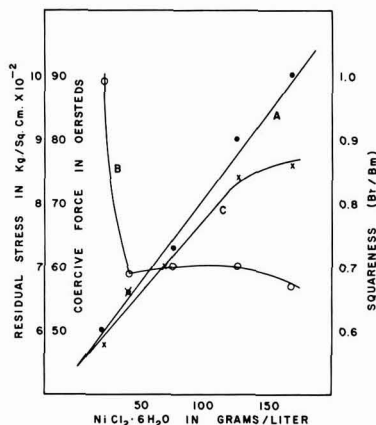


Fig. 6. Effect of nickel chloride concentration on the residual stress and magnetic properties of electrodeposited nickel; (A) residual stress; (B) squareness ( $\text{Br}/\text{Bm}$ ); and (C) coercive force vs.  $\text{NiCl}_2 \cdot 6\text{H}_2\text{O}$  concentration.

range of 0.3 $\mu$  appear over approximately 15–20% of the surface but are not shown in Fig. 5A.

**Nickel deposits.**—The internal stress was determined in nickel deposits from solutions containing the following amounts of nickel chloride hexahydrate: 0.084M (20 g/l), 0.168M (40 g/l), 0.294M (70 g/l), 0.526M (125 g/l), and 0.702M (167 g/l). The current density was 16 ma/cm<sup>2</sup>. The internal stress increases as the nickel chloride concentration increases. In fact the increase is linear and is approximately 2.7 kg/cm<sup>2</sup>/gram/liter addition of nickel chloride hexahydrate (Fig. 6A).

The magnetic characteristics of the deposits were obtained by observation of the hysteresis loop of the deposits. The squareness of the deposits decreases with increasing nickel chloride concentration from approximately 0.9 Br/Bm to 0.57 Br/Bm (Fig. 6B). Thus the remanent magnetization decreases with increasing metal salt concentration. The coercive force of the deposits increases from 48 oersteds at the lowest salt concentration to 76 oersteds at highest salt

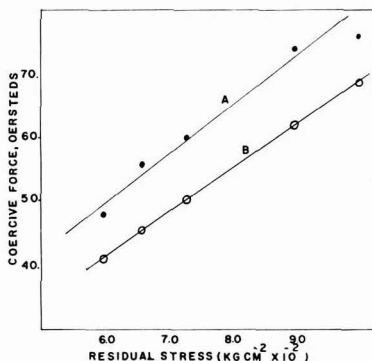


Fig. 7. Experimental and theoretical coercive force of nickel as a function of the residual stress: (A) experimental coercive force vs. stress; (B) theoretical coercive force ( $H_c = \sigma\lambda/l_s$ ) vs. residual stress.

concentration (Fig. 6C). Thus the coercive force increases with increasing internal stress. This has also been pointed out by Polukarov (5). The coercive force as a function of the internal stress is shown in Fig. 7A.

X-ray diffraction patterns of the deposits indicate a face-centered cubic structure typical of nickel with a decreasing (220) orientation of the deposit as the nickel chloride concentration increases from 20 to 125 g/l. The deposit at 167 g/l nickel chloride concentration appears to be random in orientation.

Electron micrographs of the deposits were obtained at a magnification of 20,000 diameters. The grain size distribution is very broad in the 20 and 40 g/l deposits making an estimate of the grain size difficult. The texture or background of the deposit is finely crystalline in nature and smooth. It would appear that the 20 g/l deposit has a larger grain size than the 40 g/l deposit. The 70 g/l deposit includes large continuous masses which are probably single crystals or grains with dimensions in the neighborhood of  $10\mu$ . These large flat crystals are connected by smaller crystals or grains in the neighborhood of  $1\mu$  (Fig. 8A). The 125 g/l deposit displays these large grain masses, but in much smaller proportions. These are occasionally joined to each other, but in most instances they are separated by areas containing crystals in the range of  $1.0\mu$  (Fig. 8B). The 167 g/l deposit does not contain any large crystal or grain masses, but consists of a relatively uniform crystallite size of  $0.5-1.0\mu$  (Fig. 8C).

Annealing of the deposits at  $440^\circ\text{C}$  in nitrogen for 2 hr results in a general increase in squareness and a decrease in the coercive force (Table II). This is in

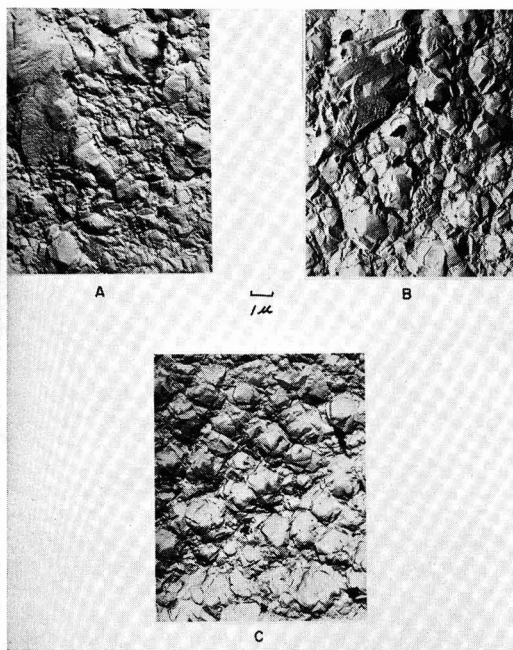


Fig. 8. Electron micrographs (magnification approximately 10,000 X) of the surface of nickel deposits prepared from a solution containing: (A) 70 g/l; (B) 125 g/l; and (C) 167 g/l  $\text{NiCl}_2 \cdot 6\text{H}_2\text{O}$ .

Table II. Nickel deposits

g/l $\text{NiCl}_2 \cdot 6\text{H}_2\text{O}$	Magnetic properties after heat treatment, $440^\circ\text{C}$		Magnetic properties prior to heat treatment	
	Coercive force, oersteds	Squareness Br/Bm	Coercive force, oersteds	Squareness Br/Bm
20	42.0	0.93	48.0	0.89
40	51.0	0.74	56.0	0.59
70	51.0	0.78	60.0	0.60
125	65.0	0.79	74.0	0.60
167	56.0	0.81	76.0	0.57

direct contrast with those results obtained with the cobalt deposits under a similar heat treatment (Table I). X-ray diffraction patterns of heat treated deposits indicate slight changes in the orientation of the deposits. The deposit which was initially random in orientation (167 g/l) showed the largest decrease in the coercive force. It should be pointed out that the results from the heat treatment could have been predicted qualitatively from the coercive force *vs.* internal stress curves if a stress relief should occur (Fig. 7A).

### Discussion

A source of internal stress may be imperfections in the crystal structure of the electrodeposited material. A tensile stress can be attributed to the existence of a certain proportion of vacant sites in each lattice layer. A compressive stress occurs with an interstitial occupancy of a foreign material in the crystal structure. The measured stress may be determined by a preponderance of one type of imperfection over the other. The stressometer used in this investigation measures the average stress. Consequently, there could be highly localized stresses of both a tensile and compressive nature in the deposit which are not detected by simply measuring the average stress. However, it can be assumed that generally the average stress is a result of localized stress gradients in the deposit. The higher the stress gradients in the deposit, the higher will be the value of the average stress. This assumption is obviously invalid if the stress gradients in the deposit are highly nonuniform in nature. Under the conditions investigated, all of the deposits exhibited a tensile stress.

No extensive effort was made in this investigation to eliminate impurities other than the use of reagent grade chemicals, and therefore the effect of impurities cannot be dissociated from those of stress. Thus, even though in certain instances the stress can be correlated directly with the coercive force, it does not necessarily mean that the stress is the cause of the coercive force. However, it is likely that whatever influences the internal stress subsequently causes the same effect on the coercive force.

Heat treatment of the cobalt deposits at  $440^\circ\text{C}$  in nitrogen for 2 hr resulted in a decrease in squareness (Br/Bm) and an increase in the coercive force of all deposits. The increase in coercive force after heat treatment may be attributed to a decrease in the internal stress of the deposits prepared from solutions containing 75, 100, and 125 g/l cobalt chloride according to the coercive force *vs.* internal stress relation as shown in Fig. 2A. However deposits prepared from the low concentration of salt (20 and 40

$g/l$ ) cannot be explained on a stress relief basis since the coercive force should have decreased with a stress relief rather than increased (see Fig. 2A). This anomalous behavior may be explained by the decrease in the cubic crystal structure of these deposits on heat treatment as shown by x-ray diffraction. Consequently, the cubic structure of cobalt decreases the coercive force over that of the hexagonal cobalt structure, and as the cubic phase decreases due to heat treatment the coercive force increases. These data substantiate results shown in Fig. 2 which indicate that the cubic phase decreases the coercive force of hexagonal cobalt deposit under the same stress conditions.

Heat treatment of the nickel deposits at 440°C in nitrogen for 2 hr decreased the coercive force and increased the squareness ( $Br/Bm$ ). The decrease in coercive force could have been predicted qualitatively from the coercive force *vs.* internal stress curve in Fig. 7A. The increase in squareness can be explained on a stress relief basis since it is well known that a tensile stress relief on a negative magnetostrictive material will increase the remanence (1). Thus the magnetic properties of nickel deposits before and after heat treatment can be explained on a stress relief basis rather than on a crystal structure-stress basis as in the case of the cobalt deposits.

The coercive force of nickel deposits is directly related to the internal stress. This suggests a model proposed by Kersten relating the coercive force to stress in the material. Kersten (6) (neglecting the energy associated with magnetic pole effects) relates the coercive force to the stress as follows:  $Hc = \sigma\lambda/Is$ , where  $\lambda$  is the magnetostriction,  $\sigma$  the internal stress, and  $Is$  the saturation magnetization. Thus the coercive force at a given composition and orientation (constant  $\lambda$  and  $Is$ ) is directly proportional to the residual stress. Calculations of the coercive force of nickel deposits prepared at various salt concentrations by substituting the experimental value of the internal stress, a magnetostrictive value of  $34 \times 10^{-6}$ , and a saturation magnetization of 484 gauss results in coercive force values of 41-68 oersteds. A plot of the calculated and experimental coercive force *vs.* the internal stress is shown in Fig. 7A and B. The agreement between the calculated and experimental results is quite good.

Calculating the coercive force of cobalt deposits on the same basis at varying salt concentrations by substituting the experimental stress values, a saturation magnetization value of 1422 gauss, and a magnetostrictive value of  $25 \times 10^{-6}$  results in coercive force values of 29-37 oersteds. The internal stress *vs.* the calculated coercive force is shown in Fig. 2B. Experimentally the coercive force ranges from 38 to 68 oersteds. Agreement between the calculated and experimental coercive force *vs.* internal stress is obviously poor due to the fact that the experimental results are not linear with stress. In the case of cobalt deposits in the presence of various amounts of saccharin similar calculations of the coercive force range from 15 to 34 oersteds, and a plot of the coercive force *vs.* residual stress is shown in Fig. 4B. Again agreement with the calculated results is poor since the experimental coercive force

*vs.* residual stress is not linear. Although the initial and final values of the calculated coercive force agrees well with the experimental values, intermediate values are generally too high. Thus the coercive force of cobalt deposits is dependent on other factors in addition to the residual stress, *e.g.*, Cu-Hex structure. In fact the coercive force of the hexagonal cobalt deposits (high salt concentration) is inversely proportional to the residual stress, *i.e.*, the coercive force increases with decreasing residual stress.

The surface characteristics of the deposited cobalt is dependent on the salt concentration and on the saccharin concentration. Increasing cobalt salt concentration increases the surface roughness of the deposited cobalt. Additions of saccharin result in a finer background texture of the cobalt deposit with the formation of large polycrystalline aggregates on the surface. Thus a stress relief can be associated with a grain refinement or a finer background texture. In the case of nickel deposits increasing salt concentration results in the formation of small crystallites at high salt concentration, but large flat crystals are formed at low salt concentrations. The internal stress increases with increasing salt concentration, and a decrease in stress can be associated with the formation of large flat crystals.

### Summary

It has been shown that a mixed cubic-hexagonal structure of cobalt occurs at a low cobalt chloride concentration. The cubic phase results in a lower coercive force since at the same internal stress value the cubic-hexagonal structure has a lower coercive force than the hexagonal structure. The effect of the cubic phase may be attributable to a lowering of the high crystalline anisotropy of the deposit which results in lower coercive force values. It should also be noted that a stress relief of a hexagonal cobalt deposit increases the coercive force. Saccharin increases the cubic phase of the cobalt with respect to the hexagonal phase and reduces the coercive force. It also reduces the residual stress considerably, but the reduction of the coercive force is more likely due to an increase in the cubic phase rather than a stress relief. The residual stress *vs.* the coercive force of cobalt deposits is not linear, and it would appear that the coercive force is primarily determined by the crystalline anisotropy. In contrast to the cobalt deposits the magnetic properties of nickel deposits appear to be directly related to the residual stress. This is shown by the linear relation of the coercive force *vs.* stress curve. In addition the coercive force calculated as proposed by Kersten ( $Hc = \sigma\lambda/Is$ ) agrees quite well with the experimental coercive force. A low stress appears to be associated with a grain refinement in the case of cobalt deposits and with the formation of large flat crystals in the case of nickel deposits.

### Acknowledgment

The author would like to acknowledge the assistance of Patrick O'Bryan, of the University of Cincinnati and The National Cash Register Company, for his effort in obtaining many of the stress meas-

urements; Donald Koopman, of The National Cash Register Company, for performing x-ray diffraction studies; and Alfred F. Prebus, of Ohio State University, for obtaining electron micrographs of the deposits.

Manuscript received Nov. 22, 1961; revised manuscript received Feb. 14, 1962. This paper was prepared for delivery before the Detroit Meeting, Oct. 1-5, 1961.

Any discussion of this paper will appear in a Discussion Section to be published in the December 1962 JOURNAL.

## REFERENCES

1. R. M. Bozorth, "Ferromagnetism," p. 595, D. Van Nostrand Co., New York.
2. J. B. Kushner, *Proc. Amer. Electroplaters' Soc.*, **41**, 188 (1954).
3. Y. M. Polukarov, *Zh. Fiz. Chim.*, **34**, 150 (1960).
4. R. M. Bozorth, "Ferromagnetism," p. 280, D. Van Nostrand Co., New York.
5. Y. M. Polukarov, *Zh. Fiz. Chim.*, **32**, 1008 (1958).
6. M. Kersten, *Probleme Der Technischen Magnetisierungskurve*, Springer, Berlin, 42-72. (Ref. 1, p. 824).

## Preparation and Magnetic Characteristics of Chemically Deposited Cobalt for High-Density Storage

R. D. Fisher and W. H. Chilton

*Physical Research Department, The National Cash Register Company, Dayton, Ohio*

### ABSTRACT

Chemically reduced cobalt coatings on a nonconductive substrate (Mylar) have been prepared which are suitable for high-density data storage applications. The influence of deposition parameters such as temperature, total solution concentration of cobalt plus hypophosphite ion, and pH on the hysteresis properties and surface characteristics of chemically reduced cobalt was investigated. The deposits are isotropic in nature so that no preferred direction of magnetization exists in the plane of the film. The coercive force of the deposits is an inverse function of the thickness, and the squareness ( $Br/Bm$ ) is primarily dependent on the thickness. The saturation magnetization may vary from 8,000 to 14,000 gauss depending on the impurity content of the deposit. A typical deposit has a coercive force of 360 oersteds at a thickness of 13,000Å. The deposits are crystalline as evidenced by x-ray diffraction patterns and electron microscopy in contrast to chemically reduced nickel deposits which are reported to be amorphous. Recording characteristics of the deposits are similar to those of commercial oxide recording tapes.

Electrodeposited cobalt-nickel films and iron oxide ( $Fe_2O_3$ ) coatings have been used as high-density data storage materials on drums, disks, and tapes. Requirements for high-density data storage are well known and have been discussed by many investigators (1). In general, the requirements are: (a) a magnetic coating with a nearly rectangular B-H loop, (b) a high coercive force generally greater than 200 oersteds, and (c) a relatively low ratio of remanent magnetization to coercive force. The work reported here was undertaken to ascertain whether chemically reduced films of cobalt could be obtained with suitable magnetic properties for high-density storage applications. Subsequently, the hysteresis properties of chemically reduced cobalt were evaluated with respect to thickness, deposition parameters, and microstructure. Chemical reduction is essentially a controlled autocatalytic reduction of cobalt and/or nickel on an active metal (Pd, Al, Ni, Co, and Fe) in the presence of hypophosphite ion. The method is attributed to Brenner (2).

### Experimental Procedure

*Film preparation.*—In this investigation Mylar was used as a substrate material. The Mylar film (7.16 cm x  $10^{-3}$  cm thick) was cleaned by: (a) dipping into a solution of 3N NaOH, (b) rinsing in distilled

water, (c) dipping into a solution of 3N HCl, and (d) rinsing in distilled water followed by rinsing in acetone. Direct deposition of cobalt onto the Mylar resulted in a deposit which did not adhere. To enhance the adhesion an intermediate organic coating (an adhesive) was placed between the Mylar and the cobalt deposit. The adhesive was applied by immersing the Mylar into a 1:3 mixture of adhesive<sup>1</sup> with methyl ethyl ketone and withdrawing at a rate of 0.84 cm/sec. The adhesive coated Mylar was then air dried for 30 min and cured for 10 hr at 80°C. To activate the Mylar-adhesive surface, stannous chloride and palladium chloride were used. The stannous chloride solution (sensitizing solution) contained 20 g/l of stannous chloride, 10 ml of concentrated HCl acid/liter, and 0.0166 g/l of sodium lauryl sulfate. The solution will not wet the Mylar-adhesive surface satisfactorily unless 2-3 hr has elapsed before immersion of the sample. The solution is used in a precipitated condition, i.e., a yellow coloration due to the formation of stannous oxychloride. The palladium chloride solution (activating solution) contained 0.5 g/l of palladium chloride and 5 ml of concentrated HCl acid/liter. The temperature of the sensitizing and activating

<sup>1</sup> Adhesive No. 200 TF supplied by the Shipley Company, Wellesley, Massachusetts.

solutions was 25°C. A standard cobalt-hypophosphite solution was prepared and contained the following unless otherwise specified: 7.5 g/l (0.031M) cobalt chloride hexahydrate, 3.52 g/l (0.033M) sodium hypophosphite monohydrate, 12.5 g/l (0.23M) ammonium chloride, 17.9 g/l (0.093M) citric acid, 0.0145 g/l sodium lauryl sulfate, and sufficient sodium hydroxide to adjust the pH to 8.2. The temperature of the cobalt-hypophosphite solution was 80°C and was controlled to  $\pm 0.5^\circ\text{C}$  by means of a heating mantle. The total volume of the solution was 27.6 liters. All solutions were prepared by dissolving reagent grade chemicals in distilled water and were used without further treatment or purification.

**Magnetic measurements.**—B-H loop measurements were made with a low-frequency (60 cycle) hysteresis loop tracer similar to that described by Howling (3). The maximum drive field without overheating was 1,030 oersteds. A Tektronix 536 oscilloscope was used with a type 53/54E preamplifier on the vertical input (B) and a 53/54B preamplifier on the horizontal input (H). The maximum vertical sensitivity was 0.29 maxwells/cm deflection.

**Electron microscopy and x-ray diffraction.**—Samples examined with the electron microscope were replicated by applying a collodion-platinum replica followed by shadowing with carbon. The magnification in all instances was 20,000 diameters. The x-ray diffraction patterns were obtained using a Norelco x-ray diffractometer. Chromium K $\alpha$  radiation was used on the cobalt deposits.

**Errors and reproducibility.**—Coating thicknesses were calculated from the coating weight and the theoretical density of cobalt corrected for the phosphorous content (approximately 4%). The phosphorous content was determined using a standard colorimetric procedure (4). Any appreciable porosity of the coating will result in thickness values that are smaller than the actual thickness. However, microscopic examination of the coatings indicated that the porosity error was small since the volume of the pores was approximately 1-4% of the total volume of the deposit.

For fixed preparation conditions the values of the coercive force of the deposits are reproducible within  $\pm 10\%$  and the flux density values (Br and Bm) within  $\pm 5\%$ . The calculated flux densities are not necessarily absolute as the applied field was only two to three times the coercive force of the deposited cobalt.

### Experimental Results

**Total concentration of cobalt plus hypophosphite.**—Initially, cobalt solutions were prepared according to Brenner (2). These solutions produced deposits with a coercive force of 20-50 oersteds depending on the experimental conditions. The deposits were unsatisfactory since the coercive force was much too low for high-density data storage applications. It was determined early in this investigation that a high concentration of cobalt and hypophosphite ions (typical of solutions described by Brenner) generally produced deposits with a low coercive force. After considerable investigation a

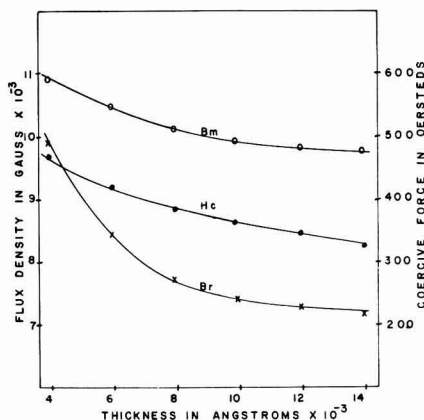


Fig. 1. Coercive force, remanent and maximum flux densities of cobalt deposits as a function of thickness.

standard solution was formulated which produced deposits with values of coercive force greater than 200 oersteds at thicknesses less than  $2\mu$ . The solution constituents are similar to those described by Brenner, the essential difference being that the solution was very dilute (see Experimental).

The magnetic properties of cobalt deposits prepared from the standard solution are a function of the thickness. The coercive force, remanent (Br) and maximum (Bm) flux density of deposits as a function of thickness are shown in Fig. 1. Both the remanent and maximum flux density appear to decrease with increasing thickness from 4,000 to 13,000Å.<sup>2</sup> The squareness (Br/Bm) of the deposits decreases with increasing thickness from 90% at approximately 4,000Å to 74% at approximately 10,000Å. The average (4,000-14,000Å) flux density of cobalt deposits was 10,500 gauss in comparison to 18,000 gauss for pure cobalt. Analysis of the deposits indicates an average phosphorous content of 4% with a trace quantity (less than 0.5%) of copper and nickel. The phosphorous content undoubtedly is primarily responsible for the loss in maximum flux density of the deposited cobalt in comparison to pure cobalt. The coercive force decreases with increasing thickness from 470 oersteds at 4,000Å to 360 oersteds at 10,000Å. In extremely thin films (<2,500Å) the coercive force may be greater than 650 oersteds (Table I). Under the conditions investigated the coercive force was determined to be an inverse function of the thickness to the one third power. By plotting the logarithm of the coercive force vs. the logarithm of the thickness a

<sup>2</sup> In the case of Bm the decrease in flux density may be fortuitous since any error in thickness will result in relatively large errors of Bm in the thin film region. However,  $\phi_r/\phi_m$  as well as Br/Bm definitely decreases as evidenced by hysteresis loops.

Table I. Grain size and coercive force of thin films of chemically reduced cobalt

Thickness, Å	Grain size, $\mu$	Coercive force, oersteds
700	0.1	>650
1,200	0.2	>600
2,300	0.45	500

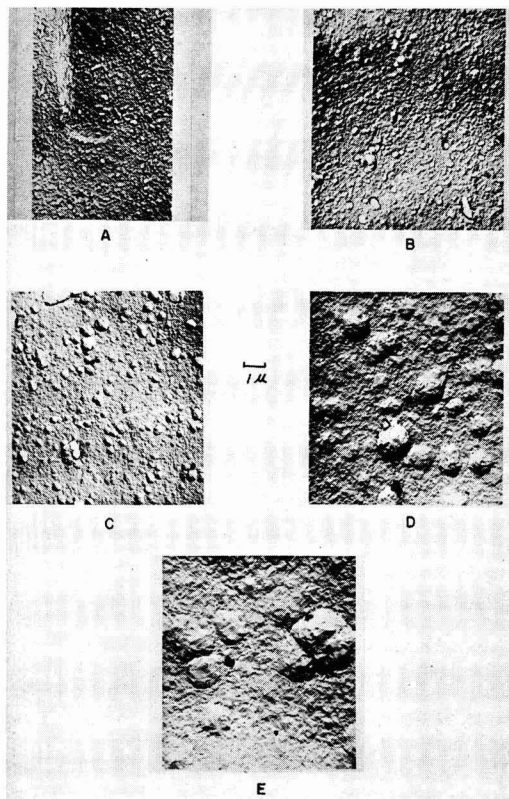


Fig. 2. Electron micrographs (magnification approximately 10,000X) of cobalt deposits at thicknesses of (A) 700Å, (B) 1200Å, (C) 2,300Å, (D) 7,000Å and (E) 14,000Å.

linear plot was obtained whose slope is one third. Thus the coercive force may be expressed as  $H_c = KT^{-1/3}$ .

Electron micrographs (20,000X) of the surface of deposits prepared at 700Å (3 min), 1,200Å (5 min), 2,300Å (10 min), 7,000Å (30 min) and at 14,000Å (60 min) were obtained to study the effect of thickness on the surface characteristics. The electron micrographs are shown in Fig. 2 A,B,C,D, and E. Examination of the micrographs indicated that initially (Fig. 2A) the deposit consists entirely of crystallites in the size range of 0.08-0.15 $\mu$  projecting above the surface; as the deposit becomes thicker these crystallites become larger (colonies, aggregates, or single crystals) but fewer in number. For example, at 10 min these crystallites have a size of approximately 0.40-0.50 $\mu$  (Fig. 2C) and at 60 min (Fig. 2E) the size (diameter) increased to 1.5 $\mu$  to 2.0 $\mu$ . The height of these crystallites above the surface (estimated from shadow) appears to decrease slightly with increasing thickness, but the number per unit area decreases rapidly. Therefore, the average smoothness increases as the deposit becomes thicker, but locally the surface may be quite rough. The surface texture or background of the deposit becomes apparent at a thickness of approximately 2,300Å (Fig. 2C). The background growth becomes more well-defined as the thickness in-

creases, i.e., edges and facets are apparent in the thicker deposits (Fig. 2E).

X-ray diffraction data indicate that the deposits are crystalline, finely grained, and have a hexagonal structure typical of cobalt. The crystallinity is in contrast to chemically deposited nickel which is reported to be amorphous (5). The diffraction patterns indicate a (10 $\bar{1}0$ ) preferred orientation parallel to the substrate. The relative peak broadening increases as the thickness decreases indicating a finer grain size and/or increasing stress with a decrease in thickness.

The deposition rate increases directly with an increase in solution concentration of cobalt plus hypophosphite ion. Therefore, to determine the effect of total concentration on the magnetic properties, deposits were compared at equal thicknesses. Solutions were prepared at 1.8, 4.0 (standard solution), 7.3, and 14.5 g/l of cobalt plus hypophosphite concentration at a fixed cobalt to hypophosphite ratio of 0.86. The magnetic properties as a function of thickness were determined at each concentration of cobalt plus hypophosphite ion. The coercive force vs. thickness for deposits prepared at 1.8, 4.0, and 7.3 g/l concentration is shown in Fig. 3 while the results for 14.5 g/l are shown in Fig. 4. Increasing the total concentration of cobalt and hypophosphite ion at a fixed ratio of cobalt to hypophosphite (0.86) increases the coercive force from 315 oersteds (10,000Å) to 390 oersteds (10,000Å) at a concentration of 1.8-7.3, but at 14.5 g/l the coercive force decreases to 47 oersteds (10,000Å). Thus a high concentration of cobalt plus hypophosphite ion, i.e., between 7.3 and 14.5 g/l at a cobalt to hypophosphite ratio of 0.86, produces deposits with a low coercive force. The remanent flux density decreases as the thickness increases in all cases (1.8, 4.0, 7.3, and 14.5 g/l Co<sup>++</sup> plus H<sub>2</sub>PO<sub>2</sub><sup>-</sup>). The deposits prepared at the low concentration (1.8) have the highest

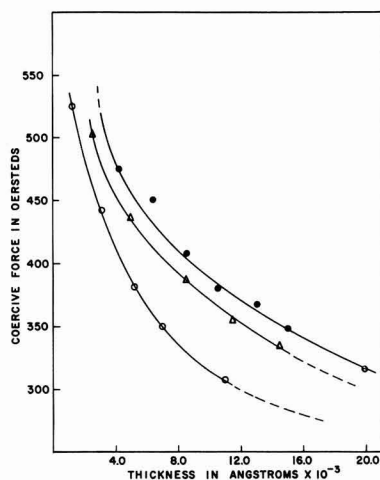


Fig. 3. Coercive force of chemically reduced cobalt as a function of thickness at various total concentrations of cobalt plus hypophosphite ion: ● Co<sup>++</sup> plus H<sub>2</sub>PO<sub>2</sub><sup>-</sup> = 7.3 g/l; △ Co<sup>++</sup> plus H<sub>2</sub>PO<sub>2</sub><sup>-</sup> = 4.0 g/l; ○ Co<sup>++</sup> plus H<sub>2</sub>PO<sub>2</sub><sup>-</sup> = 1.8 g/l; cobalt ion to hypophosphite ion ratio = 0.86.

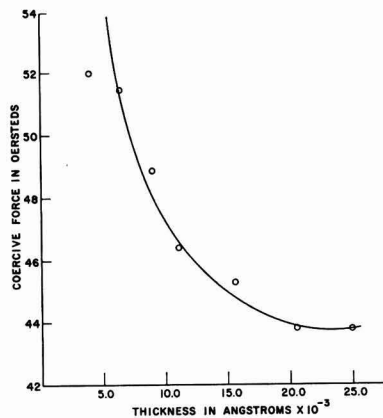


Fig. 4. Coercive force of chemically reduced cobalt as a function of thickness from a solution containing 14.5 g/l of  $\text{Co}^{++}$  plus  $\text{H}_2\text{PO}_4^-$  ion; ratio of cobalt ion to hypophosphite ion = 0.86.

remnant and maximum flux densities. The squareness ( $\text{Br}/\text{Bm}$ ) of the deposits generally decreases with increasing thickness, but deposits from the dilute solutions tend to have a slightly higher squareness in comparison with deposits prepared at the higher (14.5 g/l) concentration of cobalt plus hypophosphite ion.

**Influence of pH.**—The influence of pH on the coercive force of chemically deposited cobalt was determined at pH values from 7.0 to 9.0 at intervals of 0.2 pH unit. The coercive force as a function of thickness was determined at each individual pH value. The coercive force decreases with increasing thickness at all pH values. The magnitude of the coercive force at a given thickness is nearly constant at pH values between 7.4 and 8.2. However, an increase in coercive force at a given thickness occurs at pH values from 8.2 to 8.6, e.g., 389 oersteds (8.2) to 406 oersteds (8.6). Between a pH of 8.6 to 9.0 a drastic decrease in coercive force occurs from 406 oersteds (8.6) to 50 oersteds. This drastic decrease in coercive force with pH is similar to that which occurs with an increase in cobalt plus hypophosphite ion concentration. Below a pH of 7.4 cobalt will not deposit readily, and at a pH of 7.0 deposition ceases.

**Volume to area ratio.**—A few experiments were performed to determine if the magnetic properties of the deposits from the standard solution were dependent on the ratio of volume of plating solution to sample surface area. The volume to area ratio was varied by a factor of 100 by varying the sample area ( $\text{cm}^2$ ) and solution volume (ml). The coercive force, remnant, and saturation flux densities were then determined as a function of thickness (time) at volume to area ratios of 8.0, 55.0 and 800. The coercive force does not appear to be appreciably dependent on the volume to area ratio. However, the lowest maximum flux density occurs at the highest volume to area ratio. The rate of deposition increases slightly with increasing volume to area ratio, e.g., approximately 330 Å/min at a volume/area ratio of 800 and approximately 240 Å/min at

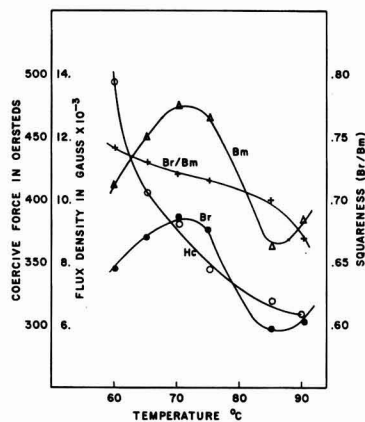


Fig. 5. Magnetic properties of chemically deposited cobalt at various temperatures but at constant time (60 min). ● Remanent flux density; △ maximum flux density; ○ coercive force; and X squareness ( $\text{Br}/\text{Bm}$ ).

a volume/area ratio of 8.0. The decrease in flux density may be associated with greater occlusion of impurities with increasing rate of deposition. However, the squareness of the deposits does not appear to be significantly different at various volume to area ratios. Consequently, all the magnetic properties remain similar with volume/area changes with the exception of the maximum flux density.

**Influence of temperature.**—The effect of temperature on cobalt deposits prepared from the standard solution was investigated by depositing for a constant time (60 min) at solution temperatures varying from 60° to 90°C at intervals of 5°C. The effect of solution temperature on the magnetic properties of the deposits is shown in Fig. 5. The coercive force decreases with increasing temperature. The saturation and remanent flux densities increase to a maximum at approximately 75°C and then decrease with further increases in temperature. The thickness (or deposition rate) increases directly with solution temperature for the 60-min deposition time. The squareness of the deposits decreases with increasing temperature. Thus the decrease in coercive force and squareness can be attributed primarily to an increase in the thickness. However, the variation of flux density with temperature cannot be explained by the change in thickness since the flux density decreases from the standard solution (80°C) without going through a maximum.

Electron micrographs (20,000X) of the surface of these deposits were examined. It can be seen from these micrographs that the deposits contain a fine textured background crystal growth with relatively large aggregates or colonies of crystallites growing perpendicular to the background. These aggregates or colonies increase in size as the solution temperature increases (increasing thickness), but the number per unit area decreases with increasing temperature. The surface roughness of the deposit is determined primarily by the height of these projections above the surface. The micrographs appear similar to those shown in Fig. 2 depending on



Table II. Recording Characteristics

Tape	Thickness, mils	Coercive force, oersteds	Pulse width, mils	Packing density, bits/in.	Signal amplitude, Mv	Saturation current, ma
Cobalt	0.03	400	1.0	800	700	60
Cobalt	0.055	330	1.5	550	925	70
3M #189	>0.3	278	1.3	665	1,200	80
3M #198	>0.3	282	1.2	770	1,100	80
Ampex 832	>0.3	278	1.2	770	1,100	65

the temperature and indicate that the primary effect of temperature on the magnetic properties is to vary the thickness. For further verification some measurements of the effect of solution temperature were made at (various deposition times) constant thickness. The coercive force was nearly constant as the temperature increased from 65° to 90°C.

**Heat treatment.**—A cobalt deposit from the standard solution was heat treated at low temperature (40°–175°C) for 24 hr in air to determine the effect of a stress relief on the magnetic properties of the cobalt deposit. Increasing temperature increases the coercive force of the deposit from 320 oersteds at 40°C to 354 oersteds at 175°C. The squareness ( $Br/B_m$ ) remains nearly constant although a slight decrease is noted from 0.80 to 0.78  $Br/B_m$  prior to and after heat treatment. Therefore a stress relief results in an increase in the coercive force of chemically reduced cobalt since at such a low-temperature grain growth, diffusion or orientation changes can hardly occur. This result is in agreement with previous results (6) showing that a stress relief of hexagonal cobalt electrodeposits results in an increase in coercive force.

**Recording characteristics.**—Preliminary recording tests of chemically deposited cobalt samples were made to determine their recording characteristics such as pulse width, packing density, signal amplitude, and saturation current. Nonreturn to zero saturation recording was used. The tests were made on a conventional closed-loop tape transport mechanism utilizing an Ampex head for recording and reading. The tape speed was 100 ips. The saturation current was determined at 20 kc as the value beyond which output and/or uniformity no longer increased. The maximum packing density in bits/in. was determined by the pulse interval at the value of recording frequency which reduced the output signal by 20%. The recording characteristics of several cobalt deposits were compared with three commercial oxide recording tapes, namely, Minnesota Mining and Manufacturing Tapes #189 and #198 and Ampex Tape #832. The tests were made under identical conditions of recording and reading. Results are shown in Table II. It is obvious that the cobalt deposits may have a slightly higher or equivalent packing density to that of oxide tapes. In addition the pulse width may be slightly higher or less than that of the tapes. However, the signal amplitudes were generally less. The saturation current is lower despite the higher coercive force of the cobalt deposits since the coating is much thinner than the oxide coatings.

### Discussion

It is apparent from the experimental data that, in order to define the magnetic properties of chem-

ically deposited cobalt, the concentration of cobalt plus hypophosphite ion, the pH, the solution volume to sample area ratio and temperature must be specified. The effect of these parameters on the magnetic properties can be explained by their subsequent effect on the thickness, crystal growth, and impurity content of the deposit. However, there does not appear to be any single factor which determines the magnetic properties.

The coercive force of the deposits is a function of the thickness. It would appear that the grain size in thin films (Fig. 2A) is approximately the same size as the background texture in thick films (Fig. 2E), i.e., if one assumes that no subdivisions of the background texture or grains in the thin films occur. Also the grains would appear to be more isolated in the thin films. In addition, thick films contain aggregates, colonies, or large crystals. These large crystals, colonies, or aggregates may be responsible for the lowering of the coercive force as the deposit becomes thicker.

Generally, a high coercive force ( $H_c > 300$  oersteds) may be attributed to a rotational mechanism either coherent or some mode (fanning, curling) of incoherent rotation of the magnetization against the anisotropy (magnetocrystalline, magnetoelastic, magnetostatic) (7). In such cases the particle size determines the coercive force, and the coercive force is independent of the thickness. In the case of these deposits, the coercive force is dependent on the thickness, but it is not entirely clear from the electron micrographs whether the grain size is dependent on the thickness. Thus it cannot be determined whether a rotational model is applicable.

It is interesting to note that Neel (8) has proposed a relationship between grain size of a multidomain grain and the coercive force as  $H_c = \gamma_w K^{1/2} I_s^{-2/3} D^{-2/3}$  where  $\gamma_w$  is the wall energy,  $K$  is the anisotropy constant,  $I_s$  is the saturation magnetization, and  $D$  is the grain size of the film. Substituting the following values of  $\gamma_w = 1$  erg/cm<sup>2</sup>,  $K = 4.0 \times 10^8$  ergs/cm<sup>2</sup>,  $I_s = 1422$  gauss for cobalt, and  $D = 0.2\mu$ , the average background grain size in thick films estimated from the electron micrographs (neglecting the clumps or aggregates), a coercive force of 350 oersteds is obtained. This agrees with the experimental coercive force of 360 oersteds at a thickness of 13,000Å. However, this model fails to explain the high coercivity in thin films which appear to have approximately the same grain size as thick films.

Thus, the source of the relatively high coercive force and the mechanism of reversal such as wall motion or rotation is unknown.

Manuscript received Dec. 8, 1961; revised manuscript Feb. 20, 1962. This paper was prepared for delivery before the Detroit Meeting, Oct. 1-5, 1961.

Any discussion of this paper will appear in a Discussion Section to be published in the December 1962 JOURNAL.

## REFERENCES

1. J. J. Miyata and R. R. Hartel, *IRE Trans. on Electronic Computers*, **EC-8** [2] (June 1959).
2. A. Brenner and G. Riddell, *Proc. Amer. Electroplaters Society*, **34**, 156 (1947).
3. D. H. Howling, *Rev. Sci. Instr.*, **27**, 952 (1956).
4. Snell and Snell, "Methods of Colorimetric Analysis," D. Van Nostrand and Co., New York (1949).
5. A. W. Goldenstein, W. Rostoker, F. Schossberger, and G. Gutzeit, *This Journal*, **104**, 104 (1957).
6. R. D. Fisher, *ibid.*, **109**, 479 (1962).
7. C. Kittel, *Revs. Modern Physics*, **21**, 541 (1949).
8. L. Neel, *J. phys. Radium*, **17**, 250 (1956).

## Effect of Binary Alloy Plating on Delayed Brittle Failure of Ultrahigh Strength Steel

Walter Beck and E. J. Jankowsky

*Aeronautical Materials Laboratory, Naval Air Material Center, Philadelphia, Pennsylvania*

## ABSTRACT

In a number of applications, involving high strength steel, tin-cadmium alloy plating has been substituted for cadmium plating. In this study, notched specimens of high strength steel were plated with tin-cadmium alloys, produced by codeposition of the components from a fluoborate bath. The steel was also plated separately with tin from the stannate bath and cadmium from the cyanide bath and the two layer system subjected to a thermal treatment. The marked differences in delayed cracking of specimens plated from baths with different compositions were discussed in the light of the coverage of the steel surface with adsorbed atomic hydrogen in conjunction with a recently advanced theory of the kinetics of crack propagation in delayed failure.

Some years ago the corrosion protection afforded a steel substrate by cadmium, zinc-cadmium, and tin-cadmium alloy coatings was evaluated at the Naval Air Material Center (1, 2). The protection offered by tin-cadmium systems was found to be most promising, and they have been used extensively on aircraft engine components since that time.

Recently, failures of tin-cadmium plated, carburized, and nitrided engine parts were reported, and hydrogen embrittlement was considered to be a possible cause. No information was available regarding embrittlement characteristics of the process, and inasmuch as hydrogen embrittlement could seriously curtail its use and extension to other high strength steel parts, it was deemed necessary to investigate the problem thoroughly.

Binary alloy coatings are formed by direct plating from an alloy bath and also may be formed by thermal treatment of separately plated layers of the constituent metals.

In either case, the embrittlement problem is probably more complex than it is for single metal deposition, as may be expected, particularly for the two-layer system. A study of this problem, therefore, appears of general interest.

The baths used in this investigation for tin and cadmium plating in producing the two layer system were different from each other and from that employed for plating the alloy directly, because they were patterned after industrial and governmental practice now extensively used for plating internal steel components of aircraft engines. The same is true for the coating thicknesses and alloy compositions selected for this study.

The principal objective of this study was the determination of the differences in embrittlement re-

sulting from the plating of tin-cadmium coatings on a high strength steel by two different processes, and if differences resulted, to determine to what extent the component parts of each process contributed to the total embrittlement.

A secondary objective was to apply an existing theory of the kinetics of delayed brittle failure to the results and to interrelate hydrogen coverage with this theory.

The embrittlement was determined by sustained loading delayed failure measurements on notched specimens of ultrahigh strength AISI SAE 4340 steel. Some delayed fracture studies were also conducted on a type H-11 hot work die steel plated with cyanide cadmium and a diffused, heat resistant nickel-cadmium alloy, respectively.

### Experimental Procedures and Results

*Specimens and testing.*—Most of the work was done with specimens fabricated from 4340 steel heat treated to a strength level of 260-280 (R<sub>50</sub> 51-52) ksi. Some studies were made on a type H-11 hot work die steel heat treated to the same strength level as the 4340 steel. Cylindrical, notched tension specimens were selected for the experiments because they are known to be very sensitive to hydrogen embrittlement. Notches were ground after heat treatment, to the dimensions shown in Fig. 1. Notches were lightly polished, gauge sections highly polished. Static tension tests were performed in a universal testing machine, at a constant cross head speed of 0.05 in./min. Times to fracture under sustained loading were determined in constant load lever arm stress rupture machines at room temperature. The loading devices used were designed to insure concentricity of load application.

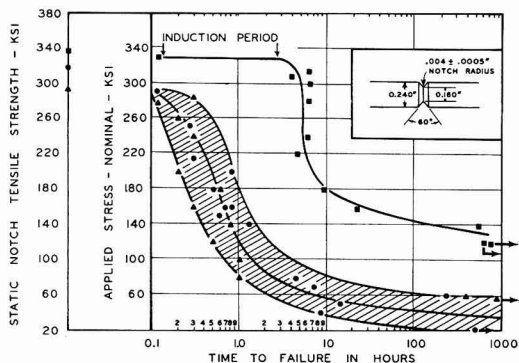


Fig. 1. Hydrogen embrittlement by plating of 4340 steel with tin, cadmium, and tin followed by cadmium and a thermal treatment. ■, Cyanide cadmium plating; ▲, stannate tin plating; ●, stannate tin, followed by cyanide-cadmium plating. All plated specimens treated for 30 min at 340°F. The tin-cadmium double coating consisted of approximately 50% tin and remainder cadmium. UTS unplated steel 260-280 ksi; NTS unplated steel 360-380 ksi;  $K_T = 4.2$ .

When no thermal treatment was to be applied, specimens were stressed 5 min after plating. Thermally treated specimens were stressed immediately after cooling down to room temperature. Threads were carefully masked before immersion in the plating bath to avoid thread breaks during load application.

*Two-layer tin-cadmium plating followed by a thermal treatment.*—Prior to plating, the specimens were anodically cleaned in a hot alkaline solution and dipped in 50% HCl solution for 50 sec at room temperature. This pretreatment insured good adhesion of the plating without affecting the notch dimensions. The acid dipped specimens, stressed immediately after dipping to 95% of the notch tensile strength of the untreated steel (4340 steel average 370 ksi, type H-11 steel average 385 ksi), did not fail when kept underload for the maximum time of 1000 hr.

Tin was plated from a stannate bath to an approximate thickness of 0.0008 in. measured on the gauge section. Immediately following tin plating and rinsing, cadmium was plated to the same thickness from a cyanide bath.

To alloy the tin with the cadmium, a recommended thermal treatment (1) at 340°F, for a period of 30 min, was used. Nominal composition of the alloy was 50% tin, 50% cadmium.

Specimens were also plated singly with tin or cadmium under the same conditions as those used for plating each of the two layers, and the same thermal treatment was applied.

Delayed failure curves are presented in Fig. 1 for tin, cadmium, and tin-cadmium plated specimens. Failure times determined for tin-cadmium plated steel and for those plated only with tin were close enough to be covered by a scatter band, typical of delayed brittle failure measurements under sustained loading.

*Tin-cadmium alloy formation by codeposition of its components.*—After alkaline cleaning and acid dipping, the alloy was directly plated from a complex fluoborate bath (1, 3, 4) recommended in the literature. The approximate thickness of the plating,

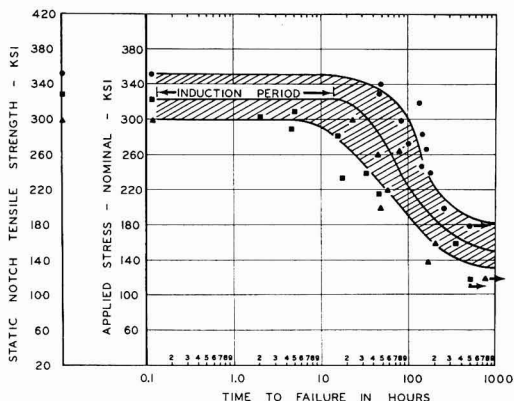


Fig. 2. Hydrogen embrittlement by plating of 4340 steel with tin-cadmium alloy and its components. ■, Fluoborate cadmium plating; ▲, fluoborate tin plating; ●, tin-cadmium alloy formed by codeposition of the metals from fluoborate bath; approximate composition of alloy 30% tin, remainder cadmium.

measured on the gauge section, was 0.0005 in. and its composition, as determined by chemical analysis, was approximately 30% tin, remainder cadmium. Tin and cadmium were also plated separately from fluoborate baths to thicknesses of approximately 0.00015 in. and 0.00035 in., respectively, corresponding to their ratio in the alloy.

Figure 2 is a plot of the failure curves recorded with specimens plated from fluoborate baths. Again, the values for the failure times are randomly distributed in the field of a comparatively wide scatter band.

*Plating of nickel followed by cadmium and a diffusion heat treatment.*—The nickel-cadmium coating system was applied on hot work die steel specimens pretreated in the same manner as the 4340 specimens. Nickel was plated to an approximate thickness of 0.0002 in. from a Watt-type bath without brightener, and cadmium to an approximate thickness of 0.0001 in. from a cyanide bath, according to ref. (5). The coating system, with a nominal composition of 65% nickel, remainder cadmium, was diffusion heat treated in a circulating air furnace at 630°F for 40 min (5).

The comparatively high diffusion temperature did not have a detrimental effect on the strength of the substrate which was an air hardening steel tempered at a temperature of 1050°F. This type of steel is used at elevated temperatures and, therefore, not plated with tin-cadmium but heat and oxidation resistant nickel-cadmium alloy. The delayed failure behavior of this steel, coated with diffused nickel cadmium or plated with 0.0005 in. cyanide cadmium<sup>1</sup> is depicted in Fig. 3. Cyanide cadmium was plated on this steel to allow comparison with 4340 steel.

*Metallographic and electrochemical evaluation.*—The work on tin-cadmium alloy plating was considered incomplete without some information about the metallurgical structure of the system obtained by thermal treatment of the separately plated layers.

The opinions concerning the question of whether or not alloy formation takes place under the thermal

<sup>1</sup> Fed. Spec. QQ-P-416a (1956).

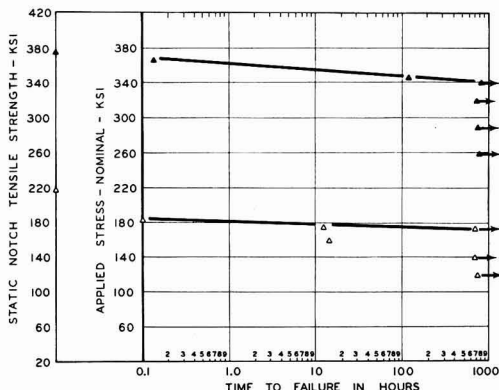


Fig. 3. Hydrogen embrittlement by plating of a hot work die steel with nickel followed by cadmium and a diffusion heat treatment, and by cyanide cadmium plating. Inverted solid triangle, Watts-type nickel plating followed by cyanide cadmium plating, diffusion heat treated for 40 min at 630°F; inverted open triangle, cyanide cadmium plating; the nickel cadmium system consisted of approximately 65% nickel and remainder cadmium; UTS unplated steel 260-280 ksi, NTS unplated steel 380-390 ksi,  $K_r = 4.2$ .

treatment conditions used in this investigation are divided. According to Britton and de Verre Stacpoole (6), the coating remains in layers; however, Scott and Gray show evidence that tin diffuses through the cadmium matrix (7).

In the studies made at this laboratory, steel panels were plated first with 0.002 in. of tin, and then with 0.002 in. of cadmium. After plating, the panels were thermally treated at 340°F for 1, 2, and 24 hr, respectively. The specimens were then sectioned at a low angle, mounted in cold hardening epoxy, rough polished with emery paper of increasingly finer grades up to 000, final polished with diamond dust of 3 and 0.5 $\mu$ , and etched for 2 min in 30% aqueous NaOH solution at room temperature.

According to the phase diagram, at 340°F, under conditions near or approaching equilibrium, the only phases that can be present are  $\alpha$ , ranging in composition from pure tin to 1% cadmium in solid solution, in contact with  $\beta$ , with from 4.0 to 5.5% cadmium in solid solution, and  $\gamma$ , ranging from pure cadmium to 0.25% tin in solid solution, in contact with  $\beta$ . The  $\alpha$  solid solution can be in equilibrium only with the  $\beta$  (4.0% tin); likewise,  $\gamma$  may only be in equilibrium with  $\beta$  (5.5% tin). Since no evidence of a eutectoid structure resulting from the decomposition of a  $\beta$  phase was observed metallographically, even after 24 hr at 340  $\pm$  3°F, it must be concluded that little or no diffusion of either tin or cadmium in other than the terminal solid solutions took place.

The metallographic findings were in excellent agreement with the electrochemical behavior of the coatings. Average steady-state potentials of two layer, thermally treated coating systems containing from 10 to 75% cadmium, measured in 0.1N NaCl solution at room temperature, were found to be -800 mv on the saturated calomel scale. Similar values were obtained on steel panels plated only with cyanide cadmium. The average potential of tin plated panels was -500 mv.

These results are in good agreement with the statements by Britton and de Verre Stacpoole (6), but do not concur with the results obtained by Scott and Gray (7). There are indications that the diffusion of tin into cadmium, demonstrated microscopically by the latter investigators, may be due to overheating, because the alloy appears homogeneous from the edge to the base, even though the time of thermal treatment (30 min at 350°F) appears much too short to ensure complete diffusion.

Because alloy formation could not be detected, the tin-cadmium system will now be designated a two-layer plating.

With respect to alloy formation by codeposition of the tin and cadmium components, attention is directed to a very recent paper by Smart *et al.* (8) who studied alloys formed by codeposition of the two metals from a complex sodium stannate-cyanide cadmium bath. According to these investigators, the plated tin-cadmium alloy is a simple eutectic system which consists of a mixture of the two high-purity components.

No metallographic investigations were made of the nickel-cadmium system. Therefore, diffusion of cadmium into nickel was only assumed to take place because it was implied in the aeronautical specification (5).

#### Discussion of Results

The discussion of the curves presented in Fig. 1-3 will be based partially on a recently advanced theory of the kinetics of crack initiation and propagation in delayed failure (9,10). According to this theory, delayed brittle cracking can be aptly described by various parameters such as the incubation period, failure time, and the static fatigue limit.

The incubation time is the period required for initiation of the first crack, and the failure time is a measure of the crack propagation rate subsequent to crack initiation. The stress below which delayed failure cannot take place for an indefinite period and above which it must occur is called the static fatigue limit.

The incubation period represents the time which is needed for the hydrogen atoms to accumulate in the region of maximal triaxial stress state until a critical concentration, required for crack initiation, has been attained. Following crack initiation, there is a period of crack propagation, and finally, failure takes place. The parameter called "induction period" in the following discussion, includes both the incubation period and the crack propagation period at the highest stress at which delayed failure occurs (see Fig. 1).

It has been shown that immediately after cadmium plating (9) or cathodic charging (10) the hydrogen atoms remain concentrated in a thin layer underneath the steel surface, and from there, they diffuse into the interior of the specimen. With decreasing surface concentration of hydrogen, incubation, fracture time, and static fatigue limit increase, progressively.

Based on the work of Troiano and his co-workers (11, 12), it is inferred that a long induction time results, at least in part, from a long incubation period.

*Induction time.*—To simplify the analysis of the results of determinations of the induction times, they

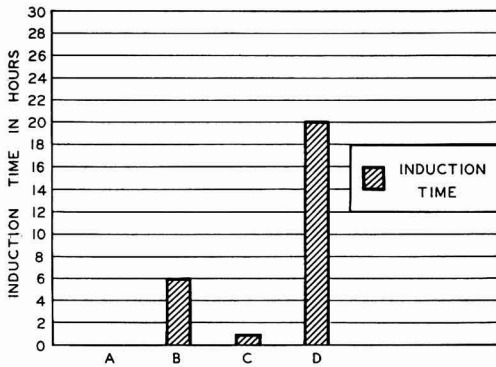


Fig. 4. Effect of plating on induction time of various steels. A, plating of stannate tin (sodium stannate bath operated at 160°F) followed by thermal treatment, plating of stannate tin followed by cyanide cadmium and a thermal treatment; B, plating of cyanide cadmium layer to approximately 0.00008 in. followed by a thermal treatment; C, plating of cyanide cadmium layer to approximately 0.0005 in.; D, platings from the fluoborate baths. A-D — 4340 steel.

are presented as bars in Fig. 4. Two interesting features of the results obtained with plated 4340 steel specimens are revealed in this figure: 1. The induction time is increased about twentyfold by plating the steel from the fluoborate bath (bar D) instead of the cyanide bath (bar C). 2. On specimens thermally treated after plating, that is, stannate tin plated specimens, and specimens plated with stannate tin and cyanide cadmium, respectively, the induction time is zero (bar A), and in the case of cyanide cadmium plated specimens, it was observed that the induction time was comparatively short (bar B).

In accordance with the theory discussed above and the results summarized under 1, it is concluded that the rate of crack initiation and propagation in specimens plated from the cyanide bath exceeds that in fluoborate plated specimens very appreciably. It is more difficult to explain the nonexistence of an induction period for the stannate tin or the stannate tin-cyanide cadmium plated specimens subjected to the same thermal treatment. It may be the result of homogenization (11) of the hydrogen distribution in the steel produced by the thermal treatment. It may also be speculated that the tin coating is a better hydrogen diffusion barrier than the thin cadmium coating (13) and that it therefore more effectively prevents outgassing of the embrittling hydrogen during thermal treatment, which would explain the short but finite induction time of the cyanide cadmium plated specimens. In any case, it is difficult to make predictions, based on induction time, about crack propagation in specimens coated with different metals and subjected to a thermal treatment.

**Static fatigue limit.**—The static fatigue limit should provide a more direct and more easily interpreted measure of embrittlement damage than the induction period. Figure 5 is a bar diagram of the static fatigue limits expressed in terms of percent of the breaking strength of the untreated notched specimens.

The differences in the static fatigue limits determined for fluoborate and cyanide cadmium plated

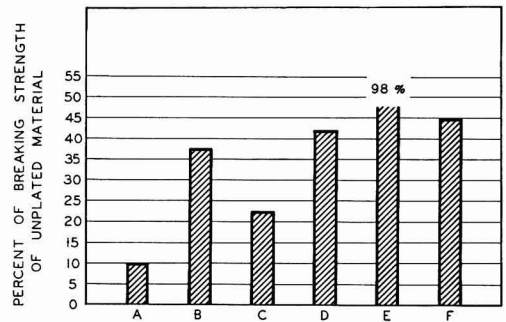


Fig. 5. Effect of plating on breaking strength of various steels, A, B, C, D as in Fig. 4. E, Plating of nickel followed by cadmium and a diffusion heat treatment; F, plating of cyanide cadmium to approximately 0.0005 in.; E-F, hot work die steel.

specimens without thermal treatment, respectively, (bars D and C), confirm qualitatively the conclusions drawn from the induction times.

The low relative breaking strength (bar A) indicates that despite a comparatively short plating time (3.5 min for stannate tin, 2 min for cyanide cadmium) and the subsequent thermal treatment, the susceptibility of the steel to brittle cracking is very high as a result of stannate tin plating.

**Hydrogen surface coverage.**—The foregoing discussion clearly illustrates the usefulness of the theory of the kinetics of crack initiation and propagation, and particularly of the static fatigue limit, in accessing hydrogen embrittlement damage. However, the theory does not suggest a mechanism which determines the accumulation of hydrogen atoms in the metal surface.

For a number of years, extensive efforts have been made in the Aeronautical Materials Laboratory to obtain more information about this mechanism during cathodic polarization or plating. These efforts have been based on electrochemical and radioactive tracer studies on ultrahigh strength 4340 steel charged cathodically in sodium hydroxide solutions with and without sodium cyanide added, as well as electrochemical studies on steel plated with cadmium from cyanide and fluoborate baths. A comprehensive report of the results will be presented in a forthcoming paper (14). A few that relate to this paper are summarized below.

By radioactive measurements on steel surfaces after cathodic polarization in a 0.1M NaOH solution containing  $\text{NaC}^{14}\text{N}$  in low concentrations, cyanide compounds were detected which tenaciously adhered to the metal. A positive heat of adsorption, in conjunction with increasing concentration of these cyanide compounds with temperature of radioactive charging solution, clearly indicated the mechanism of layer formation to be controlled by chemisorption. Hydrogen overvoltage measurements on steel electrodes with chemisorbed cyanide indicated a retardation of the hydrogen recombination reaction and hence a rise in the coverage of the surface with hydrogen. By means of the hydrogen permeation current method of Bockris and Devanathan (15) important information has been secured about this hydrogen coverage.

Addition of 0.02M sodium cyanide to a 0.1M sodium hydroxide solution raised the steady-state coverage of the steel surface with adsorbed atomic hydrogen during cathodic hydrogen evolution about 4.5 times above that in the pure sodium hydroxide solution.

In the case of cadmium plating from the cyanide bath, the coverage was only 3 times greater than that in the pure sodium hydroxide solution. It dropped further when cadmium was plated from the fluoborate bath, which was ascribed to the absence of a highly capillary active anion such as cyanide.

The extraordinarily high susceptibility of the stannate tin plated specimens to delayed failure is believed to be related to chemisorption accelerated by the comparatively high temperature of the plating bath. The rate of diffusion of the hydrogen atoms into the steel depends on the coverage of the surface with hydrogen (16). A high coverage will ensure that the hydrogen atoms diffusing from the thin layer underneath the specimen surface into its interior will be replenished at a high rate.

It is suggested that the differences in delayed brittle failure behavior of the specimens plated with tin followed by cadmium and those plated directly from an alloy bath be explained by combining the concept of hydrogen surface coverage with the theory of the kinetics of crack propagation.

In the case of the tin-cadmium coating applied by plating the constituent metals separately, the short stress rupture life is intimately related to a high hydrogen surface coverage, and it follows that the lower embrittlement imparted to the alloy plated specimens is the result of a comparatively low surface coverage with adsorbed hydrogen atoms, surface coverage being determined by the electrochemical action of the different bath anions.

Finally, the effect of plating on delayed failure of the hot work die steel will be discussed briefly.

As shown in Fig. 3, the embrittlement response of this type of steel is somewhat different from that of the 4340 steel. As can be seen from the diagram, the static notch tensile strength of the nickel-cadmium plated steel and its static fatigue limit are very close to the notch tensile strength (380 to 390 ksi) of the untreated specimen. The cyanide cadmium plated specimens again showed severe embrittlement (bar F in Fig. 5) but they were not as badly embrittled as the 4340 specimens (bar C in Fig. 5).

The almost complete absence of embrittling hydrogen in the steel (bar E in Fig. 5) may be the result of the high-temperature diffusion treatment or the proven effectiveness (17) of the low embrittling Watts nickel plating as a hydrogen diffusion barrier.

It is hoped that the studies now being conducted in this laboratory will give more information about the response to delayed brittle fracturing of H-11 and similar high strength hot die steels.

### Summary

Delayed brittle cracking of ultrahigh strength 4340 steel, plated with stannate tin, followed by cyanide cadmium and a thermal treatment, is controlled by the tin phase of the plating process.

Embrittlement induced by plating the metals in two separate layers from the above baths appreciably

exceeds that by codeposition of tin and cadmium from a complex fluoborate bath.

Delayed brittle failure in an ultrahigh strength hot work die steel plated with nickel from Watts type bath, followed by cyanide cadmium and a thermal treatment at a comparatively high temperature, was only of a negligible order.

The relative breaking strength derived from the static fatigue limit is representative of the embrittlement damage imparted to the steel. The marked differences in the stress rupture behavior of the plated specimens were related to differences in the surface coverage with adsorbed atomic hydrogen and discussed in the light of a recently advanced theory of the kinetics of crack propagation in delayed failure.

### Acknowledgment

The authors are much indebted to Mr. F. S. Williams, Superintendent of the Metallurgical Division and Mr. Samuel Goldberg, Special Materials Section of the Bureau of Naval Weapons for the great interest taken in this study, to Mr. Manuel Raefsky for his assistance with the metallographic evaluations, and to Mr. Peter Sabatini, who performed much of the experimental work.

Manuscript received Oct. 30, 1961; revised manuscript received Feb. 8, 1962. This paper was prepared for delivery before the Detroit Meeting, Oct. 1-5, 1961. The opinions or assertions expressed in this paper are the private ones of the writers and are not to be construed as official or reflecting the view of the Department of the Navy or the Naval service at large.

Any discussion of this paper will appear in a Discussion Section to be published in the December 1962 JOURNAL.

### REFERENCES

1. Aeronautical Materials Laboratory NAM AE 41, 1027, Pt. I and II issued April 28, 1948 and May 12, 1950, by J. H. James and C. M. Dougherty.
2. N. E. Promisel and G. S. Mustin, *Corrosion*, **7**, 379 (1951).
3. Bennie Cohen, *Plating*, **44**, [9], 965 (1957).
4. E. S. Hedges, et al., "Tin and Its Alloys," p. 104-106, E. Arnold Ltd., London (1960).
5. Aeronaut. Materials Specifications AMS 2416A issued by SAE (1956).
6. S. C. Britton and R. W. de Vere Stacpoole, *Trans. Inst. Met. Finishing*, **32**, 237 (1955).
7. B. E. Scott and R. D. Gray, Jr., *Iron Age*, **167** (Jan. 18), 60 (1951).
8. R. F. Smart, R. M. Angles, and D. A. Robins, *J. Inst. Metals*, **89** [9] 351 (1961).
9. H. H. Johnson, J. G. Morlet, and A. R. Troiano, *Trans. Met. Soc. AIME*, **212**, 528 (1958).
10. Taiji Toh and W. M. Baldwin, Jr., "Stress Corrosion Cracking and Embrittlement," p. 185, John Wiley & Sons, Inc., New York (1956).
11. A. R. Troiano, *Trans. ASM*, **52**, 61 (1960).
12. E. A. Steigerwald, F. W. Schaller, and A. R. Troiano, *Trans. Met. Soc. AIME*, **218** [5], 832 (1960).
13. H. H. Johnson, E. Schneider, and A. R. Troiano, *Iron Age*, **182** (July 31), 47 (1958).
14. W. Beck, Al Glass, and Ed Taylor, to be submitted to *This Journal*.
15. J. O'M. Bockris and M. A. V. Devanathan, University of Pennsylvania, Tech. Report No. 4 to ONR Contract Nonr 551 (22) N.R. 036-028 28 Feb. 1961.
16. L. I. Freiman and V. A. Titov, *Russian J. Phys. Chem.*, **34**, [1], 11 (1960).
17. W. Beck and E. J. Jankowsky, *Proc. Am. Electroplaters Soc.*, **47**, 152 (1960).

# Rotating Disk Electrode Techniques for the Study of Addition Agents

## I. Preliminary Studies with Cupric Sulfate Solutions

Seward E. Beacom and Robert N. Hollyer, Jr.

Research Laboratories, General Motors Corporation, Warren, Michigan

### ABSTRACT

The rotating disk electrode is being used as a tool to study the influence of organic addition agents on the electrodeposition of metals; the initial phases of the study are reported in this paper. Rotating disk electrode theory has been verified for deposition of copper from cupric sulfate solutions in the presence of certain ratios of inert electrolyte ions. The experimental conditions required to proceed with a study of the role of organic additives have been established. It is found that current density is distributed uniformly across the surface of the disk electrode.

Many details of the influence of organic addition agents on the electrodeposition of metals are still unresolved. To attack certain phases of this problem, it is desirable to study the electrodeposition process under the most elementary conditions, *i.e.*, with the number of uncontrolled variables at a minimum. Because of its simplicity, an electrode system consisting of a stationary anode and a rotating disk cathode was chosen for the present investigation. This system has been successfully employed by a number of investigators to study redox reactions (1-7), but its use for the examination of the electrodeposition of a metal ion is relatively recent; the few reports in the literature indicate only limited success (4, 8, 9).

The rotating disk cathode is attractive because of the large volume of readily available literature concerning its flow pattern and the related mathematical analyses (1, 2, 5, 10-14). Examination of the equations shows that deposition must be carried out at the limiting current plateau and that migration due to electrical fields must be made negligible; the latter is accomplished by the use of a large excess of indifferent electrolyte.

The primary aim of the experimental program is to establish the conditions for which the mathematical description can be applied to the deposition of copper from an aqueous cupric sulfate solution. This is a necessary step in a program to employ the rotating disk electrode for examination of the influence of organic addition agents on the electrodeposition of metals.

### Experimental

*Description of apparatus.*—Figure 1 is a block diagram of the apparatus which permits the rotation of a disk electrode at accurately controlled angular velocities. The shaft is driven by a variable speed motor. The frequency of rotation, recorded as revolutions per minute, is counted electronically by a scaler. Electrical contact to the shaft is made through a toroidal mercury cup. The glass vessel which holds the electrolyte is equipped with a side arm to permit the introduction of the 5 x 5 cm copper anode without disturbing the solution flow sym-

metry. The vessel, 12.7 cm in diameter, is sufficiently large to prevent the walls from interfering with the solution flow about the disk. A tight-fitting Lucite cover permits the maintenance of a nitrogen atmosphere above the electrolyte.

The potential, which is supplied by 1.5v dry cells and varied by means of a potentiometer, is measured with a vacuum tube voltmeter while current is measured with a milliammeter.

*Electrodes.*—The cathodes are stainless steel or solid copper disks, 6 mm thick and 1.27, 1.91, and 2.54 cm in diameter, respectively, mounted normal to the drive shaft. The sides and backs of the disks, as well as the drive shaft, are insulated from contact with the electrolyte. Very careful polishing and cleaning procedures are required. When the stainless steel disks are used they must be flash plated, first with a Wood's nickel strike, and then with cyanide copper. Experience has shown that the disks must be polished between runs and, if any roughness or staining develops, the complete plating preparation must be repeated. Because trouble was experienced with porosity in the cyanide copper deposit, the more recent work has been done with electrodes machined from high-purity copper.

*Composition of electrolytes.*—The electrolyte used in the majority of the work done thus far is an aqueous solution of cupric sulfate containing potassium sulfate as inert electrolyte. The cupric sulfate concentrations range from 0.001 to 0.020M and the po-

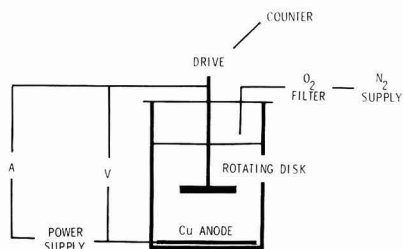


Fig. 1. Schematic diagram of apparatus

Table I. Composition of solutions used

Solution No.	CuSO <sub>4</sub> concentration (molar)	K <sub>2</sub> SO <sub>4</sub> concentration (molar)
1A	0.001	0.1
4A	0.004	0.1
6A	0.006	0.1
1B	0.001	0.2
4B	0.004	0.2
6B	0.006	0.2
12B	0.012	0.2
20B	0.020	0.2
1C	0.001	0.3
4C	0.004	0.3
6C	0.006	0.3
4D	0.004	0.05

tassium sulfate concentrations from 0.05 to 0.3M. The pH of all solutions was adjusted to 3.0 by the addition of sulfuric acid. The composition of the solutions is recorded in Table I.

**Removal of oxygen.**—To provide an oxygen-free environment, the nitrogen used for gassing is purified by passage through a solution containing vanadyl sulfate over amalgamated zinc as recommended by Meites (15). Gassing is carried out for 30 min before the start of each experiment, and a nitrogen atmosphere is maintained above the electrolyte during the run.

### Procedure and Results

The plateau voltage, that is, the cell voltage required for the deposition of cupric ions at the limiting current, is determined from the current-potential curve obtained at a constant frequency of rotation. The plateau for the CuSO<sub>4</sub> solutions extends over a range of 0.35–0.45v; the value 0.4v was used for all experiments. The same general shape of the curve and the same plateau voltage is obtained regardless of disk size or of the frequency of rotation. As expected, the magnitude of the current varies with disk size and the frequency of rotation used.

Under the experimental conditions being employed, the mathematical description predicts that a plot of current density *vs.* the square root of the frequency of rotation will yield a straight line passing through the origin. A further consequence of the theory, which holds that the distribution of current will be uniform across the surface of the disks irrespective of size, was checked by using three disks of different diameters. As shown in Fig. 2, both of these requirements are met. The fact that the average current density is the same for all three disk sizes can be assumed to indicate that the local current

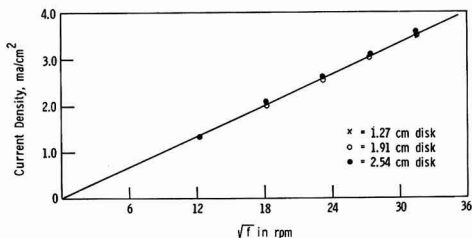


Fig. 2. Current density vs. root frequency for various sized disks

density is everywhere the same. An additional check of this point was made by measuring the thickness of copper deposits along the radii of the 1.91- and 2.54-cm disks using the interference microscope. Within the limit of experimental error ( $\pm 5\%$ ) the deposit thicknesses are uniform over the disk surfaces.

Since the general objective of this investigation is to use the controllable deposition conditions at the rotating disk electrode to examine the role of addition agents in the electrodeposition of metals, it is important to determine a range of cupric ion and potassium sulfate concentrations over which the requirements of the rotating disk theory may be met. When this range is once established, it then becomes possible to investigate the influence of organic addition agents.

Using the electrolytes listed in Table I, the current density *vs.* root frequency relationship is determined over a range of solution compositions. A plot, typical of the results obtained, is given in Fig. 3. It will be noticed that the plots, which are straight lines passing through the origin, meet the predictions of rotating disk theory. A plot of the slope  $i/\sqrt{f}$ , *vs.* the cupric sulfate concentration should be a straight line intersecting the origin. Figure 4 is a plot of this expression for the A, B, and C solutions. The agreement with theory is apparent.

Inspection of Fig. 5 shows that the plots of solutions 12B and 20B deviate from a straight line. The

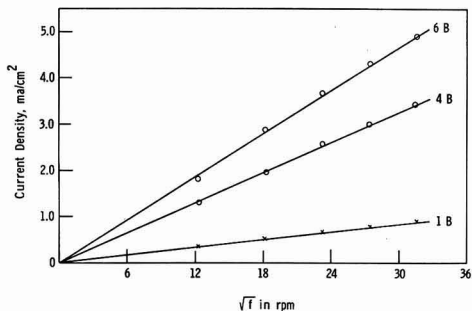
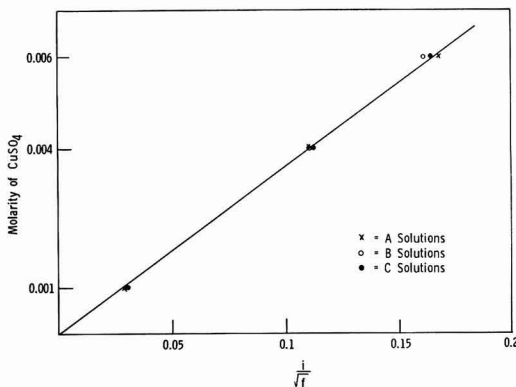


Fig. 3. Current density vs. root frequency for a series typical of electrolytes used.

Fig. 4. Plot of slope,  $i/\sqrt{f}$ , *vs.* molarity of cupric sulfate solutions



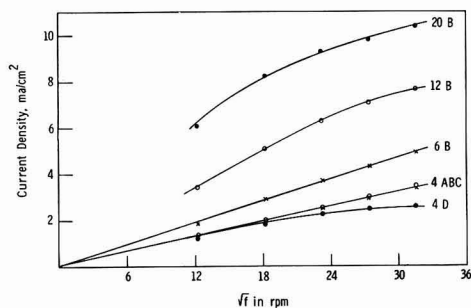


Fig. 5. Current density vs. root frequency for some extreme values of electrolyte composition.

plot for solution 6B is included for comparison. A similar deviation is observed for the plot of solution 4D which is compared with solutions 4A, B, and C. Apparently the compositions of solutions 12B, 20B, and 4D do not provide the electrolyte characteristics required to meet the predictions of rotating disk electrode theory.

#### Discussion

It is apparent that the predictions of rotating disk electrode theory may be met under certain very carefully controlled conditions. Analysis of the results shows that plots of current density vs. root frequency are straight lines passing through the origin when the ionic ratio of potassium ions to cupric ions is fifty or larger. Solutions with a ratio of fifty and up show straight lines; solutions 12B, 20B, and 4D, having ionic ratios of 33.3, 20, and 25, respectively, deviate from a straight line. Apparently an electrical transport factor is introduced, and

transfer of metal ions to the electrode is no longer diffusion and convection controlled. It appears safe to assume that ionic ratios above fifty provide electrolyte conditions which are suitable for investigating the influence of organic additives on the electro-deposition of copper.

Manuscript received Dec. 21, 1961; revised manuscript received Feb. 19, 1962. This paper was prepared for delivery before the Detroit Meeting, Oct. 1-5, 1961.

Any discussion of this paper will appear in a Discussion Section to be published in the December 1962 JOURNAL.

#### REFERENCES

1. V. G. Levich, *Acta Physicochim., URSS*, **17**, 257 (1942).
2. V. G. Levich, *Discussions Faraday Soc.*, **1**, 37 (1947).
3. Yu. G. Siver and B. N. Kabanov, *Zhur. Fiz. Khim.*, **22**, 53 (1948).
4. E. A. Hogge and M. B. Kraichman, *J. Am. Chem. Soc.*, **76**, 1431 (1954).
5. D. P. Gregory and A. C. Riddiford, *J. Chem. Soc.*, **1956**, 3756.
6. J. D. Newson and A. C. Riddiford, *This Journal*, **108**, 695 (1961).
7. *Ibid.*, **108**, 699 (1961).
8. Yu. Yu. Matulis and M. A. Mitskus, *Trudy Akad. Nauk Litvoskii, SSSR*, Ser. B, **1958**, [1], 39.
9. E. Baydevskii and S. Toskev, *Doklady Akad. Nauk. SSSR*, **130**, 1047 (1960).
10. T. von Karman, *Z. angew. Math. Mech.*, **1**, 244 (1921).
11. W. G. Cochran, *Proc. Camb. Phil. Soc.*, **30**, 365 (1934).
12. C. Wagner, *J. Appl. Phys.*, **19**, 837 (1948).
13. K. Millsaps and K. Polhausen, *J. Aeron. Sci.*, **19**, 120 (1953).
14. N. Gregory, J. T. Stuart, and W. S. Walker, *Phil. Trans. Royal Soc.*, **248**, 155 (1955).
15. L. Meites and T. Meites, *Anal. Chem.*, **20**, 984 (1948).

## A Flow Synthesis of Gallium Phosphide and Some Properties of Gallium Phosphide Powder Layers

Lewis J. Bodi<sup>1</sup>

General Telephone & Electronics Laboratories, Incorporated, Bayside, New York

#### ABSTRACT

A simplified synthesis of gallium phosphide powder in an open flow-system is described. Phosphorus vapor is carried over gallium(III) oxide by a stream of hydrogen. The oxide undergoes complete conversion to phosphide at about 1000°C. A thermal treatment enhances average particle size, and electroded GaP powder layers are fabricated. Electrical properties and electroluminescence characteristics of these layers are reported.

The projected utilizations of the unique properties of gallium phosphide have effectively dictated approaches to its synthesis which are directed at yields of single crystals. The simplest synthesis from a chemical standpoint is the most complicated in terms of implementation. Gallium is generally induction heated in a graphite container which is part of a two or three thermal-zone, sealed-quartz system. A phosphorus atmosphere is maintained by one of

<sup>1</sup>On leave from Department of Chemistry, Brooklyn College, Brooklyn, New York.

the heated zones which acts as a phosphorous reservoir. The attainment of sound polycrystalline ingots in such a system requires the maintenance of the equilibrium phosphorous pressure (~20 atm) at the melting point of the stoichiometric material (~1500°C) to facilitate zone refining. These conditions of pressure and temperature are stringent impositions on such systems, and the system of Froesch and Derick (1) aptly illustrates the degree of sophistication necessary to idealize the experi-

mental conditions. Other syntheses have been published, however, in which the synthesis' reaction is not a direct combination of elements. Notable among these are the efforts of Antell and Effer (2, 3) which, in addition to providing a variety of approaches utilizing sealed systems, also include an open-flow-system procedure. Recently, Gershenzon and Mikulyak (4) described a preparation in which a mixture of gallium and gallium (III) oxide reacted to form the suboxide which in turn reacted with phosphorus vapor in a sealed two-thermal-zone system. An interesting variety of single crystal morphologies resulted, but the reaction failed to go to completion.

Among the properties of gallium phosphide which suggest device application the electroluminescent character is of particular interest in these Laboratories. The possibility of employing this material in the preparation of a broad area light source is especially intriguing because of its fast ( $\sim 10^{-8}$  sec) response to stimulating fields (5). One broad area electroluminescent source of simple conception but of considerably more challenging execution is the single crystal containing a p-n junction which has been effected by impurity in-diffusion. The difficulty of attaining this end begins with the aforementioned, nontrivial problem of producing uniform-cross section, single-crystal ingots of GaP. It is evident that a broad area light source consisting of gallium phosphide powder should have the double advantages of simplified fabrication of the light producing layer and of an easing of the stringent pressure-temperature conditions attending synthesis. It was this interest in a powder technology of gallium phosphide, promoted to some extent by occasional calamitous experiences with sealed system syntheses of GaP, which provoked a search for a chemically reliable powder preparation which presents no explosion hazard.

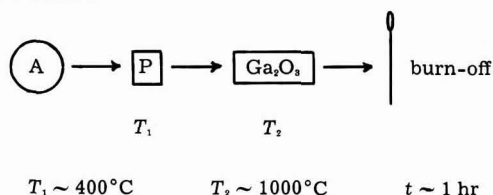
### Synthesis

Previous to the development of an open-flow synthesis of gallium phosphide, sealed tube syntheses were successfully carried out which established the method which would eventually be employed. Phosphorus and gallium (III) oxide were sealed into a quartz ampoule. The ampoule was sufficiently long to permit heating in a two-zone furnace. The vapor pressure controlling end was heated to about  $400^\circ\text{C}$ , the reaction end containing the oxide to about  $1000^\circ\text{C}$ . A brownish granular product resulted which gave a clean, GaP x-ray diffraction pattern. All of the oxide underwent conversion. The reaction is presumed to be the reduction of the oxide to the phosphide accompanied by the formation of oxides of phosphorus.

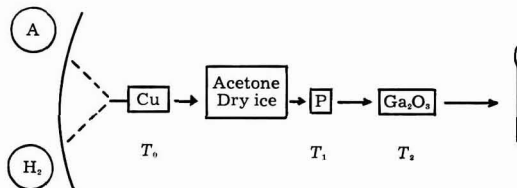
The GaP produced consisted of powder, of about the fine state of subdivision of the starting oxide, and a surface mat of needles. It would seem that the latter is a recrystallization of the initially formed powder by a vapor phase transport mechanism.

Although the approach described was successful chemically, it did not provide the stability guarantees which were desired; several such tubes achieved self-destruction while undergoing post-reaction cooling. Examination of the tube fragments in those cases revealed the existence of an inner surface

layer of a gallium silicate (indicated by x-ray diffraction analysis) suggesting that the synthesis runs were terminated by differential thermal contraction between the quartz envelope and the adhering silicate. Although surface silicate formation could have been prevented by appropriate modification of the oxide position within the tube, it was decided to attempt the same synthesis in an open system. An inert carrier gas was to be used to transport phosphorus vapor over the gallium oxide. To that end, the following system was set up employing argon as the carrier



The product was an orange-pink material which, under the microscope, was seen to consist of a mixture of separate orange and white granules. X-ray diffraction analysis indicated the presence of GaP and GaPO, as major phases. The incompleteness of the reaction (or re-oxidation of product) was attributed to the presence of oxygen and/or moisture in the system. To reduce these the system was modified to include a copper trap for oxygen which was maintained at  $500^\circ\text{C}$  and a dry-ice, acetone moisture trap. The product which resulted from the modified system was not an improvement over the initial flow-system material. The copper turnings exhibited no darkening indicating the low oxygen content of the argon. The acetone-dry ice trap did, however, pick up observable moisture. At this point it seemed evident that an additional source of oxidizing impurity must be the phosphorus itself (Fisher P. 99). It is known that this grade of phosphorus contains moisture, phosphoric acid, oxides of phosphorus, and water soluble salts. Because of the oxidizing nature of the impurities a reducing carrier was utilized to resolve the difficulty. (Although purer phosphorus was available the necessity for break seals for such phosphorus detracted from the over-all objective of operating simplicity.) A consequent system modification resulted in:



Conditions of time and temperature were those of the preceding synthesis attempt. Argon was used to flush the system prior to and following the hydrogen flow which was maintained during heating of the gallium oxide. The effect of the reducing atmosphere was decisive. The product was a granular orange-brown material covered with a mat of needles (Fig. 1 and 2). A well-defined x-ray diffraction pattern verified the presence of a single

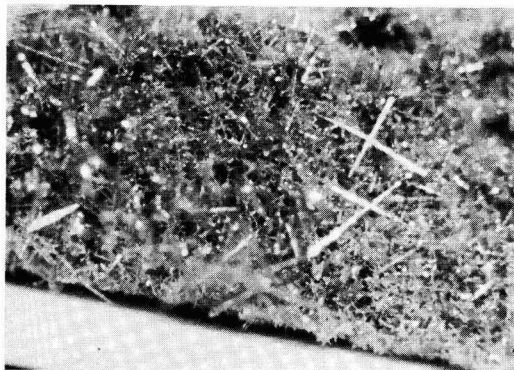


Fig. 1. Mat of GaP needles covering crucible resulting from reaction of phosphorus with gallium (III) oxide. Magnification about 30X.



Fig. 2. Fine grained GaP underlying the surface mat of GaP needles. Magnification about 30X.

cubic phase consisting of gallium phosphide. Spectroscopic examination of the starting  $\text{Ga}_2\text{O}_3$  (prepared in our laboratories by high-temperature oxidation of  $9^\circ$  gallium in a vitreous vessel) revealed the presence of traces of Al, Cu, Fe, and Mg as well as Si at higher levels ( $\sim 200$  ppm). The resulting GaP contained the preceding plus additional traces of Ni, Mn, and Cr which had evidently been introduced when the  $\text{Ga}_2\text{O}_3$  was milled. The red phosphorus seems not to have been a source of additional impurities.

#### Recrystallization and Layer Preparation

The product obtained in the described synthesis was of approximately the same grain size as the parent gallium oxide, namely submicron to micron. In the applications for which the powder was intended, particle size is important and growth from the micron range was necessary. Because of the relatively high volatility of gallium phosphide, the appreciation of particle size posed no real difficulty. That vapor transport is the probable grain growth mechanism is indicated by our experiments in which appreciable crystal growth was observed on the upper walls of crucibles in which GaP powder was heated at as low as  $900^\circ\text{C}$ . The small grained gallium phosphide was sealed into an evacuated quartz ampoule which was rotated in a furnace

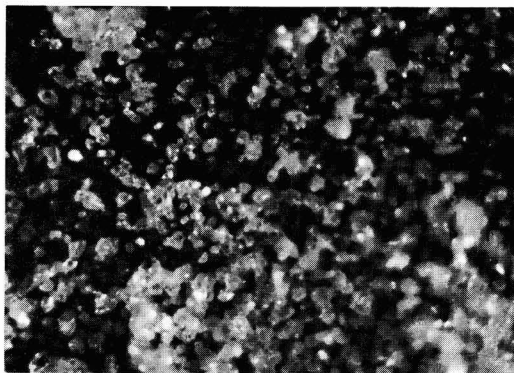


Fig. 3. Material of Fig. 2 after recrystallization. Magnification about 30X.

at  $1050^\circ\text{C}$  for several hours. The appreciation in particle size can be readily observed by reference to Fig. 2 and 3. Although it would have been possible to conduct experiments which would relate time and temperature of heating to particle growth, granules in the desired size range were obtained by conventional milling and sieving of the recrystallized material. The usual techniques of layer preparation were utilized. The properties of such layers do, not unexpectedly, exhibit some dependence on the mode of construction. In these laboratories powder layers of gallium phosphide have been prepared by spraying, settling, and blade spreading. Each method involves the use of a binder. Various organics and low-melting inorganics have fulfilled that function. Phosphor particle size is limited to a narrow range to eliminate the problems attending layer preparation when an indiscriminated milling mix is employed. The foremost of these problems is that of obtaining a continuous evaporated aluminum electrode on the exposed side of the powder layer. The other and transparent electrode is tin oxide coated glass.

#### Current-Voltage Characteristics of GaP Powder Layers

The presence of p-n junctions in gallium phosphide is indicated by the light emission observed in excited crystallites at intergranular boundaries (6). In addition there seem to be point-like regions in the crystalline material with p-n junction character judging by the roles of these sites as well-defined light sources in electric field (7-9). That preferred junction sequences seem to exist in crystallites of GaP is indicated by the rectifying properties they exhibit when identical electrodes are used as anode and cathode. Because of the randomness of grain orientation in a powder layer it would not be expected that the layer exhibit rectification except as the possible result of differences between the contacts, in this case  $\text{SnO}_2$  to GaP and Al to GaP. Such differences are mitigated in the present consideration by the intervening binder. It cannot be stated with certainty, however, that all of the grains are completely encapsulated. A voltage-current plot for a gallium phosphide powder layer with a plastic binder is represented in Fig. 4. It can

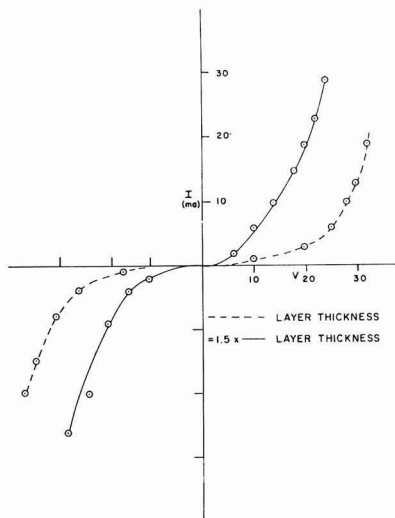


Fig. 4. Current-voltage plot for a gallium phosphide powder layer with a plastic binder. The contacts are  $\text{SnO}_x$  and evaporated aluminum.

be readily appreciated that significant rectification does not take place. (However, below the milliampere level there is frequently an order of magnitude or so difference between the conductivities corresponding to the two polarities). Figure 5 depicts a log-log plot of current *vs.* voltage. No simple relationship of the type  $I = KV^n$  fits the data. The nonlinear character of current as a function of voltage is reflected in the slopes of the plot. At low voltages, the current increases as roughly the square of the voltage, whereas at high voltages for some layers an extrapolated  $n$  value of 13 has been observed. Plotting the log of  $I$  *vs.*  $V$  yields connected linear segments. Each segment obeys the diode equation:  $I = I' \exp(V/V' - 1)$ , Fig. 6. The discontinuities represent abrupt changes of the parameters  $I'$  and  $V'$  as a function of the applied voltage. Individual crystallites exhibit a similar  $I$ - $V$  relationship.

#### Electroluminescent Characteristics

Figure 7 shows a gallium phosphide powder layer as it appears under d.c. excitation and viewed through the transparent contact. Brightness measurements were made as functions of voltage and current. The photo measurements were made employing a Wratten No. 106 eye response compensated filter and a 1P21 photomultiplier feeding a Photovolt Model 520-M photometer. Brightness measurements were limited in voltage range by the sensitivity of the measuring system on the low voltage side and by excessive heating of the cell on the high voltage side.

A plot of brightness *vs.* power is presented in Fig. 8. The linearity observed for powder layers has also been observed for the emission from sintered pressed-pellets of gallium phosphide powder. A plot of the log of the brightness against  $V^{-1/2}$  also yields a linear plot. The functional relationship between brightness and voltage for the two cases is vastly different and the simultaneous linearities must be

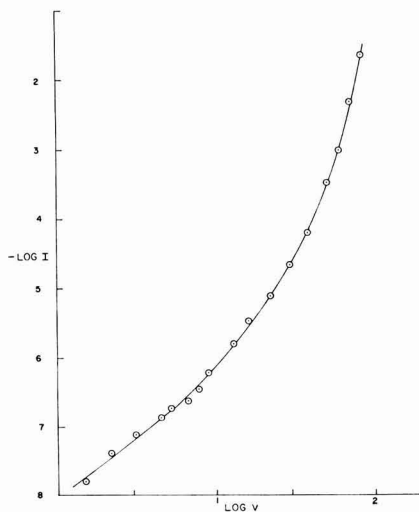


Fig. 5. General current-voltage relationship for a layer as in Fig. 4 on a log-log plot.

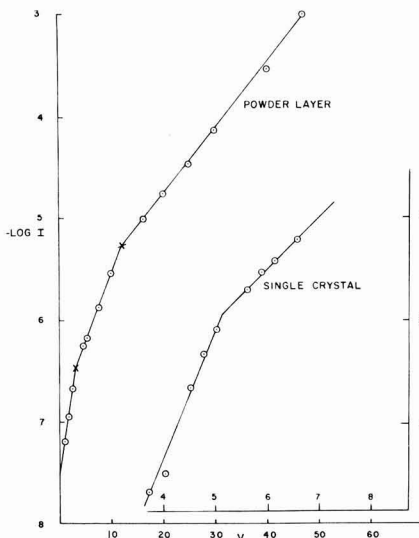


Fig. 6. Log  $I$  *vs.*  $V$  plot for a GaP powder layer and for a small single crystal illustrating adherence to the diode equation.

an accident of the narrowness of the voltage range encountered in these measurements. Wolff, Hebert, and Broder (10) have previously reported the linear character of a  $\log B$  *vs.*  $V^{-1/2}$  plot over a range of voltages somewhat broader than those of the author's measurements.

Microscopically the layer looks identical for reversed polarities. Light is seen to originate in point-like regions within the granules (not all of the granules by any means). The light emitted at these sites appears to be of considerably different spectral distribution than that which seems to characterize the layer as a whole. The latter is somewhat orange while the former is yellow-green. The difference between the two is due to optical filtering by the



Fig. 7. GaP powder layer photographed under its own emission while d.c. excited.

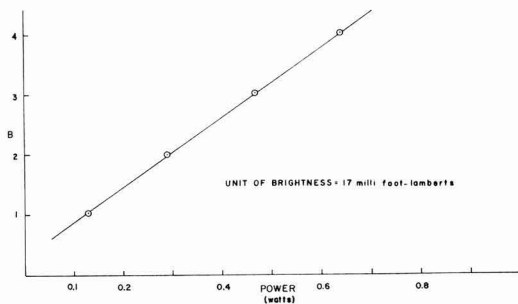


Fig. 8. Brightness vs. power for a gallium phosphide powder layer

granules. The efficiency of the powder layer as a light source has been calculated to be of the order of  $10^{-4}$  lumens per watt. After the eye response character of the measured brightnesses has been taken into account, as well as internal absorption, the efficiency is of the order of  $10^{-7}$  photons per electron.

### Summary

Gallium phosphide can be synthesized by flowing phosphorus vapor in a hydrogen carrier gas over gallium (III) oxide. The oxide should be maintained at about  $1000^{\circ}\text{C}$ ; the phosphorous reservoir at about  $400^{\circ}\text{C}$ . Moisture and oxygen traps in the flow train reduce the oxidant content of the carrier gases. The product can undergo a subsequent heat-

ing in a sealed-evacuated ampoule to effect particle size appreciation. The recrystallized material, after mechanical sizing has been carried out, may be used to make powder layers of gallium phosphide. Such layers have been fabricated and exhibit minimal rectification. Light emission from the layers is simultaneously linear in  $I \times V$  and in  $\exp(aV^{-1/2})$ . This seems to be a consequence of the limited range in  $V$  over which brightness measurements were made. As light sources, the layers have efficiencies of approximately  $10^{-4}$  lumens per watt which correspond to about  $10^{-7}$  photons per electron.

### Acknowledgments

The technical assistance provided by Mr. James Yee, Jr. and Mr. Robert Fuller was of great value in the course of this investigation. Also contributing significantly to this research effort was Dr. Rubin Summergrad who initiated the powder layer studies. Special thanks are the due of Dr. Albert K. Levine for the encouragement which led to the author's researches in semiconductors. Dr. Paul Goldberg and Dr. Donald Baird made helpful suggestions pertaining to the manuscript.

Manuscript received Jan. 4, 1962; revised manuscript received Feb. 26, 1962.

Any discussion of this paper will appear in a Discussion Section to be published in the December 1962 JOURNAL.

### REFERENCES

1. C. J. Frosch and L. Derick, *This Journal*, **108**, 251 (1961).
2. G. R. Antell and D. Effer, *ibid.*, **106**, 509 (1959).
3. D. Effer and G. R. Antell, *ibid.*, **107**, 252 (1960).
4. M. Gershenson and R. M. Mikulyak, *ibid.*, **108**, 548 (1961).
5. J. W. Allen, Tech. Rpt. No. 119, Services Electronics Research Lab., July 1961.
6. G. F. Alfrey and C. S. Wiggins, International Congress on the Physics of Solid State, Brussels, 1958, vol. 2, part 2, p. 747, Academic Press, Inc., New York (1960).
7. M. Kikuchi and I. Iizuka, *J. Phys. Soc. Japan*, **15**, 935 (1960).
8. J. W. Allen and P. E. Gibbons, *J. Electronics and Control*, **7**, 518 (1959).
9. M. Gershenson and R. M. Mikulyak, *J. Appl. Phys.*, **32**, 1338 (1961).
10. G. A. Wolff, R. A. Hebert, and J. D. Broder, *Phys. Rev.*, **100**, 1144 (1955); Proceedings of the International Colloquium on Semiconductors and Phosphors in Garmisch, Interscience Publishers Inc., New York (1958).

# Preparation and Properties of ZnO Phosphors

Arnold Pfahnl

Bell Telephone Laboratories, Incorporated, Murray Hill, New Jersey

## ABSTRACT

ZnO phosphors were prepared at a variety of firing temperatures according to the reaction  $2\text{ZnO} + \text{ZnS} \rightarrow 3\text{Zn (excess)} + \text{SO}_2$ . The absolute values of the cathodoluminescent intensity,  $I$ , and the decay time,  $\tau$ , were determined for the green emission band of these phosphors at 5 ma/cm<sup>2</sup> and 10 kv excitation. The temperature dependence of  $I$  and  $\tau$ , the form of the decay, the dependence of  $\tau$  on exciting current density, the aging characteristics, and the spectral distribution were also measured.

It was found that, at liquid nitrogen temperature,  $I$  and  $\tau$  are nearly constant for all samples regardless of the firing temperature used during the phosphor preparation. As the sample temperature is raised above that of liquid nitrogen,  $I$  and  $\tau$  both become temperature dependent, which is attributed to nonradiative quenching processes that compete with the luminescent transitions. At room temperature a nearly linear relationship exists between  $I$  and  $\tau$ . This behavior is independent of sample preparation methods or commercial source of the phosphor. It was also observed that the decay was nonexponential and that  $\tau$  is dependent on the exciting current density, which shows that the green luminescence is the result of a second-order recombination process. The influence of the firing temperature on the structure of the luminescent center is also evident from the increased aging rate of those samples which were prepared at higher temperatures.

Many different conditions and methods of preparation are reported in the literature for luminescent ZnO (Table I). The present work describes some of the properties of phosphors obtained according to the reaction  $2\text{ZnO} + \text{ZnS} \rightarrow 3\text{Zn (excess)} + \text{SO}_2$ .

Emphasis in this study has been placed on the relationship between emission intensity and decay time of the green emission, and no attempt was made to investigate the relationship between the green and the u.v. emission. High emission intensities and decay times  $\leq 250$  nanosec were desired, in view of the intended use of a phosphor of this type in a special purpose flying-spot scanner cathode-ray tube (1,41).

Results also were sought which may contribute to a better understanding of the basic processes involved in the green luminescence of ZnO.

Table I. Preparation conditions for ZnO phosphors as indicated in the literature

Emission	Preparation	Reference
Blue	Zn in O	(2-5)
	Zn in N <sub>2</sub>	(6)
Green	Zn in O, incomplete	(7)
	ZnS in O or air	(4, 6-10)
	ZnO in CO	(3)
	ZnO in H <sub>2</sub>	(3, 6, 8, 10-13)
	Zn(OH) <sub>2</sub> in H <sub>2</sub>	(7, 14)
	ZnCO <sub>3</sub> in H <sub>2</sub>	(6, 8, 10, 15)
	ZnO in vacuum	(16)
	ZnO + ZnS in N	(6, 13)
	ZnO + S in N	(17, 18, 26)
	ZnS + Pb in O	(17)
	ZnO + Bi in H <sub>2</sub>	(11, 18, 19, 27)
Orange	ZnO + MgO + LiSO <sub>4</sub>	(20, 28)
	ZnO + NH <sub>4</sub> Cl	(16)
	Zn + S	(25)
	ZnO in O	(7, 12, 21)
	ZnO in O + Ga, Al, Gd, Cl, Br	(22)

## Experimental

For the preparation of the phosphors, 5 or 10g of ZnO (r.p.) + X weight % ZnS (X = 0,1,5,10,15) were fired for 1 hr at various temperatures in covered quartz crucibles and in an atmosphere of nitrogen. The samples were cooled rapidly after firing.

All samples used in the present experiments were prepared from the same batches of ZnO and ZnS, as some variations in the emission intensity were found among batches from different producers. It was necessary that the luminescent pure (l.p.) grade of ZnS be used, since the use of reagent pure (r.p.) grade resulted in a considerable reduction of the emission intensity (Table II).

For the cathode-ray tube screen preparation, the phosphor was suspended in a solution of potassium silicate using ultrasonic agitation and was then settled on microscope slides with barium nitrate as the coagulant. A series of tests on several selected samples showed that the ultrasonic treatment did not change the intensity or the decay time. For each phosphor sample, the optimum screen weight was determined by measuring the emission intensity as a function of the screen weight.

Table II. Emission Intensity of ZnO + 5% ZnS Samples prepared with combinations of base materials from various producers

Firing time: 1 hr; firing temperature: 850°C; excitation: mercury lamp with blue glass filter

ZnO batches (all r.p.)	ZnS batches (all l.p. except c)	Intensity
A	a	29
A	b	30
B	a	30
B	b	31
A	c (r.p.)	10

The particle size of the phosphors increases with the firing temperature and reaches an average of about 30-40 $\mu$  for the samples fired at the highest temperatures. This is well within the limits of the particle size of commercial samples. On the other hand it was found that it is possible to change the particle size distribution considerably without reducing the maximum intensity if careful mechanical treatment (grinding) is applied. The grain of the screens obtained with the present powders is comparable to that of screens prepared with commercial samples of ZnO (Zn).

A demountable cathode-ray tube was used to measure the emission intensity and decay time. All data (except aging data) were taken under identical excitation conditions (anode voltage 10 kv; current density 5 ma/cm<sup>2</sup>; pulse length 5  $\mu$ sec; repetition frequency 1000 pulses/sec). These are the operation conditions under which the cathode-ray tube would be finally used (1), but they are milder than those of other flying-spot scanner operations where the product of excitation time for a screen element and the current density may be increased by a factor of ten.

The green emission from the side opposite from that of excitation was detected by a photomultiplier with S11 response. The u.v. emission band was filtered out (Corning filter CS3-72, 2.9 mm thick). The photocurrent was displayed on an oscilloscope. The time constant of the circuit was small enough to permit measurement of decay times down to 50 nanosec.

The aging data, needed in practical phosphor applications for the determination of the useful screen life, were obtained with sealed-off cathode-ray tubes having aluminized screens (seal-off pressure 10<sup>-7</sup> mm Hg). Clean vacuum conditions were required during aging measurements, since burn from positive ions or contamination from back-streaming pump fluid vapors might otherwise have introduced major errors (29). To reduce the aging time, a stationary beam was used with the beam focused to a power density of 0.5 w/cm<sup>2</sup> at the phosphor screen. This is low enough to avoid thermal damage.

The spectral distribution of the fluorescent emission was determined with a Bausch and Lomb "Model 250 mm" monochromator and a photomultiplier tube. An absolute calibration of the ensemble was made.

## Results

**Emission intensity and decay time.**—At and above room temperature, the emission intensity and the decay time (measured at the 1/e point) depend strongly on the firing temperature (Fig. 1). The intensity increases with the firing temperature up to about 1100°C and then decreases monotonically. The decay time goes through a similar maximum, which is about 100°C lower than that of the intensity. Samples fired at higher temperatures have, consequently, shorter decay times for equal emission intensities. Similar curves are obtained for preparation with 1%, 10%, and 15% ZnS content.

The data for the 20°C curve of Fig. 1 are replotted in Fig. 2 showing the decay time  $\tau$  as a function of

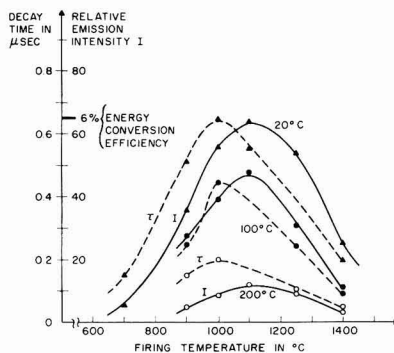


Fig. 1. Relative emission intensity  $I$  and decay time  $\tau$  of ZnO(Zn) phosphors as a function of the firing temperature. Base material: ZnO + 5% ZnS; atmosphere: nitrogen; firing time: 1 hr. Phosphor temperature varied from 20° to 200°C.

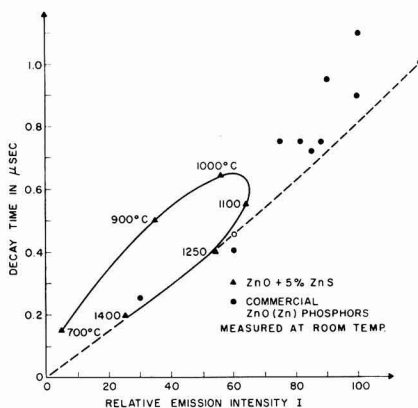


Fig. 2. Decay time  $\tau$  vs. emission intensity  $I$  for ZnO(Zn) phosphors prepared at various firing temperatures, as well as for several industrial samples.

the emission intensity  $I$ . This is a convenient method of determining the quality of a phosphor sample when the shortest decay time at a given intensity is sought. The lower part of this curve, corresponding to the higher firing temperatures, can be continued through the points representing the best ZnO phosphor samples obtained from various industrial sources. This shows that, at the present state of the art, most of the industrially produced ZnO phosphors possess nearly the optimum combination of decay time and intensity, but it does not mean that this curve necessarily represents a physical limit. Improvements in the quality (purity) of the base materials may lead to improved quality of the phosphors (see Table II).

A comparison between the commercial samples and those prepared in the present experiments shows that most of the former have higher intensities than the latter (Fig. 2). The method used for the preparation has certainly a strong influence on the maximum intensity as can be seen in Fig. 3 where the results of various preparation methods and commercial samples are compared. The highest intensity in the present experiments was obtained by the oxidation of luminescent pure ZnS, but this

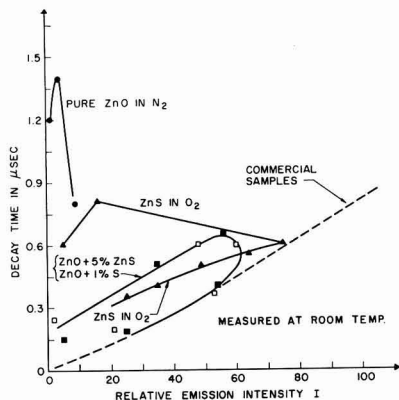


Fig. 3. Relative emission intensity  $I$  vs. decay time  $\tau$  for ZnO(Zn) phosphors prepared by various methods.

is still about 20% below the maximum found for commercial samples. Another possible method to achieve higher intensities would be doping [ref. (17), Table I]. Further investigation would be necessary to elucidate this point.

It is interesting to note that ZnO phosphors prepared according to various other methods have quite similar properties. This is shown in Fig. 3, where the emission intensities and the decay times of ZnO + 5% ZnS are compared with the values measured on ZnS oxidized in pure  $O_2$  for 20 min, ZnO + 1% S fired in  $N_2$ , and reagent-pure ZnO fired in  $N_2$ . ZnS oxidized at a temperature greater than  $1000^\circ C$  rapidly loses its green luminescence and acquires properties similar to calcined pure ZnO.

Data for a fixed firing temperature of  $1000^\circ C$  and varying ZnS concentrations are given in Fig. 4. ZnO without a special addition of ZnS exhibits very low intensities but long decay times of the order of  $1 \mu sec$  when fired at  $1000^\circ C$ . Addition of 1% ZnS causes an increase of the intensity and a decrease of the decay time. Greater concentrations of ZnS have relatively little effect.

The presence of larger quantities of sulfur in the samples fired below  $1000^\circ C$  (see section on Analysis of samples) indicated that, at these firing temperatures, a firing time of 1 hr may not suffice to complete the reaction. A few experiments with various

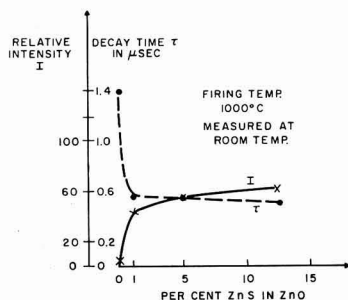


Fig. 4. Emission intensity  $I$  and decay time  $\tau$  as a function of increasing ZnS content in the ZnO + ZnS preparation. Firing time, 1 hr.

firing times, up to 6 hr, at a firing temperature of  $850^\circ C$  showed a continuous increase of  $I$  with firing time, in which  $I$  was proportional to the logarithm of the firing time. To reach the full intensity of 65 rel. units measured at room temperature, a firing time of over 12 hr would be necessary as shown by an extrapolation. At  $910^\circ C$ , the intensity reaches 90% of its saturation value after 1 hr. At  $1100^\circ C$ , less than 7 min are necessary. For the purpose of practical ZnO phosphor preparation, firing temperatures at or above  $1000^\circ C$  therefore seem advisable.

If the temperature of the sample is lowered, the intensity,  $I$ , increases monotonically, the rate of increase being a function of the firing temperature. If the temperature is lowered from 20 to  $-180^\circ C$  the intensity increases 1.8 times if the sample was fired at or below  $1000^\circ C$ , 2.0 times for a firing temperature of  $1250^\circ C$ , and 4.3 times for a firing temperature of  $1400^\circ C$ . In the vicinity of  $-180^\circ C$  the slopes level off, and a common value of the intensity is reached for all samples except those fired below  $1000^\circ C$  for which the firing time of 1 hr was not long enough to give the maximum possible intensity (Fig. 5). The decay times measured at the 37 and 5% points are also practically constant and independent of the firing temperature if measured at  $-180^\circ C$  (Fig. 5).

Figure 6 shows the decay time,  $\tau$ , as a function of the sample temperature. For the samples fired up

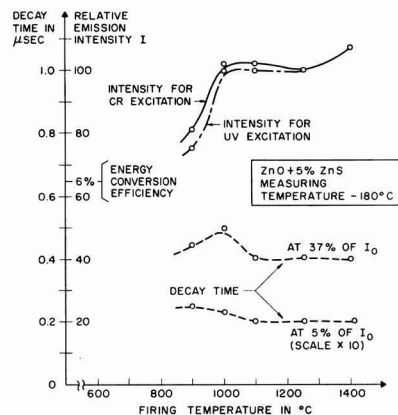


Fig. 5. Emission intensity  $I$  and decay time  $\tau$  of ZnO(Zn) phosphors prepared from ZnO + 5% ZnS as a function of the firing temperature (measured at  $-180^\circ C$ ). Firing time, 1 hr.

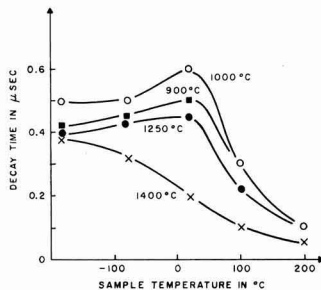


Fig. 6. Variation of the decay time as a function of temperatures. ZnO + 5% ZnS. Firing time, 1 hr.



to 1250°C there is a slight increase of  $\tau$  up to room temperature and then a rather sharp decrease. The sample fired at 1400°C exhibits a steady decrease of  $\tau$  with increasing temperature.

The absolute value of the energy conversion efficiency, which depends on the experimental conditions, was determined by comparison with optical measurement standards developed at this laboratory (30). It was found that the value of 65 rel. units of the intensity scale as used in Fig. 1-5 corresponds to an energy conversion efficiency of 6% for the excitation conditions mentioned in the experimental section above. This is in good agreement with other published data (31) taken at 1-10  $\mu\text{a}/\text{cm}^2$  at 6-8 kv, which indicate an efficiency of 7.5% for a ZnO (Zn) phosphor having approximately 1  $\mu\text{sec}$  decay time.

*Other parameters.*—The form of the decay is nonexponential regardless of the firing temperature of the samples (Fig. 7) or the temperature at which the measurement is taken (Fig. 8).

The decay time is also a function of the current density, as shown in Fig. 9. It decreases by approximately 30% if the current density is increased by a factor 10. This has been found to hold over a range of 1  $\mu\text{a}/\text{cm}^2$  to 50  $\text{ma}/\text{cm}^2$ , with either pulse or raster excitation.

Figure 10 shows the relative aging characteristics of four ZnO phosphors fired at different temperatures. The decrease in intensity due to electron bom-

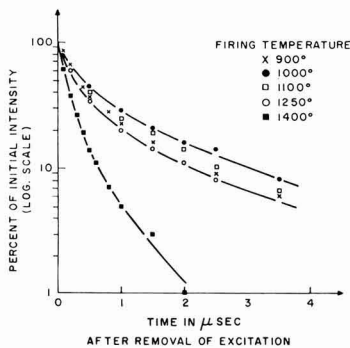


Fig. 7. Form of the decay of ZnO(Zn) phosphors prepared at various firing temperatures. Preparation conditions as in Fig. 6.

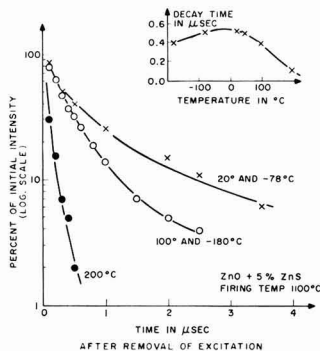


Fig. 8. Form of the decay and decay time  $\tau$  as a function of the temperature for a ZnO(Zn) sample fired at 1100°C.

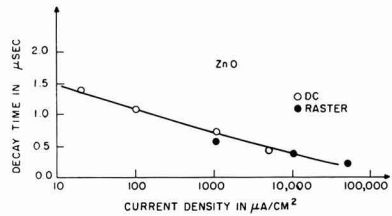


Fig. 9. Decay time of a representative ZnO(Zn) phosphor as a function of the exciting current density.

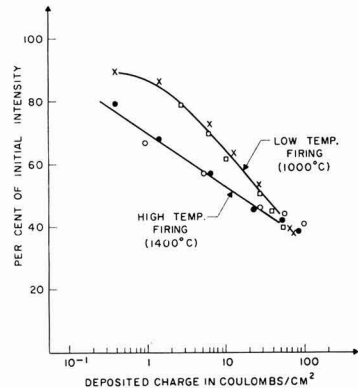


Fig. 10. Relative aging characteristics of ZnO(Zn) phosphors fired at high and low temperature.

bardment has been observed to be most sensitive to the accumulated charge per unit area deposited by the beam and is relatively independent of accelerating voltage; hence coulombs/cm<sup>2</sup> is used as the abscissa of the aging curve. The samples fired at a higher temperature (1400°C) age slightly more rapidly at the beginning than those fired at a lower temperature (1000°C). This is in agreement with observations of the sensitivity of the luminescence to mechanical damage (*e.g.*, grinding) recorded by other authors (32). The curves coincide after a deposited charge of about 100 coulombs/cm<sup>2</sup> has been reached. Some aging data obtained under raster excitation were also available but only for a total deposited charge up to 10 coulombs/cm<sup>2</sup>. No difference in the results was found.

The green emission spectrum of six representative samples fired between 900° and 1400°C was determined at various temperatures ranging from -180° or +130°C. The spectra were found to be identical, each having its maximum at 500  $m\mu$  regardless of the firing temperature, the measurement temperature, or the amount of ZnS in the base material before firing. This is in good agreement with data published in the literature (40).

*Analysis of samples.*—A mass-spectrometric analysis of the gases liberated from three representative fired samples by reheating at 650°C under high vacuum showed that sulfur is still present in quantities up to about 0.01% of the initial content (Table III). The quantities of SO and SO<sub>2</sub> liberated decrease exponentially for a linear increase of the firing temperature. The remaining sulfur is present in the form of ZnS which was shown by the

Table III. Gas quantities (in  $\text{cm}^3\text{-mm}$ ) liberated from 1g samples of ZnO phosphors heated under vacuum at 650°C, as determined by mass-spectrometric analysis

Sample composition before firing: ZnO + 5% ZnS							
Firing temp, °C	H <sub>2</sub>	CO	H <sub>2</sub> O	CO <sub>2</sub>	SO	SO <sub>2</sub>	CH <sub>4</sub>
700	91.2	90.3	243.4	82.3	20.4	26.3	—
1100	22.9	93.5	51.1	55.2	5.2	1.9	—
1400	8.2	12.6	0.6	13.2	0.1	1.4	—
Commercial sample	57.0	11.5	14.0	68.0	—	—	0.63

detection (by means of x-ray diffraction) of  $\alpha$ -ZnS crystals in the green luminescent samples fired at 1000° and 1400°C. At 1400°C the crystallites have grown large enough to give a relatively strong diffraction pattern. The analysis of an industrial sample with similar luminescent properties revealed no sulfur.

### Discussion

ZnO is typically an n-type semiconductor, with donor levels at 0.04 to 0.05 ev. They result from an interstitial excess of Zn in concentrations ranging from  $10^{15}$  to  $10^{18}$  atoms/cm<sup>3</sup>, depending on the mode of preparation of the material (33). Green luminescence appears if ZnO is prepared under reducing conditions (see Table I), which produces a further excess of Zn. The oxygen vacancies corresponding to the deviation from stoichiometry must be produced during the formation of the crystal and cannot be obtained by a reducing agent acting solely on the surface (7).

Based on these and other considerations, it has been proposed by various authors that the green luminescence corresponds to a transition from Zn<sup>+</sup> to Zn<sup>2+</sup> in the excess Zn ions (23) or to a transition in an oxygen vacancy (7, 42b).

As an alternative explanation, it has been advanced that the green band could be the result of a small amount of ZnS (0.1% or less) present in solid solution in the ZnO (26).

On the basis of the experiments previously reported, it is not possible to decide between these two interpretations, even though the mass spectrometric analysis of the green luminescent industrial sample did not reveal any sulfur content (see the Experimental section above). Therefore high-purity Zn 99.9998% was oxidized, and it was found, in agreement with other authors (22), that a green luminescent ZnO was formed. The reducing agent (ZnS, S, etc.,) consequently would serve only to create oxygen vacancies in the ZnO lattice. Considering the high sensitivity of the luminescent materials to small amounts of impurities further investigations would be necessary to ascertain the absence of sulfur in these experiments.

At a given firing temperature certainly only a limited number of excess Zn ions and oxygen vacancies can be incorporated in the crystal. This explains the leveling-off of the intensity even when increasing quantities of reducing agent are added to the base material (Fig. 4). (The form of the curves is similar for firing temperatures up to 1400°C where

the reaction is completed before one hour of firing time.)

At low concentrations of the reducing agent (e.g., in the r.p. ZnO containing less than 0.001% S used in the present sample preparation) only a few luminescent centers are formed and the intensity is low. It is also possible in this case that a small amount of oxygen leaves the lattice without requiring the action of a reducer. This also agrees with the observation of the appearance of a new band of dipolar Debye absorption above 1000°C, corresponding to an activation energy of 0.25 ev (35).

From the data shown in Fig. 5 and from the experiments relating the intensity to the firing time it can be concluded that, for the present preparation method, the number of luminescent centers produced in the crystal is independent of the firing temperature. For firing temperatures below 1000°C longer firing times than 1 hr are necessary to incorporate the maximum possible number of luminescent centers, but an increase of the firing temperature from 1000° to 1400°C increases only the number of quenching processes which may be associated with some lattice defects.

The number of these quenching processes is strongly temperature dependent and seems to disappear completely below -180°C. Other limitations on the maximum attainable efficiency must nevertheless still be present, due probably to the basic absorption processes of cathode rays in the phosphor, as the best efficiency at -180°C is only 10% (Fig. 5).

The form of the *I vs. T* curves can be represented by the equation:  $\eta = L/(L+N)$  where  $\eta$  is the luminescent efficiency, *L* the number of radiative, and *N* the number of radiationless transitions. It is generally assumed, that *L* is nearly independent of *T* and that *N* increases rapidly with the ambient temperature of the phosphor. Further measurements extending the range to liquid helium temperature would here be valuable.

The nonexponential decay (Fig. 7, 8) indicates a second-order recombination process between holes and electrons. As green luminescent ZnO has a high dark conductivity (23, 42) there should not be a great change of the electron concentration in the conduction band during the excitation. It could therefore be assumed that the rate-determining process is the trapping of holes in the center. The green emission then takes place immediately after the hole has been trapped. This would be in agreement with the different temperature dependence of decay time as compared to that of intensity, the latter being determined by the action of the quenching process on the luminescent transition, the former by the thermal action on the hole-capture process.

The increase of the decay time at low excess Zn concentrations (Fig. 4) could be explained by the sensitivity of the lifetime of the holes to lattice imperfections (43), which probably increase with increasing amounts of excess Zn. Possibly no impurity conduction band has yet been formed, and the luminescent centers are independent of one another.

At high excitation densities and low center concentration, two effects should consequently be observed: (a) a relative increase of the intensity of the u.v. emission as a consequence of the reduced possibility for recombination via activator centers, and (b) an exponential form of the decay of the green band due to the fact that the number of holes is much greater than the number of centers (at least at the beginning of the decay). Unfortunately the decay form of these samples could not be measured, but an increase in u.v. emission was observed in the present experiments. The hypothesis could also explain that exponential decay forms have repeatedly been indicated in the literature (8, 42).

The decrease of the luminescent efficiency with electron bombardment may result from damage to the luminescent centers (37) or from an increase in the number of radiationless transitions by formation of lattice defects (38). If the luminescent process takes place in a center formed by one or several ions and the electron does not leave this center during the excitation, destruction of a center decreases only the intensity and the decay time remains practically constant. This is the case, for example, with  $\text{CaWO}_4$  (29). Measurements on several samples of ZnO showed (29) that the decay time decreases about 30% after a bombardment with 100 coulombs/cm<sup>2</sup>. This would indicate an increase of the possibility for radiationless transitions. The different aging behavior of crystals prepared at various temperatures indicates also that the aging process is sensitive to structural differences in the lattice.

#### Acknowledgments

This project was under the general direction of R. W. Sears, whose encouragement throughout the study has been most valuable. Mr. R. S. Ehle performed many of the measurements, and his help is greatly appreciated. Mrs. M. H. Read did the x-ray analysis, and E. J. Becker provided the mass spectrometric data.

Manuscript received Nov. 6, 1961; revised manuscript received Feb. 20, 1962. This paper was prepared for delivery before the Indianapolis Meeting, April 30-May 3, 1961.

Any discussion of this paper will appear in a Discussion Section to be published in the December 1962 JOURNAL.

#### REFERENCES

1. C. W. Hoover, G. Haugh, and D. R. Herriot, *Bell System Tech. J.*, **38**, 365 (1959).
2. H. W. Leverenz, "Luminescence of Solids," chap. 3, p. 74, J. Wiley & Sons, New York (1950).
3. R. E. Shrader and H. W. Leverenz, *J. Opt. Soc. Am.*, **37**, 939 (1947).
4. E. Mollwo, *Z. Physik*, **138**, 478 (1944).
5. Gmelin's, "Handbuch d. Anorganischen Chemie," Vol. Zn, p. 125 (1924); pp. 805, 788 (1956).
6. G. Heiland, E. Mollwo, and F. Stockmann, "Solid State Physics," vol. 8, p. 228, Academic Press, New York (1959).
7. N. Riehl and H. Ortmann, *Z. Elektrochem.*, **60**, 149 (1956).
8. H. Gobrecht, D. Hahn, and K. Scheffler, *Z. Physik*, **139**, 365 (1954).
9. Telefunken, Swedish Pat. 97059, 1938/1939.
10. G. Brauer, "Handbuch d. Präparativen Anorg. Chemie," p. 1332, F. Enke, Stuttgart (1951).
11. C. A. Nickle, Fluorescent ZnO, U. S. Pat. 2,408,475, (1951).
12. Keiji Maeda, *Bull. Chem. Soc. Japan.*, **33**, 456 (1960).
13. F. A. Kröger and J. A. M. Dickhoff, *Physica*, **16**, 297 (1957).
14. J. Klikora, J. Horak, and A. Celikovskiy, *Chem. list.*, **52**, 2226 (1958).
15. E. Beutel and A. Kutzelnigg, *Monatsh. Chem.*, **70**, 297 (1957).
16. I. K. Versechagin and V. S. Teslyuk, *Izvest. Vysshikh Ucheb. Zavedenii*, Fig. 6, 114 (1958).
17. H. W. Leverenz, *R. C. A. Rev.*, **7**, 199 (1946).
18. British Thomson-Houston Co., British Pat. 558, 213, 1943.
19. E. G. Pettsold, *Izvest. Akad. Nauk. S.S.S.R.*, Ser. Fiz., **24**, 104 (1960).
20. L. J. Reimert and E. A. Futzinger, U. S. Pat. 2,481,344, 1947/49.
21. V. V. Osiko, *Optika i Spektrosk.*, **7**, 770 (1959).
22. F. A. Kröger and H. J. Vink, *J. Chem. Phys.*, **22**, 250 (1954).
23. F. I. Vergunas and G. A. Konivalov, *J. Exp. H. Theoret. Phys. (U.S.S.R.)*, **23**, 712 (1952).
24. S. R. Morrison, "Advances in Catalysis," vol. 7, p. 262, Academic Press, New York (1955).
25. K. Kamm, German Pat. 859, 782, 1952.
26. S. M. Thomsen, *J. Chem. Phys.*, **18**, 770, 1950; U. S. Pat. 2,573,817, 1949.
27. A. H. Joung, U. S. Pat. 2,734,872, 1956.
28. P. R. Celmer, U. S. Pat. 2,683,293, 1954.
29. A. Pfahnl, "Advances in Electron Tube Techniques," p. 204, Pergamon Press, New York (1961).
30. C. W. Hoover and H. Raag, "Solid State Physics in Electronics and Telecomm.," vol. 4, p. 688, Academic Press, New York (1960).
31. A. Bril and H. A. Klasens, *Philips Res. Repts.*, **7**, 401 (1952).
32. A. Kutzelnigg, *Sitzber. Wiener Akad. Wiss.*, **142**, 715 (1933).
33. A. R. Hutson, *Bull. Am. Phys. Soc.*, **2**, 56 (1957).
34. F. A. Kröger, "Some Aspects of the Luminescence of Solids," pp. 205 ff, Elsevier, New York (1947).
35. M. L. Blanchard, *Compt. rend.*, **244**, 757 (1957).
36. G. F. J. Garlik and M. F. H. Wilkin, *Proc. Roy. Soc.*, **A184**, 408 (1945).
37. Bandow, "Luminescence," pp. 166-170, Wiss. Verlagsges., Stuttgart (1950).
38. I. Broser and W. Reichardt, *Naturforsch.*, **6a**, 466 (1951); *Z. Physik*, **134**, 222 (1953).
39. J. A. Amik, *R. C. A. Rev.*, **20**, 753 (1959).
40. F. H. Nicoll, *J. Opt. Soc. Am.*, **38**, 817 (1948).
41. H. G. Cooper, *Bell System Tech. J.*, **39**, 1161 (1961).
42. (a) A. Pfahnl, to be published; (b) also: E. Mollwo, *Z. Physik*, **162**, 557 (1961).
43. See for example, C. Kittel, "Solid State Physics," p. 369, J. Wiley & Sons, New York (1956).

# Dissolution of Germanium in Aqueous Hydrogen Peroxide Solution

N. Cerniglia and P. Wang

Semiconductor Division, Sylvania Electric Products Inc., Woburn, Massachusetts

## ABSTRACT

The dissolution of germanium in aqueous hydrogen peroxide of from 3 to 90%  $H_2O_2$  and pH from 1 to 9 has been studied at temperatures varying from 25° to 90°C. It has been found that dissolution rate remains constant in solutions of 3-30% by weight of  $H_2O_2$  at low pH, then decreases with increasing  $H_2O_2$  content. The reaction is highly pH dependent above pH 4, and this pH dependence varies as a function of  $H_2O_2$  concentration. This indicates that the rate-controlling step in low and high  $H_2O_2$  concentration solutions at pH 5 and above may be different. Reaction mechanism to explain this situation is proposed.

The use of hydrogen peroxide solution as a final clean-up etch for germanium is an established practice in the semiconductor industry. The use of dilute aqueous hydrogen peroxide solutions as an etch for germanium was first suggested by Camp (1). Miller (2) determined the dissolution rate of germanium at various temperatures in 3.4% by volume hydrogen peroxide solutions of pH 5. The present study has been carried out in order to obtain a better understanding of the mechanism of the dissolution reaction and to determine its dependence on the hydrogen peroxide concentration, temperature, and pH of solution. The effects of the resistivity, resistivity type, and crystalline perfection of the germanium on the dissolution rate also have been studied.

## Experimental

The samples used were 1 x 1.5 x 0.010 in. single crystal n- and p-type germanium of 2 to 6 ohm-cm resistivity.<sup>1</sup> Samples were oriented with the major surfaces in the <111> plane within one degree and were prepared with an aluminum oxide lapped finish. Random area measurements on the slices showed less than 2% variation in apparent surface area. Resistivity measurements on individual samples showed variations less than 5%. Prior to etching, each sample was degreased in trichloroethylene, chloroform, and methanol, dried, cleaned in hydrofluoric acid, and rinsed in distilled, deionized water of better than 15 megohm resistivity. After drying, samples were weighed to the nearest hundredth of a milligram and thickness was measured with a dial micrometer to the nearest tenth of a mil.

Samples were placed in small passivated stainless steel wire baskets and were etched individually in separate beakers containing 150 ml of solution, each maintained within  $\pm 1^\circ C$  of temperature. No agitation of the etchant was used. The heat of reaction was low and quickly dissipated through the beaker so that the reaction was effectively carried out at constant temperature in all cases. At the end of each etch period, the germanium samples were

quickly removed and quenched in a large volume of deionized water. After rinsing and drying, the samples were measured and weighed again.

Samples were etched a number of times in the same solution in order to establish a constant etch rate. The assumption was made that the constant etch rate reached after the work damaged layer had been removed was close to the true etch rate. Since the decrease in thickness per etch period was below the sensitivity of the dial micrometer for the slow etching in very high concentration hydrogen peroxide, the majority of data for etch rate is presented in units of milligrams per square centimeter-hour, in order to be consistent from low to high hydrogen peroxide concentrations.

The etching solutions were prepared by diluting Becco reagent grade 90% hydrogen peroxide (in some cases, electronic grade 30% hydrogen peroxide from Solvay was used to prepare the solutions). Dilutions were volumetrically measured from a burette to the nearest 0.1 ml. Control of the composition for any etch run was established by analyzing for hydrogen peroxide composition using potassium permanganate titration. For dilute solutions in the neutral and alkaline pH regions, the peroxide solutions were neutralized with 10% reagent grade  $NH_4OH$ . Stability of high pH solutions at elevated temperatures was accomplished by addition of a small amount of hydrated sodium stannate. The higher pH samples taken for analysis were acidified with dilute sulfuric acid immediately after quenching in order to minimize hydrogen peroxide decomposition. Precautions to maintain hydrogen peroxide stability during etching made it possible to control the  $H_2O_2$  composition to  $\pm 0.5\%$ . This variation in hydrogen peroxide concentration was less at lower pH and temperatures. During the etching period pH measurements were taken periodically and adjustment was made whenever necessary to control variations within  $\pm 0.1$  pH unit.

## Results

*Dependence of germanium dissolution rate on  $H_2O_2$  concentration.*—A plot of dissolution rate of nondegenerate germanium with respect to  $H_2O_2$  con-

<sup>1</sup> Specific experiments were carried out with germanium specimens of other resistivity ranges.

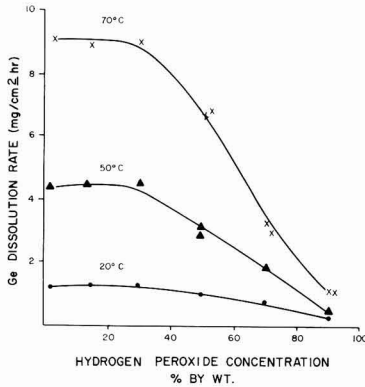


Fig. 1. Germanium dissolution rate as a function of H<sub>2</sub>O<sub>2</sub> concentration.

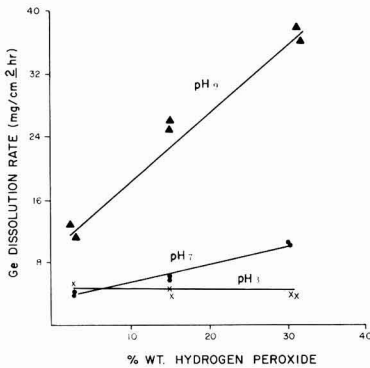


Fig. 2. Dependence of etch rate on H<sub>2</sub>O<sub>2</sub> concentration, pH 3, 7, 9

centration is given in Fig. 1. In H<sub>2</sub>O<sub>2</sub> solutions of 3-30% H<sub>2</sub>O<sub>2</sub> by weight, the dissolution rates at each temperature are essentially constant. Above 30% concentration, they decrease linearly with increasing H<sub>2</sub>O<sub>2</sub> concentration. All the solutions were prepared by diluting 90% H<sub>2</sub>O<sub>2</sub> with water, and no attempt was made to control the pH.

In Fig. 2, germanium dissolution rate is plotted as a function of H<sub>2</sub>O<sub>2</sub> concentration at three pH values. At pH 3 the rate is independent of H<sub>2</sub>O<sub>2</sub> concentration in the range 3-30%. At pH values of 7 and 9, there is a linear relationship between dissolution rate and H<sub>2</sub>O<sub>2</sub> concentration.

*Dependence of dissolution rate on solution temperature.*—The relation between germanium dissolution rate and solution temperature was studied for n-type and p-type nondegenerate germanium and for degenerate n-type germanium. Etching experiments were performed at several H<sub>2</sub>O<sub>2</sub> concentrations ranging from 15 to 90% H<sub>2</sub>O<sub>2</sub> by weight, at several pH values ranging from 1.0 to 9.0, and at four temperatures, 25°, 50°, 70°, and 90°C. In general a 50% increase in dissolution rate is obtained with each 10°C temperature rise. Figure 3 is a plot of dissolution rate as a function of 1/T x 10<sup>3</sup> for n- and p-type germanium of 10<sup>15</sup> atom/cm<sup>3</sup> impurity level etched in 30% H<sub>2</sub>O<sub>2</sub> solution at pH 4.0. The activation energy  $\bar{E}$  is estimated at

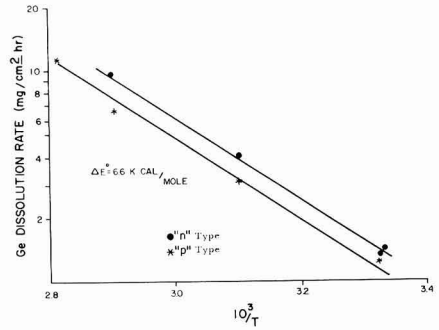


Fig. 3. Dissolution vs. temperature for n and p type germanium in 30% H<sub>2</sub>O<sub>2</sub> aqueous solutions pH 4.

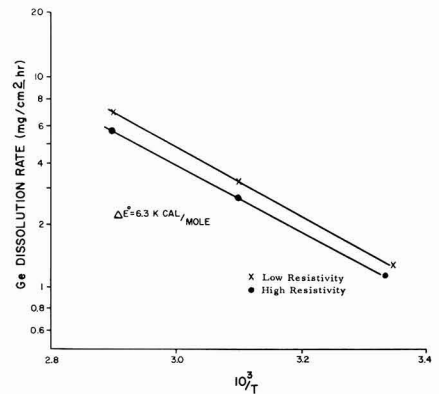


Fig. 4. Dissolution rate vs. temperature for high and low resistivity n type germanium in 30% H<sub>2</sub>O<sub>2</sub> aqueous solutions at pH 4.

6.6 kcal/mole by application of the Arrhenius equation.

Figure 4 plots dissolution rate as a function of temperature for n-type germanium samples of 10<sup>15</sup> and 10<sup>16</sup> atom/cm<sup>3</sup> impurity levels in 30% H<sub>2</sub>O<sub>2</sub> solutions at pH 4.0. The activation energy is estimated at 6.3 kcal/mole.

Table I gives values of estimated activation energy for the dissolution of n-type germanium in aqueous H<sub>2</sub>O<sub>2</sub> solutions determined by these investigations at various solution pH and % composition by weight. Values determined for p-type germanium are quite similar. From these data it is seen that at pH 5 and above the activation energy is about 10.5 kcal/mole and at pH 4 and below the value

Table I. Activation energy for various H<sub>2</sub>O<sub>2</sub> etching compositions using n-type germanium (2-6) ohm-cm

Composition, % by weight H <sub>2</sub> O <sub>2</sub>	pH	Activation energy, kcal/mole
90	1.0	6.4
70	2.1	6.8
50	3.0	7.9
30	4.0	6.6
30	5.1	11.0
30	7.1	11.0
15	4.9	10.0
15	7.0	10.5
15	9.1	10.3

is approximately 6.5 kcal/mole. The activation energy is the same for germanium of both n-type and p-type conductivity and for low and high impurity levels up to  $10^{19}$  atom/cm<sup>3</sup>.

*Dependence of dissolution rate on pH of solution.*

—In Fig. 5, germanium dissolution rates are plotted against pH of solution for etching experiments carried out with n-type nondegenerate germanium in 15, 30, and 50% H<sub>2</sub>O<sub>2</sub> solutions at 50°C. At each H<sub>2</sub>O<sub>2</sub> concentration the dissolution rate stays relatively constant until a critical pH is reached and increases rapidly thereafter. The critical pH is a function of H<sub>2</sub>O<sub>2</sub> concentration. At 50% H<sub>2</sub>O<sub>2</sub> it is 4.5, at 30% H<sub>2</sub>O<sub>2</sub> it is 5.5, and at 15% H<sub>2</sub>O<sub>2</sub> it is 6.0. In Fig. 6 and 7, similar plots are given for dissolution rates in 15 and 30% H<sub>2</sub>O<sub>2</sub> solutions at 25°, 50°, and 70°C. The dependence of dissolution rate on pH increases at higher temperatures.

*Effect of impurity concentration and crystal perfection on germanium dissolution rate.*—Etching experiments were carried out using n-type germanium specimens with resistivities from about 30 down to 0.007 ohm-cm, corresponding to an im-

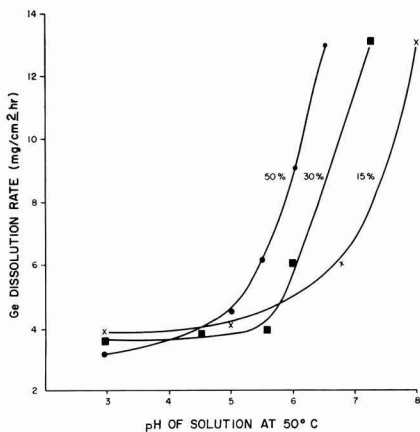


Fig. 5. Dependence of germanium dissolution rate on pH of solution for three H<sub>2</sub>O<sub>2</sub> concentrations.

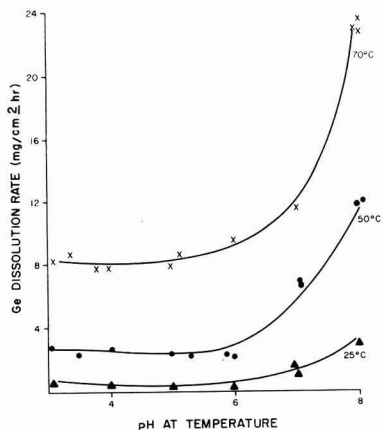


Fig. 6. Variation in dissolution rate as function of pH in 30% H<sub>2</sub>O<sub>2</sub>.

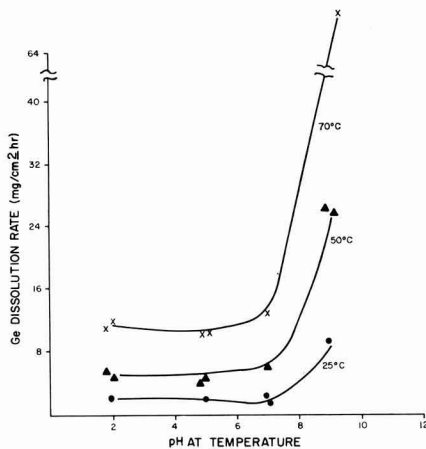


Fig. 7. Dependence of dissolution rate on pH in 15% H<sub>2</sub>O<sub>2</sub> aqueous solution.

purity concentration range from  $10^{13}$  to  $10^{19}$  atom/cm<sup>3</sup>. The high impurity germanium has a dissolution rate about 30% higher than near intrinsic germanium. Typical results are given in Table II.

Dislocation density variation in the  $1 \times 10^3$  to  $1 \times 10^7$ /cm<sup>2</sup> range does not change the dissolution rate appreciably, although macroscopic crystal imperfections such as lineage appear to increase the dissolution rate.

### Discussion

From the experimental results it is clear that: (a) the germanium dissolution rate remains essentially constant in aqueous H<sub>2</sub>O<sub>2</sub> solutions of from 3 to 30% by weight H<sub>2</sub>O<sub>2</sub> in the pH 1 to 5 range, even at elevated temperatures; (b) in the concentration range above 30% H<sub>2</sub>O<sub>2</sub> and at low pH the rate decreases linearly with increasing H<sub>2</sub>O<sub>2</sub> content; (c) in pH range above 5, there is a certain critical pH value above which the rate increases linearly with increasing pH as seen in Fig. 2. This critical pH varies with H<sub>2</sub>O<sub>2</sub> concentration, as seen in Fig. 5 and 6; (d) in solutions of pH 4 and below the activation energy of the reaction is approximately 6.5 kcal/mole and at pH 5 and above it is approximately 10.5 kcal/mole. Activation energy given by Miller

Table II. Dissolution rate vs. impurity concentration for n-type germanium at 70° ± 1°C

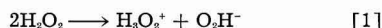
Impurity level, atom/cm <sup>3</sup>	H <sub>2</sub> O <sub>2</sub> weight percentage	pH at 70°C	Dissolution rate, mg/cm <sup>2</sup> -hr
$10^{13}$	30	4.0 ± 0.1	6.60
$10^{15}$	30	4.0 ± 0.1	7.38
$10^{19}$	30	4.0 ± 0.1	8.64
$10^{13}$	32-33	3.9 ± 0.1	7.50
$10^{19}$	32-33	3.9 ± 0.1	8.82
$10^{16}$ *	32-33	3.9 ± 0.1	10.68
$10^{19}$ **	32-33	3.9 ± 0.1	10.14
$10^{13}$	33-35	7.0 ± 0.1	25.2
$10^{15}$	33-35	7.0 ± 0.1	25.8
$10^{19}$	33-35	7.0 ± 0.1	27.6

\* Heavy lineage.  
\*\* Lineage.

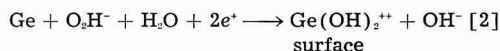
(2) is 11 kcal/mole in a solution of 3% H<sub>2</sub>O<sub>2</sub> of pH 5; (e) p-type germanium etches at a slightly faster rate than n-type germanium; (f) germanium with gross imperfections and high impurity concentration has a higher dissolution rate than nondegenerate germanium of better crystalline perfection.

On the basis of the above experimental results, the following two-step mechanism for germanium dissolution in H<sub>2</sub>O<sub>2</sub> is proposed.

In aqueous solutions of H<sub>2</sub>O<sub>2</sub>, as suggested by Schumb *et al.* (3), the dissociation of H<sub>2</sub>O<sub>2</sub> occurs as in reaction Eq. [1]



When the O<sub>2</sub>H<sup>-</sup> ions diffuse to the germanium surface, they attach instantly to surface germanium atoms forming surface complex > Ge(OH)<sub>2</sub>, or Ge(OH)<sub>2</sub><sup>++</sup>, by reaction shown in Eq. [2]

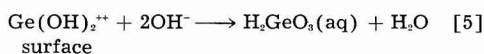
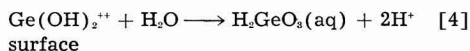


The chemical bonds between the surface germanium atom and underlying atoms remain unbroken. The rate of this reaction is determined by the supply of O<sub>2</sub>H<sup>-</sup> ions and supply of holes, and the number of available surface germanium atoms. If the supply of holes is more abundant than O<sub>2</sub>H<sup>-</sup> ions at the interface, the reaction rate will be limited by the diffusion of O<sub>2</sub>H<sup>-</sup> ions to the interface. In this aqueous system it is proposed that holes are supplied by the reaction between H<sup>+</sup> ions and H<sub>2</sub>O<sub>2</sub>, as shown in Eq. [3]



The supply of holes is abundant and not rate determining. In p-type Ge, the availability of holes in the germanium bulk may aid this supply, resulting in slightly faster dissolution rates in p-type Ge under similar experimental conditions.

The formation of the final dissolution products, metagermanate ions or metagermanic acid, can proceed by one of the following two reactions, Eq. [4] and [5]

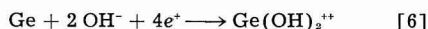


Either reaction will occur instantly as soon as the reactants are brought together. In solutions of low pH, the final dissolution reaction is believed to proceed primarily according to Eq. [4]. In the pH range of 1 to 5 where the dissolution rate remains essentially constant, the O<sub>2</sub>H<sup>-</sup> ion availability at the interface is probably quite constant. This occurs because the variation in H<sub>2</sub>O<sub>2</sub> concentration and pH does not change the (O<sub>2</sub>H<sup>-</sup>) gradient in the diffusion layer and the layer thickness. At higher temperatures, the availability of O<sub>2</sub>H<sup>-</sup> ion will improve and give faster dissolution rates.

In Fig. 1 it is seen that at 30% hydrogen peroxide the dissolution rate begins to decrease linearly with

increasing H<sub>2</sub>O<sub>2</sub> concentration or decreasing H<sub>2</sub>O concentration. The formation of metagermanic acid involves a Ge(OH)<sub>2</sub><sup>++</sup> ion and a H<sub>2</sub>O molecule as evidenced by the linear relation indicating that under these conditions reaction [4] becomes rate limiting. The rate for a certain Ge(OH)<sub>2</sub><sup>++</sup> surface concentration is limited primarily by the availability of H<sub>2</sub>O molecules at the interface, *i.e.*, a diffusion mechanism. The activation energy for all these cases is approximately 6.5 kcal/mole.

According to Greischer (4) germanium reacts preferentially with hydroxyl ions in aqueous solutions. When OH<sup>-</sup> ions are consumed as fast as they reach the surface by Eq. [5], dissolution takes place with H<sub>2</sub>O molecules as shown in Eq. [4]. With increasing pH, the reaction with OH ions becomes more important. Since OH<sup>-</sup> ions react much faster than H<sub>2</sub>O molecules in the formation of H<sub>2</sub>GeO<sub>3</sub>, the dissolution steps become very fast in neutral and basic solutions where reaction [5] predominates. In a basic solution, the situation is further complicated by another mechanism in forming the Ge(OH)<sub>2</sub><sup>++</sup> surface complex, as shown in Eq. [6]



This reaction may become competitive with Eq. [2], involving a different activation energy. The experimental value here is 10.5 kcal/mole. Since each germanium surface atom requires two OH<sup>-</sup> ions to form the surface complex Ge(OH)<sub>2</sub><sup>++</sup> and requires two additional OH<sup>-</sup> ions for the final dissolution product, the dependence of the rate on OH<sup>-</sup> ion concentration is very strong. Because the reaction can proceed by Eq. [2] and [4] just as well, there is no simple relationship established between rate and pH. It is interesting to note in Fig. 5 that after reaching the critical pH, the germanium dissolution rates in 50, 30, and 15% H<sub>2</sub>O<sub>2</sub> solutions increase in the same fashion with increasing pH, indicating the same mechanism where OH<sup>-</sup> ion availability plays an important role. Since reactions [2] and [6] proceed simultaneously in the more concentrated H<sub>2</sub>O<sub>2</sub> solutions the effect of increasing OH<sup>-</sup> ion concentration becomes more noticeable at lower pH.

For very impure germanium (*i.e.*, 10<sup>10</sup> atoms/cm<sup>3</sup>) and germanium with macroscopic imperfections such as gross lineage, the dissolution rates are higher. This may be due to the electric field built-in with these imperfections or by postulating that the chemical bond between Ge surface atoms and the bulk can be broken more readily by H<sub>2</sub>O<sub>2</sub> when the presence of these defects weakens the bond. At the present time we have no quantitative explanation of the dependence of the dissolution rate on the degree of crystal perfection in germanium.

This proposed mechanism can only explain the experimental facts qualitatively. Experimental difficulties limit the conditions where controlled dissolution can be obtained. For instance, experiments in a 30% H<sub>2</sub>O<sub>2</sub> solution of pH greater than 9 at high temperatures or in a 90% H<sub>2</sub>O<sub>2</sub> concentration solution of pH greater than 9 cannot be carried out. Extreme instability of the H<sub>2</sub>O<sub>2</sub> solution makes it impossible to maintain constant temperature and com-

position. However, it is feasible to carry out experiments at temperatures below 25°C. For more quantitative results, further experimental work at lower temperature is required.

#### Acknowledgment

The authors wish to thank Mrs. A. R. Waters for her assistance in the experimental work, and to Mr. S. Crytzer and Mrs. B. Zaffina for their help in the chemical analyses of the hydrogen peroxide solutions. They would also like to acknowledge the assistance of Mr. F. Bower in preparation of the manuscript.

Manuscript received Oct. 16, 1961; revised manuscript received Feb. 14, 1962. This paper was prepared for delivery before the Houston Meeting, Oct. 9-13, 1960.

Any discussion of this paper will appear in a Discussion Section to be published in the December 1962 JOURNAL.

#### REFERENCES

1. P. R. Camp, *This Journal*, **102**, 586 (1955).
2. K. J. Miller, *ibid.*, **108**, 296 (1961).
3. W. C. Schumb, C. N. Satterfield, and R. L. Wentworth, "Hydrogen Peroxide," p. 370, Reinhold Publishing Co., New York (1955).
4. Greischer, "The Surface Chemistry of Metals and Semiconductors," H. C. Gatos, editor, p. 183, John Wiley and Sons, Inc., New York (1960).

## Batch Evaporation or Crystallization at Constant Composition by a Two-Container Method

W. G. Pfann, J. R. Patel, and H. C. Theuerer

*Bell Telephone Laboratories, Incorporated, Murray Hill, New Jersey*

#### ABSTRACT

A two-container method is described for producing a vapor or pulling a crystal of constant composition from a binary or multicomponent liquid solution. As the liquid level falls in the first container due to evaporation or crystal growth, liquid enters from the second container. The cross section and liquid composition of the second container are selected in a manner such that the composition in the first container remains constant.

In a companion paper (1) a method is described for evaporating essentially all of a batch of liquid solution at constant vapor composition. In this paper we describe a different method of achieving the same result, which is also applicable to crystallization. Our method is less generally useful, as it requires a knowledge of the volatilities of the components of solution and vapor and is less flexible in other respects. Nevertheless, it appears to be a useful alternative.

The basis of the method is as follows. Because the vapor differs in composition from the liquid, continued evaporation changes the composition of the remaining liquid. This change is automatically nullified by introducing feed liquid of appropriate composition.

The apparatus consists essentially of two columns or reservoirs of liquid connected by a one-way passage that permits flow only from the second to the first, as shown in Fig. 1. The liquid heads are the same in the two columns, both being maintained at the same atmospheric pressure. As liquid is removed from column 1 by evaporation (either by heating it or by a hydrogen bubbler, for example), the level falls and liquid flows into column 1 from column 2 so as to equalize the heads.

If the cross-sectional area,  $A_2$ , of column 2 is chosen correctly with respect to the area,  $A_1$ , of column 1, the vapor leaving 1 will be of constant composition. (We assume rapid mixing in 1, which a bubbler would provide.)

The required area ratio,  $(A_1/A_2)$  is given by:

$$\frac{A_1}{A_2} = \frac{M_0(1-x_2/x_1)}{M_2(1-x_0/x_1)} - 1 \quad [1]$$

where subscripts 0, 1, and 2 refer to the product vapor, the liquid in 1, and in 2, respectively,  $M$  denotes average molecular weight of the solution, and  $x$  denotes mole-fraction of heavy (less volatile) component. Equation [1] is derived in the Appendix. The ratio  $(x_0/x_1)$  may be called a distribution coefficient,  $k$ .

In terms of  $M_H$  and  $M_L$ , the molecular weights of heavy and light components, respectively, [1] may be written:

$$\frac{A_1}{A_2} = \frac{[x_0 M_H + (1-x_0) M_L](1-x_2/x_1)}{[x_2 M_H + (1-x_2) M_L](1-k)} - 1 \quad [2]$$

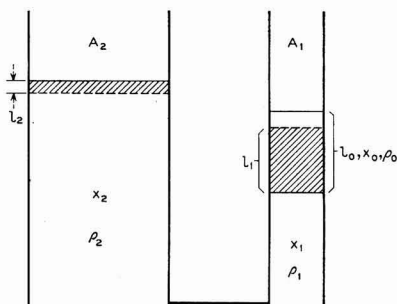


Fig. 1. Schematic illustrating quantities involved in the two-container method.



In general, it will be preferable to have pure light component in column 2, i.e.,  $x_2 = 0$ , in which case 2 reduces to

$$\frac{A_1}{A_2} = \frac{k + x_0 \left( \frac{M_H}{M_L} - 1 \right)}{1 - k} \quad [3]$$

If the liquids in 1 and 2 differ in density, they will be at different levels. But if they do not (as when  $x_0$  is very small), they will be at the same level. Equation [3] shows that the ratio ( $A_1/A_2$ ) depends only on  $k$  at small  $x_0$ , but on  $x_0$  as well, at larger  $x_0$ , because of the density difference which large  $x_0$  introduces.

The apparatus can be adapted for solutions of different  $k$ -values by designing for small  $k$  (that is,  $A_1/A_2$  small), and either providing inert glass rods to reduce  $A_2$  to the proper value, or adjusting the composition of column 2 as described in the next section.

#### Extension to Ternary or Higher Order Solutions

The method can be generalized to accommodate a higher-order system having solutes, a, b, c . . . ( $n - 1$ ), and "solvent," n. It is merely necessary to choose the proper mole fraction,  $x_{2a}$ ,  $x_{2b}$ , etc., of these solutes in column 2. This is done by selecting ( $A_1/A_2$ ) to match the solute of lowest  $k$  (call it solute "a"), with  $x_{2a} = 0$ . It is then possible to choose values of  $x_{2b}$ ,  $x_{2c}$ , etc., for which this same area ratio will be correct.

Let  $R$  designate ( $x_2/x_1$ ), then, in accord with Eq. [1], and since  $M_2$  and  $M_0$  pertain to the solutions as a whole, we may write

$$\left( 1 + \frac{A_1}{A_2} \right) \left( \frac{M_2}{M_0} \right) = \frac{1 - R_a}{1 - k_a} = \frac{1 - R_b}{1 - k_b} = \dots = \frac{1 - R_{n-1}}{1 - k_{n-1}} \quad [4]$$

It is evident from [4] that as  $k$  increases (from component to component),  $R$  must also increase.

The generalized expression for  $M_0$  is

$$M_0 = x_{0a}M_a + x_{0b}M_b + x_{0c}M_c \dots + x_{0(n-1)}M_{n-1} + (1 - x_{0a} - x_{0b} - x_{0c} \dots - x_{0(n-1)})M_n \quad [5]$$

An analogous expression holds for  $M_2$ .

The value of ( $A_1/A_2$ ) for  $R_a = 0$  is

$$\frac{A_1}{A_2} = \frac{M_0}{M_2} \cdot \frac{1}{1 - k_a} - 1 \quad [6]$$

The value of  $x_{2b}$ , for  $R_a = 0$ , is

$$x_{2b} = x_{0b} \cdot \frac{1 - k_a/k_b}{1 - k_a} \quad [7]$$

The value of  $x_{1b}$  is

$$x_{1b} = x_{0b}/k_b \quad [8]$$

Equations analogous to [7] and [8] hold for each of the other solutes.

#### Relationship to Crystallization

These considerations apply to the withdrawal of a solid, rather than a vapor, from column 1, as by crystal pulling. In fact, Patel and Mullen (2) have

described the application of the two-container technique to the pulling of germanium crystals lightly doped with gallium. The equations derived in the present paper represent a generalization which accounts for density differences and for the presence of two or more solutes.

There is a zone leveling technique (3) which accomplishes for solids the same result described here. This is the method in which a zone containing solute advances into a charge of pure solid solvent, and in which the zone-length,  $l$ , decreases linearly with distance,  $s$ , at a rate,  $dl/ds$ , given by

$$\frac{dl}{ds} = -k \quad [9]$$

where  $k$  now refers to the solid rather than the vapor. The zone length falls to zero at  $s = l_0/k$ , where  $l_0$  is the initial length. As described, the method was restricted to values of  $k$  less than unity. By analogy with the two-container technique, it can be seen that this zone leveling technique can be extended to  $k$ 's greater than unity by having a uniform concentration  $x_2$  in the charge, in which case the required rate of change of zone length is:

$$\frac{dl}{dx} = -k \cdot \frac{1 - x_2/x_0}{1 - k} \quad [10]$$

For  $k$ 's  $> 1$ , Eq. [10] permits operation at increasing zone length (for  $x_2/x_0 > k$ ). However, this leaves one at the end of the operation with a large zone of concentration  $x_0/k$ .

Manuscript received Jan. 4, 1962.

Any discussion of this paper will appear in a Discussion Section to be published in the December 1962 JOURNAL.

#### REFERENCES

1. H. C. Theuerer, Being reviewed for *This Journal*.
2. J. R. Patel and J. Mullen, *This Journal*, **105**, 253C (1958); Abstract of paper presented at Ottawa Meeting, Sept. 29, 1958.
3. W. G. Pfann, *Trans. AIME*, **194**, 747 (1952).

#### APPENDIX

##### Derivation of Eq. [1]

Assume the liquid heads in columns 1 and 2 of Fig. 1 to be initially equal. Imagine a length  $l_0$  of the liquid in 1 to be made to have composition  $x_0 < x_1$  (where  $x$  denotes mole fraction of heavy component) by a segregation process occurring within column 1, where  $x_0$  is the desired vapor composition. Remove length  $l_0$  of this liquid whose composition is  $x_0$  and density is  $\rho_0$ .

Then allow the pressure heads to equalize by flow of volume  $l_0 A_2$  of liquid from 2 into 1. The net changes in head as a result of these two operations must be equal. Therefore:

$$-l_2 \rho_2 = -l_0 \rho_0 + l_1 \rho_2 = -l_0 \rho_0 + l_2 \left( \frac{A_2}{A_1} \right) \rho_2 \quad [A-1]$$

From which:

$$\frac{l_2}{l_0} = \frac{\rho_0}{\rho_2} \cdot \frac{A_1}{A_1 + A_2} \quad [A-2]$$

If the composition of the liquid in column 1 is to be unchanged by these operations (and we assume complete mixing in 1), then the composition of the net material leaving 1 must equal  $x_1$ . We therefore obtain an expression for the mole fraction of heavy component,  $H$ , leaving 1, using the relation:

$$\text{mole } H = \text{mole fraction } H \times \frac{\text{total moles}}{\text{unit volume}} \times \text{volume} \quad [A-3]$$

Let  $B$  denote total moles per unit volume of solution. Then:

$$\begin{aligned} \text{Moles } H \text{ leaving in vapor} &= x_0 B_0 l_0 A_1 \\ \text{Moles } L \text{ leaving in vapor} &= (1-x_0) B_0 l_0 A_1 \\ \text{Moles } H \text{ entering from 2} &= x_2 B_2 l_2 A_2 \\ \text{Moles } L \text{ entering from 2} &= (1-x_2) B_2 l_2 A_2 \end{aligned}$$

$$x_1 = \frac{x_0 B_0 l_0 A_1 - x_2 B_2 l_2 A_2}{x_0 B_0 l_0 A_1 - x_2 B_2 l_2 A_2 + (1-x_0) B_0 l_0 A_1 - (1-x_2) B_2 l_2 A_2} \quad [\text{A-4}]$$

which reduces to

$$\frac{A_1}{A_2} = \frac{l_2 B_2 (x_1 - x_2)}{l_0 B_0 (x_1 - x_0)} \quad [\text{A-5}]$$

Substituting for  $(l_2/l_0)$  from [A-2], we obtain

$$1 + \frac{A_1}{A_2} = \frac{B_{\rho 0} (x_1 - x_2)}{B_{\rho 2} (x_1 - x_0)} \quad [\text{A-6}]$$

which can be used to solve for area ratio  $(A_1/A_2)$ . However, a more useful form of [A-6] can be obtained using the relation

$$B = \rho/M \quad [\text{A-7}]$$

where  $M$  denotes average molecular weight of the solution, and for solutions 2 and 0 is given by

$$\begin{aligned} M_2 &= x_2 M_H + (1-x_2) M_L \\ M_0 &= x_0 M_H + (1-x_0) M_L \end{aligned} \quad [\text{A-8}]$$

where subscripts H and L refer to heavy and light components. Equation [A-6] then reduces to

$$\begin{aligned} 1 + \frac{A_1}{A_2} &= \frac{M_0 (x_1 - x_2)}{M_2 (x_1 - x_0)} \\ 1 + \frac{A_1}{A_2} &= \frac{M_0 (1 - x_2/x_1)}{M_2 (1 - k)} \end{aligned} \quad [\text{A-9}]$$

## Epitaxial Deposition of Silicon in a Hot-Tube Furnace

Bruce E. Deal

Raytheon Company, Mountain View, California

### ABSTRACT

A method has been developed for depositing single crystal silicon epitaxially in a conventional hot-tube furnace. Silicon is deposited on a silicon substrate by the reduction of a silicon halide at temperatures in excess of 1200°C. A modification of the gas inlet system prevents decomposition of the silicon halide before contacting the silicon substrate. Several silicon slices can be treated simultaneously with good reproducibility of deposit thicknesses and resistivities.

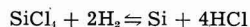
The announcement of the successful fabrication of an epitaxial transistor was made a little over a year ago (1). There has been much interest in the subject since then, as is demonstrated by the large number of papers concerning epitaxial deposition presented at technical societies and in the literature (2-8). There appear to be many possibilities for improved semiconductor devices using epitaxial material. At the same time, many problems exist regarding the actual deposition of an epitaxial layer suitable for a particular device. Reported here are the results of a particular program in which it was demonstrated that single crystal silicon can be successfully deposited using a conventional diffusion furnace. The program was undertaken to determine if the more expensive, less common types of apparatus using resistance heated or induction heated substrates are necessary for silicon epitaxial deposition. These methods involve the use of a relatively cool reaction tube or chamber, as contrasted to a diffusion apparatus where the tube is as hot as the specimen being treated.

### Apparatus and Materials

The furnace used in our experiments was a Hevi-Duty Globar furnace, 26 in. long, with three heat zones. All three zones were controlled to  $\pm 1^\circ\text{C}$  with a L&N Speedomax H recorder with C.A.T. controller. Reaction tubes, 45 mm ID, constructed of either Mullite or quartz were used in the experiments. The silicon used for the substrate material was single crystal, (111) oriented, n-type, antimony-doped with resistivities ranging from 0.01 to 0.05 ohm-cm. The slices were prepared similarly to those used for

conventional transistors. After being sliced and coarse-lapped to 9-mils thickness, they were polished with Linde A on one side to 8 mils. They were given a hot acetone rinse, two rinses in hot trichloroethylene, one rinse in warm isopropyl alcohol (with the appropriate deionized water rinses), and dried. They were then oxidized 1 hr in steam at 1250°C and the oxide removed by a standard oxide etch solution. The purpose of the oxidation procedure was to remove any lapping damage as well as to provide a cleaner surface.

The method of silicon deposition chosen for this program was that of hydrogen reduction of silicon tetrachloride



Various sources of silicon tetrachloride were used in this program, including some prepared in our own laboratory. For most of the experiments described here, however, ultrapure  $\text{SiCl}_4$  was obtained from Matheson Coleman and Bell Co. with boron specified as being less than 10 ppb and phosphorus less than 50 ppb.

### Experimental—Single Slice Deposition

Initially, hydrogen gas was passed through a bubbler of  $\text{SiCl}_4$  maintained at  $-25^\circ\text{C}$  and directly into the reaction tube as in a diffusion process. The silicon substrate was placed flat on a quartz slab at about 1200°C. Some slices were first subjected to a hydrogenn treatment, others were not. However, results were all unsatisfactory. Reduction of the silicon tetrachloride was occurring well ahead of the silicon substrate or at too low a temperature. Numerous

reaction products were being carried to the substrate, tube wall, and elsewhere. No suitable deposits were obtained.

These results suggested that reduction of the silicon tetrachloride should be prevented until it reached the substrate. This would have to be accomplished by cooling the reacting gas mixture of hydrogen and silicon tetrachloride as it flowed into the furnace. Therefore, the system shown in Fig. 1 was designed and constructed. A 4 mm ID quartz insert tube, surrounded by a cooling jacket, extended into the furnace tube. Nitrogen gas was found to be the most efficient coolant. The optimum rate of nitrogen flow, determined experimentally, was 25 liters/min. The furnace temperature profile with and without a flow of cooling gas is shown in Fig. 2. It is evident from this profile that the reacting gases are maintained below 1000°C until contacting the silicon substrate. The use of a cooled insert tube resulted in smooth silicon deposits, later shown to be single crystal. As is shown in Fig. 1, the reaction gases were directed vertically and perpendicular to the substrate through a nozzle. The latter had an opening diameter of approximately 15 mm. The silicon substrate was about 10 mm beneath the nozzle opening. By varying the flow rate and the deposition time, optimum process conditions were determined for uniform deposit formation. A silicon deposit about 10-20 $\mu$  thick could be produced in from 5 to 15 min. Flow rates of between 1 and 2 liters/min were found to be the most satisfactory. Resistivities were in the neighborhood of 2 ohm-cm, n-type. The deposits appeared uniform across the surface except for a slight

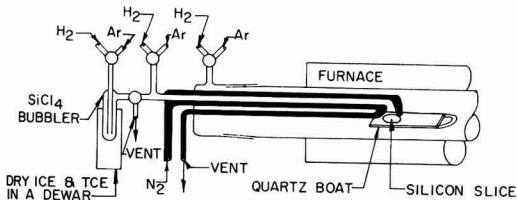


Fig. 1. Apparatus for epitaxial deposition of silicon in a hot-tube furnace.

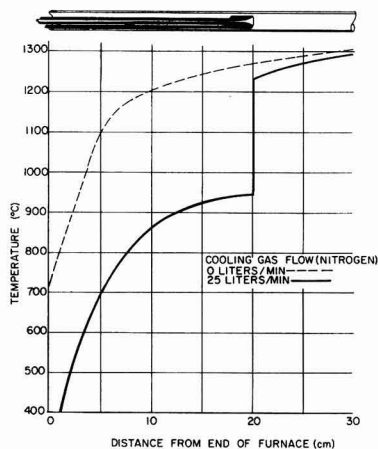


Fig. 2. Temperature profile of epitaxial reaction chamber

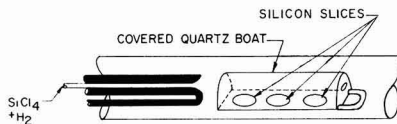


Fig. 3. Modified apparatus for epitaxial deposition on more than one silicon slice.

tapering at the edges. No deposit was observed on the underside of the substrate.

For a typical run, silicon tetrachloride was maintained at  $-25^{\circ}\text{C}$ , providing a mole fraction of about 0.025 in hydrogen. The system was first purged with argon. The substrate was placed in position on a flat quartz boat and was exposed to hydrogen for 15 min at  $1250^{\circ}\text{C}$ . Deposition was then carried out under conditions necessary to obtain a desired deposit thickness. For instance, if the flow rate was 1.5 liters/min, a deposit thickness of about 18 $\mu$  could be obtained in 6 min. After purging again with argon, the slice was removed from the furnace and evaluated. The total time that the slice remained in the furnace was about 30 min.

It was demonstrated that the process is extremely sensitive to any water vapor or air admitted to the system through leaks in the apparatus. Thus a very tight system is required.

#### Deposition of Several Slices

After successful deposition on a single slice, three slices were treated simultaneously using the modification of the system shown in Fig. 3. As can be observed, the stream of reacting gases was directed straight out from the insert tube into a covered quartz boat. The latter was referred to as a "covered wagon." It was approximately 10 cm long, 2.8 cm high, and 2.5 cm wide at the bottom. The distance between the covered boat and the nozzle opening was about 5 cm. The nozzle opening was 10 mm in diameter. The covered boat was used originally to prevent reaction products from dropping from the top of the furnace tube onto the substrates. In addition, deposited silicon could be removed from the sides of the boat between runs. But it was soon found that by selecting the correct size of hole in the end of the boat and the correct flow rate, the covered boat would permit better control of the reacting gas mixture. A hole diameter of 10 mm and flow rates of 2-4 liters/min provided satisfactory results. As was the case for the single slice system, the mole fraction of  $\text{SiCl}_4$  in hydrogen was 0.025, and the substrate temperature was maintained in the range of  $1230^{\circ}\text{C}$ - $1270^{\circ}\text{C}$ . The 15-min hydrogen pretreatment was also used for the multislice depositions. Deposition times were longer than for the single slice depositions, about 10-15 min.

By using this system, uniform deposits could be produced on several slices. Deposit thicknesses were equal among the slices and from run to run for a given set of operating conditions. Resistivities were also reproducible among runs, provided the same source of  $\text{SiCl}_4$  was used. No tapering at the edges of the deposits was observed as was the case in the previous one-slice system. This was undoubtedly due to the more uniform gas concentration above the substrates in the covered boat system.

Table I. Thickness and resistivity profile of silicon epitaxial deposits produced in hot-tube furnace

Slice No.	Position	Deposit thickness, $\mu$	Resistivity, ohm-cm
58R	1	21.6	1.4
	2	27.8	1.6, 1.3
	3	22.5	1.2, 1.3
	4	23.0	1.4
	Average	23.5	1.4
	Standard deviation	2.4	0.1
70R	1	23.0	—
	2	27.1	—
	3	28.6, 26.1	—
	4	25.8	—
	Average	26.1	—
	Standard deviation	1.8	—

To better understand the deposition process, a smoke chamber was assembled which duplicated the geometry of the multislice system. Nitrogen flowing through hydrochloric acid and ammonium hydroxide represented the hydrogen-silicon tetrachloride flow pattern. By observing these patterns, process variables could be optimized for uniform deposition on several slices. The smoke chamber experiments also indicated where certain beneficial changes in the geometry of the system could be made. One proposed modification was the formation of a grid of quartz fibers across the opening of the covered boat, thus providing better dispersion of the gas mixture. The smoke chamber also permitted the evaluation of other sizes and shapes of boats, including some with more than one shelf.

During continuing deposition experiments, it was found the quartz insert tube would last several weeks if used under proper conditions. If the outlet of the tube became plugged or broken, the entire insert assembly was removed from the furnace and the tube end replaced by the glassblower. Thus, the main portion of the insert assembly had a relatively long life.

### Evaluation of Deposits

Deposits were evaluated in the following manner. All slices were weighed before and after deposition. In addition, deposit thickness values were obtained by angle lapping and staining. As mentioned above, deposit thicknesses across a sample prepared in the multislice system were quite uniform. Profiles of

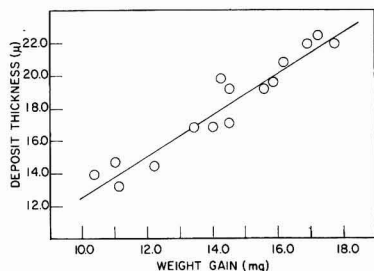


Fig. 4. Relationship of weight gain to deposit thickness for hot-tube, epitaxial deposition of silicon.

thicknesses for two typical, deposited slices are listed in Table I. These values were obtained at various locations on the slice. It was soon found that a definite relationship existed between deposit weight per unit area and thickness, approximating the density of silicon. A plot of weight-thickness data is presented in Fig. 4. Weights are expressed as weight gain per total slice, the slices being 20.6 mm in diameter and 0.2 mm thick. We were able, therefore, to estimate the thickness values to  $\pm 10\%$  from the weight measurements. This would not have been possible if deposition occurred to any extent on the underside of the substrate.

Resistivities were determined from capacitance-voltage measurements (9) and were generally found to be quite uniform across the deposit and through the deposit. An example of a resistivity profile is given in Table I. Early in our experiments it was obvious that the resistivity of the deposits was dependent on the specific supply of silicon tetrachloride. Later, it was observed that the hydrogen source is also a factor. For a given source of these reactants, we could obtain good reproducibility of resistivities. Special experiments were conducted in which boron tribromide was added to the silicon tetrachloride. Predicted increases in deposit n-type resistivities were obtained initially. However, if the doped silicon tetrachloride was allowed to stand for 24 hr, resistivities dropped back down to close to the original value. It was concluded, therefore, that boron tribromide was probably unstable in silicon tetrachloride and that doping should be carried out at the time of deposition.

A series of runs was made using the single slice system. The same supply of silicon tetrachloride was used for all runs of this series. Deposition conditions were as follows:  $\text{SiCl}_4$  was maintained at  $-24^\circ\text{C}$ , substrate temperature was  $1200^\circ\text{C}$ , flow rate was 1.5 liters/min, and deposition time was 6 min. Deposit weight and resistivity results as well as calculated thickness values are tabulated in Table II. All deposits were n-type. These results indicate reasonable reproducibility of deposit characteristics.

Similar data are listed in Tables III and IV for the multislice system. The reproducibility among

Table II. Results of a series of silicon vapor depositions in a hot-tube furnace using the single slice system

Slice No.	Weight gain, mg	Deposit thickness, $\mu^*$	Resistivity, ohm-cm
B-9B	14.0	17.5	2.2
B-10B	13.5	17.0	2.6
B-11B	13.2	16.5	1.8
B-12B	14.5	18.2	2.7
B-13B	14.1	17.6	3.6
B-14B	18.3	22.8	2.3
B-15B	15.8	19.8	3.0
B-16B	11.5	14.5	2.3
B-17B	18.7	23.0	2.6
B-19B	12.0	15.0	2.5
B-20B	12.4	15.5	2.3
Average	14.4	17.9	2.5
Standard deviation	2.3	2.7	0.4

\* Deposit thicknesses were calculated from weight measurements.

Table III. Reproducibility of deposit properties among slices in individual runs using multislice system

Run No.	Deposition conditions	Weight gain, mg	Deposit thickness, $\mu^*$	Resistivity, ohm-cm
88	Deposition time:			
	10 min	10.9	13.6	—
	Flow rate: 3 l/min	11.8	14.7	—
	SiCl <sub>4</sub> temp: -24°C Si temp: 1255°C	10.5	13.1	—
91	Deposition time:			
	15 min	17.7	22.2	0.5
	Flow rate: 3 l/min	19.1	23.9	1.0
	SiCl <sub>4</sub> temp: -22°C Si temp: 1255°C	14.5	18.1	0.9
89	Deposition time:			
	12 min	15.7	19.7	1.4
	Flow rate: 3.5 l/min	14.1	17.6	1.4
	SiCl <sub>4</sub> temp: -24°C Si temp: 1255°C	13.5	16.9	1.1
97	Deposition time:			
	15 min	16.7	20.9	—
	Flow rate: 3.5 l/min	17.5	21.9	—
	SiCl <sub>4</sub> temp: -25°C Si temp: 1255°C	14.4	18.0	—

\* Deposit thicknesses were calculated from weight measurements.

Table IV. Results of a series of silicon vapor depositions in a hot-tube furnace using the multislice system

Run No.*	Weight gain, mg	Deposit thickness, $\mu$	Resistivity, ohm-cm
138	17.0	23.6	2.0
	17.2	24.0	1.9
139	15.8	19.5	3.3
	16.2	20.7	1.3
140	11.0	14.6	2.6
	11.5	9.1	1.3
141	17.2	22.4	1.3
	18.4	18.4	1.5
		Average =	1.9
		Std. deviation =	0.7
142	17.2	18.4	0.2
	17.5	19.1	1.3
144	17.7	21.9	0.8
	15.9	15.7	0.8
145	16.6	17.4	0.8
	16.9	21.9	1.5
		Average =	0.9
		Std. deviation =	0.4
Average	16.2	19.1	
Standard deviation	2.1	3.8	

\* Runs 138-141 used SiCl<sub>4</sub> Batch A.  
Runs 142-145 used SiCl<sub>4</sub> Batch B.

slices in each of four runs is indicated in Table III. Runs 88 and 91 are both for depositions using a flow rate of 3 liters/min but for different times. A slightly higher flow rate was used for runs 89 and 97. The deposit weights are reasonably reproducible among the three slices of each run, as are resistivities.

Table IV demonstrates reproducibility of deposit weights, thicknesses, and resistivities for a series of runs in the multislice system. Only two slices were deposited per run. Substrate temperature was 1270°C, flow rate was 4 liters/min, deposition time was 12 min, and SiCl<sub>4</sub> was maintained at -25°C for this series of runs. It should be noted that the silicon tetrachloride was changed between runs 141 and 142. This change affected the resistivity values, as is indicated in the table. With one or two exceptions, all values are fairly consistent.

Various deposited slices were turned over to our development pilot line for fabrication of transistors. A number of mesa switching transistors were completed and tested for electrical properties. As expected, collector-emitter saturation voltages as well as storage times were considerably lower than those of similar nonepitaxial transistors.

### Conclusions

The results of this program have demonstrated that silicon can be deposited epitaxially on a silicon substrate in a conventional hot-tube diffusion furnace. Several slices can be treated simultaneously. Deposits produced are uniform in thickness and resistivity and have very few surface irregularities. For a given source of silicon tetrachloride and hydrogen, results are reproducible from run to run. As is the case with any silicon vapor deposition process, the process is highly sensitive to the presence of water vapor or air. Resistivities of deposit can be controlled by doping the reacting materials at the time of deposition. It is probable that this system can be used for the vapor deposition of other materials, both elements and compounds, required in the various phases of electronic device fabrications.

### Acknowledgments

The author wishes to thank W. Peterson for his help in the experimental portion of this program. Also, W. R. Lamb and E. A. Swanson of these laboratories provided valuable assistance in evaluating the deposits.

Manuscript received Oct. 19, 1961; revised manuscript received Jan. 15, 1962. This paper was prepared for delivery before the Detroit Meeting, Oct. 1-5, 1961.

Any discussion of this paper will appear in a Discussion Section to be published in the December 1962 JOURNAL.

### REFERENCES

- H. C. Theuerer, J. J. Kleimack, H. H. Loar, and H. Christensen, *Proc. IRE*, **48**, 1642 (1960).
- J. E. Allegritti, D. J. Shombert, E. Schaarschmidt, and J. Waldman, "Metallurgy of Elemental and Compound Semiconductors," Vol. 12, p. 255, R. O. Grubel, Editor, Interscience Publishers, New York (1961).
- R. Glang and B. W. Kippenhan, *IBM J. Rsch. Dev.*, **4**, 299 (1960).
- J. C. Marinace, *ibid.*, **4**, 248 (1960).
- A. Mark, *This Journal*, **108**, 880 (1961).
- W. G. Spitzer and M. Tanenbaum, *J. Appl. Phys.*, **32**, 744 (1961).
- H. C. Theuerer, *This Journal*, **108**, 649 (1961).
- E. S. Wajda, B. W. Kippenhan, and W. H. White, *IBM J. Rsch. Dev.*, **4**, 288 (1960).
- J. S. Saby and W. C. Dunlap, *Phys. Rev.*, **90**, 630 (1953).

# Polarography of Mercaptoalkyl Compounds and Their Disulfides

Walter Stricks, J. K. Frischmann, and R. G. Mueller

Department of Chemistry, Marquette University, Milwaukee, Wisconsin

## ABSTRACT

The polarography of 2-mercaptoethylguanidine (RSH), 2-mercaptoethylguanidine ( $R_1$ SH), 2-mercaptoethylamine ( $R_{II}$ SH), and 2-mercaptoethanol ( $R_{III}$ SH) and their disulfides (RSSR,  $R_1$ SSR $_1$ ,  $R_{II}$ SSR $_{II}$ , and  $R_{III}$ SSR $_{III}$ ) has been studied. The mercaptans behave in the same way as other mercaptans described previously in the literature. RSSR gives well-defined reduction waves. The characteristics of the RSSR waves in the absence and presence of RSH are the same as those of oxidized glutathione and can be accounted for by the sequence of the two reactions:  $RSSR + e + H^+ \rightleftharpoons RS^- + RSH$ ,  $RS^- + e + H^+ \rightarrow RSH$  in which the first reaction is the rate and potential determining step.  $R_1$ SSR $_1$ ,  $R_{II}$ SSR $_{II}$ , and  $R_{III}$ SSR $_{III}$  are reduced irreversibly at the dropping mercury electrode.

In recent years a large number of mercaptoalkyl compounds have been studied with regard to their properties as radiation protective drugs for animals. In the course of systematic investigations of reactions of these compounds with metal ions and proteins it appeared to be useful to study the polarographic behavior of a few typical mercaptoalkyl compounds under various experimental conditions.

This paper deals with a polarographic study of 2-mercaptoethylguanidine (denoted as RSH), 2-mercaptoethylguanidine ( $R_1$ SH), 2-mercaptoethylamine ( $R_{II}$ SH), and 2-mercaptoethanol ( $R_{III}$ SH) and their disulfides which for the sake of brevity will be referred to as RSSR,  $R_1$ SSR $_1$ ,  $R_{II}$ SSR $_{II}$ , and  $R_{III}$ SSR $_{III}$ , respectively. The results obtained for these compounds are compared with each other and with those obtained for other mercaptans and disulfides described in the literature (1-3).

## Experimental

**Materials.**—Solutions of mercaptoalkyl guanidine were prepared from S<sub>2</sub>-aminoalkylisothiuronium bromide hydrobromide which undergoes rearrangement in neutral solution to form mercaptoalkylguanidine (4). Stock solutions of  $10^{-2}$ M mercaptan were prepared by weighing an appropriate amount of the isothiuronium compound in a glass cap which together with the compound was introduced into a bottle provided with metal screw cap into which a few holes were bored. In order to obtain an airtight seal the cap was fitted with a self sealing Buna N rubber gasket. Now a given volume of air free sodium hydroxide solution containing an amount of sodium hydroxide exactly equimolar to the isothiuronium salt was added in order to neutralize the liberated hydrobromic acid. The bottle was sealed immediately and after dissolution of the sample the solution was purged thoroughly with nitrogen introduced by means of a hypodermic needle which pierced the cap of the bottle. Samples were withdrawn from the bottle by means of a 2 ml calibrated syringe. When not in use the solution was stored in a refrigerator. The mercaptan solutions were found to be stable for a week. Stock solutions

of mercaptoethylamine and mercaptoethanol were prepared in the same way as described for RSH and  $R_1$ SH except that no sodium hydroxide was added to the solution.

The isothiuronium compounds were obtained from Dr. D. G. Doherty of the Biology Division, Oak Ridge National Laboratory. The mercaptoethylamine hydrochloride was obtained from the Walter Reed Army Medical Center, and the mercaptoethanol was an Eastman Kodak white label product. The mercaptan solutions were analyzed by amperometric titration with ethylmercury chloride at the rotated dropping mercury indicator electrode (5).

The disulfide solutions were obtained by air oxidation of the mercaptans. A slow stream of carbon dioxide and dust free air was passed through 50 ml of 0.01M mercaptan solution. The progress of the oxidation was followed polarographically. The air bubbling was continued until the anodic wave of the mercaptan had disappeared. The oxidation of RSH and  $R_1$ SH was performed in neutral medium and found to be complete after 15-20 hr. The oxidation of  $R_{II}$ SH and  $R_{III}$ SH was sluggish in neutral medium and faster in alkaline solutions. The solutions of these compounds were therefore made 0.1M in ammonia which was driven out from the solution with air toward the end of the reaction. The oxidation of  $R_{III}$ SH was slow even in alkaline medium and a trace of copper ( $10^{-6}$ M) was added as a catalyst in order to accelerate the oxidation. The resulting stock solutions were  $5 \times 10^{-6}$ M in disulfide.

All the other chemicals used were commercial C.P. reagent grade products.

**Methods.**—Current-voltage curves were obtained at  $25.0 \pm 0.1^\circ$  with a Fisher Electropode, Model 65, the manual apparatus and circuit described by Lingane and Kolthoff (6) and with a self-recording Sargent Polarograph, Model XXI. All potentials were measured against the saturated calomel electrode (S.C.E.). Oxygen was removed from the solution with a stream of nitrogen (Linde nitrogen, 99.996% pure). During an experiment an atmosphere of nitrogen was maintained over the solution. Corrections were made for the residual current.

Two capillaries were used: capillary I:  $m = 1.76$  mg sec<sup>-1</sup>;  $t = 4.4$  sec (in 0.10N KCl, open circuit);  $h = 75.5$  cm; capillary II:  $m = 1.98$  mg sec<sup>-1</sup>;  $t = 4.1$  sec (open circuit);  $h = 67.4$  cm.

The pH of the solutions was measured with a Beckman zero-matic pH meter. A Beckman "General Purpose" glass electrode was used.

The ionic strength of the supporting electrolyte was adjusted by the addition of appropriate quantities of potassium chloride or sodium nitrate.

## Results and Discussion

### Mercaptans

Some 100 polarograms were taken with solutions of various concentrations in mercaptan in buffers at pH 1-12.1. The polarographic behavior of the mercaptans is similar to those of other mercaptans such as cysteine (1), glutathione (3), and thioglycolic acid (7) described previously in the literature and the equations for the electrode reactions are therefore not derived in this paper. In contrast to cysteine the mercaptans investigated in this work give a well defined anodic wave, the shape and the height of the wave being somewhat affected by the pH of the solution. RSH gives steep waves at pH higher than 4.6 (curve B of Fig. 1) while at pH equal to or smaller than 4.6 the wave becomes drawn out (curve A, Fig. 1). The diffusion current is markedly smaller at the lower pH. R<sub>11</sub>SH and R<sub>111</sub>SH give drawn out waves in solutions of pH smaller than 2. In contrast with glutathione no specific buffer effect was observed with the mercaptans investigated and reversible waves were obtained in acetate, phosphate, and ammonia buffers and in dilute sodium hydroxide.

Surface active substances like gelatin (0.01%) or polyacrylamide (0.01%) have no effect on the shape of the anodic wave. The mercaptans markedly reduce the surface tension of mercury as is evident from the electrocapillary curves which are similar in shape to those obtained with glutathione (3).

The waves obtained with solutions at pH 5.4-11.6 at ionic strength one and 0.1 were analyzed as described previously (3) and found to correspond to the reversible formation of mercurous mercaptide (RSHg).

The half-wave potential can be expressed by

$$E_{1/2} = E' + 0.059 \log \{[H^+] + K\} \quad [1]$$

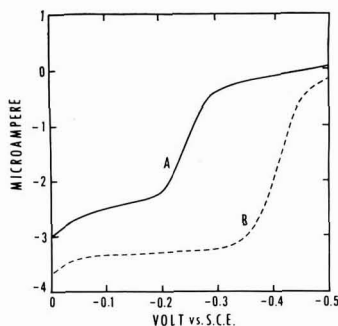


Fig. 1. Polarograms of 10<sup>-3</sup>M RSH in various buffers ( $\mu = 1$ ). A, acetate, pH 4.67; B, phosphate, pH 7.4.

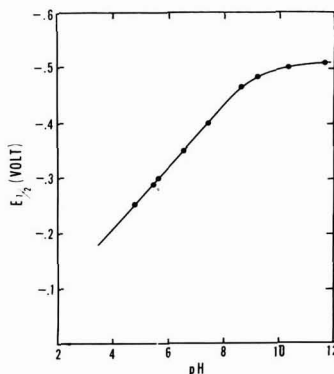


Fig. 2. Half-wave potential of RSH vs. pH ( $\mu = 1$ ).

where the constant  $E'$  is  $E^\circ + 0.059 \log k_1/k_2$  at 25°C,  $K$  is the dissociation constant of the sulfhydryl group,  $k_1$  and  $k_2$  are constants which are proportional to the square roots of the diffusion coefficients of RSH and RSHg, respectively, and  $E^\circ$  is the standard potential of the electrode reaction.

The half-wave potentials of RSH which were taken from the plots  $\log (i_a - i)/i$  vs. the potential are plotted in Fig. 2. By extrapolation of the curve of Fig. 2 the value of  $E'$  which corresponds to the half-wave potential at a pH of zero is obtained. Values of  $E'$ , the half-wave potentials at pH 11.5 corresponding to the horizontal portion of the  $E_{1/2} - \text{pH}$  plot, and the apparent dissociation constants of the sulfhydryl group of the mercaptans are listed in Table I. The apparent dissociation constants  $K$  of the sulfhydryl group were obtained from titrations of the mercaptans with sodium hydroxide, using a glass electrode. With the exception of cysteine which forms a film at the electrode (1) the half-wave potentials in acid medium are approximately of the same order of magnitude, while the

Table I. Polarographic data of mercaptans and disulfides.  $\text{pK}$  of the sulfhydryl groups of mercaptans

Compound	$E' \times 100$ , volt vs. S.C.E.	$E_{1/2}$ at pH 11.5 volt vs. S.C.E.	pK	$D \times 10^6$ , $\text{cm}^2 \text{sec}^{-1}$
RSH	1.4	-0.508	8.8	7.1 (G)
R <sub>1</sub> SH	4.1	-0.534	9.4	4.4 (G)
R <sub>11</sub> SH	6.0	-0.560	10.75	8.9 (G)
R <sub>111</sub> SH	3.0	-0.537	9.6	13.0 (G)
Thioglycolic acid (8)	0.62	-0.580	10.68	8.6 (A)
Cysteine (1)	10.6	-0.580	10.28	7.0 (B)
Glutathione (3)	3.0	-0.480	9.12	4.7 (C)
RSSR				8.8 (G)
R <sub>1</sub> SSR <sub>1</sub>				6.7 (D)
R <sub>11</sub> SSR <sub>11</sub>				11.0 (G)
R <sub>111</sub> SSR <sub>111</sub>				37.0 (D)
Dithiodiglycolic acid (7)				6.0 (E)
Cystine (2)				5.3 (F)
Oxidized gluta- thione (3)				4.5 (G)

(A) pH not given in literature; (B) in 0.1M HClO<sub>4</sub>; (C) at pH 10.82; (D) at pH 9.2; (E) at pH 3.0; (F) in 0.1M HCl; (G) at pH 10.3.

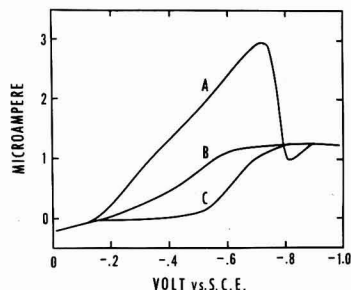


Fig. 3. Reduction waves of  $2.5 \times 10^{-4}$  M RSSR in (A) acetate buffer (pH 2.8), (B) same as (A) with  $5 \times 10^{-3}\%$  gelatin, (C) borax buffer (pH 9.2).

half-wave potentials in the alkaline pH region vary according to the variation of the pK values of the sulphydryl group as required by Eq. [1].

Diffusion currents of the anodic wave of the mercaptans were measured in the concentration range between  $2.6 \times 10^{-4}$  to  $1.4 \times 10^{-3}$  M. The diffusion current is independent of the pH in the pH region from 5 to 12. At pH smaller than 5 the diffusion current decreases. Thus the diffusion current of a  $10^{-3}$  M RSH solution was found to be 3.30 and 2.36  $\mu$ A at pH 11.6 and 4.7, respectively. Polarographic diffusion coefficients of the various mercaptans and disulfides are compared in Table I.

#### Disulfides

Guanidinoethylidysulfide (RSSR) gives a single reduction wave over the entire pH range investigated. In  $2.5 \times 10^{-4}$  M RSSR solutions a pronounced maximum occurs at pH 2.8 (curve A of Fig. 3). As the pH of the solution is increased the maximum becomes considerably flatter. At pH equal to or higher than 7 the maximum disappears (curve C of Fig. 3). Gelatin at concentrations of 0.001–0.003% suppresses the maximum at low pH and has hardly any effect on the half-wave potential and on the diffusion current. Increasing amounts of gelatin give rise to waves which are drawn out, the effect becoming more pronounced with decreasing pH (curve B, Fig. 3).

Electrocapillary curves taken with RSSR solutions have exactly the same shape as those obtained with RSH.

Analysis of current voltage curves obtained with RSSR solutions of various concentrations (1 to  $3.8 \times 10^{-4}$  M) at pH 11.6 to 5.82 at ionic strength 1 and 0.1 in the absence and presence of 1.23 to  $6.17 \times 10^{-4}$  M RSH revealed that the characteristics of the wave is exactly the same as that of oxidized glutathione (3). The equation of the wave at 25°C is therefore given by

$$E = E' + 0.059 \log \{ [H^+] + K \} + 0.059 \log (i_a - i) / i^2 \quad [2]$$

where  $E'$  is a constant. The reaction mechanism suggested for the reduction of oxidized glutathione also explains the experimental results obtained with RSSR ( $RSSR + e + H^+ \rightleftharpoons RS^{\cdot} + RSH$ ,  $RS^{\cdot} + e + H^+ \rightarrow RSH$ , the first reaction being the rate and potential determining step).

The diffusion current of RSSR hardly changes with pH in solutions at pH lower than 10 ( $i_a/c=6.0$ ) but is higher at pH above 10 ( $i_a/c=6.8$ ). At a concentration range between  $6.7 \times 10^{-5}$  to  $3.2 \times 10^{-4}$  M the diffusion current was found to be proportional to the concentration.

The experiments performed with guanidino propylidysulfide ( $R_1SSR_1$ ), aminoethylidysulfide ( $R_{11}SSR_{11}$ ), and hydroxyethylidysulfide ( $R_{111}SSR_{111}$ ) were essentially of the same kind as those mentioned for RSSR.

The current voltage curves of  $R_1SSR_1$  and  $R_{11}SSR_{11}$  have the appearance of reversible waves. However, the analysis of the  $R_1SSR_1$ -wave gave a plot  $\log (i_a - i) / i^2$  vs. potential which was a curved line. In the presence of an excess of  $R_1SH$  ( $2.5 \times 10^{-4}$  M  $R_1SSR_1$ ,  $5 \times 10^{-4}$  to  $4 \times 10^{-3}$  M  $R_1SH$ ) the plots  $\log (i_a - i) / i$  gave straight lines of slope 0.052 to 0.062 as required by Eq. 2. The plot  $\log C_{RSSR}$  ( $C_{RSSR}$  is molar concentration of RSH) vs.  $E_{1/2}$  gave a straight line of slope 0.071 instead of the theoretical value of 0.059. The wave of  $R_{11}SSR_{11}$  analyzed to give a plot  $\log (i_a - i) / i^2$  vs.  $E$  which was a straight line of the theoretical slope of 0.059. The plot  $\log i_a / 2$  vs.  $E_{1/2}$  was a straight line of slope 0.076 instead of the theoretical value of 0.059. Mixtures of  $2.5 \times 10^{-4}$  M  $R_{11}SSR_{11}$  with varying concentrations of  $R_{11}SH$  ( $2.5 \times 10^{-4}$  to  $1.2 \times 10^{-3}$  M) gave plots  $\log (i_a - i) / i$  vs.  $E$  which were straight lines of theoretical slopes of about 0.060 similar to the waves obtained with  $R_1SSR_1$ . The plot  $\log C_{R_{11}SH}$  vs.  $E_{1/2}$  was found to be a curved line and therefore does not conform to the requirements of Eq. 2.

The observations with  $R_1SSR_1$  and  $R_{11}SSR_{11}$  indicate that the reduction of these two compounds at the dropping mercury electrode is not reversible since the experimental results do neither satisfy the conditions for a two electron reduction nor do they agree with the conditions for a free radical mechanism (Eq. [2]).

Polarograms of  $R_{111}SSR_{111}$  were taken with solutions at various pH (12 to 4) in the absence and presence of gelatin. All waves obtained with  $R_{111}SSR_{111}$  were distorted and drawn out, indicating an irreversible electrode process. Therefore an analysis of these waves was not attempted.

It is of interest to note that, while the polarographic behavior of all mercaptans reported in the literature is essentially the same, the disulfides differ rather markedly as far as their polarography is concerned. The difference between RSSR on one hand and  $R_1SSR_1$ ,  $R_{11}SSR_{11}$ , and  $R_{111}SSR_{111}$  on the other hand is remarkable, considering that all these compounds are of a similar structure. In contrast to this it is noteworthy that compounds as different as oxidized glutathione and RSSR show the same polarographic behavior.

#### Acknowledgment

This investigation was supported by the U.S. Army Medical Research and Development Command, Department of the Army, under Research Contract No. DA-49-193-MD-2146. Part of this work is based on the M.S. Thesis of one of the authors (J.K.F.).



Manuscript received Sept. 18, 1961; revised manuscript received Jan. 26, 1962.

Any discussion of this paper will appear in a Discussion Section to be published in the December 1962 JOURNAL.

## REFERENCES

1. I. M. Kolthoff and C. Barnum, *J. Am. Chem. Soc.*, **62**, 3061 (1940).
2. I. M. Kolthoff and C. Barnum, *ibid.*, **63**, 520 (1941).
3. W. Stricks and I. M. Kolthoff, *ibid.*, **74**, 4646 (1952).

4. D. G. Doherty, R. Shapira, and W. T. Burnett, Jr., *ibid.*, **79**, 5667 (1957).
5. W. Stricks and S. K. Chakravarti, *Anal. Chem.*, **33**, 194 (1961).
6. J. J. Lingane and I. M. Kolthoff, *J. Am. Chem. Soc.*, **61**, 825 (1939).
7. D. L. Leussing and I. M. Kolthoff, *This Journal*, **100**, 334 (1953).
8. A. Liberti and E. Cerone, *Ann. Chim. Rome*, **41**, 95 (1951).

## Equilibrium Studies in the Reduction of Thorium Oxide by Aluminum

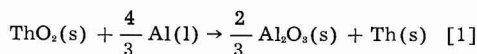
Douglas O. Raleigh

*Atomics International, Canoga Park, California*

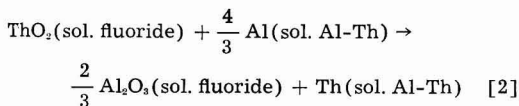
## ABSTRACT

When metallothermic reductions are carried out with an excess of the reducing metal, formation of an intermetallic compound between the reactant and product metals can make reduction energetically more favorable. Thorium oxide can be reduced by an excess of aluminum despite unfavorable standard-state energetics. The intermetallic compound involved is shown to be  $\text{ThAl}_3$ . From equilibrium experiments, its standard free energy of formation is estimated to be  $-36$  kcal.

Recent interest in our laboratory in alloys of thorium and their preparation led us to experimental work on the reduction of thorium oxide by metals less reactive than calcium. The reduction of thorium oxide by aluminum as a process for preparing thorium-aluminum alloys was achieved; studies on the optimum conditions for reduction are reported elsewhere (1). The occurrence of the reduction despite nominally unfavorable energetics was of interest to us. The standard-state reaction

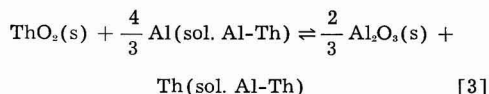


is associated with a positive free energy of reaction at all temperatures of interest. At  $1050^\circ\text{C}$ , the temperature chosen for our work,  $\Delta F = +38$  kcal from the reported (2) standard free energies of formation of  $\text{ThO}_2(\text{s})$  and  $\text{Al}_2\text{O}_3(\text{s})$ . In the process developed by us, however, the thoria is suspended or dissolved in a molten fluoride mix in contact with liquid aluminum and, since the product thorium is dissolved in the aluminum, the actual reaction is



It was suspected that the required chemical potential for the reaction was derived primarily from the formation of one or more intermetallic Th-Al compounds and their solution in the metallic melt. The possibility, however, of strong solute-solvent interaction between the alumina and the fluoride melt could not be eliminated. To clarify the situation, the series of experiments reported here was

carried out. Thorium-aluminum melts were equilibrated with a molten fluoride salt that was saturated with thoria and alumina and contained a solid excess of both. Under these conditions, the dissolved and solid oxides are in equilibrium, so that the reaction occurring may be written



By determining the equilibrium concentration of thorium in aluminum in this system and carrying out the necessary supplemental work, it was shown that the primary driving force for the reaction is the free energy of formation of  $\text{ThAl}_3$ , and an estimate of its value was made. The results indicate that intermetallic compound formation may play a useful role in promoting metallothermic reductions in a number of systems.

## Experimental

*Apparatus.*—The experimental work required a high-temperature inert atmosphere furnace system with provision for outgassing, stirring, and withdrawing samples from the reaction mix. The apparatus is shown in Fig. 1. The chemical systems of interest were heated in cylindrical graphite crucibles set inside a Vycor tube vacuum furnace as shown. Heating was provided by an induction coil connected to a  $2\frac{1}{2}$  kv-amp Lepel induction unit. Temperature was measured with a nickel-sheathed chromel-alumel thermocouple set into the crucible as shown and connected, through sealed copper leads, to a type 8662 L & N Millivolt Indicator. The thermocouple sheath was carefully grounded to

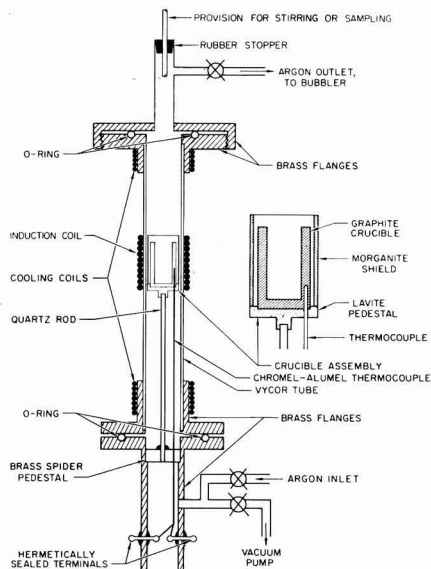


Fig. 1. Apparatus

insulate the thermocouple from induction currents. The temperature measured with this arrangement checked that of a test quantity of molten aluminum in the crucible as measured with a calibrated optical pyrometer to within several degrees at 1050°C. The temperature was controlled to  $\pm 5^\circ\text{C}$  by a Wheelco Capacitrol controller.

Vacuum and argon lines allowed outgassing and provision of the required inert atmosphere. The argon used was purified by passing it over uranium turnings at 500°C. The vacuum line was connected to a Kinney KC-5 vacuum pump and the vacuum pressure measured with a standard thermocouple gauge. By use of a greased rubber stopper, the furnace top was equipped for gastight operation of either a motor-driven stirring rod or a sampling tube.

The metals used in this work were reactor grade thorium and 99.99% ingot aluminum. The chemicals employed were reagent grade lithium fluoride, aluminum oxide, and thorium oxide. No further purifications were carried out.

**Selection of salt phase.**—To carry out the equilibration studies between Al-Th alloy and the oxides of aluminum and thorium with favorable kinetics, a suitable molten salt flux was required. Since the salt mix was to be saturated with both oxides, the oxide solubilities in the mix needed to be moderate, but not high, to achieve saturation conveniently and avoid unfavorable increases in the viscosity of the melt. Further, no reaction or compound formation is allowable between the salt melt and either the oxides or the molten metal phase. Fluoride salts were favored because of their solubilities for metallic oxides, but cryolite mixes were found to be unsuitable because of reaction with the aluminum<sup>1</sup> and excessive alumina solubility. The following experiments showed lithium fluoride to be inert toward alu-

minum under the planned equilibration conditions.

Identical mixtures of lithium fluoride and aluminum were heated for 1 and 2 hr, respectively, at 1050°C under 1 atm of argon in the described apparatus. Analysis of both metal phases by flame photometry showed less than 0.03 w/o (weight per cent) Li present. The aluminum content in the molten LiF was found to be 2.28 w/o in both runs as determined by EDTA titration, but the absence of the corresponding amount of Li in the metal phase and the constancy of the Al content indicated that this represented the solubility of aluminum in molten LiF at 1050°C.

That no solute-solvent reactions occurred between the oxides and LiF was shown later, in the equilibrium reduction runs, where x-ray diffraction analyses on the salt phase showed patterns only for  $\text{ThO}_2$ ,  $\text{Al}_2\text{O}_3$ , and LiF.

As will be seen later, solution of the thorium in aluminum reduces its activity sufficiently that it could not be expected to react with the LiF.

**Solubilities of oxides.**—To obtain useful background information for the equilibration studies, the solubilities of  $\text{Al}_2\text{O}_3$  and  $\text{ThO}_2$  in molten LiF at 1050°C were determined separately and in common solution. In several preliminary runs, limits of solubility and relative supernatant and precipitate volumes were determined by heating LiF- $\text{ThO}_2$  and LiF- $\text{Al}_2\text{O}_3$  mixtures for ½ hr at 1050°C in our apparatus and examining the frozen melts. In each case, sharp separation into precipitate and supernatant regions was evident.

To determine the solubilities, two experimental procedures were used. In the first, a mixture of 0.4g of  $\text{Al}_2\text{O}_3$  and 7.1g LiF was placed in the furnace setup, outgassed, and heated at 1050°C under argon. After heating for ½ hr at this temperature, a quartz tube in the apparatus was lowered into the crucible to just above the melt surface. After several minutes to allow the tube end to come to the melt temperature, the tube was lowered into the supernatant zone and a melt sample withdrawn by means of a suction gun. The tube was then removed from the furnace, the sample recovered, and the tube replaced. Acceleration of the argon flow during tube removal minimized entry of air into the system. Following replacement of the tube, the crucible temperature was raised to 1100°C, held at this temperature for ½ hr to hasten saturation, lowered to 1050°C, held at 1050°C for ½ hr, and the next sample taken. This procedure was then repeated twice more for a total of four samplings. Samples were analyzed for Al by EDTA titration. The procedure was repeated in a second run with a mixture of  $\text{ThO}_2$ ,  $\text{Al}_2\text{O}_3$ , and LiF to determine the solubilities of the oxides in common solution.

In the second procedure, used as a partial check, the apparatus was equipped with a motor-driven, graphite-tipped stirring rod. A  $\text{ThO}_2$ -LiF mixture was outgassed, heated to 1050°C, and held at this temperature. Three cycles were then carried out in which the mixture was stirred for 3 min, allowed to settle for 25 min, and sampled as before. The furnace was then shut down, a portion of  $\text{Al}_2\text{O}_3$  added atop the cooled mix, the crucible reheated to 1050°C, and

<sup>1</sup>  $\text{Na}_3\text{AlF}_6 + \text{Al} \rightarrow 3\text{Na}\uparrow + 2\text{AlF}_3$ .

Table I. Solubilities of  $\text{Al}_2\text{O}_3$  and  $\text{ThO}_2$  in LiF at 1050°C

Run	Procedure	Solute	w/o Solute in sample				Assumed solubility
			1	2	3	4	
1	1st	$\text{Al}_2\text{O}_3$	0.26	0.26	0.28	0.32	0.30 (?)
2	1st	$\text{Al}_2\text{O}_3$	0.28	0.32	0.38	0.38	0.38
		$\text{ThO}_2$	0.05	0.05	0.08	0.06	0.06
3	2nd	$\text{ThO}_2$	<0.04	<0.03	<0.04	—	<0.04
4	2nd	$\text{Al}_2\text{O}_3$	0.41	0.43	0.38	—	0.41
		$\text{ThO}_2$	0.05	0.09	0.06	—	0.07

three more cycles of stirring, settling, and sampling carried out.

The results of all solubility determinations appear in Table I. Accuracies of individual sample analyses were about 0.01 w/o for the  $\text{ThO}_2$  contents and 0.02 w/o for the  $\text{Al}_2\text{O}_3$  analyses. Of primary interest in our work were the solubilities of the oxides in common solution, which agree well in the two procedures, despite the nearness to the limits of analysis for the thorium content. In interpreting sample analyses from the runs carried out by the temperature cycling (first) procedure, constant solute contents in the last few samples are taken to indicate saturation. Thus, the choice of 0.38 w/o as the alumina solubility in run 2 seems reasonable, and the absence of any significant progression in the  $\text{ThO}_2$  content in this run allows us to take a simple average. Results, however, are not as clear-cut in run 1. One believes that the runs with stirring (second procedure) are more reliable in that the constancy of alumina contents in the samples indicate a rapid attainment of saturation. The thorium solubility in run 3 is seen to be below the limit of analysis, but the general picture indicates somewhat of an increase of the solubilities of both  $\text{ThO}_2$  and  $\text{Al}_2\text{O}_3$  when present in common solution in LiF.

*Equilibration experiments.*—Several preliminary runs, in which LiF- $\text{ThO}_2$ - $\text{Al}_2\text{O}_3$  mixes were heated in contact with Th-Al alloy melts for several hours at 1050°C, indicated that great care was needed to achieve equilibrium. Continuous stirring was required, so the motor-driven graphite-tipped stirring rod was installed in the apparatus. The arrangement, however, led to poor phase separation and extensive aluminum carbide formation from the metallic aluminum, so the graphite crucible was fitted with a liner of recrystallized alumina and a stirring rod tip of the same material was used. Partial solution or disintegration of the stirring rod tip occurred during runs, despite the presence of more than the saturation limit of  $\text{Al}_2\text{O}_3$  in the initial salt mix. However, since the runs were to be carried out at any rate with the salt flux saturated with both oxides, this constituted no problem.

The series of equilibration runs was carried out as follows. Preliminary runs showed an achievable thorium build-up of at least 10 w/o in the metal phase, so a quantity of Al 10 w/o Th alloy was prepared by heating the alloy components for several hours at 1050°C in an argon atmosphere. A mixture of LiF and enough  $\text{ThO}_2$  and  $\text{Al}_2\text{O}_3$  to well exceed their solubility limits was then outgassed and heated for 15 min at 1050°C under argon to provide a suitable salt phase. The metal and salt phases were then

heated together to 1050°C under argon, the motor-driven stirring rod gradually lowered into the melt, and the mixture heated for 2 hr, with continuous stirring, at 1050°C. The stirrer was then withdrawn, the mix cooled quickly, and the metal phase from the run recovered and analyzed *in toto*. The analysis showed a considerable increase in the metal phase thorium content, so a metal phase of the approximate new alloy composition was prepared and another run carried out with a salt phase of the same composition. This was repeated until the metal phase showed only a small further increase in thorium content, whereupon a metal phase with a much higher thorium content was prepared and a similar run carried out. This run showed a decrease in thorium content of the metal phase, so the procedure was repeated with initial metal phases of successively smaller thorium content.

The results of the experiments are shown in Table II. It is seen that the procedure resulted in a near-approach to equilibrium. The assumed equilibrium concentration of Th in the metal phase is  $28.1 \pm 0.2$  w/o thorium.

*Metal phase studies.*—As seen later, the above equilibrium concentration can be used with the known free energy of reaction of Eq. [1] to estimate the standard free energy of formation of the intermetallic compound involved in Eq. [3]. To do this, however, requires knowing the exact identity of this compound and the solubility of thorium in aluminum at the temperature of interest. In both cases, reported work is in some disagreement. For our work, the intermetallic compound of interest was the one which is in equilibrium with a saturated solution of thorium in aluminum at 1050°C. Aluminum-thorium phase diagrams by different workers (3-5) however, variously indicate this compound to be  $\text{ThAl}$ ,  $\text{ThAl}_2$ , and  $\text{ThAl}_3$ . Work by Leber (3) indicated the solubility of Th in Al at 1050°C to be 55 w/o, but other work (4) was in disagreement.

The solubility of thorium in liquid aluminum at 1050°C was determined by the first procedure used for oxide solubilities. A mixture of 10g aluminum and 26.5g thorium, the latter in small pieces, was heated to 1050°C in argon, under 0.5g LiF to serve

Table II. Weight per cent Th in equilibration run metal phases

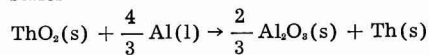
Run	Initial	Final
1	10.0	20.3
2	18.9	26.2
3	25.0	27.9
4	40.0	35.2
5	35.0	28.3

as a flux. The mixture was heated at 1050°C for ½ hr and a sample of the melt withdrawn. Then, as in previous runs, the melt was heated at 1100°C for ½ hr, cooled and held at 1050°C for ½ hr, and the second sample taken. The process was repeated to obtain a third sample, using, as before, a quartz tube and suction gun. The thorium analyses on the three samples were 52.4, 54.6, and 54.6 w/o, respectively. Since the previous solubility data of Leber were obtained by cooling curve analysis, it was felt that an adequate check was obtained and that 55 w/o is the correct solubility of thorium in aluminum at 1050°C.

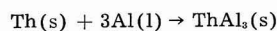
The identity of the intermetallic compound in equilibrium with a saturated solution of thorium in aluminum at 1050°C was established as follows. A mixture of Th and Al corresponding to a 55 w/o thorium alloy was heated at 1060°C for 2 hr to dissolve all of the thorium. The melt was then cooled to 925°C over a period of ½ hr, and the temperature held at 925°C for another half-hour. The bulk of the melt liquid was then removed from the crucible at 925°C by means of a quartz tube and suction gun. The material remaining in the crucible was a mat of well-defined needlelike crystals. The crucible was quickly cooled to room temperature and the crystals separated from an adhering residue of solidified melt liquid by dissolving away the latter with 10% aqueous NaOH. Chemical analysis and x-ray diffraction identified the crystals as ThAl<sub>3</sub>. Since none of the phase diagrams reported showed any phase changes or thermal arrests between 1060° and 925°C, and since melt liquid was not available for reactions below 925°C, it was assumed that the crystals recovered are those of the stable aluminide at 1050°C. The result is in agreement with the work of Murray (5), which is the most recent work on this portion of the Th-Al phase diagram.

### Discussion

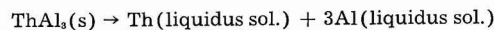
The results of the preceding experimental work can be used to estimate the standard free energy of formation of ThAl<sub>3</sub>. The reduction of thorium oxide to produce thorium-aluminum alloy can be considered in terms of the virtual formation of ThAl<sub>3</sub> and its solution in a sufficient excess of aluminum to result in the metal phase of equilibrium composition. Accordingly, Eq. [3], for the reaction at 1050°C, can be written in terms of the equivalent series



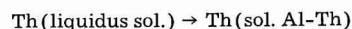
$$\Delta F_1 = +38 \text{ kcal}$$



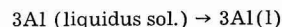
$$\Delta F_2 = \Delta F_f^\circ (\text{ThAl}_3)$$



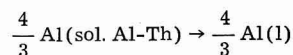
$$\Delta F_3 = 0$$



$$\Delta F_4 = -RT \ln \frac{a_{\text{Th}}^{\text{sol}}}{a_{\text{Th}}}$$



$$\Delta F_5 = -RT \ln (a_{\text{Al}}^{\text{sol}})^3$$



$$\Delta F_6 = -RT \ln (a_{\text{Al}})^{4/3}$$

where  $\Delta F_f^\circ (\text{ThAl}_3)$  is the standard free energy of formation of ThAl<sub>3</sub>,  $a^{\text{sol}}$  refers to activities in the liquidus Th-Al melt (i.e., saturated solution of Th in Al), and  $a_{\text{Al}}$  and  $a_{\text{Th}}$  to activities in the melt of equilibrium composition. Since the over-all reaction is an equilibrium reaction,  $\Sigma \Delta F = 0$ , and thus

$$-\Delta F_f^\circ (\text{ThAl}_3) = 38 - RT \ln (a_{\text{Al}}^{\text{sol}})^3 (a_{\text{Al}})^{4/3} \left( \frac{a_{\text{Th}}^{\text{sol}}}{a_{\text{Th}}} \right)$$

We recall that the concentrations of thorium in the equilibrium and liquidus melts at 1050°C were 28 w/o and 55 w/o, respectively. In terms of mole fractions, however, the solutions are considerably more dilute, the mole fractions being 0.043 and 0.125. Thus, there is some basis for evaluating the above activities by the use of Raoult's and Henry's laws. While the concentrations involved are admittedly marginal for this approach, no specific data on activity coefficients exist. Further, it will be seen that the activity factor term in the above expression provides only a small contribution to the calculated free energy of formation, so that even large inaccuracies in evaluating the term will have a small effect on the final result. The assumption of Raoult's and Henry's laws, then, allow the following substitutions:  $a_{\text{Al}} = N_{\text{Al}}$  and  $a_{\text{Th}}^{\text{sol}}/a_{\text{Th}} = N_{\text{Th}}^{\text{sol}}/N_{\text{Th}}$ , and accordingly,

$$-\Delta F_f^\circ (\text{ThAl}_3) = 38 - RT \ln (N_{\text{Al}}^{\text{sol}})^3 (N_{\text{Al}})^{4/3} \left( \frac{N_{\text{Th}}^{\text{sol}}}{N_{\text{Th}}} \right)$$

Using the stated values for the indicated mole fractions, one obtains, for the standard free energy of formation of ThAl<sub>3</sub> at 1050°C, an estimate of 36 kcal.

It is seen that the predominant driving force for the nominally unfavored reduction of thorium oxide by aluminum is the free energy of formation of the intermetallic compound ThAl<sub>3</sub>; associated dilution effects play an energetically small role. Even large errors in the activities, which may be involved in assuming the applicability of Raoult's and Henry's laws, will not significantly affect the calculated free energy of formation. What is more important in this respect, however, is the accuracy to which the relative free energies of formation of thoria and alumina at 1050°C are known. Estimated limits of error from Kubaschewski (2) and various original reports of these measurements indicate that the 38 kcal figure may be in error by as much as 5 kcal. Accordingly, until more accurate data become available, the -36 kcal free energy of formation of ThAl<sub>3</sub> at 1050°C must be regarded as subject to the same uncertainty. It is felt, however, that this value at least gives some indication of the stability of such compounds. It would be of interest if this quantity could be determined experimentally by an independent method.

### Acknowledgments

The author wishes to thank Mr. W. D. Turner for considerable assistance in the experimental work reported. The support of the United States Atomic Energy Commission is gratefully acknowledged.

Manuscript received Sept. 25, 1961; revised manuscript received Feb. 16, 1962.

Any discussion of this paper will appear in a Discussion Section to be published in the December 1962 JOURNAL.

## REFERENCES

1. D. O. Raleigh, *Ind. Eng. Chem.*, **53**, 445 (1961).
2. O. Kubaschewski and E. L. Evans, "Metallurgical

Thermochemistry," John Wiley & Sons, Inc., New York (1956).

3. A. Leber, *Z. anorg. u. allgem. Chem.*, **166**, 16 (1927).
4. F. A. Rough and A. A. Bauer, U. S. Atomic Energy Commission Report BMI-1300 (1958).
5. J. R. Murray, *J. Inst. Metals*, **87**, 349 (1959).

## Diagrammatic Representation of the Thermodynamics of Metal-Fused Chloride Systems

R. Littlewood<sup>1</sup>

*Tube Investments Research Laboratories, Hinxton Hall, Saffron Walden, Essex, England*

## ABSTRACT

Previously, diagrammatic methods of presentation have been used to study the thermodynamics of metallic corrosion in fused chlorides, and the method has now been extended to metal-winning reactions. Diagrams in which the equilibrium potential  $E$  (relative to the standard chlorine electrode) in the system is plotted against the activity of oxide ion in the chloride melt (expressed as its negative logarithm,  $pO^{2-}$ ) are presented for the metals Mg, Ni, Zr, and Ti in contact with one or more of the chlorides LiCl, KCl, NaCl, and MgCl<sub>2</sub> at 800°C. As an example of the use of  $E$ - $pO^{2-}$  diagrams, it is shown how they can be applied to metal extraction processes involving chlorides. The main advance here is that the method offers an approach to the prediction of impurity levels and is applicable equally well to electrowinning from fused chlorides and to reduction of chlorides by base metals. Levels of impurity, particularly of oxygen, in the metal product are obtainable directly from the diagrams.

The thermodynamics of metal-fused chloride systems is more complicated than appears at first sight especially when reactions involving impurities, particularly anions, are taken into consideration. The success of graphical methods of presenting thermodynamic data for aqueous systems led us to develop similar ways of presentation for fused salt systems, and we have already applied some of these to study the thermodynamics of metallic corrosion in fused chlorides (1, 2).

The presentation of thermodynamic data in a diagram has certain advantages which have not always been fully appreciated. When considering a system of a number of components, one method involves conversion of the data into linear equations linking free energy with logarithmic functions of composition. There is one such equation for each possible reaction of all the various constituents present. The relations are plotted graphically, and the resulting diagram summarizes the thermodynamic properties of the system at a given temperature. This simplicity of presentation is to be compared with the application of a similar series of equations to each particular set of conditions, from which the behavior of the system under that particular set of conditions is inferred. In this case, if the properties of the system under several different conditions are required, the whole procedure usually has to be repeated. Where a general appreciation of the effect on the system of a variety of different conditions is required, presentation of the properties of the system in a diagram has obvious advantages.

The thermodynamic diagrams of Pourbaix (3) have been particularly useful in understanding the

behavior of metals in contact with aqueous solutions. Pourbaix plots equilibrium potential against  $pH$ , and the diagrams divide themselves into regions of stability of different solid phases (compounds of the metal in question).

In the fused salts also, free energies can be expressed as equilibrium potentials, and there are a number of functions of composition which might be used as the other variable. In the present paper, the composition variable chosen is the activity of oxide ion in the melt, expressed in terms of its negative logarithm,  $pO^{2-}$ . The resulting  $E$ - $pO^{2-}$  diagrams are particularly useful when considering systems involving oxides, or oxygen, in contact with fused chlorides, and in practice this covers all conditions under which fused chlorides are normally used. As an example, the paper shows in particular how  $E$ - $pO^{2-}$  diagrams are applicable to metal extraction processes involving chlorides.

*Conventions.*—In aqueous systems, the conventions used in a thermodynamic treatment are well established. With reactions in fused salts, the conventions adopted in a particular treatment need to be defined at the outset. The conventions chosen for the present paper are identical with those used previously by the author (1, 2). Free energies are converted to an emf scale using the expression

$$E^{\circ} = -\Delta G^{\circ}/nF \quad [1]$$

and the potential zero is taken as the potential of a chlorine electrode (1 atm pressure) in contact with a chloride melt at unit chloride activity. Activities in condensed phases are based on the pure component as the standard state, or in the case of gases, the gas at unit fugacity, approximately 1 atm pressure.

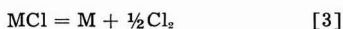
<sup>1</sup> Present address: The British Iron and Steel Research Association, London, England.

## Principles

A fused chloride melt is stable over a range of potential, which at one atmosphere pressure extends from zero on the chlorine electrode scale, where the melt will be in equilibrium with chlorine at 1 atm pressure, to a negative value of potential equal to the decomposition potential of the melt. The latter is related to the free energy of formation of the chloride by Eq. [1], and the decomposition potential will be more negative the more stable the chloride. Between these two potentials, the chloride will always be partially dissociated and the activities of metal and chlorine in the melt will vary with potential, while conforming to the equilibrium constant (parentheses denote activities).

$$K = \frac{(Cl_2)^{1/2} (M)}{(MCl)} \quad [2]$$

of the reaction



This equilibrium constant is obtainable from the expression

$$\log K = -\Delta G^\circ_{MCl}/2.303 RT \quad [4]$$

where  $\Delta G^\circ_{MCl}$  is the free energy of dissociation of the chloride MCl. The activity of free metal and of free chlorine present in the melt at any given potential  $E$  can be calculated from the Nernst equations for the two half-reactions.



Thus, when MCl is present at unit activity,

$$E = E^\circ_{Cl} + (2.303 RT/F) \log (Cl_2)^{1/2} \quad [7]$$

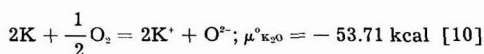
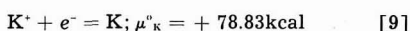
for half-reaction [5], and

$$E = E^\circ_M - (2.303 RT/F) \log (M) \quad [8]$$

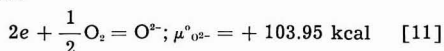
for half-reaction [6], where  $E^\circ_M$  can be calculated from relation [1].

The two expressions for  $E$  (Eq. [7] and [8]) are identities, since the equilibrium potential in the system has a unique value, and in fact Eq. [7] and [8] are interrelated by Eq. [2].

To deal with a system containing oxygen and oxides, it is necessary to define a standard state for the oxide ion, and in accordance with the conventions adopted, we have chosen the pure oxide of the cation of the chloride melt under consideration as unit activity of oxide ion. For example, in the case of a KCl melt the standard state for oxide ion would be pure  $K_2O$  and the standard free energy of formation of  $O^{2-}$  ion would be calculated as follows:



therefore



A standard free energy of formation of the oxide ion defined in this way will differ in value accord-

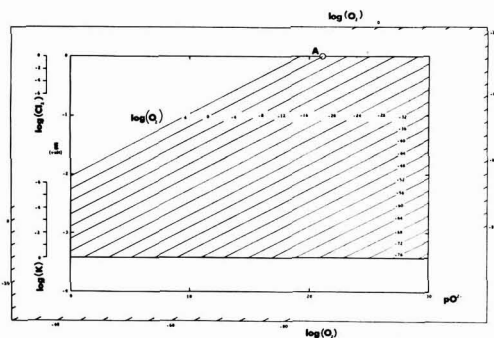


Fig. 1. Relationship between oxygen pressure, oxide activity, and potential for KCl at 800°C.  $E$  is electrode potential relative to the standard chlorine electrode. For point A, see text.

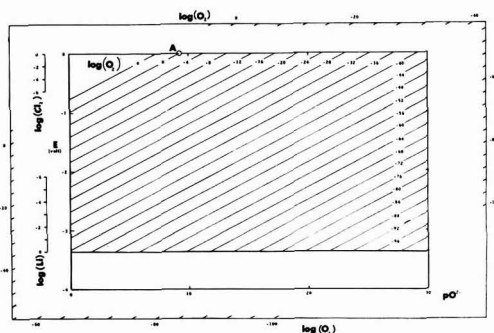


Fig. 2. Relationship between oxygen pressure, oxide activity, and potential for LiCl at 800°C.

ing to the particular melt chosen. In mixed chlorides, the activity of  $O^{2-}$  will be expressed in terms of one particular oxide, but provided a single definition is adhered to throughout the treatment, the final results will be the same whichever oxide is chosen, although oxides of cations other than the standard one might have either extremely large or extremely small activity coefficients.

The standard free energy of formation for the oxide ion can now be used to express the relationship between potential, oxygen pressure, and oxide activity

$$E = E^\circ_{O^{2-}} + (2.303RT/2F) \log [(O_2)^{1/2}/(O^{2-})] \quad [12]$$

This relationship is shown graphically for KCl at 800°C in Fig. 1 and for LiCl at 800°C in Fig. 2. For a given oxygen pressure, Eq. [12] gives rise to a straight line dependence of  $E$  on  $pO^{2-}$  and in the figures, oxygen pressures at intervals of  $10^4$  apart are shown, giving a grid of parallel lines. The position of these lines corresponds with the two oxygen pressure scales external to the diagrams (the line for a given oxygen pressure is found by laying a ruler on the diagram joining the appropriate points on the two scales). The upper and lower limits to the diagrams are set by the potentials at which the melt is oxidized to chlorine or reduced to metal, respectively. The other two external scales on the left-hand side give the activity of chlorine or metal present at a given potential, according to Eq. [7] and [8].

Figures 1 and 2 illustrate the marked differences in properties between melts of LiCl and KCl, which will be discussed in more detail later. Note, however, that the oxide activities in melts of LiCl and KCl prepared under atmospheres of identical composition will be very different. For example, the equilibrium conditions in melts prepared under an atmosphere of equal parts of oxygen and chlorine at a total pressure of 2 atm would be represented by the points marked A in Fig. 1 and 2. These correspond to oxide activities of  $10^{-9.8}$  in LiCl and  $10^{-21.1}$  in KCl, illustrating the effect of the higher affinity for oxygen of Li relative to K.

There is provision in the diagram for oxygen pressures down to extremely low values. These pressures are still meaningful and are particularly important when dealing with systems under reducing conditions, such as in the presence of metals which are strong oxygen getters, or in hydrogen atmospheres. For example, hydrogen gas at 1 atm pressure containing 1 volume per million of water vapor would be in equilibrium with an oxygen partial pressure of about  $10^{-40}$  atm, and these conditions could therefore in principle be represented on the  $E-pO^2$  diagram by the line corresponding to an oxygen pressure of  $10^{-40}$  atm.

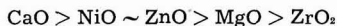
The solubility product of any oxide in a given chloride MCl can also be calculated, relative to the oxide  $M_2O$ . For example, the solubility product of nickel oxide in a KCl melt at 800°C is obtained as follows. When the melt is saturated with NiO, excess solid oxide will be present at unit activity, and since the system is at equilibrium, the free energy change for the dissolution reaction



will be zero, so that

$$\log S = \log (\text{Ni}^{2+}) (\text{O}^{2-}) = (\mu_{\text{NiO}} - \mu_{\text{Ni}^{2+}} - \mu_{\text{O}^{2-}}) / 2.303RT \quad [14]$$

Table I gives the values of activity solubility products of some oxides in melts of LiCl and in KCl calculated in this way. These illustrate the greater solubility of oxides in LiCl than in KCl, as observed experimentally (4). In addition, the relative magnitudes of solubility product of the oxides in either chloride are in the order



which corresponds well with experimental observations of oxide solubilities in LiCl (4), KCl (4), and LiCl-KCl eutectic (5).

Experimental data on oxide solubilities in fused chlorides are very scanty, and no attempts to de-

termine solubility products appear to have been made. Solubility products cannot, of course, be obtained directly from simple solubility measurements of the oxide in the chloride alone, but this point will be commented on later. It will only be possible to assess fully the significance of the calculated values when experimental values of activity solubility products become available, but it appears justifiable at the moment to accept solubility products calculated in this way.

The grid showing equilibria in the system KCl —  $\text{O}_2$  —  $\text{O}^{2-}$  (Fig. 1) can now be used as a reference frame on which to superimpose domains of thermodynamic stability of compounds formed between components of this system and another metal, such as in Fig. 3, which is for the Mg—KCl system. For clarity, the reference grid of oxygen pressure lines has been omitted, but any line may be found simply by laying a ruler on the diagram joining the appropriate points on the two external oxygen pressure scales. Scales showing the activity of chlorine and of potassium in the melt are also given on the left as before. KCl is stable at 800°C down to a potential of  $-3.42v$ . The region of stability of KCl divides up into three domains (as shown by the heavy lines in Fig. 3) in each of which one and only one compound of Mg can be present at unit activity. In the domain marked MgO, MgO (solid, unit activity) is in equilibrium with a melt of KCl containing  $\text{MgCl}_2$  and  $\text{O}^{2-}$  ions. The activity of  $\text{Mg}^{2+}$  in the melt can be found from the vertical isoactivity lines connecting with the  $\log (\text{Mg}^{2+})$  scale directly above the diagram. It can be seen that as the activity of  $\text{O}^{2-}$  ion in the melt falls, the activity of  $\text{Mg}^{2+}$  rises until at a value of  $pO^{2-}$  of 21.83 (and provided  $E$  is above  $-2.47v$ ), solid MgO at unit activity can coexist with  $\text{MgCl}_2$  at unit activity. At values of  $pO^{2-}$  greater than 21.83, MgO can only exist at an activity less than unity (i.e., in solution) and we pass into the domain marked  $\text{MgCl}_2$ . At values of  $pO^{2-}$  greater than 21.83, Eq. [19], in which the activity of MgO is taken to be unity, tells us that  $(\text{Mg}^{2+})$  must be greater than unity. This is physically meaningless, since activities can never exceed unity using the present conventions. Hence the activity of MgO must be less than unity.

In the domain  $\text{MgCl}_2$ , the melt may contain  $\text{Mg}^{2+}$ ,  $\text{O}^{2-}$ , and Mg in solution in KCl, but the only compound of Mg which can be present at unit activity is  $\text{MgCl}_2$ . Its activity is not necessarily unity, and it can have any value between unity and values approaching zero. This is because the value of  $E$  defines only the value of the ratio  $(\text{Mg}^{2+})/(\text{Mg})$  and not the absolute values of  $(\text{Mg}^{2+})$  or  $(\text{Mg})$  which accordingly can vary over a wide range while keeping the ratio of their activities constant. The same components  $\text{Mg}^{2+}$ ,  $\text{O}^{2-}$ , and Mg are present in the melt in the domain marked Mg metal, which is divided from the  $\text{MgCl}_2$  domain by a horizontal line at a value of  $E$  of  $-2.47v$ , but in this domain, it is possible for Mg metal to be present at unit activity. The potential of  $-2.47v$  is simply that potential at which Mg metal at unit activity can coexist with unit activity of  $\text{MgCl}_2$ . The horizontal isoactivity lines, which connect with the  $\log (\text{Mg}^{2+})$  scale to the

Table I. Calculated solubility products of oxides in fused chlorides at 800°C

Oxide	$\log S$ in LiCl	$\log S$ in KCl
NiO	-7.8	-19.7
CaO	-3.8	-15.8
ZnO	-8.2	-20.0
MgO	-9.9	-21.8
ZrO <sub>2</sub>	-26.8	-50.6

right of the diagram, can be used to find the activity of  $Mg^{2+}$  in the melt which would be in equilibrium with Mg metal at any given potential. The boundary between the Mg metal and MgO domains is a line representing the conditions under which Mg metal and MgO can coexist, each at unit activity, and corresponds to a value of  $\log(O_2)$  of  $-47.72$ , the dissociation pressure of MgO.

Figure 3 shows that solubility of an oxide in a fused chloride at a given temperature depends on several factors, an understanding of which is needed to obtain values of solubility products from solubility measurements. The solubility of MgO in KCl would be estimated by measuring the concentration of  $Mg^{2+}$  ions in the KCl melt, but this will depend on the value of  $pO^{2-}$  in the melt as in the case of an oxide in contact with an aqueous solution. For example, at a value of  $pO^{2-}$  of 21.83, the  $Mg^{2+}$  activity in the melt would be unity; at a value of  $pO^{2-}$  of 15.83, it would be  $10^{-5}$  (Fig. 3). The results of solubility measurements will therefore depend very markedly on the value of  $pO^{2-}$  in the melt and this will need to be closely controlled. Solubility experiments described in the literature (4, 5) have not been deliberately controlled in this way, although contact with a glass or ceramic container would fix  $pO^{2-}$  at a value dependent on the nature of the oxides present in the container material (1, 6, 7) (contact with an air atmosphere would not fix the value of  $pO^{2-}$ , Fig. 1 and 2). The experimental solubilities obtained in a particular case, can in fact, be used to estimate the conditions in the melt during the experiment. Voskresenskaya and Kashcheev (4) obtained a value for the solubility of MgO in KCl at  $900^\circ C$  of about 0.002%: for the purpose of this example at  $800^\circ C$ , let us say a mole fraction of  $Mg^{2+}$  in the melt, of  $10^{-5}$ . The measurements were made in an air atmosphere (oxygen at 0.2 atm pressure), so that writing mole fraction of  $Mg^{2+}$  as activity of  $Mg^{2+}$ , after Temkin (8), we can plot a point representing this result on Fig. 3 (point A). The conditions in the melt during these experiments must therefore have been as follows

potential  $-0.5v$ ,  $pO^{2-}$  16.83

Diagrams similar to Fig. 3 can be constructed for any metal and those for nickel in KCl and in LiCl at  $800^\circ C$  are shown in Fig. 4 and 5. For metals hav-

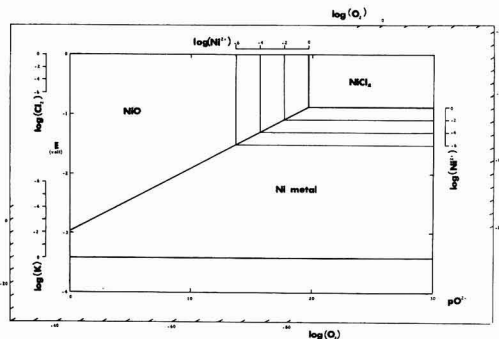


Fig. 4.  $E$ - $pO^{2-}$  diagram for the system Ni-KCl at  $800^\circ C$

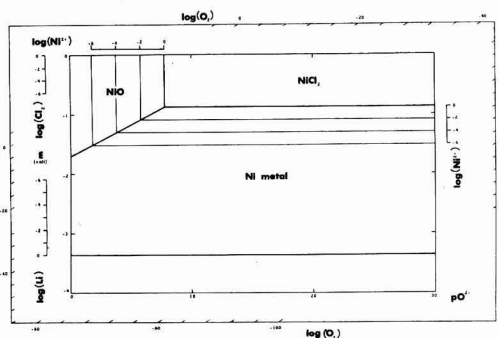


Fig. 5.  $E$ - $pO^{2-}$  diagram for the system Ni-LiCl at  $800^\circ C$

ing more than one stable chloride (Figs. 6, 7, 9, 10), the situation is more complex because there is more than one way of presenting the data. For example, a set of isoactivity lines corresponding to the equilibrium of each chloride could be plotted, and at some potential the sum of the activities would become equal to unity. At potentials above this value, the only significance of the scales would be to indicate the ratios of the ion activities to that of the metal in the melt, and since the latter would be undefined, this would be a somewhat indefinite way of presenting the data. It is more convenient not to attempt to show separately the activity of every possible metal ion, but instead to express melt compositions in terms of other variables. In the diagrams presented here, the variables chosen were the sum of the activities of all ions of the metal,  $(M^+) + (M^{2+}) + (M^{3+}) + \text{etc.}$ , and the ratios of the activities of ions with a valency difference of one,  $(M^{n+}) / (M^{n-1})$ , etc. The latter are plotted as scales external to the diagram in Fig. 6 and 7, while the sum of the metal ion activities is plotted as isoactivity lines on the diagram. Changes in redox equilibria in the melt cause these lines to curve, but nevertheless, this type of diagram is much simpler than one showing separately the activities of all possible chlorides. A diagram for Zr in contact with a KCl melt at  $800^\circ C$  is shown in Fig. 6. The domains are exactly analogous to the magnesium case, but are distorted in shape at potentials where changes in redox equilibria occur. The two scales at the right-hand side of the diagram indicate the position of redox equilibria of zirconium ions in the melt. These, in con-

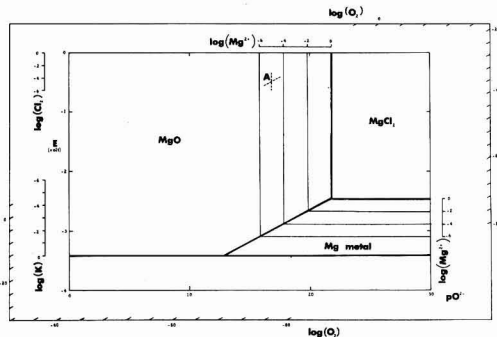


Fig. 3.  $E$ - $pO^{2-}$  diagram for the system Mg-KCl at  $800^\circ C$ . For point A, see text.



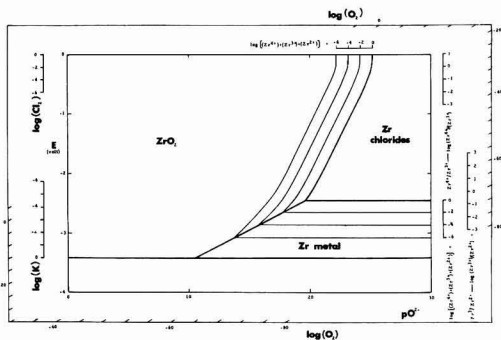


Fig. 6.  $E$ - $pO_2$  diagram for the system Zr-KCl at 800°C

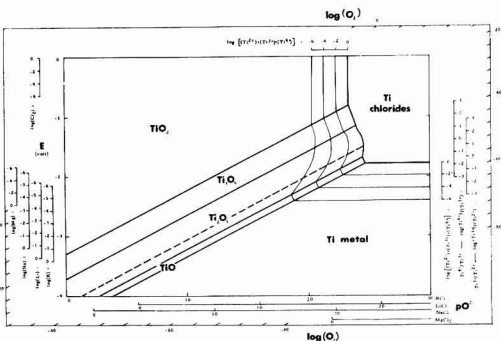


Fig. 7.  $E$ - $pO_2$  combined diagram for the systems Ti-MgCl<sub>2</sub>, Ti-NaCl, Ti-LiCl, and Ti-KCl at 800°C.

junction with the isoactivity lines on the diagram showing the sum of the activities of Zr ions, allow the exact composition of the melt in terms of KCl, ZrCl<sub>4</sub>, ZrCl<sub>3</sub>, and ZrCl<sub>2</sub> to be found.

For metals with more than one oxide, there are further domains, one for each stable oxide, as in the case of titanium (Fig. 7). In addition to domains showing the conditions under which each of the oxides is thermodynamically stable, domains can also be delineated in which one of two solid substances is stable with respect to the other. For example, the dotted line shows where TiO<sub>2</sub> becomes stable with respect to Ti metal. (The corresponding lines for the other oxides are not shown, as they would increase the complexity of the diagram without materially increasing its usefulness). It should be clearly understood that TiO<sub>2</sub> is stable only in the region within the TiO<sub>2</sub> domain, but in view of the sluggishness of solid-state transformations, it might be kinetically favored over a wider range of conditions than indicated by the stability region of the diagram. The position of the dotted line gives an indication of this extension of the range of conditions under which TiO<sub>2</sub> might exist, for reactions involving metallic titanium.

In Fig. 7, a further modification has been introduced which makes the diagram applicable to titanium in LiCl, NaCl, or MgCl<sub>2</sub> as well as in KCl. The scales to the left of the diagram show the limits of stability of these melts, and the parts of the diagram extending below these limits in each particular case have, of course, no physical significance.

$pO_2$  scales for each chloride are given on the lower edge of the diagram and again, parts of the diagram to the left of the zero value of  $pO_2$  for each particular chloride have no meaning. The O<sub>2</sub> pressure scales and isoactivity lines referring to titanium ions are common to all the four chlorides, LiCl, NaCl, KCl, and MgCl<sub>2</sub>.

Details of the construction of these diagrams are given in the appendix.

### Applications of the Diagrams

The present diagrams have much in common with  $E$ - $pH$  diagrams for aqueous systems, which have become well-known largely through the work of Pourbaix and his collaborators (3). It is expected that  $E$ - $pO_2$  diagrams for fused salts will prove at least as useful as these and if anything, they should be more directly applicable because at the higher temperatures common in salt melts, reactions have a greater chance of reaching equilibrium than in aqueous solutions at room temperature. In other words, predictions made about metal-fused salt systems from  $E$ - $pO_2$  diagrams are likely to be as exact as the thermodynamic data on which they are based, since most reactions in melts at high temperatures are reversible.

The condition of any system is represented on the diagrams by a point, and the equilibrium positions of all the reactions which the constituents can undergo is determined by projecting this point on to the appropriate scales, or by noting its position relative to appropriate isoactivity lines. The position of the system-point can be found if any two independent variables in the system are known. For example, if besides potential, we know either the activity of oxide ion in the melt or the partial pressure of oxygen at equilibrium, the position of the system-point is defined.

Some general conclusions regarding the possible applications of  $E$ - $pO_2$  diagrams in fused chlorides can be reached without recourse to detailed practical examples, and it is felt that the following are some of the main fields in which they might be used. The list is not considered to be exhaustive and simple cases are chosen to make the principles clear.

*Aggressiveness of melts.*—Consideration of the factors affecting corrosion of metals in fused chlorides has shown (1,2) that the stability of the chloride is of primary importance. Since the decomposition potentials of LiCl and KCl have similar values, it might be expected that their aggressiveness would be similar under comparable conditions. It is well known, however, that this is not so and under the same conditions of temperature, atmosphere composition, drying procedure etc. LiCl is the more aggressive towards metals. This is often loosely ascribed to the greater ease of hydrolysis of LiCl during drying or melting which leads to a greater amount of oxide or oxychloride in the LiCl melts, but it is felt that this idea is incomplete and inexact. While there will no doubt be different amounts of oxide in LiCl and KCl melts prepared by identical procedures, the greater the amount of oxide in the melt, the lower will be the redox potential of the melt at any given oxygen pressure (Fig. 1) and therefore the lower

its initial aggressiveness should be. This is the reverse of what is found in practice, and hence this effect must in practice be offset in the opposite direction by some other essential difference between melts of LiCl and KCl. Comparison of Fig. 1 and 2 shows that at any given oxygen pressure and value of  $pO^{2-}$  the redox potential of a LiCl melt is about 1.2v higher than that of a KCl melt. In other words, even if the two melts have the same oxide activity and are under atmospheres of identical composition, a LiCl melt will still be more oxidizing than a KCl melt and will thus be more aggressive. This intrinsic difference in redox potential is due to differences between the free energies of formation for oxides and chlorides of lithium and potassium and is likely to have a far-reaching effect on many chemical reactions in melts besides corrosion reactions.

It should be pointed out that the effect of water on the reactivity of chloride melts may be more complicated, since hydrolysis leads to the formation of  $H^+$  ions as well as  $O^{2-}$  ions and the water will also dissociate to  $H_2$  and  $O_2$ . These effects have been discussed at length elsewhere (1, 2), and the effects of water on redox potential of chloride melts are still incompletely understood experimentally (6). However, when comparing redox potential behavior in melts so different in properties as KCl and LiCl, such complications will probably be secondary to the differences due to relative oxide stability described above.

*General application to corrosion in fused chlorides.*—As already pointed out, the properties of  $E$ - $pO^{2-}$  diagrams are similar in many respects to those of  $E$ - $pH$  diagrams for aqueous solutions. For aqueous systems, Pourbaix (3) has defined domains in which the corrosion of metals is thermodynamically possible or impossible by assuming that a metal will only corrode when the substance forming its surface has a solubility in excess of an arbitrary value of  $10^{-6}M$ . He distinguishes between two types of "domains of noncorrosion," one where the surface is actually bare metal (immunity domain) and the other where the metal is covered with a deposit of oxide or salt (passivity domain), and in the latter case, only if the substance covering the metal forms a completely perfect and nonporous screen will corrosion be prevented.

The  $E$ - $pO^{2-}$  diagrams for fused chlorides may be divided into analogous domains, but effective passivity is less likely to occur in fused chlorides than in aqueous solution and any conclusions made from such diagrams regarding "passive" behavior should be treated with reserve. It appears safer to designate simply as "oxide-covered" the region equivalent to the passive domain, as in Fig. 8. These regions represent the conditions under which the corrosion product is insoluble in the melt, and whether these conditions do in fact lead to passivity will depend on details such as the morphology of the oxide and its tenacity to the metal surface. Figure 8 shows the nickel-KCl diagram divided into domains of corrosion and noncorrosion on the assumption that no corrosion occurs if the solubility of the metal in the melt (as ions) is less than  $10^{-6}$  activity. Such dia-

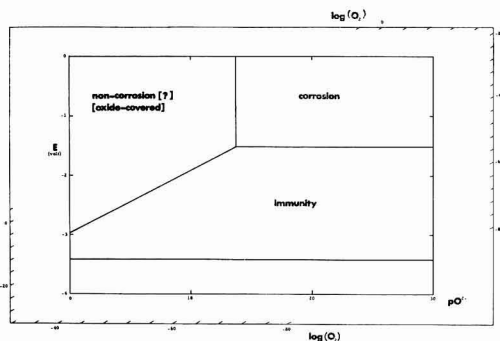


Fig. 8. Application of  $E$ - $pO^{2-}$  diagram to corrosion of nickel in KCl melt at  $800^{\circ}C$ .

grams predict whether the corrosion products of a given metal in a given fused chloride medium will be soluble metal ions or solid oxide, which may be an important consideration in some types of operation using fused chlorides.

It is not proposed to consider here in detail the application of  $E$ - $pO^{2-}$  diagrams to corrosion in fused salts, as a generalized treatment is available elsewhere (1, 2).

*Electrowinning of metals from fused salts.*—One of the most promising applications of  $E$ - $pO^{2-}$  diagrams appears to be to electrowinning of metals from fused chlorides where in particular the diagrams give some guidance on the effect of variables on product purity.

Let us consider as an example the extraction of nickel by electrolysis of a bath of molten KCl containing  $10^{-2}$  activity of  $Ni^{2+}$  ions. This is not at present a commercial process and is used only to illustrate the principles involved. Figure 4 shows that, provided the value of  $pO^{2-}$  exceeded 17.7, the  $Ni^{2+}$  ions would remain in solution as  $NiCl_2$ , but if the value of  $pO^{2-}$  was less than 17.7, a proportion of the  $Ni^{2+}$  ions would be precipitated as NiO. The activity of  $Ni^{2+}$  remaining in solution in the chloride melt at any  $pO^{2-}$  value less than 17.7 could be found by reference to the vertical isoactivity lines or to the scale of  $Ni^{2+}$  activities along the top of the diagram. An alternative point of view is that if the oxygen activity (partial pressure) in the system exceeded the dissociation pressure of NiO (about  $10^{-18.5}$  atm), NiO would be precipitated, but if the partial pressure of oxygen were less than  $10^{-18.5}$  atm, the  $Ni^{2+}$  ions would stay in solution (Fig. 4).

Deposition of nickel metal from a KCl melt containing a  $Ni^{2+}$  activity of  $10^{-2}$ , according to Fig. 4, would not begin to occur until the potential of the cathode had fallen below  $-1.09v$ . [The potential is given by the  $\log(Ni^{2+})$  scale to the right of the diagram.] As regards the impurities in the product, the potassium content of the nickel electrodeposited at any given potential can be found from the  $\log(K)$  scale on the left hand side of the diagram (extrapolation would be necessary in this particular example), and the chlorine content can be found in a similar manner. The oxygen content of the product electrodeposited at a given potential from a melt of given  $O^{2-}$  ion activity can be estimated by finding

from the external oxygen scales the value of oxygen pressure (activity) corresponding to the position of the system-point. The oxygen content of the metal product will be less, the lower the oxide ion activity in the melt and the lower the potential at which the product is deposited, but low potentials lead also to excessive contamination by potassium metal.

Besides giving quantitative guidance to the extent of product contamination in a given process under various operating conditions,  $E$ - $pO^{2-}$  diagrams can be used as a guide to possible ways of improving product purity by altering the process itself. One possible way of obtaining a product with a lower oxygen content would be to use a solvent with a higher affinity for oxygen, *i.e.*, with a more stable oxide. For example, LiCl might be substituted for KCl. Figures 4 and 5 show that electrolysis of a melt of given  $NiCl_2$  content under identical conditions of potential and  $pO^{2-}$  will lead to a product containing less oxygen if LiCl is used as solvent rather than KCl. For example, nickel metal with an oxygen activity of  $10^{-16}$  would be obtained by electrolysis of a KCl melt with a  $pO^{2-}$  value of 20 at a potential of  $-1.0v$ , whereas the product from an LiCl melt under the same conditions would contain an oxygen activity of only  $10^{-10}$ . In practice, of course, the preparation of a melt with a low oxide content might be more difficult for LiCl than for KCl, but these difficulties could in any case be overcome by use of an oxide "getter," which will be discussed now.

The purpose of adding a getter to the melt is to raise the  $pO^{2-}$  value and/or lower the oxygen activity in the system. For example, magnesium metal or magnesium chloride might be added to the bath to precipitate oxygen as MgO, and the values of  $pO^{2-}$  and  $O_2$  activity obtainable in this way in KCl could be obtained from Fig. 3. For example, if Mg were gradually added so that MgO was precipitated at a constant  $Mg^{2+}$  activity of  $10^{-2}$ , the potential of the system would fall along the vertical isoactivity line for  $10^{-2}$  ( $Mg^{2+}$ ) until a potential of  $-2.68v$  was reached, after which further additions of Mg would produce no further gettering. The addition of Mg might also lead to reduction of the  $NiCl_2$  in the melt at a potential higher than  $-2.68v$ , leading to precipitation of metallic nickel, and the potentials at which precipitation would begin to occur at a given activity of  $NiCl_2$  could be obtained from Fig. 4. If electrolytic separation of nickel was the requirement, the gettering process would, of course, be halted at a potential higher than that at which precipitation of metallic Ni began to occur in the body of the melt.

These simple principles are equally applicable to more complicated cases such as the winning of Ti or Zr from chloride melts, where the metal has more than one oxide or chloride. In such cases, the isoactivity lines are not always straight, and interpolation or extrapolation of activity values is sometimes less straightforward than in the simple case.

*Reduction of chlorides by reactive metals.*—Part of the previous section was concerned with the application of  $E$ - $pO^{2-}$  diagrams to chloride reduction by reactive metals in the presence of a chloride sol-

vent taking no direct part in the reaction. Many technologically important metals such as Ti or Zr are produced on a commercial scale by chloride reduction, but usually there is no "inert" chloride melt present in these processes and in its initial state the system base metal/chloride is highly reactive. However, when reduction is complete, the final products will be at, or near, equilibrium at a potential which determines the composition of all the phases then present.  $E$ - $pO^{2-}$  diagrams can therefore be used to describe the final state of the system, the base metal chloride by-product filling the role of the "inert" chloride in previous examples, and this is particularly useful because the purity especially the oxygen content, of the product is often an important factor in determining its metallurgical properties.

As an example, the  $E$ - $pO^{2-}$  diagram for Ni in KCl (Fig. 4) could be applied to the reduction of  $NiCl_2$  to nickel by potassium metal, and to predict impurity levels in the product. If excess potassium were used, the final equilibrium potential in the system would be  $-3.42v$  and the nickel metal product would be contaminated with potassium (the extent of contamination would be determined by the solubility of K metal in Ni metal at  $800^\circ C$ ). If less potassium were used, the equilibrium potential in the system could be measured either directly or by analysis of the KCl slag for  $NiCl_2$  [which is connected with the equilibrium potential by the log ( $Ni^{2+}$ ) scale to the right of the diagram]. Measurement of the oxide content of the slag would give the value of  $pO^{2-}$ . From these data, the content of oxygen and other impurities in the metallic product could be estimated as already described.

Reasoning based on these principles can give considerable guidance when a choice of process is to be made, and for example, comparison of Fig. 4 and 5 leads to the conclusion that, provided the two systems can be operated at the same levels of oxide contamination, reduction of  $NiCl_2$  by Li metal is likely to lead to a metal product containing less oxygen than reduction by K metal. The extent of contamination by alkali metal would probably be roughly the same in the two cases.

As another example, let us consider the production of titanium by the reduction of  $TiCl_4$ . Both Mg and Na have been used as reducing agents on an industrial scale, and from Fig. 7 the relative purities of product from the two processes can be estimated for reductions at  $800^\circ C$ . For clarity, simplified, approximate diagrams for Ti in NaCl and Ti in  $MgCl_2$  have been redrawn in Fig. 9 and 10. Comparison of these two diagrams shows immediately that for a given value of  $pO^{2-}$  the oxygen activity in the Ti metal product would be much lower for magnesium reduction than for sodium reduction. For example, let us suppose that the oxide contamination present in the two cases has been sufficient to produce a  $pO^{2-}$  value of 20 in the slag, and that in both cases excess of reductant has been used. The equilibrium potentials after reaction has gone to completion will be  $-3.20v$  in the case of sodium and  $-2.47v$  in the case of magnesium. Figure 9 shows that under these conditions, the oxygen activity in the titanium metal produced by sodium reduction would be about  $10^{-10}$ ,

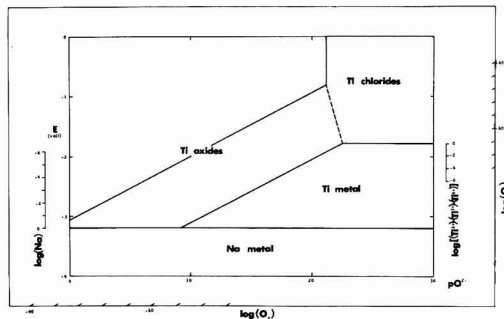


Fig. 9.  $E$ - $pO_2$  diagram for Ti-NaCl system at 800°C (approximate)

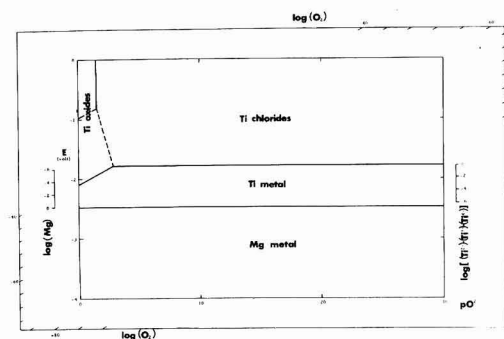


Fig. 10.  $E$ - $pO_2$  diagram for Ti-MgCl<sub>2</sub> system at 800°C (approximate).

while that in titanium produced by magnesium reduction would be about  $10^{-20}$ . The amount of contamination by Mg or Na would depend on their solubility in titanium at 800°C, which would need to be determined experimentally. Any attempt to reduce Na or Mg contamination by carrying out reduction under conditions of a deficiency of reductant would produce titanium with a higher oxygen content, besides increasing the amount of unreacted titanium chlorides left in the MgCl<sub>2</sub> melt. The interplay of the three factors, titanium chloride content of MgCl<sub>2</sub> melt, Mg or Na content, and oxygen content of product, can be readily investigated by detailed comparison of Fig. 9 and 10. The more detailed Ti diagram (Fig. 7) would also give the actual composition of the melt in terms of TiCl<sub>3</sub>, TiCl<sub>2</sub>, and TiCl, if this were required.

In exactly the same way, factors affecting the purity of other metals produced by chloride reduction can be investigated, and similar trends are apparent.

### Discussion

No attempt has been made to discuss in detail all possible applications of the present method, but it can be seen from the examples given that  $E$ - $pO_2$  diagrams are applicable to a wide variety of physicochemical processes in metal-fused chloride systems. The ideas presented are still at the development stage, and the approach a tentative one, but the present treatment makes an important contribution to thought in at least one major technology, the winning of metals from fused salts. The main

advance here is that the method offers an approach to the prediction of impurity levels in the products of such processes. Impurity levels are calculated as activities of the impurity under equilibrium conditions and thus represent the highest product purity that could be obtained from the process under ideal conditions. Oxygen is one of the most important impurities encountered in refractory metals such as Ti or Zr, and the treatment is especially suited to deal with this impurity. It has also been shown how the levels of contamination by other metals involved in fused-salt reductions can be estimated and the treatment could easily be extended to include any impurity present in feed materials either as chloride or as metal. The treatment is applicable to electrolytic reduction processes in fused chlorides and to chloride reduction by base metals, but it obviously cannot take account of additional impurities introduced during subsequent operations, such as leaching-out of the product. In many cases, oxide contamination during leaching far exceeds the oxygen originally present in the metal product, but as non-aqueous methods become available for extracting the metal product, the purity of the original product will become more important. Unfortunately at the present time the purity of the original product cannot be maintained through the subsequent recovery operations.

Besides giving general guidance on the relative impurity levels to be expected in products from different types of processes or from a single process operated in different ways, the data may be applied to predict impurity levels in specific practical cases, when any deviation in the expected purity could be taken to indicate departure from ideal processing conditions. To make purity predictions from the  $E$ - $pO_2$  diagrams, values of only two independent variables need be known at the completion of reduction, which then fix the position of the system-point on the diagrams. It is relatively easy to measure the redox potential of a chloride melt, either directly (6, 7), or by chemical analysis for the components of any suitable redox system present. Oxide activity could also be measured by a suitable electrode, or alternatively the oxygen pressure in the system could be measured either directly or in some cases calculated from the pressures of two other suitable constituents of the atmosphere (H<sub>2</sub> and H<sub>2</sub>O, for example). The measurement of redox potential and  $pO_2$  in fused salts may ultimately become as routine as potential and pH measurement in aqueous systems.

Impurity levels in the products are given by the diagrams as activities and these could be translated into, say, percentages where oxygen solubilities in the product metal are available or in the case of a metallic impurity, where activity data in the appropriate alloy are available.

Besides making this contribution to an understanding of metal-winning processes, the present treatment seems also applicable to a wider field of fused-salt chemistry, and some examples involving reaction of fused chlorides with metals—the reverse of electrowinning processes—have been given. The calculation of solubility products will probably be

of particular importance. The treatment can be extended to other halides where sufficient thermodynamic data are available; the most urgent extension now is probably to fluorides because of current interest in metal winning from fluorides. It is suggested that the general features of the present method may prove of value over a wider field than fused halides; in fact, attempts have already been made to understand certain metallurgical problems by plotting thermodynamic data in a somewhat similar manner (9).

The treatment described in this paper is thermodynamic and has the limitations common to all thermodynamic treatments. The advantage of a diagrammatic method over simple consideration in terms of equations is that it allows the relative importance of all the possible reactions of the constituents of the system to be assessed at a glance.

### Acknowledgment

The author wishes to thank Dr. C. Edeleanu for many stimulating discussions during the development of the ideas presented in this paper, which is published by permission of the Chairman of Tube Investments Ltd.

Manuscript received Sept. 18, 1961; revised manuscript received Feb. 12, 1962. This paper was prepared for delivery before the 18th International Congress of Pure and Applied Chemistry, Montreal, Aug. 6-12, 1961.

Any discussion of this paper will appear in a Discussion Section to be published in the December 1962 JOURNAL.

### REFERENCES

1. C. Edeleanu and R. Littlewood, *Electrochimica Acta*, **3**, 195 (1960).
2. R. Littlewood and C. Edeleanu, *Silicates Industriels*, **26**, 447 (1961).
3. M. Pourbaix, "Thermodynamics of Dilute Aqueous Solutions," Arnold, London (1949).
4. M. K. Voskresenskaya and G. N. Kashcheev, *Isvest. Sektora. Fiz. Khim. Anal.*, **27**, 255 (1956).
5. G. Delarue, *Recueil*, **79**, 510 (1960).
6. R. Littlewood and E. J. Argent, *Electrochimica Acta*, **4**, 114 (1961).
7. R. Littlewood and E. J. Argent, *ibid.*, **4**, 155 (1961).
8. M. Temkin, *Acta Physicochemica U.R.S.S.*, **20**, 411 (1945).
9. L. S. Darken and R. W. Gurry, "Physical Chemistry of Metals," McGraw-Hill Book Co., London (1953).
10. O. Kubaschewski and E. L. Evans, "Metallurgical Thermochemistry," Pergamon Press, London (1958).
11. W. J. Hamer, M. S. Malmberg, and B. Rubin, *This Journal*, **103**, 8 (1956).
12. A. Glassner, ANL-5107, Argonne National Laboratory (1953). (This is now superseded by ANL-5750).

### APPENDIX

*Sources of thermodynamic data.*—In equilibrium calculations, it is essential to use a self-consistent set of basic data. Standard free energies of formation were calculated from the equations given by Kubaschewski and Evans (10) where possible. Where no data was available in reference (10), the chloride data of Hamer *et al.* (11) and the oxide data of Glassner (12) were used. Where data from more than one reference was available for a particular compound, these invariably agreed with each other to within a few kilocalories. In a few cases (*e.g.*, ZrCl<sub>3</sub>, ZrCl<sub>2</sub>), extrapolation of data to 800°C was necessary.

Table II. Standard free energies of formation at 800°C

Compounds	cal/mole	Reference
LiCl	-77,580	(12)
Li <sub>2</sub> O	-109,660	(12)
KCl	-78,830	(10)
K <sub>2</sub> O	-53,710	(10)
NaCl	-73,680	(10)
Na <sub>2</sub> O	-65,350	(10)
MgCl <sub>2</sub>	-113,940	(10)
MgO	-117,210	(10)
NiCl <sub>2</sub>	-40,350	(11)
NiO	-33,180	(10)
ZrCl <sub>2</sub>	-112,300	(11)*
ZrCl <sub>3</sub>	-165,300	(11)*
ZrCl <sub>4</sub>	-170,000	(11)*
ZrO <sub>2</sub>	-210,590	(10)
TiCl <sub>2</sub>	-81,560	(11)*
TiCl <sub>3</sub>	-120,300	(11)*
TiCl <sub>4</sub>	-152,370	(10)
TiO	-99,440	(10)
Ti <sub>2</sub> O <sub>3</sub>	-292,590	(10)
Ti <sub>2</sub> O <sub>5</sub>	-472,560	(10)
TiO <sub>2</sub>	-173,630	(10)

\* Extrapolated value.

The standard free energies used in all the calculations are given in Table II. The standard free energies of formation of oxide ion in LiCl, KCl, NaCl, and MgCl<sub>2</sub> at 800°C, calculated as in relations [9], [10], and [11], were as follows

in LiCl	:	+ 45,500 cal/mole
in KCl	:	+ 103,950 cal/mole
in NaCl	:	+ 82,010 cal/mole
in MgCl <sub>2</sub>	:	- 3,270 cal/mole

*Construction of the diagrams.*—The condition for equilibrium of the electrochemical reaction

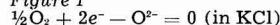
$$\sum \nu M + n e^- = 0 \quad [15]$$

is given by (3)

$$-\sum \nu \mu + 23,060 n E = 0 \quad [16]$$

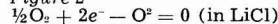
where the constituents M have free energies of formation of  $\mu$  (cal/mole) and  $E$  is expressed in volts. Relation [16] enables equilibrium relations to be set up in terms of the two variables of interest,  $E$  and  $pO^{2-}$ . The basic equations used in constructing the diagrams are given below; Fig. 5, 8, 9, and 10 were constructed graphically from the other diagrams.

Figure 1



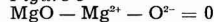
$$E = -2.255 + 0.1065 \log (O_2)^{1/2} + 0.1065 pO^{2-} \quad [17]$$

Figure 2

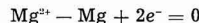


$$E = -0.9865 + 0.1065 \log (O_2)^{1/2} + 0.1065 pO^{2-} \quad [18]$$

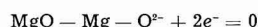
Figure 3



$$\log (Mg^{2+}) = -21.83 + pO^{2-} \quad [19]$$

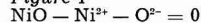


$$E = -2.469 + 0.1065 \log (Mg^{2+}) \quad [20]$$

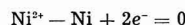


$$E = -4.796 + 0.1065 pO^{2-} \quad [21]$$

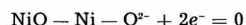
Figure 4



$$\log (Ni^{2+}) = -19.71 + pO^{2-} \quad [22]$$

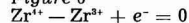


$$E = -0.875 + 0.1065 \log (Ni^{2+}) \quad [23]$$

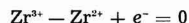


$$E = -2.973 + 0.1065 pO^{2-} \quad [24]$$

Figure 6



$$E = -0.204 + 0.213 \log (Zr^{4+}) / (Zr^{3+}) \quad [25]$$



$$E = -2.299 + 0.213 \log (Zr^{3+}) / (Zr^{2+}) \quad [26]$$

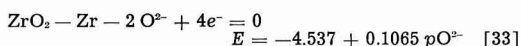
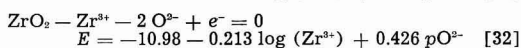
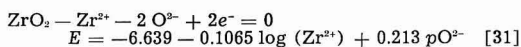
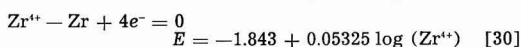
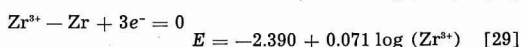
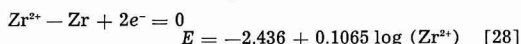
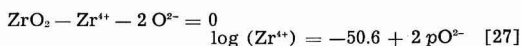
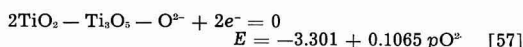
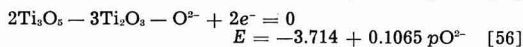
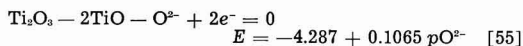
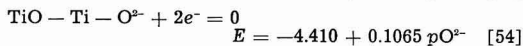
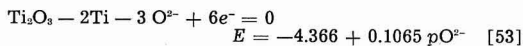
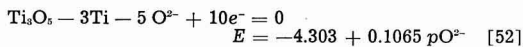
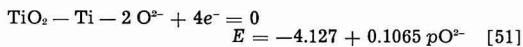
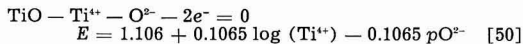
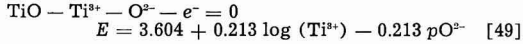
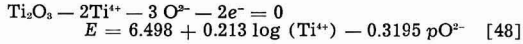
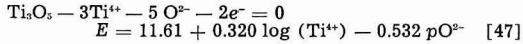
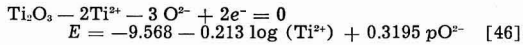
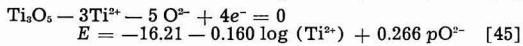
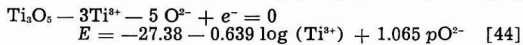
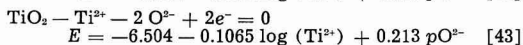
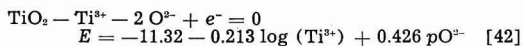
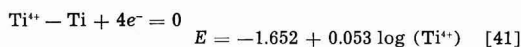
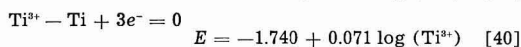
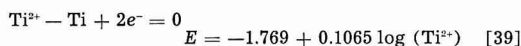
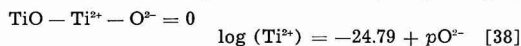
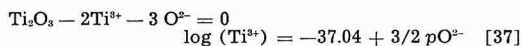
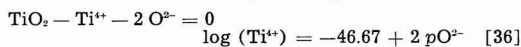
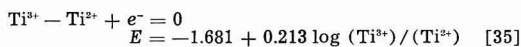
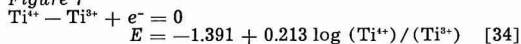


Figure 7



## Technical Notes



### A Pulse Measurement of the Semiconductor-Electrolyte Space Charge Capacity

Paul T. Wrotenbery

*The University of Texas and Texas Research Associates, Austin, Texas*

A. W. Nolle

*The University of Texas, Austin, Texas*

Measurements of the space charge capacity of a semiconductor surface in contact with an electrolytic environment have been made recently by Bohnenkamp and Engell (1), Hurd and Wrotenbery (2), Efimov and Erusalimchik (3), and Zviagin and Liutovich (4). All of these measurements were made using standard bridge techniques. In these previously reported measurements the magnitude of the measured capacity at 1-10 kc measuring frequency has been at least an order of magnitude higher than values expected on the basis of theoretical space charge calculations. This deviation has been assumed to be at least partially due to the presence of surface states with time constants small

relative to the period of the measuring frequency used in these bridge measurements. Hurd and Wrotenbery have utilized a radio-frequency bridge system and extended the range of measuring frequency to a megacycle in an attempt to eliminate the discrepancy between theory and experiment; however, due to the low value of the reactive component of the measured impedance, significant results could be obtained only up to about 200 kc (2). It was with this problem of obtaining a measurement of the capacity of the space charge independent of surface states that the writers conceived the idea of utilizing a current pulse method. Pulse techniques have been used previously in metal-

electrolyte capacity measurements by Hackerman and co-workers (5). In this paper the initial results of application of this method to silicon and germanium in basic environments are reported and compared to similar results obtained previously by the bridge method (2).

The method used consists of applying a constant current pulse with rise time of less than  $0.2 \mu\text{sec}$  to the silicon surface through a platinum electrode in the electrolyte. The platinum electrode is also utilized to apply a controlled polarizing potential to the surface so that the space charge distribution can be altered. Changes in the electrode potential are measured relative to a saturated calomel half cell. Initially, the constant current pulse was obtained by use of a mercury switch and a constant current source. However, the results reported here were obtained by use of the pulse generator described by Riney, Schmid, and Hackerman (5). The voltage-time relationship between the platinum electrode and the bulk of the semiconductor is recorded photographically by means of an oscilloscope which is triggered as the current pulse is applied. From this recorded response, the capacity,  $C$ , of the surface at the time the pulse is applied, i.e., at  $t \cong 0$ , can be computed. The calculation is valid even though  $C$  may be time dependent.<sup>1</sup> The presence of surface states would, after some finite time of the order of the response time of the state, tend to cause a deviation of the observed response from that expected without surface states. The detection of this deviation is interpreted as evidence for the presence of surface states. The experimental system used in this work is shown in Fig. 1. The inductor,  $L$ , in the d-c bias circuit is used to prevent shorting of the current pulse through the bias supply. It can be replaced by a large resistor; however, this makes necessary a much larger bias supply voltage source. In the Riney apparatus used to obtain all results reported in this paper with the exception of the results shown in Fig. 3, a resistance is used in place of  $L$ . The Riney pulse generator contains internally the bias supply and the rectification represented by the diode,  $D$ , which is necessary to prevent the pulse generator from shorting the bias supply on application of the pulse. The resistor,  $R_s$ , was used to allow measurement of the amplitude of the current pulse. Prior to electro-

chemical measurements, the system was checked by use of standard components of appropriate magnitude which were inserted in place of the cell. The pulse rise time was checked by use of a resistor in place of the cell. The normally assumed semiconductor surface equivalent circuit, ignoring for the moment any possible surface states, is enclosed in dotted lines. If surface states exist, additional components must be introduced into the equivalent circuit so as to make  $C_p$  effectively a time varying capacitance. In Fig. 1,  $C_p$  represents the true space charge capacity and  $R_p$  represents an effective shunting resistance, necessary since d-c current flow occurs across the interface. The resistance,  $R_s$ , is the equivalent series resistance of the semiconductor crystal, electrolyte, and contact. If the response of this circuit to a constant current pulse of magnitude,  $I_0$ , is analyzed, it is found that the capacity,  $C_p$ , is given by

$$C_p \Big|_{t=0} = I_0 \left( \frac{dE}{dt} \Big|_{t=0} \right)^{-1} \quad [1]$$

In the absence of surface states,  $E$  would be an exponential function of time, and the voltage response would be linear over a time  $\ll R_p C_p$ ; and under these conditions, the slope is easily and quite accurately obtained and the capacity at  $t \cong 0$  consequently determined. The only effect of  $R_p$  in determination of the initial slope is in the length of time over which the response is linear. It is not necessary for  $C_p$  to be time independent (and thus the response exponential) for this equation to hold. If surface states or other possible charge transfer sites exist, the measured capacity will in effect be frequency dependent, since it will depend on the surface-state distribution. However, in a pulse measurement this frequency dependence will be observed as a time dependence. For example, if one assumes that the frequency dependence is brought about because of a set of surface states of some response time, say,  $1 \mu\text{sec}$ , then the measured capacity will be frequency dependent in the vicinity of a megacycle. At frequencies with periods small compared to a microsecond, these surface states are incapable of equilibrating, while at frequencies with periods of the order of a microsecond or greater, these states will equilibrate and thus contribute to the capacity. When the constant current pulse is applied, the surface states will accept appreciable charge after a time of the order of a microsecond has elapsed; thus, the capacity, as measured by the slope of the recorded response, will initially represent the true space charge capacity and will change with the presence of new charge transfer sites. Assuming that this change occurs at  $t \ll R_p C_p$ , i.e., over the linear region, the voltage response as a function of time can thus be utilized to detect the presence of surface states by observing the change of slope of the recorded response from that at times less than the time constant of the surface state to that at times greater than the time constant of the state. If it is assumed that the capacity changes from some value  $C_p$  to some value  $C_p + C_{ss}$ , then the second slope would allow computation of  $C_p + C_{ss}$ . On the basis of this simplified model, some very interesting and informative results have been obtained.

<sup>1</sup> Where we find that  $dE/dt$  decreases with time for  $t \ll R_p C_p$ , we shall arbitrarily describe the system as having a time varying effective capacitance.

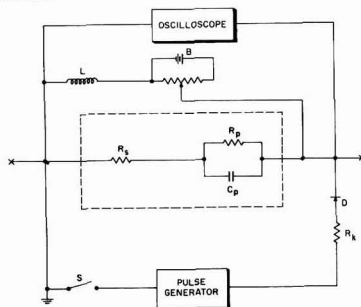


Fig. 1. Circuit diagram for pulse measurements, including semiconductor surface equivalent circuit.

The basis for estimating the effective value of  $R_p$  was the Bridge result of Bohnenkamp and Engell on germanium and Hurd and Wrotenbery on silicon (1, 2). In the vicinity of the capacity minimum, where the measurements being reported were made, and at the highest measuring frequency of 160 kc,  $R_p$  for germanium in 1N KOH (1) is in the range of 200-1000 ohm/cm<sup>2</sup>. As the frequency is decreased,  $R_p$  approaches 10,000 ohm/cm<sup>2</sup> at 1 kc. In transforming to the time domain necessary in time dependent measurements, the approximate corresponding time dependence of  $R_p$  would be obtained by considering the  $R_p$  values associated with the reciprocal of the frequency, thus yielding from the above stated values a value of  $R_p$  at 5  $\mu$ sec of 200-1000 ohm/cm<sup>2</sup> and increasingly larger values at greater times. The exact time dependence would have to be obtained from the Fourier Transform of the power spectrum of  $R_p$ . The results on silicon are essentially identical, with slightly higher values throughout the frequency range of 1-200 kc (2). As previously pointed out, the only effect of  $R_p$  in the linear response region is in the determination of the length of time over which the response is linear. Based on these values of  $R_p$  and theoretically computed values of  $C_p$ , the corresponding values of  $R_p C_p$  at times of the order of a microsecond and at the potentials used in this work are greater than 50  $\mu$ sec in the vicinity of the minimum where good agreement with theory was obtained. At the most negative potential used in the case of germanium, *e.g.*, -0.925v relative SCE, the value of  $R_p C_p$  is in the vicinity of 20-30  $\mu$ sec. For this smallest value of  $R_p C_p$ , the nonlinearity at 2  $\mu$ sec would be only a few per cent, and for the majority of the measurements reported,  $R_p C_p$  is sufficiently great that negligible nonlinearity would occur at 1-10  $\mu$ sec.

Evidence of fast surface states with response times of the order of a few microseconds have been observed in germanium; however, in the case of silicon, no similar states were indicated. This implies that in the case of silicon, fast states, if existent, have time constants of less than a microsecond, whereas in germanium, at least some of the fast surface states have time constants greater than a microsecond. It is pointed out that the pulse rise time of 0.2  $\mu$ sec sets the lower limit on observation of the voltage response.

Typical traces recorded for 10 ohm-cm n-type silicon and for 10 ohm-cm n-type germanium in 1N KOH are shown in Fig. 2a and 2b, respectively. The change in slope noted, in the case of germanium, during the first 2 or 3  $\mu$ sec is assumed to be the result of fast surface states with time constants of the order of this time. It was found that this slope change occurs primarily on the 2-4  $\mu$ sec range and that a second rather well-defined linear region follows. This rather distinct change in slope would be expected if the surface states responsible for it were of a distinct time constant of the order of 2-4  $\mu$ sec. The response on silicon is linear to less than a microsecond, thus, leading to the tentative conclusion that fast states on silicon, if existent, have time constants of less than a microsecond. It is evident from the values of  $R_p C_p$ , discussed previously

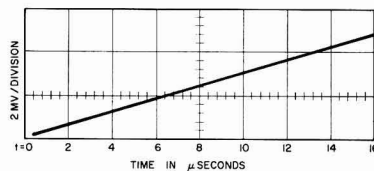


Fig. 2a. Typical voltage-time response for 10 ohm-cm n-type Si

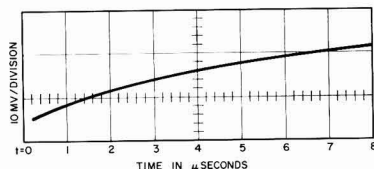


Fig. 2b. Typical voltage-time response for 10 ohm-cm n-type Ge

for germanium that this relatively large change in slope is not associated with the  $R_p C_p$  time constant.

In Fig. 3 and 4 are shown some results of capacity measurements made by this method on silicon and germanium in 1N KOH. In Fig. 3, a capacity measurement on silicon made by Hurd and Wrotenbery (2) by the bridge method is included for comparison. The bridge measurements were made at 10 kc, and the slope obtained from the pulse method was taken after an elapsed time of 10  $\mu$ sec. It is noted that the measured capacity on silicon by the pulse method corresponds closely to the values obtained by the bridge technique at 10 kc, which would include the effect of fast surface states. The deviation between the two curves is probably due to slightly different premeasurement conditions, since the two measurements were not made on the same sample, and difference in true surface area alone can contribute significantly to this deviation. In the case of germanium (see Fig. 4), the values of capacity computed for the two slopes observed in Fig. 2b show the reduction in capacity which would be expected as the effect of equilibrating states is eliminated. It is emphasized that the difference in capacity values between the two curves in Fig. 4 is independent of direction of the current pulse, *i.e.*, whether or not it is anodic or cathodic, and also that the values are obtained

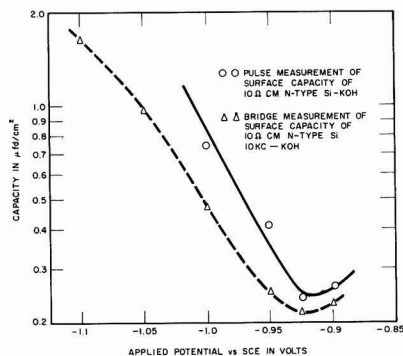


Fig. 3. Comparison of capacity of 10 ohm-cm n-type silicon measured by pulse method and by bridge method.



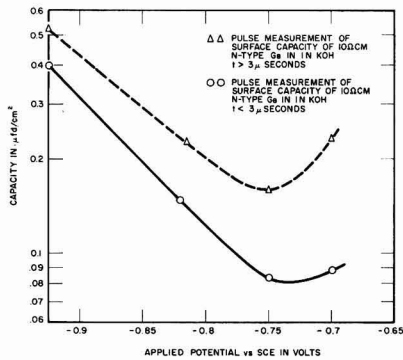


Fig. 4. Capacity of 10 ohm-cm n-type Ge, measured by pulse method showing decrease in slope obtained for times less than 3  $\mu$ sec.

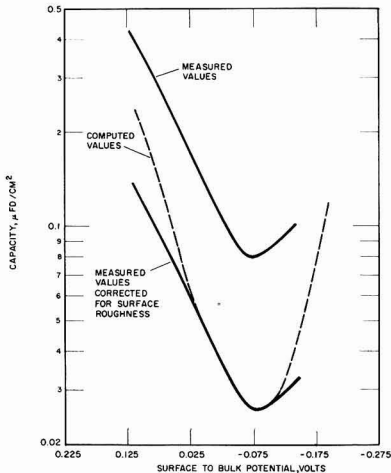


Fig. 5. Comparison of results of pulse measurement on 10 ohm-cm n-type Ge with computed values.

simultaneously in time on the same surface. The measured values on germanium at the minimum is  $0.08 \mu\text{f}/\text{cm}^2$ , whereas the theoretically predicted value for the space charge of this sample is  $0.027 \mu\text{f}/\text{cm}^2$ . The measured capacity of the germanium surface obtained by the above described technique

is only a factor of about three greater than values predicted on the basis of previous space charge calculations (1, 2). Deviations between the true and projected surface areas could reasonably account for some or all of this difference. In Fig. 5, the measured capacity for 10 ohm-cm n-type germanium for times less than  $3 \mu\text{sec}$  is compared with values theoretically calculated from the well-known Poisson-Boltzman approach.<sup>2</sup> The upper curve in Fig. 5 gives the measured values while the lower dotted curve gives the measured value corrected for a surface roughness factor of 3. The good agreement in the vicinity of the minimum is noted. This agreement on 10 ohm-cm germanium is somewhat better than that obtained by Bohnenkamp and Engell (1) at 160 kc bridge measurement on intrinsic germanium.

The interpretation of larger deviations from the theoretical values, obtained in all previous measurements (1-4), as being at least partially due to the fast surface states, is supported by these results. Closer agreement to theoretical space charge capacities are obtained than have previously been reported. Further application of this technique to semiconductor electrolyte systems appears a promising approach to the solution of many of the unresolved problems in these systems.

#### Acknowledgment

This work was supported in part by Texas Instruments, Inc., Dallas, Texas.

Manuscript received Oct. 23, 1961; revised manuscript received Feb. 11, 1962.

Any discussion of this paper will appear in a Discussion Section to be published in the December 1962 JOURNAL.

#### REFERENCES

1. K. Bohnenkamp and H. J. Engell, *Z. Elektrochem.*, **61**, 1184 (1957).
2. R. M. Hurd and P. T. Wrotenbery, Paper, Electrochemical Soc. Meeting, Houston, 1960; Indianapolis, 1961.
3. E. A. Efimov and I. G. Erusalimchik, *Doklady Akad. Nauk S.S.S.R.*, **124**, 609 (1959).
4. V. I. Zviagin and A. S. Liutovich, *Izvest. Akad. Nauk Uzbek S.S.S.R.*, Physics—Math. series No. **1**, 25 (1959).
5. J. S. Riney, G. M. Schmid, and Norman Hackerman, *Rev. Sci. Instr.*, **32**, 588 (1961).

<sup>2</sup> See, for example, ref. (1).

## Electrolytic Etching of Germanium in Water

W. Rindner and R. C. Ellis, Jr.

Research Division, Raytheon Company, Waltham, Massachusetts

Chemical etching with water (1) has several advantages were it not for the impractically slow rate at which water attacks Ge. It is the purpose of this paper to discuss electrolytic etching with water which has been found to attack Ge at a useful rate. In addition to Ge the III-V semiconducting compounds GaAs and GaP have been etched by the same method.

Most of the work reported was done with Ge slices about 15 mils thick. These slices were held horizontally either by clip leads or metallic bases on which they were mounted by gold bonding. A positive potential was applied to the slice in actual contact with or in close proximity to a thin wire used as the negative electrode. Etching was performed by placing on the substrate a drop of water

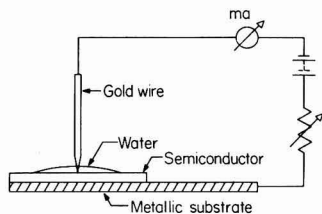


Fig. 1. Experimental arrangement for electrolytic etching in water

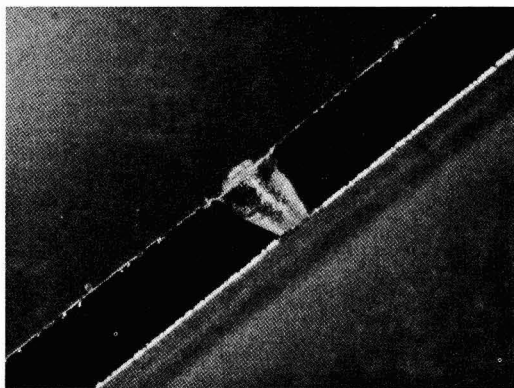


Fig. 2. Etching of a hole in Ge with a thin Au cathode. Magnification approx. 40X.

around the wire and passing currents of a few milliamperes through the system. Tap water and distilled gave the same results. Figure 1 shows the experimental arrangement and Fig. 2 a cross section of a slice etched through in the manner described.

Various materials such as Au, W, Cu, steel, and Ge were used as cathodes without very significant differences being observed among them. Similarly, Ge substrates covering the resistivity range from degenerate to near-intrinsic, both n- and p-type, were found to be equally attacked within experimental error. For good resolution the cathode had to be very close to the substrate. With high resistivity semiconductors and a sharply pointed cathode the resolution could be improved by actually making light contact between the substrate and the cathode. As the pressure was increased the resolution deteriorated and the etching rate eventually decreased by about two orders of magnitude. In the case of low resistivity material actual contact had to be avoided to allow etching to take place.

Usually current densities at the cathode were of the order of 100 amp/cm<sup>2</sup>. With a 2 mil diameter cathode, about  $5 \times 10^{-7}$  cm<sup>3</sup> Ge was removed per hour. To improve resolution the current path was confined as nearly as possible to the direction of the cathode axis by immersing only the very tip in water. Alternatively, good results were obtained using a wire insulated everywhere except on the part facing the substrate.

Surrounding the point facing the cathode a concentric structure of the surface was observed as shown in Fig. 3. Around the strongly etched region



Fig. 3. Appearance of the Ge surface around the area facing the cathode.

(central white spot) there is a flat, shallow, dish-shaped depression about 3/16 in. in diameter. The entire area under the drop of water is slightly stained and is bordered by a circular white deposit. The latter was identified as hexagonal germanium oxide by its electron diffraction pattern. Removal of the oxide ring with tartaric acid solution revealed that some contact etching had taken place underneath. The dish-shaped depression is surrounded by a halo-shaped stained or etched region which corresponds in size to the extent of great turbulence during etching. The striations visible around the central spot were brought out by the etching and are due to disturbances introduced in the process of slicing the semiconductor. Etching leaves undamaged material with a smooth surface.

One experiment was performed in the following manner. A germanium slice was cut in half. The two halves were connected to a d-c power supply and brought in contact with their edges at right angles, and immersed in water. In this way the effect of current polarity on etching rate was determined under otherwise equal conditions. It was found that etching took place on both slices, but at different rates. The volume removed from the slice under positive potential was about five times larger than that removed from the other slice.

When no current was passed through the system but contact was established between cathode and substrate in the presence of water, preferential etching at the point of contact was observed after about 12 hr. This appears to be the previously described effect of contact etching (2) with water as the etchant.

Etching of GaAs and GaP was performed in a manner similar to that described for Ge.

The two conditions required for etching are met in this process: the impetus for oxidation is supplied by the potential between anode and cathode and the removal of oxidized germanium is accomplished by the slight solubility of germanium oxide in water. Excess oxide precipitates and collects in those volumes of the solution with the least turbulence.

Definition is obtained by the greatest current density being supported through the shortest distance. The greater etching rate of this region is

abetted by local heating and a subsequent increase in the solubility of  $\text{GeO}_2$ . The increased solubility facilitates the germanium removal and results in a greater conductance in the solution.

The reason for the improved resolution obtained with high resistivity substrates and light contact between the cathode and the semiconductor is probably due to the confinement of current flow being more effective than the current flow lost due to direct passage from cathode to substrate.

Hydrogen gas is formed at the cathode as expected, while little observed gas is given off at the anode. Germanium is therefore probably being oxidized to  $\text{Ge}^{4+}$  directly, unlike the case of silicon where hydrogen is found escaping from both anode and cathode in a slightly conducting solution. It has been postulated that this is due to the silicon being oxidized to  $\text{Si}^{+2}$  electrolytically with a subsequent decomposition of water by this active species (3).

Superimposed on the germanium etching is the straight electrolysis of water which in addition introduces oxygen into the water. This oxygenation

by electrolysis and air solubility can account for the various contact etching phenomena observed on germanium.

#### Acknowledgment

The authors wish to express their appreciation of the efficient assistance in the experimental work by J. Gould and R. Flagg.

Manuscript received Aug. 14, 1961; revised manuscript received Feb. 14, 1962. This paper was prepared for presentation before the Detroit Meeting, Oct. 1-5, 1961.

Any discussion of this paper will appear in a Discussion Section to be published in the December 1962 JOURNAL.

#### REFERENCES

1. W. Harvey and H. Gatos, *This Journal*, **105**, 659 (1958).
2. W. Rindner and J. Lavine, *Contact-Etching of Semiconductors*, *Solid-State Electronics*, **2**, 190 (1961).
3. W. Erikson and A. Baker, *Reactions of Silicon with Aqueous Solutions of HF and Various Oxidizing Agents*, *Electrochem. Society Meeting*, Ottawa, 1958.

# Discussion Section



This Discussion Section includes discussion of papers appearing in the *JOURNAL of The Electrochemical Society*, Vol. 108, No. 5-11 (January-November 1961). Discussion not available for this issue will appear in the Discussion Section of the December 1962 *JOURNAL*.

## Photoluminescent Effects in Contact Electroluminescence

B. Morosin and F. A. Haak (pp. 477-478, Vol. 108, No. 5)

**W. Lehmann**<sup>1</sup>: The emission of visible radiation from a mechanical mixture of an ordinarily non-electroluminescent phosphor powder and a metal (or well-conducting semiconductor) powder, suspended in castor oil and subjected to an alternating electric field, was described by Lehmann in 1957.<sup>2</sup> The effect was qualitatively explained as electroluminescence of the phosphor particles in the extremely high electric field strength near sharp edges of the metal particles and, because of the necessary close contact between the phosphor and the metal, was termed "Contact Electroluminescence." These experiments recently were repeated by Morosin and Haak. They explain the light emission as due to the glow of local discharges which partly can be seen directly by eye (violet in air) or which may excite adjacent phosphor particles to photoluminescent emission, which is characteristic of the particular phosphor. They supported their view by the observation that emission could even be obtained with cells containing metal powder but no phosphor.

Morosin and Haak's explanation is identical to that presented by Herwelly<sup>3</sup> who tried to understand the Destriau Effect, i.e., the "intrinsic" electroluminescence of ZnS-type phosphors, as photoluminescence excited by the ultraviolet generated in glow discharges near the phosphor particles. It has been shown fairly convincingly by Destriau<sup>4</sup> that this explanation does not hold in the case of "intrinsic" electroluminescence, and it will be shown here that it does not hold either in the case of contact electroluminescence. The arguments to be used are almost identical to those used by Destriau to oppose Herwelly's view.

A glow discharge can, indeed, be observed in many cases under improper operating conditions. It may occur in air bubbles accidentally present in the cell or in bubbles caused by gaseous decomposition products of the oil and, in either case, is favored by the presence of metal or other conducting particles. Such glow can also visibly photoexcite adjacent phosphor particles. However, it is fairly easy to distinguish this photoluminescence from real electro- or contact-electroluminescence. The following facts may be mentioned.

1. Many, but not all, phosphors respond with different emission colors to photo- and electroluminescence.<sup>5</sup> The color of contact electroluminescence also

may vary with variation of the frequency of the exciting field in the same fashion as for intrinsic electroluminescence (e.g., blue at high and green at low frequencies). The color of photoluminescence is independent of the exciting frequency of the glow discharge.

2. If contact electroluminescence were actually photoluminescence, then all efficient photoluminescent phosphors should respond about equally well. This is by far not the case. As an example, green-emitting zinc silicate activated by manganese responds very well to an alternating electric field if mixed with a metal powder while red-emitting magnesium fluorogermanate, also activated by manganese, does not respond at all. One may even mix equal parts of these two phosphors with a metal powder. The germanate can well be excited by ultraviolet of wave length 2537Å or 3650Å, the silicate practically only by 2537Å. Hence, the photoluminescent emission spectrum consists of the green band of the silicate and of the red of the germanate simultaneously if excited by 2537Å, and practically only of the red germanate emission if excited by 3650Å. However, if subjected to contact electroluminescence, the spectrum of the blend shows only the green emission of the silicate phosphor while the germanate remains completely dead.

3. Morosin and Haak explain the color differences between contact electroluminescence and photoluminescence, which can sometimes be observed, by a superposition of the violet color of the glow with the emission of the phosphor excited by this glow. If so, then the color shift should be observed with all phosphors, not only with a few as actually is the case. Further, Morosin and Haak obviously do not realize that a superposition of the color of photoluminescence with the violet of the glow discharge in air does not always agree with the observed color of contact electroluminescence. As an example, the yellow photoemission of the (Zn,Cd)S:Ag phosphor mentioned in the table in Footnote 2 superimposed to the violet of a glow in air should result in a pink to reddish purple color, while yellow-green actually

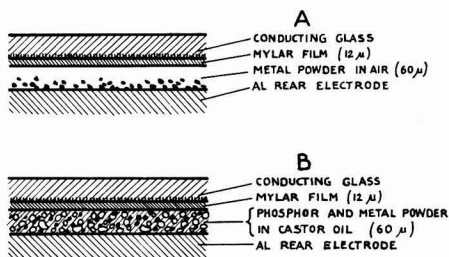


Fig. 1. The experimental arrangement used. A—Metal (or semiconductor) powder in air producing glow discharge. B—Phosphor and metal (or semiconductor) powder in castor oil producing contact electroluminescence.

<sup>1</sup> Research Dept., Westinghouse Electric Corp., Bloomfield, N. J.

<sup>2</sup> W. Lehmann, *This Journal*, 104, 45 (1957).

<sup>3</sup> A. Herwelly, *Acta Physica Austriaca*, 5, 30 (1951).

<sup>4</sup> G. Destriau, *J. phys. radium*, 14, 307 (1953).

<sup>5</sup> The table in Footnote 2 lists six examples instead of only one as stated by Morosin and Haak.

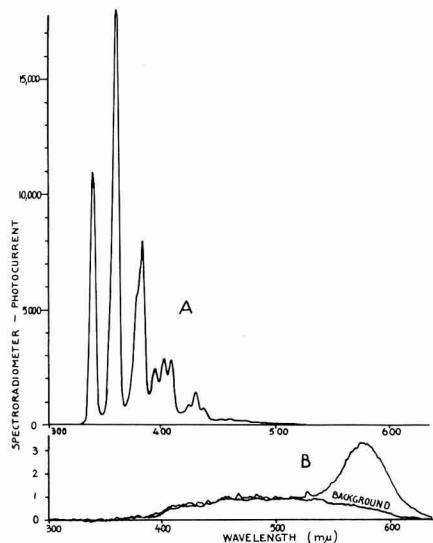


Fig. 2. A—Spectrum of a glow discharge in air (arrangement of Fig. 1A). B—Spectrum of contact electroluminescence of a ZnS:Mn phosphor and aluminum powder in castor oil (arrangement of Fig. 1B). Both spectra are uncorrected, as recorded. The background in spectrum B is due to stray light from room illumination.

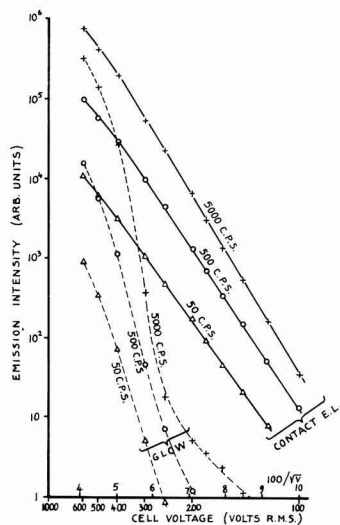


Fig. 3. Brightness-voltage dependences of a glow discharge (aluminum powder in air, arrangement of Fig. 1A) and of contact electroluminescence (green ZnS:Cu,Cl phosphor in contact with Cu<sub>2</sub>S, arrangement of Fig. 1B).

was observed. Finally, the characteristic line spectrum of a glow discharge should be easily detectable in the spectrum of contact electroluminescence if it were present. The examples of Fig. 2 of this discussion (using the experimental arrangement of Fig. 1) show that this is not the case and that the emission of contact electroluminescence under proper conditions consists only of the spectrum emitted by the phosphor.

4. The emission of contact electroluminescence normally is confined to many small "spots" scattered over the area of the cell. If such spots were due to photoexcitation, the exciting glow discharge would also have to be concentrated in very small spots and, hence, to be very intense within each spot (otherwise, the intense but very localized emission of the phosphor could not be understood). However, microscopic examination of contact electroluminescence reveals no visible glow discharge in the vicinity of emitting spots. On the other hand, glow discharges require dimensions of many times the mean free path of the gas molecules, which in air at atmospheric pressure is about  $10^{-5}$  cm, *i.e.*, just slightly below the limit of resolution of a good microscope ( $2$  to  $3 \times 10^{-5}$  cm). Hence, an intense glow discharge in submicroscopically small dimensions is most unlikely.

5. The time-average of the light emitted by a phosphor excited by contact electroluminescence is fairly stable. Its dependence on the exciting voltage can well be described by the same equations which hold in the case of intrinsic electroluminescence, *e.g.*, by  $L = L_0 \exp [-(V_0/V)^{1/2}]$ , where  $L_0$  and  $V_0$  are constants. An example of a green ZnS:Cu,Cl phosphor (originally nonelectroluminescent) in contact with Cu<sub>2</sub>S (arrangement of Fig. 1B) is shown in Fig. 3. The emission created by a glow discharge in air (arrangement of Fig. 1A) ordinarily is much less stable and tends to strong fluctuations in intensity. The time average of its emission does not approach straight lines in Fig. 3 and, hence, cannot be described by the above equation.

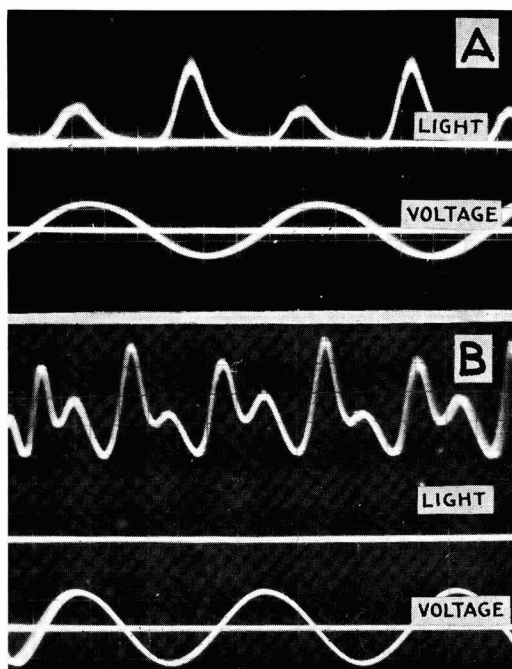


Fig. 4. Light waves of a glow discharge in air (A—arrangement of Fig. 1A, aluminum powder) and of contact electroluminescence (B—arrangement of Fig. 1B, blue-green ZnS:Cu,Cl phosphor in contact with Cu<sub>2</sub>S), both excited by a sinusoidal voltage of 100 cps.

6. The brightness waves of contact electroluminescence excited by a sinusoidal voltage resemble those observed in "intrinsic" electroluminescence and frequently show, as do the latter, a main and a secondary peak for each half cycle of the exciting voltage. An example is shown in Fig. 4B. The brightness waves of a glow discharge in air are quite different (Fig. 4A) and never show secondary peaks.

These effects prove that contact electroluminescence can very easily be distinguished from photoluminescence excited by local glow discharges and that its mechanism in all likelihood is identical to that of intrinsic electroluminescence. In all cases, a well-conducting second phase must be present and in intimate contact with the phosphor. This may be metal particles, etc., in case of contact electroluminescence, or thin coats of copper sulfide or metallic copper on the surfaces,<sup>6</sup> or inclusions of  $\text{Cu}_2\text{S}$  inside of the phosphor particles.<sup>7</sup> Inclusions of  $\text{Cu}_2\text{S}$  segregate predominantly in lattice faults, e.g., in stacking faults, rather than in the otherwise undisturbed  $\text{ZnS}$  lattice. A correlation between the occurrence of electroluminescence and of stacking faults thus can readily be understood.

**B. Morosin<sup>8</sup> and F. A. Haak<sup>2</sup>:** Our Technical Note gave experimental evidence of the generation of ultraviolet light in these so-called contact EL cells. To state that cells in which this u.v. light is observed are operating under "improper operating conditions" is justified only if one defines what the "proper" conditions are. The occasional apparent absence of u.v. emission from certain cells may well be due to the high efficiency of absorption of short wave-length radiation by the phosphor and by the experimental cell, and is determined by the thickness and packing density of the cell. Also: the presence of only a small amount of u.v. with respect to visible light in the output of such cells does not mean that only a small amount of u.v. is internally produced. Probably it should be pointed out that we observed the u.v. bands only on photographs of several hours' exposure. Let us keep in mind the well-known wave-length dependence of intensity as far as our eye is concerned in the evaluation of comments by Lehmann regarding the addition of colors.

Conclusion: We have shown that u.v. light is generated in contact EL cells which, to the best of our knowledge, are operating properly. We obviously were aware of Herwelly's paper (our reference 3) and Destriau's response to it (Lehmann's Footnote 4); however, in our note we did not question the existence of "intrinsic" electroluminescence. The only pertinent criticism of our paper would be to show unambiguously that in certain cases no u.v. radiation is generated internally (which is not the same as emitted from the cell). Interested scientific investigators may easily quench their intellectual curiosities by performing a few simple experiments which will elucidate for them the so-called phenomenon of "contact" electroluminescence.

## The Conductivity of Undehydrated Insulating Liquids

R. Guizonnier (pp. 519-522, Vol. 108, No. 8)

**E. Baumann<sup>9</sup>:** Professor Guizonnier has shown that the conductivity of insulating liquids and waxes must be due to the moisture content in these materials. We measured<sup>10,11</sup> the conductivity of paraffin oil with a moisture content of less than 50%. Thus we found the activation energies and the gram molecules produced per unit of volume and time of dissociated light and heavy water, respectively. The transformer insulating oil examined contained 13.3% aromatic bond parts, 22.3% naphthenic, and 64.4% paraffinic bond parts. Its mean molecular weight was 267. At 20°C the oil water-saturation content was 50 ppm<sup>11</sup>  $\text{H}_2\text{O}$ . The results described in this paper were obtained at a water content of 12 ppm. Consequently, at 20°C our oil had a relative humidity of 24%. The relative humidity decreases at steady water content with increasing temperature. So the measurements were carried out far from the saturation point of water solubility and there could be no disturbing minimum of the conductivity (see Fig. 5 of the discussed paper).

**Measuring set.**—First, the examined oil was moistened with distilled light water ( $\text{H}_2\text{O}$ ) and then with heavy water ( $\text{D}_2\text{O}$ ) having a purity of 96.7 mole %. We measured the conduction current in three oil samples of light and heavy water, respectively, at temperatures from 20° to 70°C with the applied voltage increasing and decreasing. Out of these six measuring points, the average was calculated. The voltage of the power supply was highly stable having an alternating current ripple of less than 0.01%.

Between 150v and 800v, the voltage could be adjusted to a certain value with an accuracy of  $\pm 0.25\%$ . The average field strength during measurements could be varied from 400 v/cm to 2300 v/cm at a gap distance of 0.376 cm  $\pm 0.5\%$  between the cylindrical measuring electrodes. We measured the current with the sensibility of  $10^{-12}\text{A}$  and an accuracy of about  $\pm 3\%$  in a measuring range up to  $7 \cdot 10^{-11}\text{A}$ . The testing cell had shielding electrodes and was airtight.

**Measuring procedure.**—As soon as the temperature balance was reached a 50-cycle a-c voltage was applied up to 9 kv and the loss factors were measured. Then we applied a continuous voltage of 400v for 6 min. The desired test d-c voltage was fixed and we waited 1.5 to 2 min until we read the current, such that it had been stable for 30 sec. Then we measured the current as a function of the voltage at different temperatures between 20° and 70°C. In all the cases, the current density first increased linearly with the applied field strength reaching a saturation point near a field strength  $E_s$  (see Fig. 1 of this discussion).

**Evaluation of the results.**—As we can see from Fig. 1, there are two components of the current density  $j_1$  and  $j_2$ , which are proportional to the test field strength. In the case of  $j_1$ , this is only true for  $E < E_s$ . If the field strength is higher ( $E > E_s$ )  $j_1$  turns into

<sup>6</sup> P. Zaim, G. Diemer, and H. A. Klasens, *Philips Research Repts.*, **9**, 81 (1954).

<sup>7</sup> W. Lehmann, *This Journal*, **107**, 657 (1960).

<sup>8</sup> Kassel-Harleshausen, Niederfeldstr. 38 E/O, Western Germany.

<sup>9</sup> K. Heldmaier, "Leitfähigkeitsmessungen und Verlustfaktormessungen an Isolieröl, abhängig von Spannung, Temperatur und relativer Feuchtigkeit," Diploma paper, Institute for High Tension Techniques, Technical University Fridericiana, Karlsruhe (1959/1960).

<sup>10</sup> My thanks are due to Professor H. Lau, director of the Institute of High Tension Techniques, Technical University of Karlsruhe; under his guidance, the tests (Footnote 9) could be completed successfully.

<sup>11</sup> ppm = parts per million and means a weight ratio.

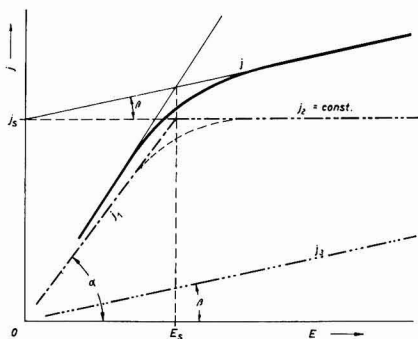


Fig. 1

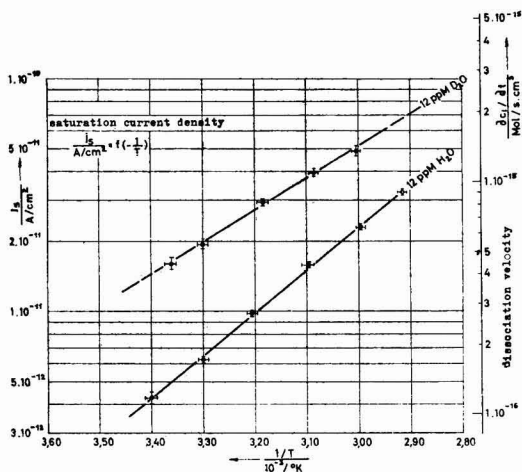


Fig. 2

the saturation current density  $j_s$  which does not depend on the electric field.

Here we are going to treat exclusively the temperature dependence of this field-independent saturation current density  $j_s = j_0$ . In our paraffin oil, we measured the saturation current and the so-called saturation field strength  $E_s$  at a humidity content of 12 ppm heavy and 12 ppm light water, respectively. While the values for  $E_s$  are very nearly independent from the temperature, the saturation current density  $j_s$  increases exponentially with the negative reciprocal value of the absolute temperature (in degrees Kelvin). Fig. 2 of this discussion shows how the saturation currents depend on the reciprocal value of the absolute temperature at a humidity content of 12 ppm  $H_2O$  and 12 ppm  $D_2O$ , respectively.

From the rise of the line

$$\ln j_s/j_0 = w/k \cdot T \quad (\text{see Fig. 2})$$

we can calculate an activation energy  $w$  ( $k$  = Boltzmann constant,  $T$  = absolute temperature in degrees Kelvin). Above the saturation field strength  $E_s$ , we found that the viscosity variation of the oil with temperature did not influence the motion of the charge carriers.

Therefore,  $w$  represents an activation energy required to produce disintegration. The saturation field strength  $E_s$  is the same at all temperatures between

20° and 70°C. For light water ( $H_2O$ ),  $E_s$  is 0.8 kv/cm, and, for heavy water ( $D_2O$ ),  $E_s$  is 1.1 kv/cm.

From the field independent components of the saturation current which were measured at field strength  $E > E_s$ , we calculated the energies required to produce disintegration for the essentially current contributing components of light and heavy water in the insulating oil.

From Fig. 2 (12 ppm  $H_2O$  in oil) follows:

$$w_{H_2O} = 0.4 \text{ eV} \pm 3\%$$

and for 12 ppm  $D_2O$  in the paraffin oil:

$$w_{D_2O} = 0.27 \text{ eV} \pm 9\%$$

The activation energy  $w$  is approximately 1.4 times greater in oil with light water than in oil with heavy water. Thereby it is proved true that the protons and deuterons, respectively, influence the conductivity in moistened oil decisively. Our former opinions about the water influence on the dielectric qualities of insulating oils<sup>13, 14</sup> are herewith well confirmed.

**Conclusion.**—By means of many measurements, Professor Guizonnier has shown that the conductivity in insulating oils and waxes must be due to their water content. We measured and examined the saturation current of paraffin oil which was moistened with light and heavy water, respectively. We found that the activation energy is 1.4 times greater in light water than in heavy water. This pronounced isotope effect means that protons and deuterons, respectively, influence the conductivity in paraffin oil decisively.

From the characteristic of the saturation current dependent on the absolute temperature [in degrees Kelvin (see Fig. 2)], we see that the thermal motion of the particles causes conductivity when the field strength is smaller than 3 kv/cm. According to Eigen and De Maeyer,<sup>14</sup> it is possible to calculate a dissociation velocity from the field independent saturation current, at a given water concentration. The dissociation velocity is shown in the right scale of Fig. 2. At the same water concentration, more dissociation processes take place per unit of time and volume with heavy water in the oil than with light water in it.

In this thermal process, the formation of free ions may take place in several phases successively. The phase which determines the speed of the whole process needs most activation energy, and it is this energy which we measured. From the very clear isotope effect, we see that it can only be a proton transition.

The absolute values of the activation energies alone are not sufficient to design the correct model of the reaction as to where the proton transition takes place. It is necessary to examine also further test results concerning the dependence of the current on the water concentration and on the field strength. Supplementary measurements, also in other oil samples, must be made in order to investigate more ex-

<sup>13</sup> E. Baumann, "Measurements of the Breakdown in Insulating Oils," Paper No. 12, Symposium on Liquid Dielectrics of The Electrochemical Society, May 5, 1959, Philadelphia, Pa.

<sup>14</sup> E. Baumann, "Messung der Durchschlagspannung in Isolierölen," *Bull. schweiz. elektrotech. Ver.*, 51, No. 6, 254 (1960).

<sup>15</sup> M. Eigen and L. De Maeyer, "Ein stationäres Feldverfahren zur Untersuchung von Dissoziationsprozessen in Flüssigkeiten und Festkörpern," *Z. Elektrochem.*, reports of the Bunsen Society for Physical Chemistry, 60, H. 9/10, 1037 (1956).

actly the proton transition we found in moistened paraffin oil.

**R. Guizonnier:** In conditions slightly different from ours, Dr. Baumann found the relation between current and temperature that we already mentioned.

While, though approximately, we sought the initial current  $i_0$  after the application of the tension, Dr. Baumann applies, first of all, an alternating current of 50 Hertz, then 400v during 6 min, and, at last, the continuous tension  $V$  in experiment during 1.5 to 2 min, the current being read as soon as it seems to be stable for 30 sec.

Instead of considering the value thus measured, he draws the curb  $i = f(V)$  and the size he thinks of is what we must call the current of saturation  $i_s$ . When the liquid is dry enough—and that is the case—the difference between  $i_0$ , that we measured, and  $i_s$ , considered by Dr. Baumann, is not very important.

Under such conditions, the value  $W = 0.4$  ev that we found, is reached when the field is superior to  $E_s$ . We made evident recently<sup>16</sup> that, when the applied field is very low (some volts/cm), the exponential form of the relation between  $i_0$  and  $T$  is preserved, but then  $W = 0.27$  ev.

It is interesting to see that this value is found by Dr. Baumann, when heavy water is added to oil. As we pointed out, that is the value obtained when using deionized water with low fields, or only distilled water.

#### Desensitization of Zirconium Powder, Especially Zirconium Powder Used in Primers

Peter Karłowicz, George Norwitz, and Joseph Cohen (pp. 659-663, Vol. 108, No. 7)

**D. R. Zaremski<sup>16</sup>:** This article, which appears in the July 1961 JOURNAL, has been reviewed with great interest in view of its close relationship to work performed by our laboratory in the year 1956. Specifically, the objectives of our experimental work at that time were to investigate the pyrophoric properties of potentially hazardous scrap materials, such as titanium and zirconium grindings, and to determine ways and means for our production plants to dispose of these materials safely. As an approach to the latter objective, treatment in acid solutions was one of the methods evaluated with the thought in mind that, if proven successful, it would readily lend itself to mill operations where spent nitric-hydrofluoric pickle liquors, available in large quantity, could be used as the treating medium.

Briefly, the results of our work indicated that disposition through acid treating was highly satisfactory although the type of acid medium used appeared to be an important factor. Greatest success was met in using solutions containing ½% to 1% hydrofluoric acid. Good results also were obtained in nitric-hydrofluoric acid solutions and aqua regia (3 HCl:1 HNO<sub>3</sub>). Sulfuric acid solutions, on the other hand, were not too effective.

Our methods for evaluating the effects of a given acid treatment were not too involved and consisted simply of dispersing treated and untreated grindings over a open flame and observing the relative tendencies for the materials to ignite. In following this procedure, untreated zirconium samples and those treated in sulfuric acid solutions were found to emit a radiant white spark. In contrast, samples treated in aqua regia and in solutions containing hydrofluoric acid were found inert, exhibiting no ignition tendencies. Spent pickle liquors, as discovered in subsequent studies, also produced the desired effect provided the solutions contained at least ½% hydrofluoric acid.

In concluding this discussion, we would like to emphasize the fact that the treatments described above and used by Allegheny Ludlum were for the sole purpose of desensitizing material which was to be disposed of. In no instance were our intentions related to reclaiming material or preparing it for another application.

#### Anodic Polarization of Stainless Steel in Chloride Solutions

G.M. Schmid and Norman Hackerman (pp. 741-744, Vol. 108, No. 8)

**U. R. Evans<sup>17</sup>:** The authors kindly quote a very early paper by myself. This, however, concerned unalloyed iron, not stainless steel. Some later papers from my laboratory describe work on stainless steel and seem to provide evidence of the existence of a film. For instance, a detailed study carried out by Berwick<sup>18</sup> aimed expressly at deciding whether the resistance of stainless steel to dilute sulfuric acid should be related to adsorbed oxygen or to an oxide film; Berwick's measurements were capable of being explained on the assumption of a film thickening by the logarithmic law, but appeared incapable of explanation by assuming adsorbed oxygen. Still later, Stern,<sup>19</sup> using a different method, reached the conclusion that there was a film growing by the logarithmic law; as he appears to have been unaware of Berwick's work, this probably can be regarded as entirely independent evidence.

It is thought that a satisfactory theory should explain not only the new experimental data put forward in the paper propounding the theory, but also the measurements of others—providing that those measurements are regarded as experimentally accurate. It would be interesting to know how the authors of the paper under discussion are inclined to interpret the results of Stern and of Berwick.

**G. M. Schmid and Norman Hackerman:** We thank Dr. Evans for his remarks and the interest he has shown in this work.

We agree that the work cited by Dr. Evans provides experimental evidence for the growth of an oxide film according to a logarithmic law. We also agree that passivity of iron and stainless steel is not caused by physically adsorbed oxygen.

<sup>16</sup> R. Guizonnier, *Comptes rendus Académie des Sciences*, July 24, 1961.

<sup>17</sup> Research & Development Labs., Allegheny Ludlum Steel Corp., Brackenridge, Pa.

<sup>18</sup> Cambridge University, Grange Rd., Cambridge, England.

<sup>19</sup> I. D. G. Berwick and U. R. Evans, *J. Appl. Chem.*, 2, 576 (1952).

<sup>19</sup> M. Stern, *This Journal*, 106, 376 (1959).



It has to be pointed out, however, that the first step in the formation of, as well as the last step in the reduction of, an oxide film must involve a chemisorbed layer of oxygen or some oxygen-containing species. Our contention is that this layer of chemisorbed oxygen causes the rapid electrochemical changes associated with passivity, permanent passivity being effected by subsequent growth of an oxide film, the structure of which depends on the nature of the earlier step.<sup>30</sup> In this laboratory, stripping experiments on iron have shown that coverages of much less than one monolayer are sufficient to cause the metal to show passive characteristics.<sup>31</sup> Both the work of Berwick and Evans and that of Stern is entirely compatible with this point of view.

### Porosity Measurements on Gold Plated Copper

M. S. Frant (pp. 774-778, Vol. 108, No. 8)

**Wm. H. Fischer<sup>32</sup>:** The use of the ammonia-ammonium persulfate solution as a test for porosity in gold plates on copper is quite interesting. About five years ago, a somewhat similar method was employed to evaluate the porosity of Inconel-clad copper.

The test solution consisted of 400g of ammonium persulfate per liter of distilled water plus 2 liters of concentrated ammonium hydroxide, thus being somewhat stronger than that used by Frant.

The test was performed by immersing a constant surface area of the Inconel-clad copper in a fixed volume of test solution in a test tube at room temperature without agitation. At 1/4, 1/2, 1 hr, and each succeeding hour, up to 8 hours, a cuvetteful of solution was removed and its copper content determined with a Fisher Electrophotometer using a 650Å red filter, against a distilled water blank. Comparison tests employing a Beckman DK-2 Ratio Recording Spectrophotometer were in good agreement with the filter photometer tests. The solution was returned to the test tube after each reading. The data were plotted as ppm copper vs. time as shown in Fig. 1 of this discussion which portrays the four main types of curves obtained.

Type 1 curves are obtained from samples having large holes in the cladding. The blue color appears

almost immediately upon immersion of the sample and rapidly increases in density. The test solution may get hot and evolve gas so vigorously as to appear to be boiling.

Type 2 curves are obtained from samples having one or both of two types of defects in the cladding: 1—copper on the surface or 2—small holes or thin spots in the cladding. The test solution may enlarge the small holes or perforate the thin spots. Hole enlargement may be due to gas evolution rather than to direct attack on the Inconel, although the test solution does attack Inconel slowly. Independent experiments have shown that etching accompanied by preferential removal of nickel from the alloy occurs. However, when solid Inconel is immersed in the test solution for periods up to 8 hr, a reading equivalent to less than 5 ppm copper is obtained. Emission spectrography of used solution indicated no significant amounts of any of the three main constituents of Inconel: nickel, chromium, or iron. Rough calculations showed that nickel is about 60 times less sensitive in this test than is copper. This means that if 60 ppm nickel were removed from the alloy by the test solution, it would be read as 1 ppm copper.

Type 3 curves are obtained from samples whose Inconel surface is contaminated by copper but which has no holes or thin spots.

Type 4 curves are given by cladded specimens free of all defects. The color developed is yellow in hue, not blue. It is due mainly to reagent deterioration.

Occasionally, an anomalous green color is developed. This is not due to nickel or very small amounts of copper. Its cause remains unknown. However, it does not interfere with interpretation of the results.

This test was designed as an incoming inspection method for cladded material to weed out unsuitable material. An unexpected bonus was that the shapes of the curves obtained allowed the identification of the causes of the rejections, thus aiding in preventing their recurrence. Thus, by using not only the amount of copper removed but also its rate of removal, additional useful information was gained.

**M. S. Frant:** Fischer's experience with the use of the ammonia-ammonium persulfate solution as a porosity test for Inconel-clad copper is most enlightening, particularly his comments on being able to use the test despite a very slight attack of nickel by the reagent, and his use of the test to distinguish different causes of failure.

About four years ago, we used the same reagent as a means of quantitatively measuring corrosion rates for nickel-plated copper in salt spray. The basic concept is that the observed "porosity" will measure the discontinuities produced in the plating as corrosion proceeds. The test is regarded as destructive, and the corroded samples are discarded after the porosity test. The test was run by exposing identical pieces from a sulfamate bath<sup>33</sup> (prepared in a single barrel load—average thickness 15μ) to varying lengths of time in salt spray, and then measuring the amount of copper dissolved by the reagent under standard conditions (the same as those described on page 775 of the discussed paper). When the log of the

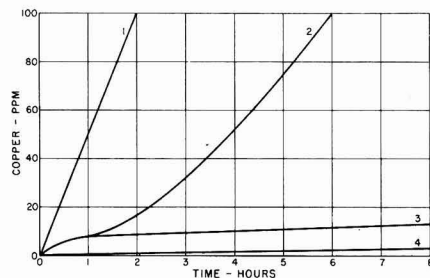


Fig. 1. Typical absorbance vs. time curves obtained in persulfate test for copper.

<sup>33</sup> R. C. Barrett, *Tech. Proc. Am. Electroplaters' Soc.*, 41, 169 (1954).

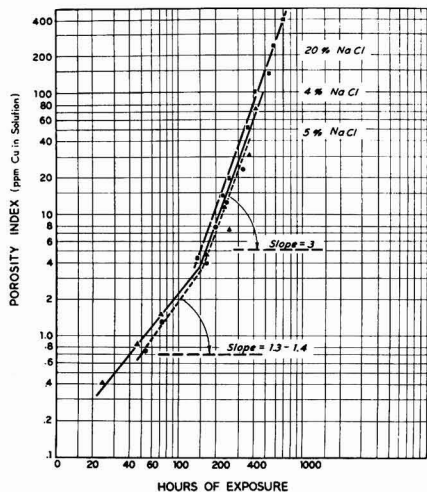


Fig. 1. Salt spray corrosion rates for sulfamate nickel, porosity index vs. time of exposure. Log-log plot: 4% NaCl solution, solid triangles; 5% NaCl solution, solid circles; 20% NaCl solution, solid squares.

amount of copper dissolved is plotted against the log of the time of salt spray exposure, an initial period is observed with a slope of 1.3 to 1.4 (See Fig. 1 published here.) After about 150 hr the slope becomes almost exactly proportional to the cube of the time of exposure. As can be seen from the graph, it is independent of the salt spray concentration.

Similar experiments on two sets of nickel samples from the Watts bath gave the following slopes: 5% NaCl—1.85, 2.10; 20% NaCl—2.45, 1.99. For Watts nickel, the amount of copper dissolved by the reagent is approximately proportional to the square of the exposure time.

A portion of the sulfamate nickel samples used above were chrome plated and the test repeated. Three distinct slopes were observed: a zero slope (at 0.6 ppm copper) for the first 60 hr; from 60 to 150 hr the slope was about 0.7; thereafter the slope was 2.0.

In our previous work in which this same reagent was used to follow the corrosion rate of tin-plated copper in salt spray,<sup>24</sup> the amount of copper dissolved was found to vary as the square of the time of exposure. Results from the persulfate reagent technique agree with the corrosion rate for tin measured by following the corrosion of thin tin films by light transmission.<sup>25</sup> The square rate was attributed to a radial (or 2-dimensional) growth of pits; while it can be visualized in terms of a single pit, the average of many pits would have the same rate of change of area.

If this line of reasoning holds for nickel and chrome plate, then a slope of 2 is believed to indicate that it is the Watts nickel or chrome which is attacked even after basis metal is exposed. The slope of 3 obtained with sulfamate nickel after a variable initial slope would indicate that, once the corrosion

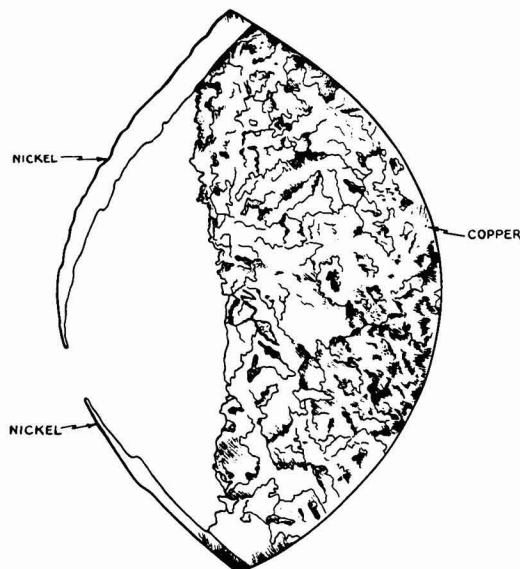


Fig. 2. Cross sectional view of a pit in sulfamate-plated nickel as seen under the microscope. Magnification of original photograph: 280X.

process has proceeded to the exposure of copper, the copper is preferentially attacked. If attack is visualized as the growth of the segment of the sphere out from an exposed point in the nickel coating, a cubic term would be expected.

Microscopic cross sections of the corroded samples have confirmed this hypothesis. For the Watts nickel samples, no attack of the copper was observed. Fig. 2 published here shows a drawing made from a micro-section of a corroded sulfamate nickel specimen which was not exposed to the persulfate reagent.

Fischer's results, like ours, indicate the range of information on coating condition and behavior which can be achieved through interpretation of results from a generally neglected technique.

### Some Observations of Copper Deposits on Single Crystals of Copper

Isaac Giron and Fielding Ogburn (pp. 842-846, Vol. 108, No. 9)

S. C. Barnes<sup>26</sup>: I was particularly interested to note that the work reported by Giron and Ogburn completely confirmed that of the Birmingham University team. That similar structures have been obtained in two independent studies is of particular importance in view of the known susceptibility of the acid copper sulfate bath to trace impurities. It seems fairly certain that the crystallographic features formed on single crystal electrodes develop by a bunching mechanism and, in this respect, the work of Poli and Bicelli<sup>27</sup> is also of relevance.

It still remains to be decided, however, whether the particular growth forms evident on crystals of a par-

<sup>24</sup> M. S. Frant, *Plating*, 45, 157 (1958).

<sup>25</sup> M. S. Frant, *Science*, 127, 288 (1958).

<sup>26</sup> Joseph Lucas Ltd., Group Research Centre, Marston Green, Birmingham 33, England.

<sup>27</sup> G. Poli and L. P. Bicelli, *Metallurgia Ital.*, 51, 548 (1959).

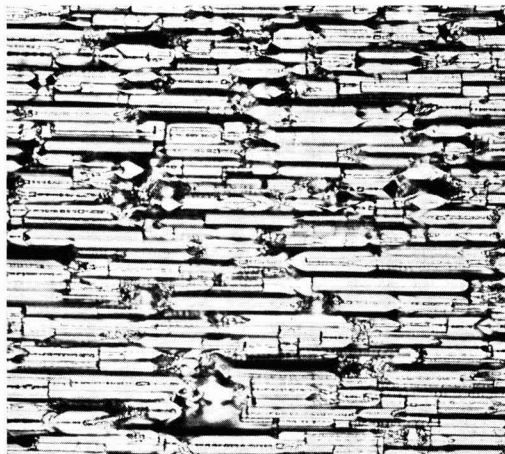


Fig. 1. Surface structure of copper deposit formed on a (110) copper single crystal cathode after plating for 20 min at 30 mA/cm<sup>2</sup> from an N.H. SO<sub>4</sub> + N. Cu SO<sub>4</sub> bath at 35°C. Magnification 575X. [110] direction parallel to long edge.

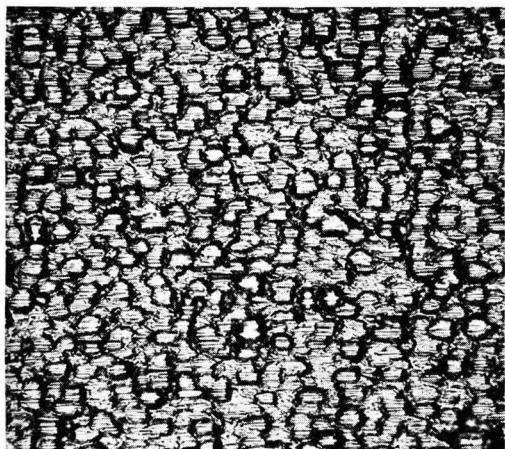


Fig. 2. Deposit obtained under the same conditions in the presence of 10<sup>-5</sup> M/l thioacetamide. Magnification 575X. [100] direction parallel to long edge.

ticular orientation are rate or potential dependent. Although the information in the paper by Giron and Ogburn does not shed any light on this topic by itself, it does when considered in conjunction with observations on the effects of addition agents on the growth habit of copper deposits.

Giron and Ogburn report that at low c.d.'s the deposit surface on (110) crystals is composed of ridges aligned at right angles to a close packed [110] direction (i.e., parallel to a [100] direction). At higher c.d.'s, the ridges extend parallel to the [110] direction. Previously unpublished results obtained by myself during an investigation into the effects of thio compounds on the structure of copper electrodeposits indicate that additions of thioacetamide (at a concentration of the order 10<sup>-5</sup> M/l) cause the deposit form on (110) crystals to change from ridges parallel

to a [110] direction to ridges at right angles to this direction (Fig. 1 and 2 of this discussion). This change is also accompanied by a large reduction in cathodic overvoltage.

It would appear, therefore, that since the habit change can be produced by either a reduction in c.d., or by the use of an addition agent which lowers polarization, the structure of the deposit is controlled by the electrode potential rather than by the applied c.d. Further work on the exact relationships between deposit structure and electrode kinetics seems warranted, and perhaps the recently developed relaxation techniques will be of use in this connection.

#### Cathodic Behavior of Iron Single Crystals and the Oxides Fe<sub>3</sub>O<sub>4</sub>, Gamma-Fe<sub>2</sub>O<sub>3</sub>, and Alpha-Fe<sub>2</sub>O<sub>3</sub>

C. D. Stockbridge, P. B. Sewell, and M. Cohen  
(pp. 928-933, Vol. 108, No. 10)

#### An Electrometric and Electron Diffraction Study of Air-Formed Oxide Films on Iron

P. B. Sewell, C. D. Stockbridge, and M. Cohen  
(pp. 933-941, Vol. 108, No. 10)

**U. R. Evans<sup>28</sup>:** The second paper ends with the words, "Stripping the film for identification, as was done by Davies and Evans, would give an erroneous result because exposure of the underlying thin magnetite layer to air would oxidize it to  $\gamma$ -Fe<sub>2</sub>O<sub>3</sub>."

These words may leave the reader with the idea that all our work is held to be invalid. It is, therefore, important to point out that, even if the three authors are right in condemning results based on film-stripping, our main conclusions remain unaffected, since the quantitative data in our two papers rest on methods independent of film-stripping. In our first paper,<sup>29</sup> the curves showing logarithmic growth at low temperatures, and parabolic at high temperatures (in general confirmation of Vernon and his colleagues<sup>30</sup>), were obtained by quite different techniques. In our second paper,<sup>31</sup> stripped films certainly were studied in two out of the three sections; the method was not felt to be ideal, and any attempt to fix exactly the composition of the film would have been unjustified; the conclusions, however, only claimed to show approximate values—e.g., that cubic oxide contained more or less than 80% Fe<sub>2</sub>O<sub>3</sub>.

Despite the authors' statement at the end of their second paper, that the oxidation of magnetite is so rapid as to render measurements based on stripped films inaccurate, their own measurements recorded in Tables II and III of the first paper suggest that the oxidation is quite a slow process. This certainly accords with our experience. We generally have found that magnetite films, in absence of liquid water, are fairly stable. If it were a fact that magnetite was oxidized too rapidly for the use of the stripped-film techniques, then any film rapidly stripped, or trans-

<sup>28</sup> Cambridge University, Grange Rd., Cambridge, England.

<sup>29</sup> D. E. Davies, U. R. Evans, and J. N. Agar, *Proc. Roy. Soc.*, **A225**, 443 (1954).

<sup>30</sup> W. H. J. Vernon, E. A. Calnan, C. J. B. Clews, and T. J. Nurse, *Proc. Roy. Soc.*, **A216**, 375 (1953).

<sup>31</sup> D. E. Davies and U. R. Evans, *J. Chem. Soc.*, 1956, 4373.

ferred to glass, should be found to be wholly ferric oxide on testing. Throughout our work, however, we have found ferrous iron in the stripped or transferred film in cases where there was reason to think that it had been present in the film before stripping or transfer. In particular, we would recall an optical difference between duplex films ( $\alpha$ -ferric oxide over magnetite) and simplex films (ferric oxide only) after transfer to glass; the simplex films showed the same color by transmitted light, whether the glass or the oxide was nearest to the eye, whereas the duplex film showed two different colors. If the magnetite layer oxidized so quickly as to invalidate methods based on stripping, the duplex specimen would surely acquire the optical properties of a simplex film on storage in air; this was not found to be the case. No doubt, methods based on film-stripping are less satisfactory than the more direct study of the films attached to the metal, but they need not be ruled out for all purposes.

The authors should be congratulated on much careful work. It is satisfactory that the thicknesses obtained by them agree fairly well with those of other authors but, as they point out, such estimates "do not serve to identify the film." Fresh information regarding composition is, therefore, particularly welcome, but their conclusions are somewhat contradictory. On page 940 it is stated that, "The two phase nature of the thin oxide film is clearly established," but lower down we read, "it seems unlikely that two discrete structures exist." Which represents the authors' final opinion?

**M. Cohen:** I would like to thank Dr. Evans for his discussion. As he points out, the thicknesses of oxide reported agree quite well with those reported by himself and others at comparable temperatures. The main disagreements between Dr. Evans' papers<sup>32, 33</sup> and those published from this laboratory<sup>34-37</sup> concern the composition of the films and the stability of  $\text{Fe}_3\text{O}_4$  in the presence of air.

Although Dr. Evans did not observe  $\text{Fe}_3\text{O}_4$  at any temperature below 250°C on Swedish iron and observed  $\text{Fe}_3\text{O}_4$  at higher temperatures only after some time of oxidation, we observed  $\text{Fe}_3\text{O}_4$  at all temperatures and from the beginning. This lack of identification of magnetite is rather surprising in view of the results obtained by annealing in vacuum by both Dr. Evans (Footnote 32, p. 454) and ourselves which show that the underlying iron reduces  $\text{Fe}_2\text{O}_3$  to  $\text{Fe}_3\text{O}_4$  very rapidly (<2 hr) even at 200°C. This would indicate that nucleation of  $\text{Fe}_3\text{O}_4$  is not a problem.

I believe that the reason for the above difference lies in the methods of cathodic reduction. In a previous study from this laboratory,<sup>38</sup> it was shown that cathodic reduction in the ammonium chloride solution used in Reference 32 gave highly variable results such that it was not possible to correlate coulometric weight loss and iron analysis measurements. It was

for this reason that the buffer solution was developed. Use of the deaerated buffer solutions allows both identification and measurement of the quantities of oxides involved. It also makes quite clear the presence of magnetite in all the cases studied. The large difference between both the immersion and reduction potentials of  $\gamma\text{-Fe}_2\text{O}_3$  and  $\text{Fe}_3\text{O}_4$  is evident in both papers.<sup>34, 35</sup> It should be noted that Dr. Evans observed  $\text{Fe}_3\text{O}_4$  from the beginning with pure iron (Reference 32, pp. 455-456).

Regarding the remarks pertaining to the color of duplex films, the low temperature oxidation of magnetite to  $\gamma\text{-Fe}_2\text{O}_3$  would still leave a duplex film of  $\gamma\text{-Fe}_2\text{O}_3$  and  $\alpha\text{-Fe}_2\text{O}_3$ .  $\gamma\text{-Fe}_2\text{O}_3$  is a good electronic conductor in comparison to  $\alpha\text{-Fe}_2\text{O}_3$  and probably has quite different optical properties.

The oxidation of magnetite to  $\gamma\text{-Fe}_2\text{O}_3$  by air at room temperature presents a real problem. With thick compact films, the percentage change in composition on exposure to air for short times can be quite small. However a film of  $\text{Fe}_3\text{O}_4$ , 40Å thick, exposed to air on both sides would oxidize completely to  $\gamma\text{-Fe}_2\text{O}_3$  in about 30 hr and would convert over half its thickness to  $\gamma\text{-Fe}_2\text{O}_3$  within 2 hr. A stripped air-formed film 25Å thick would oxidize to  $\gamma\text{-Fe}_2\text{O}_3$  within ½ hr on exposure to oxygen. Although this is not rapid oxidation in the ordinary sense, it is sufficiently rapid to cause errors in analyses for ferrous-ferric ion ratios and to change electron diffraction patterns.

The points brought up in the last paragraph relate to the word thin and the two quotations refer to an 80Å film formed at 200°C and a 25Å film formed at room temperature on a (112) single crystal pure iron. In both cases, all the oxides are cubic and the cathodic reduction curves show evidence of a duplex film. With the 80Å film there is an appreciable amount of both  $\text{Fe}_3\text{O}_4$  and  $\gamma\text{-Fe}_2\text{O}_3$ . At these thicknesses, it is probably permissible to write in terms of two distinct phases. With the thinner air-formed film, although the outer part of the film is  $\gamma\text{-Fe}_2\text{O}_3$  and the inner part of the film is  $\text{Fe}_3\text{O}_4$ , the phase boundary probably occupies such a large portion of the thickness that it may not be permissible to insist on two discrete structures in the total thickness of 25Å. One should keep in mind that the structures of  $\gamma\text{-Fe}_2\text{O}_3$  and  $\text{Fe}_3\text{O}_4$  are very similar so that one might expect a thick phase boundary between them.

**D. Gilroy and J. E. O. Mayne**<sup>39</sup>: In the second paper, the authors claim that it is possible to differentiate between  $\text{Fe}_3\text{O}_4$  and  $\gamma\text{-Fe}_2\text{O}_3$  owing to different efficiencies of cathodic reduction at constant current density. In view of the similarity in structure of these two oxides, it seems very remarkable that there should be such a sharp change in reductive efficiency as suggested by the authors in their interpretation of Curve 1, Fig. 4. The air-formed film is very thin and it may not behave on reduction in a similar way to the much thicker duplex film formed at higher temperatures.

Hancock<sup>40</sup> examined the cathodic reduction of the air-formed film in 0.2N potassium chloride and 0.1N

<sup>32</sup> D. E. Davies, U. R. Evans, and J. N. Agar, *Proc. Roy. Soc.*, A225, 443 (1954).

<sup>33</sup> D. E. Davies and U. R. Evans, *J. Chem. Soc.*, 1956, 4373.

<sup>34</sup> C. D. Stockbridge, P. B. Sewell, and M. Cohen, *This Journal*, 108, 928 (1961).

<sup>35</sup> P. B. Sewell, C. D. Stockbridge, and M. Cohen, *This Journal*, 108, 933 (1961).

<sup>36</sup> E. J. Caule, K. H. Buob, and M. Cohen, *This Journal*, 108, 829 (1961).

<sup>37</sup> E. J. Caule and M. Cohen, *This Journal*, 108, 834 (1961).

<sup>38</sup> H. G. Oswin and M. Cohen, *This Journal*, 104, 9 (1957).

<sup>39</sup> Dept. of Metallurgy, University of Cambridge, Cambridge, England.

<sup>40</sup> Hancock, *J. Chem. Soc.*, 1958, 4167.

sodium hydroxide. Virtually no iron passed into solution and the coulombs passed at the points of inflexion were identical. These experiments have been repeated with neutral 0.1*N* sodium sulfate and benzoate; again, virtually no iron passed into solution. However, with the borate/chloride buffer, used by the authors, ferrous ions passed into solution, but not in sufficient quantity to account for the entire film. It appears that in neutral unbuffered or alkaline solutions the cathodic process is the reduction of oxide to iron; whereas, in buffered solutions, this is accompanied by the reduction of ferric to ferrous ions, which pass into solution. A probable explanation is that upon cathodic reduction the liquid in contact with the surface of the specimen becomes alkaline; in the presence of a buffer the rise in pH will be delayed, but not indefinitely. It is suggested that in Curve 1, Fig. 4, on Section  $E_A-E_B$  the process is essentially a one-electron reduction, whereas on Section  $E_B-E_C$  a three-electron process is involved.

If these suggestions are accepted, then it follows that the values given for the film thickness in the Tables should be recalculated, and higher values will be obtained; furthermore, the difference in the efficiency of reduction of the two oxides is not a characteristic of the oxides, but arises owing to the buffering action of the solution.

Hancock's value of  $26 \pm 3 \text{ \AA}$  for the thickness of the air-formed film on iron, reduced in hydrogen, has been criticized because he assumed that the film was composed of  $\gamma\text{-Fe}_2\text{O}_3$ . Had he assumed that it was composed entirely of  $\text{Fe}_3\text{O}_4$ , the value would be greater by less than 9%. It is generally agreed that the film is of intermediate composition; the corrected value would, therefore, be within the limits of his measurements.

**M. Cohen:** With regard to the remarks of D. Gilroy and J. E. O. Mayne, the work in the two papers differentiates between  $\gamma\text{-Fe}_2\text{O}_3$  and  $\text{Fe}_3\text{O}_4$  by immersion potential and reduction potential as well as current efficiency of reduction. In some thousands of cathodic reduction runs made in either the borate/chloride buffer or a borate/boric acid buffer at a pH of 8.4, we always have found that the outer layer reduces to form ferrous ion in solution with high current efficiency. That the buffer appears to be quite effective for long periods of time is shown in Curves 1 and 2, Fig. 11, where the time to reach the magnetite potential obviously is dependent on the thickness of the outer  $\gamma\text{-Fe}_2\text{O}_3$  layer.

I agree that with the thin films some of the magnetite is reduced to iron. This assumption was made to obtain the thicknesses shown in Table IX. As can be seen in this table, the thickness and composition of a film on polycrystalline iron will depend on the distribution of orientations of the individual grains, and probably on the oxidation characteristics of grain boundaries as well. We also have some evidence of the formation of iron from reduced magnetite by electron diffraction. From the point of view of identification and measurement of the thin films on iron, the difference in behavior of  $\gamma\text{-Fe}_2\text{O}_3$  and  $\text{Fe}_3\text{O}_4$  on cathodic treatment in the buffered solution is very useful.

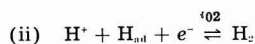
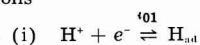
### The Application of an X-Y Pulsed Measuring System to Polarization Studies, I. The Hydrogen Reaction on Platinum

C. H. Presbrey, Jr., and Sigmund Schuldiner (pp. 985-995, Vol. 108, No. 10)

**M. W. Breiter<sup>11</sup>:** Presbrey and Schuldiner report experimental results which are in agreement with the results on hydrogen evolution published by the late Professor Knorr, by me, or our co-workers in recent years. However, the interpretation of the measurements by the two schools differs greatly. The results of Presbrey and Schuldiner can be explained satisfactorily by the interpretation of hydrogen overvoltage phenomena on activated platinum metals which has been given by us without drastic changes in the years since 1954:

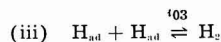
(A) Mass-transport processes are rate determining for stationary current potential curves over a wide potential range.

(B) The exchange current densities of the two discharge reactions



are large at  $\eta = 0$  ( $i_{01} \approx i_{02} \approx 0.3 \text{ \AA/cm}^2$ ).

(C) The equilibrium of the recombination reaction



is established for  $\eta < +0.08\text{v}$ . It does not exist for  $\eta > +0.08\text{v}$ .

The experiments which lead to the above conclusions were discussed and summarized by me recently.<sup>12</sup> Our interpretation is in qualitative agreement with the important contributions to the understanding of hydrogen overvoltage by Frumkin's school.

Schuldiner's interpretation ( $i_{01} \gg i_{02} \gg i_{03}$ ) is based to a large extent on the occurrence of cathodic Tafel lines with  $b \approx 30$  mv. These curves are measured at a high flow rate of the stirring gas. A further increase of the flow rate does not influence the current potential curves any more. So Schuldiner concludes that reaction (iii) is rate determining. However, his observation does not necessarily imply that diffusion is eliminated. It means that the thickness of the diffusion layer does not change to a measurable extent any more if the flow rate is increased above a certain value. An anodic limiting current density  $i_{01}$  of diffusion (and convection) of molecular hydrogen of  $15 \text{ ma/cm}^2$  is required to reduce the influence of the transport processes to 10% if  $i_{02}$  is  $1.5 \text{ ma/cm}^2$ . Such a high  $i_{01}$ -value has not been reported in literature even under the most extreme stirring conditions (flow of electrolyte or rotating disk) at  $p_{\text{H}_2} = 1 \text{ atm}$ .

It is felt that the Tafel relations in Fig. 7 and Fig. 8 of Schuldiner's present paper and in many of his former publications are valid for a very small range of current densities only. The range is too small to

<sup>11</sup> Research Lab., General Electric Co., Schenectady, N. Y.

<sup>12</sup> M. Breiter in "Transactions of the Symposium on Electrode Processes," Edited by E. Yeager, pp. 307-324, John Wiley & Sons, Inc., New York (1961).

draw reliable conclusions. The assumption of a slow combination step requires that the concentration of atomic hydrogen which is involved in the reaction is very small at  $\eta \approx +0.06\text{v}$ . Therefore it cannot be large at  $\eta = 0$  either. This forces Schuldiner to postulate the formation of a second monolayer of hydrogen atoms which is completed at negative potentials. However, the a-c impedance measurements at cathodic overvoltages in 8N H<sub>2</sub>SO<sub>4</sub> show conclusively that a second monolayer of hydrogen atoms is not formed up to cathodic current densities of 0.3 A/cm<sup>2</sup>. The high capacity of the platinum electrode during the cathodic pulse is due to the accumulation of molecular hydrogen in the diffusion layer, not to the formation of a second monolayer. The anodic charging curves in Fig. 10, like our charging curves, do not give evidence for a third "plateau" due to the anodic removal of a second monolayer. A better picture of the anodic oxidation of hydrogen atoms is obtained by the potentiostatic application of a sawtooth.<sup>43, 44</sup> The so-called plateaus of the charging curves are not well enough distinguishable to determine their length. Only part of the hydrogen associated with the surface at equilibrium is ionized near the equilibrium potential because the adsorption isotherm is very flat in the vicinity of  $\eta = 0$ .

The "reversible" hydrogen adsorption on platinum in the gaseous phase occurs at pressure  $p_{\text{H}_2} < 1$  atm. As hydrogen adsorption in electrolytes without specifically adsorbable ions starts at about the same low pressure as in the gaseous phase, the "reversible" hydrogen adsorption was attributed by me<sup>45</sup> to the region of the left peak<sup>43, 44</sup> of the potentiostatic i-U curves.

**S. Schuldiner:** Unfortunately, Dr. Breiter has misconstrued several important points in our paper. His statement that we are "forced to postulate the formation of a second monolayer of hydrogen atoms which is completed at negative potentials," is not correct. What we do postulate is that, since a double atomic layer is unfeasible, a quantity of H atoms, which coulometrically may amount to a second layer, forms Pt-H alloy on the surface layer of platinum.

Concerning the diffusion *vs.* slow combination rate-controlling mechanisms, I shall not reiterate here detailed arguments in favor of the combination mechanism since this type of redundancy is an unnecessary rehashing of the literature. A comparison of a steady-state hydrogen overvoltage curve<sup>46</sup> (Fig. 2) with the transient overvoltage curves shown in Fig. 8 of the paper under discussion shows a convergence at increasing current densities. If mass transport were rate controlling, then the steady-state overvoltage should diverge from the transient overvoltage curve as the current density increases.

In addition, in Fig. 2,<sup>46</sup> Tafel curves which extend over two and one half orders of magnitude of current density are shown. Fig. 8<sup>46</sup> of the same reference shows Hammett relations for three orders of magnitude of current density. These are long enough ranges of current density to be highly significant.

Since both the X-Y and sawtooth methods use measuring instruments of essentially the same precision and resolution (commercial oscilloscopes, etc.), neither has an advantage over the other in this respect. The disadvantage of the sawtooth method is that at fast sweep rates a displacement current, which cannot be corrected for, is included in the oscilloscope trace. The X-Y method avoids this difficulty.

### Rhenium-Tungsten-Carbon Interactions

R. F. Havell and Y. Baskin (pp. 1068-1069, Vol. 108, No. 11)

**Charles P. Kempter<sup>47</sup>:** The authors state that "Interactions between rhenium and carbon are limited to absorption of about 1% carbon in the rhenium lattice producing slight changes in the lattice constants and a reduction of the c/a ratio from 1.615 to 1.600," quoting only the early work of Trzebiatowski.<sup>48</sup> They did not quote the recent articles by Hughes<sup>49</sup> ("A Survey of the Rhenium-Carbon System") or Nadler and Kempter<sup>50</sup> ("Some Solidus Temperatures in Several Metal-Carbon Systems"). Hughes reviewed work on the Re-C system prior to that of Trzebiatowski, and published the Re-C phase diagram above 1500°C from 0 to ~30 atomic per cent (a/o) carbon. He reported a simple eutectic system at 16.9 a/o carbon and 2480 ± 50°C, with the solid solubility of carbon in rhenium varying from 11.7 a/o at the eutectic temperature to 4.2 a/o at 1800°C. In an alloy of 20 a/o carbon, the "a" parameter increased from 2.760Å to 2.792Å and the "c" parameter increased from 4.458Å to 4.471Å—thus the axial ratio decreased from 1.615 to 1.601. In agreement with Hughes, Nadler and Kempter reported the minimum solidus temperature in the rhenium-carbon system to be 2486 ± 18°C. In addition, although Havell and Baskin quoted a recent reference<sup>51</sup> for the Re-W phase diagram, they quoted no references pertaining to the W-C system, but did state a 2600°C melting point for WC and a 2475°-2730°C range for melting points of tungsten carbides and/or eutectics in the W-C system. Nadler and Kempter<sup>50</sup> have reviewed work on the W-W<sub>2</sub>C eutectic and the WC melting point, and have determined values of 2732 ± 22°C and 2720 ± 20°C for these, respectively. (A final pertinent reference, which appeared after the submission of the Havell and Baskin note, is a paper by Sara<sup>52</sup> entitled "Phase Equilibria in the System Tungsten-Carbon." Sara found the minimum solidus temperature in the W-C system to be the W-W<sub>2</sub>C eutectic temperature and agreed well with the above N. and K. value.)

The Miller indices tabulated for the "rhenium-WC solid solution" in Table III are consistent with space group D<sub>6h</sub>-P6<sub>3</sub>/mmc, which occurs for Re (Strukturbericht type A3) and W<sub>2</sub>C (type L<sub>3</sub>). Both types<sup>53</sup>

<sup>47</sup> Los Alamos Scientific Lab., University of California, Los Alamos, N. Mex.

<sup>48</sup> W. Trzebiatowski, *Z. anorg. Chem.*, **233**, 376 (1937).

<sup>49</sup> J. E. Hughes, *J. Less-Comm. Met.*, **1**, 377 (1959).

<sup>50</sup> M. R. Nadler and C. P. Kempter, *J. Phys. Chem.*, **64**, 1468 (1960).

<sup>51</sup> J. M. Dickinson and L. S. Richardson, *Trans. Am. Soc. Metals*, **51**, 758 (1959).

<sup>52</sup> R. V. Sara, 14th Regional Meeting, American Ceramic Society, Oct. 26, 1961, San Francisco, Calif.

<sup>53</sup> W. B. Pearson, "A Handbook of Lattice Spacings and Structures of Metals and Alloys," Pergamon Press, New York (1958).

<sup>43</sup> F. G. Will and C. A. Knorr, *Z. Elektrochem.*, **64**, 258, 270 (1960).

<sup>44</sup> W. Bildt and M. Breiter, *Z. Elektrochem.*, **64**, 897 (1960).

<sup>45</sup> M. Breiter, *Electrochimica Acta*, in press.

<sup>46</sup> S. Schuldiner, *This Journal*, **106**, 891 (1959).

have two metal atoms per unit cell in set (c) at  $1/3$ ,  $2/3$ ,  $1/4$ , and  $2/3$ ,  $1/3$ ,  $3/4$ , and  $W_2C$  also has a carbon atom in an octahedral hole. Thus, it seems reasonable that Re would form solid solutions with  $W_2C$ , and, therefore, the use of "(Re, WC)ss" in Table I and in reference to Table III might be misleading. Although WC has a hexagonal lattice, the space group<sup>64</sup> is  $D_{3h}^5-P\bar{6}m2$  and the assignment of Miller indices is different from the case of Re or  $W_2C$ . Even though the *initial* tungsten to carbon molar ratio was unity, this does not preclude the existence of W-C structures other than WC in the observed solid solution. Until further characterization of the solid solution is carried out, it seems appropriate to refer to it as the Re-W-C solid solution as Havell and Baskin did in Table II.

**R. F. Havell and Y. Baskin:** We are thankful to Mr. Kempter for citing the recent work on the binary systems Re-C and W-C which bear directly on our study. We agree that the expression (Re, WC)ss is somewhat misleading, as it implies that the structure WC exists in the solid solution. We prefer either (Re-W-C)ss or Re- $W_x$ - $C_x$  solid solutions. The Re- $W_x$ - $C_x$  solid solution is structurally similar to that of  $W_2C$  despite the fact that the W/C mole ratio is a unity. As discussed in the article, rhenium and tungsten powders with a W/C mole ratio of 2 were not reacted, since contact of these samples with the graphite plate at 2300°C would have resulted in carbon absorption, thus shifting the ratio toward unity.

We feel that Mr. Kempter's implication that the W/C mole ratio of our powders changed on firing is not justified. Accurate weighings showed negligible weight change and, consequently, no shift in this ratio. Actually, it is not necessary to alter the W/C mole ratio from unity to obtain solid solutions having a close-packed hexagonal structure. The solid solution composition (Re, W, C) possesses this structure and, except for a different metal constitution, has the same metal to carbon ratio as the composition (Re,  $W_x$ , C), which would be intermediate between Re and  $W_2C$ . Moreover, the lattice constants of (Re, W, C) ( $a = 2.877$ ,  $c = 4.561$ ,  $c/a = 1.585$ ) are very close to those calculated for Re,  $W_2C$  on the basis of Vegard's Law ( $a = 2.88$ ,  $c = 4.59$ ,  $c/a = 1.59$ ). The small difference in atomic radius between rhenium and tungsten might account for some of the above difference.

### On the Electrodeposition of Arsenic and Its Role in Corrosion Prevention

Gösta Wranglén (pp. 1069-1070, Vol. 108, No. 11)

**R. Piontelli and G. Poli<sup>65</sup>:** According to Dr. Wranglén's opinion, the insulating properties of the amorphous arsenic layers, obtainable by plating or displacement, involve the following consequences:

(A) The intervening of an ohmic drop contribution in the overvoltages, concerning both arsenic and hydrogen reduction as given by the direct method,

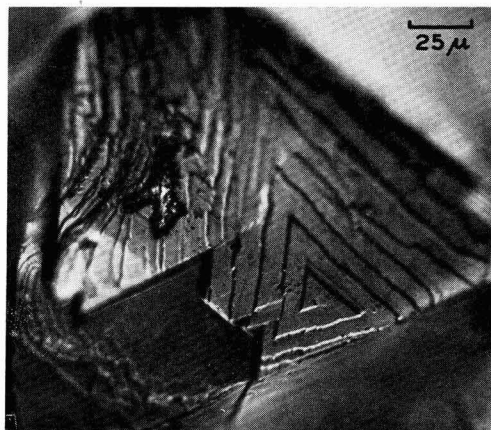


Fig. 1. Arsenic deposited in crystalline form (chloride bath); example of growth spiral. Magnification 400X.

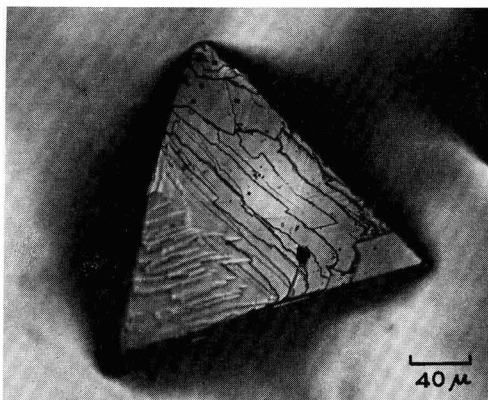


Fig. 2. Arsenic deposited in crystalline form (chloride bath). Magnification 270X.

so as to render meaningless the results thus obtainable;

(B) High voltages and a very poor current efficiency in the arsenic electrowinning;

(C) A very efficient inhibitive influence of arsenic with respect to the corrosion of iron materials, formerly explained<sup>66</sup> by considering the hydrogen overvoltages.

1. We agree on the point that the "cumulative overvoltages" given by the direct methods in a quasi-steady condition, although representing the item to be considered in the cell voltage-balance, are affected in this case by a quite significant ohmic contribution, which may become largely predominating for thick arsenic layers.

2. The "true overvoltages" (that is, corrected from any ohmic contribution), in the arsenic separation on arsenic layers, are definitely high (in the order of several tenths of a volt), however, also at low c.d.<sup>67</sup>

3. Arsenic may be plated, at least partially, also in crystalline form (see Fig. 1 and 2 of this discussion),

<sup>66</sup> O. P. Watts, *Trans. Am. Electrochem. Soc.*, **21**, 339 (1912).

<sup>67</sup> In the succession, Bi, Sb, As, a strong increase of these "true overvoltages" corresponds to the increase of the metalloidal character (see R. Piontelli, *Z. Elektrochem.*, **55**, 128 (1951)).

<sup>64</sup> J. Leciejewicz, *Acta Cryst.*, **14**, 200 (1961).

<sup>65</sup> Lab. of Electrochemistry, Physical Chemistry, Metallurgy, Politecnico di Milano, Milan, Italy.

the corresponding "true overvoltage" again being quite high.<sup>58</sup>

4. In any case, the low and decreasing current efficiency encountered by Wranglén could not be accounted for on the basis of the assumed insulating power of the arsenic layer, which would influence both of the concurrent cathodic processes. The current efficiency in the As deposition is low, due to the high true overvoltage involved by this process, while its decrease in time, in Wranglén's experiments, is due perhaps: (a) to composition changes in the bath; (b) to the structure changes of the cathodes. As a matter of fact, we found evidence that these last, although not involving any appreciable decrease in the (true) overvoltage in the As deposition, may appreciably decrease the hydrogen overvoltage.

5. The conclusion that the strong inhibition that As may exert on the corrosion of Fe cannot be explained solely on the basis of the hydrogen overvoltage has been largely substantiated by previous experiments from this laboratory.<sup>59</sup>

In our opinion, however, this very efficient protection is due largely to the structure and, in particular, to the very peculiar perfection of the separated layers (which eliminate any potentially anodic area), in spite of their origin by a displacement reaction, and thanks to the very high throwing power which characterizes, under favorable conditions, arsenic deposition on some foreign metals.

The opinion that this protective influence cannot merely be attributed to the insulating power of the As layer, as Wranglén seems to consider, may be directly confirmed as follows. An iron specimen, after adequate treatment in an inhibiting arsenical solution, does not displace hydrogen from strong acids, nor copper from copper sulfate.

Let us eliminate the arsenic layer from the contour or from some other localized area, by scraping.

The specimen will now displace hydrogen, or respectively copper, but the cathodic process will then occur not only on the newly exposed area but, moreover, on a rather large fraction of the still covered one.

The very presence of the arsenic layer would be unable, therefore, to prevent the occurrence of cathodic processes complementary to the anodic ones when these last are made possible by the availability of anodic areas.

**G. Wranglén:** The discussion by Professors Piontelli and Poli, complementing their previous extensive work in this field, is most welcome. They have correctly interpreted and summarized the conclusions of the present writer. It seems necessary to emphasize, however, that the nonconductivity of the arsenic electrodeposited by the author was not "assumed" but experimentally established.

It is now very interesting to learn that arsenic can be deposited, "at least partially," also in crystalline form, as the micrographs 1 and 2 show. It also would

have been of great interest to learn the conditions of deposition, however, since it would seem as if crystalline electrodeposits of arsenic are exceptional at low temperatures and normally to be expected only in fused salt electrolysis. Amorphous deposits (according to x-ray diffraction analysis) were obtained not only by the present writer but also by Stillwell and Audrieth<sup>60</sup> from solutions of  $\text{AsCl}_3$  in glacial acetic acid, and by Finch, Quarrel, and Wilman<sup>61</sup> from aqueous cyanide baths. Deposits from the  $\text{AsCl}_3$ -HAc bath were used by Salzberg and Goldschmidt<sup>62</sup> in their studies of hydrogen overvoltage on arsenic. It is also known that arsenic precipitated chemically from aqueous solutions by reducing agents is obtained in various amorphous forms.<sup>63</sup> These are considered to be transition forms between the nonmetallic yellow, cubic, and the metallic gray, rhombohedral modification of elementary arsenic. They are transformed to the metallic modification on heating. According to origin, the transformation temperature varies from 100° to 377°C.<sup>64</sup> Their nonconductivity seems to be a direct consequence of their amorphous structure. This connection often seems to have been overlooked, however, particularly in electrochemical studies.

Piontelli and Poli maintain that the insulating properties of electrodeposited arsenic would affect the two concurrent cathodic processes equally and thus not influence the current efficiency of arsenic deposition. It must be observed, however, that the arsenic is deposited in a noncoherent condition (porous from the acid chloride bath, flaky from the alkaline arsenite bath) leaving small areas of the basis metal uncovered. On these the current density will be very high, much higher than the limiting c.d. for arsenic deposition. This is particularly true for arsenite solutions where the  $\text{AsO}_2^-$ -ions migrate away from the cathode, resulting in a low limiting c.d. Hence, copious hydrogen evolution from water will take place resulting in a low current efficiency of arsenic deposition. It seems natural that this effect is accentuated during the course of an electrolysis experiment.

The high throwing power in the electrodeposition of arsenic, referred to by Piontelli and Poli, is also a natural consequence of the low conductivity of the deposit, transferring the electrodeposition reaction to still uncovered areas. In this respect, the electrodeposition of arsenic resembles certain anodic processes, such as anodizing of aluminum.

The corrosion experiment described by Piontelli and Poli and involving the local removal of the nonconducting arsenic film very much resembles localized corrosion, such as pitting, on metals passivated by an oxide film, e.g., aluminum and stainless steel. There the cathode reaction also occurs all over the passivating film or on active parts of it.

<sup>58</sup> C. W. Stillwell and L. F. Audrieth, *J. Am. Chem. Soc.*, **54**, 472 (1932).

<sup>59</sup> G. E. Finch, H. G. Quarrel, and H. Wilman, *Trans. Faraday Soc.*, **31**, 1051 (1935).

<sup>60</sup> H. W. Salzberg and B. Goldschmidt, *This Journal*, **107**, 348 (1960).

<sup>61</sup> Gmelin's Handbuch der Anorganischen Chemie, 8:te Aufl., Verlag Chemie, GmbH., Weinheim/Bergstr. (1952).

<sup>64</sup> Work cited in Footnote 63, p. 121.

<sup>58</sup> For further details, see R. Piontelli and G. Poli, In print.  
<sup>59</sup> See for this purpose the following papers (concerning the inhibition by As, Sb of the corrosion of Fe, Ni, Co, and similar phenomena): R. Piontelli, et al., *Chimica Industri.*, **24**, 122 (1942); *ibid.*, **25**, 203 (1943); *Gazz. chim. Ital.*, **77**, 45 (1947); *ibid.*, **79**, 279, 293, 297, 533, 722 (1949).



# FUTURE MEETINGS OF The Electrochemical Society



★ ★ ★

**Boston, Mass., September 16, 17, 18, 19, and 20, 1962**

Headquarters at the Statler-Hilton Hotel

Sessions will be scheduled on

Batteries (General Sessions on primary and secondary batteries, and fuel cells),  
Battery—Theoretical Electrochemistry Joint Symposium on Porous Electrodes, Corrosion,  
Corrosion—Electronics Joint Symposium on Phenomena at Interfaces, Electrodeposition  
(including a Symposium on Alloy Electrodeposition), Electrodeposition—Electronics  
Joint Symposium on Electrochemical Processes for Semiconductor Devices,  
Electronics—Semiconductors (including a Symposium on Semiconductor Phenomena),  
Electrothermics and Metallurgy (including a Symposium on Hot Pressing), Electrothermics  
and Metallurgy—Corrosion Joint Symposium on High-Temperature Corrosion

★ ★ ★

**Pittsburgh, Pa., April 14, 15, 16, 17, and 18, 1963**

Headquarters at the Penn Sheraton Hotel

Sessions probably will be scheduled on

Electric Insulation, Electronics (including Luminescence and  
Semiconductors), Electrothermics and Metallurgy,  
Industrial Electrolytics, and Theoretical Electrochemistry

★ ★ ★

**New York, N. Y., September 29, 30, and October 1, 2, and 3, 1963**

Headquarters at the New Yorker Hotel

★ ★ ★

**Toronto, Ont., Canada, May 3, 4, 5, 6, and 7, 1964**

Headquarters at the Royal York Hotel

★ ★ ★

**Washington, D. C., October 11, 12, 13, 14, and 15, 1964**

Headquarters at the Sheraton-Park Hotel

Papers are now being solicited for the meeting to be held in Pittsburgh, Pa., April 14, 15, 16, 17, and 18, 1963. Triplicate copies of each abstract (*not exceeding 75 words in length*) are due at Society Headquarters, 30 East 42 St., New York 17, N. Y., *not later than December 14, 1962* in order to be included in the program. *Please indicate on abstract for which Division's symposium the paper is to be scheduled, and underline the name of the author who will present the paper.* No paper will be placed on the program unless one of the authors, or a qualified person designated by the authors, has agreed to present it in person. An author who wishes his paper considered for publication in the JOURNAL should send triplicate copies of the manuscript to the Managing Editor of the JOURNAL, 30 East 42 St., New York 17, N. Y.

Presentation of a paper at a technical meeting of the Society does not guarantee publication in the JOURNAL. However, all papers so presented become the property of The Electrochemical Society, and may not be published elsewhere, either in whole or in part, unless permission for release is requested of and granted by the Editor. Papers already published elsewhere, or submitted for publication elsewhere, are not acceptable for oral presentation except on invitation by a Divisional program Chairman.



## Symposium on Stress Corrosion of Metals, ECS Fall 1963 Meeting

The Corrosion Division is planning a Symposium on Stress Corrosion of Metals for the 1963 Fall Meeting of The Electrochemical Society to be held in New York City, September 29 to October 3, 1963.

Subjects suggested for this symposium are: classical stress corrosion; hydrogen embrittlement as a factor in stress-corrosion cracking; brittle fracture as affected by environmental conditions; and the application of modern concepts of solid-state physics to stress corrosion.

Papers giving data to support or disprove one of the current theories of the mechanism of stress-corrosion cracking would be considered under the classification of classical stress corrosion. Papers merely summarizing data on a particular alloy or group of alloys are not considered to have a place in the symposium.

Inasmuch as results of center or edge notch tests on very high-strength alloys are reported to be highly sensitive to the test environment, the Chairmen feel that papers giving results and particularly sug-

gested mechanisms for these phenomena should be included.

Metal physics is an increasingly important field and papers in which the modern concepts of solid-state physics are applied to the theory of stress-corrosion cracking would be desirable.

Additional information on plans for the symposium can be obtained from one of the Co-Chairmen: E. H. Phelps, Applied Research Lab., U.S. Steel Corp., Monroeville, Pa., and Hugh L. Logan, National Bureau of Standards, Washington, D. C.

### Section News

#### News from India

*Symposium on Electrochemistry.*—The National Institute of Sciences of India arranged a Symposium on Electrochemistry at New Delhi during October 1961. Thirty-nine papers were presented covering various aspects of electrochemistry: theory of electrolytes; electrode processes and potentials; electrochemistry in relation to structure. There were contributions from Australia, Italy, the U.K., U.S.A., and U.S.S.R. Abstracts of the papers have been issued in a printed booklet.

*Electrochemistry Seminar.*—The Third Seminar on Electrochemistry was held at the C.E.C.R.I., Karakudi, from December 26 to 29, 1961. Seventy-seven papers were presented in six sections: 1—electrode kinetics, electrochemical equilibria, and electroanalysis; 2—electroorganic and inorganic products; 3—electrothermics and electrometallurgy; 4—metal finishing and electrodeposition; 5—corrosion; 6—batteries. Scientists from France, Holland, Hungary, Japan, the U.S.A., and U.S.S.R. contributed papers to the seminar. Abstracts of the papers have been published in a booklet by the C.E.C.R.I.

*Indian Science Congress.*—The 49th annual session of the Indian

Science Congress was held at Cuttack from January 3 to 9, 1962. The program covered sectional meetings, symposia, popular and special lectures, visits to institutions and other places of interest, and social functions. An exhibition of scientific and laboratory equipment was arranged.

Delegates from many foreign countries participated in the deliberations. Several papers on electrochemistry and allied branches were presented. The following were among the symposia topics: physicochemical methods in the determination of structure of molecules;

### Papers Solicited for New ECS Magazine to be Published in 1963

As announced in the February issue of the JOURNAL (page 37C), The Electrochemical Society will publish a new magazine under a name and cover design yet to be adopted. The first issue will be published in January-February 1963. Initially, the new publication will be issued bimonthly. It will become a monthly publication as soon as enough papers are received to justify such a step.

The new magazine will cover electroprocesses in areas of technology, engineering, design, devices, economics, and appropriate reviews. The same review procedures which apply to the present JOURNAL will also obtain with regard to the new magazine.

A. C. Loonam, Editor, is now soliciting papers for publication in the new magazine. All members and others concerned, who are engaged in the applied areas of electroprocesses, who can submit papers on timely subjects are urged to do so as soon as possible.

Triplicate copies of each manuscript, prepared in accordance with the Instructions to Authors of Papers published on pp. 131C-132C of the May JOURNAL, should be submitted to the Editor of the new magazine, A. C. Loonam, The Electrochemical Society, Inc., 30 East 42 St., New York 17, N. Y.

Manuscripts so submitted become the property of The Electrochemical Society and may not be published elsewhere, in whole or in part, unless permission is requested of and granted by the Editor.

high-temperature properties and techniques; coordination complexes.

*Symposium on Corrosion of Metals.*—A Symposium on Corrosion of Metals will be held from November 7 to 10, 1962 at the Defense Research Lab. (Stores), Kanpur. The following subjects will be covered in about 55 papers: 1—fundamental studies; 2—corrosion inhibitors; 3—nonmetallic protective coatings; 4—metallic coatings and paints; 5—corrosion problems in industry; 6—environmental studies; 7—laboratory methods; 8—special corrosion problems; 9—practical corrosion problems; 10—cathodic protection. There will be contributions from defense organizations, national laboratories, research institutions, universities, and industries, including papers from foreign countries.

*Symposium on Ferroalloy Industry in India.*—A Symposium on the Ferroalloy Industry in India was organized by the National Metallurgical Lab., Jamshedpur, during February 1962. Twenty-nine papers were presented and discussed in the following sessions: 1—survey of raw materials, sampling and role of research; 2—extraction and production technology; 3—scope of ferroalloy industry, by-products, standardization, etc.; 4—physicochemical reactions; 5—general aspects of ferroalloy technology. Abstracts of the papers have been published in the *NML Technical Journal*, Vol. 4, No. 1 (1962).

T. L. Rama Char,  
India Correspondent

### Ontario-Quebec Section

The final meeting for the 1961-1962 season was held on March 30, 1962 in Montreal at the Laurentien Hotel. The following were elected officers of the Section for the 1962-1963 season:

*Chairman*—R. A. Campbell, Dept. of Mines & Technical Surveys, Ottawa, Ont.

*Vice - Chairman (Program)*—A. Hone, University of Montreal, Montreal, Que.

*Vice-Chairman (Membership)*—T. R. Pezzack, Union Carbide Canada Ltd., Toronto, Ont.

*Secretary-Treasurer*—W. C. Cooper, Canadian Copper Refiners Ltd., Montreal, Que.

*Committee Members*—G. M. Mason, Aluminum Co. of Canada Ltd., Montreal, Que.; P. G. Walker, Union Carbide Canada Ltd., Montreal, Que.; A. J. Chavez, Electric Reduction Co. of Canada Ltd., Varennes, Que.;

Howard Adair, Ontario Research Foundation, Toronto, Ont.

The first paper in the technical program was presented by T. G. Edgeworth of Aluminum Co. of Canada Ltd., and was entitled "Some Developments in Aluminum Smelting." This was a review paper on recent developments in aluminum smelting, including developments reported at the recent AIME aluminum symposium. The second paper, presented by F. B. Grosselfinger of Hoechst-Uhde Corp., New York City, entitled "Mercury Cells for Chlorine Production," dealt with a number of aspects of mercury cell design and operation, including such items as denuder power recovery, anode design, and the influence of trace element poisons.

T. R. Pezzack,  
Secretary-Treasurer

### Washington-Baltimore Section

The fifth meeting of the season was held at the National Bureau of Standards at 8:00 P.M. on March 15, 1962. Nominations for officers for the 1962-1963 season were presented.

The speaker was Henry B. Linford, President of the Society, who discussed National Society affairs, in particular plans for the new journal, tentatively named *Electrochemical Technology*. His technical talk was on the subject "The Effect of Soils on the Electrodeposition Process." The effect of soiling of copper with stearic acid on the overpotential for deposition of copper from the sulfate bath was discussed. The presence of even traces of contaminant causes reduction of the double layer capacity. Sequential charging curves reveal that, as plating proceeds, the electrode contaminants eventually are covered by freshly deposited copper, and therefore, the charging curves approach those for clean surfaces. Application of a computer to solving of the equation relating overpotential to time is being studied to ease the experimental burden.

V. A. Lamb, Secretary

### New Members

In May 1962, the following were elected to membership in The Electrochemical Society by the Admissions Committee:

#### Active Members

S. S. Aconsky, Clairex Corp.; Mail add: 123 E. 37 St., New York 16, N. Y. (Electronics—Semiconductors, Electrothermics & Metallurgy)

By action of the Board of Directors of the Society, all prospective members must include first year's dues with their applications for membership.

Also, please note that, if sponsors sign the application form itself, processing can be expedited considerably.

D. J. Anderson, P. R. Mallory & Co., Inc.; Mail add: 7412 Graham Rd., Indianapolis 50, Ind. (Corrosion, Electric Insulation)

David Birtles, Sheffield Smelting Co. Ltd., Royds Mill St., Sheffield 4, England (Industrial Electrolytic)

Jean Briant, Institut Francais du Petrole, 1-4 Ave. du Bois-Preau, Rueil-Malmaison, S.&O., France (Theoretical Electrochemistry)

A. H. Bushey, Kaiser Aluminum & Chemical Corp.; Mail add: N. 1101 Argonne Rd., Spokane 69, Wash. (Industrial Electrolytic, Theoretical Electrochemistry)

A. B. Callhan, Blaw-Knox Co.; Mail add: 405 Wimer Dr., Pittsburgh 37, Pa. (Industrial Electrolytic, Theoretical Electrochemistry)

W. G. Carriero, Engelhard Industries, American Platinum Div., 231 N.J.R.R. Ave., Newark, N. J. (Electrodeposition, Theoretical Electrochemistry)

Y. F. Chang, Purdue University, Electrical Engineering School; Mail add: 1989 Indian Trail Dr., West Lafayette, Ind. (Electronics—Semiconductors)

R. S. Cooper, Victor Chemical Works, Div. of Stauffer Chemical Co., 11th & Arnold Sts., Chicago Heights, Ill. (Industrial Electrolytic, Theoretical Electrochemistry)

J. H. Eddleston, Westinghouse Electric Corp.; Mail add: 372 Avocado Place, Camarillo, Calif. (Electronics)

A. F. Forziati, Diamond Ordnance Fuze Lab.; Mail add: 9812 Dameron Dr., Silver Spring, Md. (Battery, Electronics—Luminescence)

D. E. Greetham, Northern Electric Co.; Mail add: 128 Mgr. Tache, Boucherville, Que., Canada (Electronics—Semiconductors)

E. A. Grens, II, University of California, Dept. of Chemical Engineering; Mail add: 2735 Regent St. Berkeley 5, Calif. (Battery, Electrodeposition, Industrial Electrolytic, Theoretical Electrochemistry)

A. P. Hardt, Lockheed Aircraft Corp., Missiles & Space Div.; Mail add: 1140 Winsor Ave., Piedmont 10, Calif. (Electro-Organic)

Max Harris, Electrolytic Metal Corp. (Pty.) Ltd., Box 6880, Johannesburg, South Africa (Electrodeposition, Electrothermics & Metallurgy, Industrial Electrolytic, Theoretical Electrochemistry)

S. W. Ing, Jr., General Electric Co.; Mail add: 4 Centennial Dr., Syracuse, N. Y. (Electrodeposition, Electronics—Luminescence and Semiconductors, Electrothermics & Metallurgy, Theoretical Electrochemistry)

T. A. Johnson, A.I.A.G. Metals, Inc., 9 Rockefeller Plaza, New York 20, N. Y. (Electronics—Semiconductors)

C. M. Kellett, Jr., Westinghouse Electric Corp.; Mail add: 578 Shuey Ave., Greensburg, Pa. (Electronics—Semiconductors)

G. M. Kent, Rosemead Plating Co., Inc., 4204 Temple City Blvd., Rosemead, Calif. (Electrodeposition)

K. E. Lemons, Fairchild Semiconductor Corp., 844 Charleston Rd., Palo Alto, Calif. (Electronics, Theoretical Electrochemistry)

A. L. McCloskey, U. S. Borax & Chemical Co., 50 Rockefeller Plaza, New York 20, N. Y. (Corrosion)

E. J. McHenry, Bell Telephone Labs., Inc.; Mail add: 28 Gales Dr., New Providence, N. J. (Battery)

G. P. Mortensen, Westinghouse Electric Corp., Lamp Div.; Mail add: 26 Washington Court, Livingston, N. J. (Electronics)

J. H. Nichols, Monsanto Chemical Co., 800 N. Lindbergh, St. Louis 66, Mo. (Industrial Electrolytic)

B. J. Nicholson, Philco Scientific Lab.; Mail add: Crescent Rd., Wyncote, Pa. (Electric Insulation)

Ken Nobe, University of California, Dept. of Engineering, Los Angeles 24, Calif. (Corrosion, Electronics—Semiconductors, Electrothermics & Metallurgy, Theoretical Electrochemistry)

J. E. O'Brien, Transitron Electronic Corp.; Mail add: 25 Muriel Ave., Wakefield, Mass. (Electronics—Semiconductors)

Guglielmo Pellegrini, Co. Accumulatori Uranio-C., S. Milano 88, Verona, Italy (Battery, Electrothermics & Metallurgy, Industrial Electrolytic, Theoretical Electrochemistry)

R. A. Ritchie, Electric Reduction Co. of Canada Ltd.; Mail add: 29 Pheasant Lane, Islington, Ont., Canada (Electrothermics & Metallurgy, Industrial Electrolytic)

R. S. Robertson, Nalco Chemical Co., 6216 W. 66 Place, Chicago 38, Ill. (Corrosion, Theoretical Electrochemistry)

### ECS Membership Statistics

The following three tables give breakdown of membership as of Apr. 1, 1962. The Secretary's Office feels that a regular accounting of membership will be very stimulating to membership committee activities. In Table I it should be noted that the totals appearing in the right-

hand column are *not* the sums of the figures in that line since members belong to more than one Division and, also, because Sustaining Members are not assigned to Divisions. But the totals listed are the total membership in each Section. In Table I, Sustaining Members have been credited to the various Sections.

Table I. ECS Membership by Sections and Divisions

Section	Division										No Division	Total as of 1/1/62	Total as of 4/1/62	Net Change
	Battery	Corrosion	Electric Insulation	Electrodeposition	Electronics	Electro-Organic	Electrothermics & Met.	Industrial Electrolytic	Theoretical Electrochem.					
Boston	20	40	15	37	89	6	28	9	36	5	197	195	- 2	
Chicago	28	34	12	40	36	18	17	16	43	6	163	162	- 1	
Cleveland	51	27	1	38	40	6	27	22	31	6	191	171	- 20	
Columbus, Ohio	4	14	2	20	17	2	27	5	9	2	67	60	- 7	
Detroit	31	23	4	50	23	8	11	9	37	6	121	116	- 5	
India	1	5	—	11	5	3	3	4	5	2	37	20	- 17	
Indianapolis	32	10	12	13	27	7	12	7	16	3	81	78	- 3	
Midland	10	16	2	5	7	3	10	17	10	—	47	50	+ 3	
Mohawk-Hudson	18	27	19	10	23	3	14	4	27	4	89	88	- 1	
New York	130	102	34	175	194	38	112	73	132	33	669	647	- 22	
Niagara Falls	12	18	2	26	29	6	59	56	10	8	168	154	- 14	
Ontario-Pacific	5	16	2	10	7	1	30	24	10	4	87	77	- 10	
Northwest	5	9	—	10	5	—	7	7	14	3	37	37	0	
Philadelphia	41	22	7	39	78	7	23	22	47	16	221	209	- 12	
Pittsburgh	6	46	7	30	51	5	33	19	37	1	144	142	- 2	
San Francisco	19	13	1	28	42	5	14	19	27	2	111	107	- 4	
S. Calif.-Nevada	29	26	5	43	77	11	32	20	50	6	173	171	- 2	
Texas	8	26	2	10	60	6	10	23	30	1	124	121	- 3	
Washington-Baltimore	41	35	8	35	30	3	14	6	26	3	145	144	- 1	
U. S. Non-Section	60	64	10	76	72	32	57	46	85	26	357	337	- 20	
Foreign Non-Section	68	69	17	74	45	33	52	66	92	79	319	313	- 6	
Total as of Jan. 1, 1962	632	671	168	811	988	213	626	502	804	233	3548			
Total as of April 1, 1962	619	642	162	780	957	203	592	474	774	216	3399			
Net Change	-33	-29	-6	-31	-31	-10	-34	-18	-30	-17			-149	

Table II. ECS Membership by Grade

	Total as of 1/1/62	Total as of 4/1/62	Net Change
Active	2983	2733	- 250
Faraday (Active)	37	33	- 4
Deutsche Bunsen Gesellschaft (Active)	21	20	- 1
Delinquent	174	303	+129
Active Representative Patron Members	10	10	0
Active Representative Sustaining Members	105	103	- 2
Total Active Members	3307	3179	-128
Life	16	16	0
Emeritus	93	93	0
Associate	56	54	- 2
Student	46	27	- 19
Honorary	7	7	0
Total	3548	3399	-149

The figures pertaining to Patron and Sustaining Member Representatives, and Faraday and Deutsche Bunsen Gesellschaft members subscribing to the JOURNAL, have been added to reflect reclassifications and changes in membership status.

Table III. ECS Patron and Sustaining Membership

	Total as of 1/1/62	Total as of 4/1/62	Net Change
Patron Member Companies	5	5	0
Sustaining Member Companies	149	147	- 2

- S. R. Shortes, Texas Instruments, Inc.; Mail add: 4605 San Marcus, Mesquite, Texas (Electronics—Semiconductors)
- Melvin Turetzky, Kearfott Div., 1500 Main Ave., Clifton, N. J. (Electronics—Semiconductors)

#### Associate Members

- E. K. Andersen, III, Sprague Electric Co., 87 Marshall St., North Adams, Mass. (Corrosion)
- P. L. Brown, Depauw University; Mail add: 800 S. Locust St., Greencastle, Ind. (Electrodeposition)
- G. J. DiMasi, U.S.A. Signal Research & Development Lab.; Mail add: P. O. Box 126, Eatontown, N. J. (Battery, Theoretical Electrochemistry)
- P. J. Dugdale, Universidad de Concepcion; Mail add: Valentin Letelier 384, Concepcion, Chile (Corrosion, Electro-Organic)
- M. L. Krzeminski, Simoniz Co.; Mail add: 11108 S. Talman, Chicago 55, Ill. (Corrosion)
- L. D. Maxim, Rm. 311, Baker Labs., College of Forestry, State University of New York, Syracuse 10, N. Y. (Electric Insulation)
- B. S. Richman, Betz Labs. Inc., Gillingham & Worth Sts., Philadelphia 24, Pa. (Corrosion)
- Maija Sklar, Raytheon Co., P. O. Box 280, Mountain View, Calif. (Corrosion, Electronics—Semiconductors)
- Martin Sulkes, U.S. Electric Mfg. Co.; Mail add: 277 E. 7 St., Brooklyn 18, N. Y. (Battery)
- R. V. Velden, Globe Union, Inc.; Mail add: 4909 N. 39 St., Milwaukee 9, Wis. (Battery)
- J. J. Werbicki, Jr., Texas Instruments, Inc.; Mail add: 28 Alma St., Providence 8, R. I. (Electrothermics & Metallurgy)

#### Student Associate Member

- J. W. Barrett, Baylor University, Chemistry Dept.; Mail add: 2724 Proctor Ave., Waco, Texas (Electrodeposition, Theoretical Electrochemistry)

#### Reinstatement to Active Membership

- T. R. P. Gibb, Jr., Tufts University, Dept. of Chemistry; Mail add: 27 Sargent Rd., Winchester, Mass. (Electrothermics & Metallurgy)

#### Transfer to Active Membership

- D. H. McClelland, Astropower Inc.; Mail add: 2621 Harbor Blvd., Costa Mesa, Calif. (Corrosion, Electrodeposition, Theoretical Electrochemistry)

#### Deceased

- B. F. Freeberg, Lombard, Ill.  
Lloyd McKinley, Wichita, Kan.

## Personals

**Harry C. Gatos**, a Lincoln Lab. scientist, has been appointed professor, jointly in the Dept. of Metallurgy and the Dept. of Electrical Engineering, at the Massachusetts Institute of Technology, Cambridge, effective July 1. Dr. Gatos' special interests are chemical and solid state metallurgy and his extensive publications include research on the surface behavior of materials and the structure of semiconductors. Dr. Gatos joined Lincoln Lab. in 1955 and, in 1957, was appointed the first leader of the Chemistry and Metallurgy Group in the solid state program. In 1959, he was appointed associate head of the Solid State Div.

He has published about 60 technical papers, and has edited "Properties of Elemental and Compound Semiconductors" for the American Institute of Mining, Metallurgical, and Petroleum Engineers, and "The Surface Chemistry of Metals and Semiconductors" for The Electrochemical Society, both published in 1960. Currently, he is Corrosion—Semiconductors Editor for the ECS JOURNAL.

**David A. Lupfer** has joined the technical staff of Nytronics, Inc., Berkeley Heights, N. J., as director of research. Mr. Lupfer, who has worked in the field of electronic component development for the past 14 years, formerly was manager of the Materials and Ceramics Div. of Gulton Industries, Inc., Metuchen, N. J., a position which he held for approximately three years.

**Maynard L. Parker**, works manager of the Niagara plant of Hooker Chemical Corp.'s Eastern Chemical Div. for the past three years, has been promoted to production manager of the Niagara plant.

**J. Sundararajan** has been awarded the Ph.D. degree of the Indian Institute of Science, Bangalore, for his thesis on "Inhibition of the Corrosion of Aluminium."

**M. S. Thacker**, of New Delhi, India, spent August-October 1961 on a tour of Europe and the U.S.S.R. Under a special invitation, he attended the UN Conference on "New Sources of Energy" which was held in Rome in August. The visit to Moscow was at the invitation of the Academy of Sciences, U.S.S.R. He also has been invited to preside over

## Manuscripts and Abstracts for Spring 1963 Meeting

Papers are now being solicited for the Spring Meeting of the Society, to be held at the Penn Sheraton Hotel in Pittsburgh, Pa., April 14, 15, 16, 17, and 18, 1963. Technical sessions probably will be scheduled on: Electric Insulation, Electronics (including Luminescence and Semiconductors), Electrothermics and Metallurgy, Industrial Electrolytics, and Theoretical Electrochemistry.

To be considered for this meeting, triplicate copies of abstracts (*not exceeding 75 words in length*) must be received at Society Headquarters, 30 East 42 St., New York 17, N. Y., *not later than December 14, 1962. Please indicate on abstract for which Division's symposium the paper is to be scheduled, and underline the name of the author who will present the paper.* No paper will be placed on the program unless one of the authors, or a qualified person designated by the authors, has agreed to present it in person. An author who wishes his paper considered for publication in the JOURNAL should send triplicate copies of the manuscript to the Managing Editor of the JOURNAL, 30 East 42 St., New York 17, N. Y.

Presentation of a paper at a technical meeting of the Society does not guarantee publication in the JOURNAL. However, all papers so presented become the property of The Electrochemical Society, and may not be published elsewhere, either in whole or in part, unless permission for release is requested of and granted by the Editor. Papers already published elsewhere, or submitted for publication elsewhere, are not acceptable for oral presentation except on invitation by a Divisional program Chairman.

the UN Conference on "Application of Science and Technology for the Benefit of the Less-Developed Areas of the World" to be held in Geneva in 1963.

**Fritz Tödt**, who celebrated his 65th birthday on January 1, 1962, has resigned from his position in the Bundesanstalt für Materialprüfung, Berlin-Dahlem, where he was in charge of the section Special Methods of Electrochemistry. Studying in the laboratories of Max Volmer and Lise Meitner, later heading a department of the Kaiser-Wilhelm-Institut of Physical Chemistry, Dr. Tödt always has been especially interested in electrochemistry. He was one of the first to investigate the influence of oxygen on the corrosion rate of metals, and on the formation of oxide layers. During this work, he developed electroanalytical methods belonging to the most sensitive methods available today. He especially has promoted the development of oxygen trace analysis. Dr. Tödt has become widely known as

the editor of the book "Korrosion und Korrosionsschutz."

It is less known that in recent years he has become engaged in work on biological and medical problems, mainly in connection with the respiration of cells. By application of his method of oxygen trace analysis, he has been able to arrive at results which so far have not been accessible with other methods.

Dr. Tödt is now lecturer at the Institut für Zuckerindustrie of the Berlin Technische Universität. Also, he still has working facilities in the Bundesanstalt für Materialprüfung.

**K. I. Vasu**, of India, has left for London to join the Dept. of Metallurgy, Imperial College of Science and Technology, for advanced studies under the Commonwealth Bursary Scheme.

**S. Venkatachalam** has been appointed junior research assistant in the Dept. of Inorganic and Physical Chemistry, Indian Institute of Science, Bangalore.

processes are derived or given for many cases. A repetition of similar equations in different parts of the book appears unavoidable. The book is recommended to all persons interested in electrochemical studies, whether from the theoretical or practical point of view. It should be included in the libraries of all laboratories where research is done in this field.

Manfred W. Breiter  
General Electric Research Lab.

---

## News Items

---

### J. E. Draley Receives NACE Whitney Award

Joseph E. Draley of the Argonne National Lab., Lemont, Ill., has been presented with the NACE's Willis Rodney Whitney Award in recognition of outstanding public contributions to corrosion science. The award was made during the 1962 NACE Annual Conference in Kansas City, Mo., during March.

Dr. Draley has been engaged in corrosion research since 1942 when he joined the staff of the Metallurgical Lab. of the University of Chicago. More recently he has been affiliated with the Kellogg Corp., Oak Ridge National Lab., and Argonne National Lab., working on atomic energy projects. His work largely has been concerned with corrosion mechanisms of aluminum, uranium, and zirconium and their alloys in pure water and dilute solutions.

A Past Chairman of the Corrosion Division of The Electrochemical Society, Dr. Draley also has served as Corrosion Division Editor of the Society's JOURNAL. He has been Chairman of the Gordon Research Conference on Corrosion and a member of the committee for fundamental work on corrosion of the Corrosion Research Council. He was instrumental in arranging annual symposia on corrosion under the auspices of the Atomic Energy Committee, and initiated an international meeting on aqueous corrosion of reactor materials in Brussels in 1959 under the joint sponsorship of EURATOM and the U. S. Atomic Energy Commission.

At present, he is a member of the Corrosion Resistant Metals Committee of the Institute of Metals Division of the Metallurgical Society of the American Institute of Mining and Metallurgical Engineers, and of a special subcommittee on light metals for nuclear applications of the American Society for Testing and materials.

---

## Book Review

---

**Elektrochemische Kinetik**, by Klaus J. Vetter. Published by Springer-Verlag, Berlin-Göttingen-Heidelberg, Germany, 1961. 698 + XV pages; DM. 160 (about \$40.00).

Vetter's book on electrochemical kinetics, written in German, is the most comprehensive modern textbook on electrode phenomena which is available on the market. The basic concepts for an understanding of electrochemical processes are presented clearly. The abundant literature is taken into consideration until 1955, partly up to 1960. Its appearance fills a gap which has become large by the progress made in this field during the last three decades.

The first part of the book deals with electrochemical thermodynamics (which includes the application of the conventional thermodynamics to electrode reactions), the theory of liquid-junction potentials and membrane potentials, and the theory of the double layer. The different types of overvoltage (caused by discharge steps, by mass transport, and by chemical reactions) and the separation of the net overvoltage into the single parts are discussed in the second part. Methods for the determination of the reaction mechanism are treated in the third part. Experimental results on redox

reactions, the hydrogen electrode, the oxygen electrode, metal deposition, and dissolution in the absence or presence of films, corrosion, and passivity of metals are interpreted extensively in the fourth part which consists of about 300 pages. The reader will find in this part that Vetter added new results obtained in his laboratory, or new interpretations to measurements of other electrochemists. An author index and a subject index at the end increase the value of the book.

The text is well written. A large amount of information with considerable illustrative quantitative data is compiled in a condensed form. Mathematical equations for the functional dependence of the fundamental parameters in electrode

**Notice to Members and Subscribers**  
**(Re Changes of Address)**

To insure receipt of each issue of the JOURNAL, please be sure to give us your old address, as well as your new one, when you move. Our records are filed by states and cities, not by individual names. The Post Office does not forward magazines.

We should have this information by the 16th of the month to avoid delays in receipt of the next issue.

Dr. Draley is the author of numerous publications and frequently has been a speaker on corrosion subjects for The Electrochemical Society, NACE, and other technical organizations.

### Electrochemistry at University of Pennsylvania

The Electrochemistry Group, under the direction of Professor John O'M. Bockris, at the University of Pennsylvania, Philadelphia, has been recognized by the university as a separate entity within the Dept. of Chemistry and has been redesignated the Electrochemistry Laboratory of the University of Pennsylvania. The Laboratory now consists of 25 co-workers, including Dr. Mino Green (associate director) and Dr. M. A. V. Devanathan (assistant director), together with eight post doctoral associates, four research associates, and thirteen graduate students. The staff includes scholars from all parts of the world.

The Electrochemistry Laboratory is concerned largely with studies of the fundamental mechanisms of electrode processes, together with investigations on the structure of ionic melts. It is becoming increasingly active in fundamental research connected with fuel cells. It is intended that the Laboratory will continue to undergo significant further expansion.

The Laboratory also is concerned with the teaching of electrochemistry, with special reference to the shortage of trained scientists in this field in the United States. Graduate students major in physical chemistry in the Dept. of Chemistry but fulfill special requirements, which insure that their knowledge of physical chemistry includes suitable amounts of fundamental electrochemistry.

### AIEE-IRE Boards Approve Merger Principles

The Boards of Directors of the Institute of Radio Engineers and the American Institute of Electrical En-

gineers, in separate meetings held in New York City during March, approved in general the broad principles of the proposed consolidation of the two engineering societies. It was proposed that the consolidated society might be known as the Institute of Electrical and Electronics Engineers—an international body with a membership of some 150,000. If the memberships approve the consolidation by a mail vote this summer, it is contemplated that the new society will be operating by January 1, 1963.

At present, the IRE's membership is 97,000 and the AIEE's is 70,000 (both figures include students). Combined assets of the two societies total approximately \$6,500,000.

The IRE was established in 1912 and the AIEE in 1884. For many years, the activities of the two organizations have overlapped, especially at the student level where joint Student Branches are common in many engineering colleges.

### Thermoelectric Material in Magnetic Field Shows High Figure of Merit

Placing a thermoelectric material in a magnetic field greatly improves its properties, Bell Telephone Laboratories announced in March. In a paper presented at a meeting of the American Physical Society in Baltimore, Bell scientists Raymond Wolfe and George E. Smith reported achieving a "figure of merit" of  $8.6 \times 10^{-3}$  per degree Kelvin in an alloy of the semimetals bismuth and antimony at 100°K in a field of 1000 gauss. This is the highest figure of merit ever measured at any temperature.

The improvement was attained by applying a magnetic field perpendicular to the flow of current in a single-crystal specimen. In an alloy of 88% bismuth and 12% antimony, the figure of merit, or "Z," at room temperature was raised from 1.2 to  $2.9 \times 10^{-3}$  per degree K by applying

a magnetic field of 17,000 gauss. This is comparable with the best commercially available materials. However, at 100°K, a field of only 1000 gauss is required for the record Z in Bi-Sb, a field readily available with a small horseshoe magnet.

This increased figure of merit implies the possibility of designing equipment for refrigeration to operate at lower temperatures than previously has been possible by electronic means. A two-stage device with a single n-type bar of the bismuth-antimony alloy in the second stage operated in a magnetic field of 12,000 gauss to a record low of 105°C below room temperature. Greater improvements can be expected when the device operates from a low-temperature environment.

This improved material should find immediate application in low-temperature electronic refrigeration. The demonstrated principle may also be applied to other thermoelectric materials.

### New Method for Preparing Ultrapure CdSe

A convenient new laboratory method for preparing ultrapure cadmium selenide and related compounds has been developed by scientists of International Business Machines Corp.'s Thomas J. Watson Research Center.

The new process permits a low-temperature synthesis of CdSe directly from the elements for the first time. Earlier attempts at direct synthesis required high temperatures and frequently produced explosive reactions. In the new method, very fine powders of Cd and Se are heated slowly to a temperature of 450°C in a high vacuum. The successful method is a result of the discovery that the powders must be composed of particles smaller than a certain critical size, and that the heating rate must be not greater than 0.5°C per minute. Under these

## Brief Communications

The JOURNAL accepts short technical reports having unusual importance or timely interest, where speed of publication is a consideration. The communication may summarize results of important research justifying announcement before such time as a more detailed manuscript can be published. Consideration also will be given to reports of significant unfinished research which the author cannot pursue further, but the results of which are of potential use to others. Comments on papers already published in the JOURNAL should be reserved for the Discussion Section published biannually.

Submit communications in triplicate, typewritten double-spaced, to the Editor, Journal of The Electrochemical Society, 30 East 42 St., New York 17, N. Y.

conditions, the elements react completely to form CdSe. A similar process has been found to be applicable to a number of other compounds, including CdS, CdTe, ZnS, ZnSe, and ZnTe.

The new preparation technique, along with results of a variety of other chemical studies of CdSe, were reported by IBM scientists Arnold Reisman and Melvin Berkenblit at an American Chemical Society symposium in Washington during March.

An additional discovery made by Dr. Reisman and Mr. Berkenblit is also of practical interest. Early in the course of their experiments, they noticed that silica containers in which reactions of CdSe were studied became severely corroded unless the pressure in the container was less than about  $10^{-4}$  mm Hg. Further work showed that the corrosion was due to the presence of CdO. This result suggested a good method for obtaining adhesion between a sintered layer of CdSe and a silica or silica-based substrate in photoconductive devices. A few tests showed that a small amount of oxygen introduced into the atmosphere during sintering of CdSe layers on glass substrates produced good bonding by means of CdO corrosion of the glass.

#### Electron Beam Technique Produces Superconductive Wire

Electron Heating Corp. has announced a new method for producing superconductive wire. The EHC system employs a zone melting technique, utilizing a self-accelerated, remotely located electron beam gun. The material to be melted is held in a horizontal-type, water-cooled mold and either the gun or the mold is traversed at a controlled rate along the axis of the ingot.

Electron Heating Corp. has used this technique to produce homogeneous, ductile ingots of niobium and zirconium alloys which, when drawn to very fine wire with conventional cold working equipment, exhibit superior electrical and magnetic properties. Compared to other methods, the new technique produces wire that can withstand higher mag-

netic flux densities before losing its superconducting properties.

The process permits severe plastic deformation without excessive embrittlement. Microstructures of these alloys show an extremely fine, uniform dispersion of impurities centering around dislocations. There is strong reason to believe that the superior electrical and magnetic properties arise from this unique impurity dispersion and from the extreme cooling rates.

For details write to H. S. Berman, Electron Heating Corp., 82 Hicks Ave., Medford 55, Mass.

#### Philco Environmental Test Center Available to Industry

Philco Corp's giant \$1,000,000 Environmental Test Center, Philadelphia, has been made available to any industry or government agency needing to test equipment in simulated environments ranging from deep under the sea to far out in space.

The 30,000-square-foot Test Center is capable of simulating environments of temperature (from extreme cold to extreme heat), altitude, humidity, outer space vacuum, salt spray, immersion, rain, vibration, and shock for equipments, components, and packages.

Test Center customers have available Philco test and laboratory facilities necessary for a comprehensive product or component analysis. The Center's customers include some of the nation's largest manufacturing firms as well as various government agencies.

#### AP&CC Takes Over Navy's Ammonium Perchlorate Plant

American Potash & Chemical Corp. recently took possession of the nation's largest ammonium perchlorate plant when transfer of title to the Henderson, Nev., facility was effected by the General Services Administration in San Francisco, it has been announced by Peter Colefax, chairman and president of the company. The plant was built by the company for the Navy and the company has operated it since its completion in 1953.

The facility is located adjacent to the company's Henderson plant and becomes an integral part of it. Sodium chlorate, sodium perchlorate, potassium perchlorate, potassium chlorate, and manganese dioxide are produced at Henderson in addition to ammonium perchlorate.

#### Merger of Hooker and Parker Rust Proof Approved

Shareholders of Hooker Chemical Corp. at New York City, and of Parker Rust Proof Co. at Detroit, Mich., have voted overwhelmingly in separate meetings to consolidate Parker Rust Proof Co. with and into Hooker Chemical Corp. The stockholders' action became official when documents of consolidation were filed on March 30, 1962, in New York State, and in the State of Michigan where Parker was incorporated in 1929.

R. W. Englehart, who has been chairman of the board and president of Parker, will become a vice-president and director of the consolidated corporation.

#### Monsanto to Build Chlorine/Caustic Plant Addition

Monsanto Chemical Co. has begun construction of a major addition to its William G. Krummrich Plant at Monsanto, Ill., which will provide new manufacturing capacity for 100 tons per day of chlorine and 110 tons per day of caustic soda, both for captive use within the plant.

The new unit is scheduled to be in operation early in 1963. It will supplement existing production of chlorine and caustic soda there to bring the plant's total capacities for these products up to 230 and 250 tons per day, respectively. Monsanto also operates a major unit for chlorine and caustic soda production at its Anniston, Ala., plant.

#### Eastman Kodak Aid-to-Education Program

Research grants totaling nearly \$250,000 will go this year to 22 college and university graduate departments under a newly announced phase of Eastman Kodak Co.'s aid-to-education program. The new

## December 1962 Discussion Section

A Discussion Section, covering papers published in the January-June 1962 JOURNALS, is scheduled for publication in the December 1962 issue. Any discussion which did not reach the Editor in time for inclusion in the June 1962 Discussion Section will be included in the December 1962 issue.

Those who plan to contribute remarks for this Discussion Section should submit their comments or questions in triplicate to the Managing Editor of the JOURNAL, 30 East 42 St., New York 17, N. Y. *not later than September 3, 1962.* All discussion will be forwarded to the author(s) for reply before being printed in the JOURNAL.





## RESEARCH ELECTROCHEMIST

Challenging opportunity in expanding research laboratory investigating electroplating and metal finishing.

Require aggressive scientist, having M.S. or B.S. degree and 2 to 4 years' experience, to conduct applied research projects with minimum of supervision. Applicant should have sound background in inorganic and physical chemistry and a real interest in research. Modern research facilities located near Finger Lakes and Adirondack recreational areas of New York State. Liberal employee benefits.

Please send detailed resumé including salary requirements to:

**Personnel Supervisor—Technical  
SOLVAY PROCESS DIVISION  
Allied Chemical Corporation  
Syracuse 1, New York**

grants, ranging from \$6000 to \$12,500, will go annually to a selected number of graduate departments. The major portion of the funds awarded will be for unrestricted use in research programs and new or improved facilities.

Each \$12,500 grant provides for a \$1000 award recognizing the achievements of an outstanding doctoral student. The awards will be made for excellence in graduate studies and research or in teaching. While the grants do not specifically provide for graduate fellowships, a portion of the funds awarded may be used for that purpose if so desired by the recipient institution.

### Symposium on Chemistry and Physics of Nonmetallic Solids

Current problems in the chemistry and physics of nonmetallic solids will be the theme of the symposium to be held by the Physical Chemistry Division of The Chemical Institute of Canada, at Laval University, Quebec City, on September 6 and 7, 1962.

The object of the symposium is to bring together physical chemists, physicists, and other interested parties to discuss some of the current theoretical and experimental problems involving insulating solids.

Specific topics to be considered are intermolecular forces, chemical bonding, lattice vibrations, and phase transitions.

The program will feature about 12 principal contributions which will be meant to inform and to initiate discussion. Approximately half of the symposium will be given over to discussion.

Accommodation will be available in the new residence buildings at Laval University.

Anyone interested in contributing a short report for presentation during the discussion period is invited to get in touch with either of the two conveners: Professor P. A. Giguère, Dept. of Chemistry, Laval University, Quebec City, or Dr. J. A. Morrison, Div. of Pure Chemistry, National Research Council, Ottawa.

### Seventh Annual Appalachian Underground Corrosion Short Course

The Seventh Annual Appalachian Underground Corrosion Short Course will be held June 12, 13, and 14 at West Virginia University, Morgantown, W. Va. New speakers, new classes, and new topics have been added for 1962, making a total of 64 classes in all. In addition, there

will be exhibits and field demonstrations of equipment and materials.

### Midwest Quality Control Conference

The 17th Midwest Quality Control Conference will be held at the Denver Hilton Hotel on October 26 and 27, 1962. For further information, write to American Society for Quality Control, P. O. Box 396, Denver, Colo.

### Announcements from Publishers

"Gmelins Handbuch der Anorganischen Chemie," published by Verlag Chemie, GmbH., Weinheim/Bergstrasse, Germany. Supplemental volumes, published 1961: "System 28, Calcium, Part B, Section 3," 1568 pages, clothbound; \$142.00. "System 58, Cobalt, Part A," 886 pages, clothbound; \$139.00. "System 60, Copper, Part B, Section 2," 352 pages, clothbound; \$58.00.

In these three supplementary volumes, published in 1961, the literature is covered from 1932 through 1949 with critical evaluation of the material. For areas in which there has been a rapid growth of interest since 1950, the literature has been partially surveyed up to 1961, without critical evaluation beyond 1949. When new headings have been initiated, the literature survey extends back to work done before 1931.

The volume on Calcium concludes the listing of calcium compounds, from Ca-S-O systems to Na-K-Ca-Mg-S-O hydrates, and includes a section on reactions of calcium ion and a section on the detection and estimation of calcium, strontium, and barium.

The volume on Cobalt covers the history, occurrence, and technology of cobalt and cobalt compounds, the physical, chemical, and electrochemical properties of cobalt, and the properties of alloys and compounds. Much attention is given to the compounds of cobalt and carbon, with 23 pages devoted to the various carbonyls. Electrochemists will be most interested in the sections on electrolytic deposition, electrowinning, and electrochemical behavior. The latter section includes 50 pages on topics such as ionic mobility, potentials vs. various solutions, behavior at the dropping electrode, overvoltage of oxygen and of hydrogen, and anodic and cathodic behavior.

The volume on Copper includes copper compounds from copper-

boron to copper-bismuth, including the compounds with silicon, carbon, phosphorus, arsenic, and antimony. The section on carbon compounds, including salts of carboxylic acids, cyanides, and thiocyanates, covers 252 pages.

All three volumes have German-English tables of contents, English headings, and English subheadings on the paragraphs. One can locate material almost without a reading knowledge of German.

"Dictionary of Chemistry," by L. Mackenzie Miall. Published by John Wiley & Sons, Inc., 440 Park Ave. South, New York 16, N. Y., 1961. vii + 593 pages; \$13.75.

This actually is a little encyclopedia, rather than a dictionary. The contents fall into three main categories. There are definitions and illustrations of many terms, such as membrane equilibrium, cytochrome, polyester, and so fourth. There are brief descriptions of many chemicals and chemical processes such as beryllium acetate, Cannizzaro reaction, cyclobutane neocinchenone, parting (of gold from silver), etc. There also are one-paragraph accounts of the lives of some chemists and contributors to chemistry.

The descriptions of chemicals include physical and chemical properties. For example, under the heading "Carbanilide" following the empirical and structural formulas, the description continues—"Silky needles, m.p. 235°, b.p. 260°. Slightly soluble in water, readily in alcohol and ether. Prepared by the action of phosgene upon aniline."

The book is more useful for workers in biology, medicine, and perhaps physics than for practicing chemists.

## Literature from Industry

**Electrochemical Machining.** Hanson-Van Winkle-Munning Co. has set up a demonstration laboratory in Matawan where sample parts sent in by interested metal producers and fabricators can be processed by Electrochemical Machining, which is capable of machining virtually all conductive metals; however, because of differences in the basic microstructure of various metals, it is necessary to test each individual application to determine

production rates, dimensional tolerance capabilities, and surface finishes possible. A four-page bulletin has been made available to all metal producers and fabricators to answer some of the basic questions, such as: How the Electrochemical Machining Process works . . . machinable metals . . . advantages of the ECM Process over conventional techniques.

For complete information, write to Hanson-Van Winkle-Munning Co., Electrochemical Machining Div., Matawan, N. J.

## Advertiser's Index

AIAG Metals, Inc. ....	156C
Great Lakes Carbon Corp., Electrode Div. ....	Cover 2
E. H. Sargent & Co. ....	146C
Solvay Process Div., Allied Chemical Corp. ....	155C
Stackpole Carbon Co. ....	145C
Yardney Electric Corp. ....	156C

# CHEMISTS and CHEMICAL ENGINEERS

Challenging positions with leading manufacturer of electro-chemical high-energy systems.

### RECENT GRADUATES:

BS in chem. or chem. engineering, with emphasis on physical chem. 0-3 years experience.

### ELECTRO-CHEMIST:

Ph.D. or equivalent experience in related fields.

.. EXCELLENT GROWTH OPPORTUNITIES.

.. LIBERAL COMPANY BENEFITS.

Send resume and salary requirements,

DIRECTOR OF PROFESSIONAL EMPLOYMENT

# YARDNEY ELECTRIC CORP.

40-52 Leonard St.,  
New York 13, N. Y.

An equal opportunity employer.



# AIAG METALS, INC.

SUBSIDIARY OF CONSOLIDATED ALUMINUM CORP.

## HIGHEST PURITY

GALLIUM

GALLIUM  
OXIDE

GALLIUM  
COMPOUNDS

ALUMINUM

SINTERED  
ALUMINUM  
POWDER

ALUMINA  
(ALUMINUM  
OXIDE)

Prompt deliveries from stock in New York City

AIAG Metals Inc.  
9 Rockefeller Plaza  
New York 20, N.Y.

Dept.

Please send information on \_\_\_\_\_

End use intended \_\_\_\_\_

Name \_\_\_\_\_ Company \_\_\_\_\_

Address \_\_\_\_\_

City \_\_\_\_\_ State \_\_\_\_\_

# The Electrochemical Society

## Patron Members

Aluminum Co. of Canada, Ltd.,  
Montreal, Que., Canada  
International Nickel Co., Inc.,  
New York, N. Y.  
Olin Mathieson Chemical Corp.,  
Chemicals Div., Industrial Chemicals  
Development Dept., Niagara Falls, N. Y.  
Union Carbide Corp.  
Divisions:  
National Carbon Co., New York, N. Y.  
Union Carbide Consumer Products Co.,  
New York, N. Y.  
Union Carbide Metals Co.,  
New York, N. Y.  
Westinghouse Electric Corp., Pittsburgh, Pa.

## Sustaining Members

Air Reduction Co., Inc., New York, N. Y.  
Ajax Electro Metallurgical Corp.,  
Philadelphia, Pa.  
Allen-Bradley Co., Milwaukee, Wis.  
Allied Chemical Corp.  
Solvay Process Div., Syracuse, N. Y.  
General Chemical Div., Morristown, N. J.  
Alloy Steel Products Co., Inc., Linden, N. J.  
Aluminum Co. of America,  
New Kensington, Pa.  
American Metal Climax, Inc.,  
New York, N. Y.  
American Potash & Chemical Corp.,  
Los Angeles, Calif. (2 memberships)  
American Smelting and Refining Co.,  
South Plainfield, N. J.  
American Zinc Co. of Illinois,  
East St. Louis, Ill.  
American Zinc, Lead & Smelting Co.,  
St. Louis, Mo. (2 memberships)  
American Zinc Oxide Co., Columbus, Ohio  
M. Ames Chemical Works, Inc.,  
Glens Falls, N. Y.  
Armco Steel Corp., Middletown, Ohio  
Basic Inc., Maple Grove, Ohio  
Bell Telephone Laboratories, Inc.,  
New York, N. Y. (2 memberships)  
Bethlehem Steel Co., Bethlehem, Pa.  
(2 memberships)  
Boeing Airplane Co., Seattle, Wash.  
Burgess Battery Co., Freeport, Ill.  
(4 memberships)  
Canadian Industries Ltd., Montreal,  
Que., Canada  
Carborundum Co., Niagara Falls, N. Y.  
Catalyst Research Corp., Baltimore, Md.

Consolidated Mining & Smelting Co. of  
Canada, Ltd., Trail, B. C., Canada  
(2 memberships)  
Continental Can Co., Inc., Chicago, Ill.  
Cooper Metallurgical Associates, Cleveland,  
Ohio  
Corning Glass Works, Corning, N. Y.  
Diamond Alkali Co., Painesville, Ohio  
Dow Chemical Co., Midland, Mich.  
Wilbur B. Driver Co., Newark, N. J.  
(2 memberships)  
E. I. du Pont de Nemours & Co., Inc.,  
Wilmington, Del.  
Eagle-Picher Co., Chemical and Metals Div.,  
Joplin, Mo.  
Eastman Kodak Co., Rochester, N. Y.  
Thomas A. Edison Research Laboratory, Div.  
of McGraw-Edison Co., West Orange, N. J.  
Electric Auto-Lite Co., Toledo, Ohio  
C & D Div., Conshohocken, Pa.  
Electric Storage Battery Co., Yardley, Pa.  
Engelhard Industries, Inc., Newark, N. J.  
(2 memberships)  
The Eppley Laboratory, Inc., Newport, R. I.  
(2 memberships)  
Exmet Corp., Tuckahoe, N. Y.  
Fairchild Semiconductor Corp., Palo Alto,  
Calif.  
Food Machinery & Chemical Corp.  
Becco Chemical Div., Buffalo, N. Y.  
Westvaco Chlor-Alkali Div., South  
Charleston, W. Va.  
Foote Mineral Co., Exton, Pa.  
Ford Motor Co., Dearborn, Mich.  
General Electric Co., Schenectady, N. Y.  
Chemistry & Chemical Engineering  
Component, General Engineering  
Laboratory  
Chemistry Research Dept.  
General Physics Research Dept.  
Metallurgy & Ceramics Research Dept.  
Aircraft Accessory Turbine Dept.,  
West Lynn, Mass.  
General Instrument Corp., Newark, N. J.  
General Motors Corp.  
Allison Div., Indianapolis, Ind.  
Delco-Remy Div., Anderson, Ind.  
Guide Lamp Div., Anderson, Ind.  
Research Laboratories Div., Warren, Mich.  
General Telephone & Electronics  
Laboratories Inc., Bayside, N. Y.  
(2 memberships)  
Gillette Safety Razor Co., Boston, Mass.  
Globe-Union, Inc., Milwaukee, Wis.  
B. F. Goodrich Chemical Co.,  
Cleveland, Ohio

(Sustaining Members cont'd)

- Gould-National Batteries, Inc.,  
Minneapolis, Minn.
- Great Lakes Carbon Corp., New York, N. Y.
- Hanson-Van Winkle-Munning Co.,  
Matawan, N. J. (2 memberships)
- Harshaw Chemical Co., Cleveland, Ohio  
(2 memberships)
- Hercules Powder Co., Wilmington, Del.
- Hill Cross Co., Inc., West New York, N. J.
- Hoffman Electronics Corp., Semiconductor  
Div., El Monte, Calif. (2 memberships)
- Hooker Chemical Corp., Niagara  
Falls, N. Y. (3 memberships)
- HP Associates, Palo Alto, Calif.
- Hughes Research Laboratories, Div. of  
Hughes Aircraft Co., Malibu, Calif.
- International Business Machines Corp.,  
New York, N. Y.
- International Minerals & Chemical  
Corp., Skokie, Ill.
- ITT Federal Laboratories, Div. of  
International Telephone & Telegraph  
Corp., Nutley, N. J.
- Jones & Laughlin Steel Corp.,  
Pittsburgh, Pa.
- K. W. Battery Co., Skokie, Ill.
- Kaiser Aluminum & Chemical Corp.  
Div. of Chemical Research,  
Permanente, Calif.  
Div. of Metallurgical Research,  
Spokane, Wash.
- Kawecki Chemical Co., Boyertown, Pa.
- Kennecott Copper Corp., New York, N. Y.
- Leesona Moos Laboratories, Div. of Leesona  
Corp., Jamaica, N. Y.
- Libbey-Owens-Ford Glass Co., Toledo, Ohio
- Lockheed Aircraft Corp.,  
Missiles & Space Div., Sunnyvale, Calif.
- Mallinckrodt Chemical Works, St. Louis, Mo.
- P. R. Mallory & Co., Indianapolis, Ind.
- Merck & Co., Inc., Rahway, N. J.
- Metal & Thermit Corp., Detroit, Mich.
- Miles Chemical Co., Div. of Miles  
Laboratories, Inc., Elkhart, Ind.
- Minneapolis-Honeywell Regulator Co.,  
Minneapolis, Minn.
- Minnesota Mining & Manufacturing Co.,  
St. Paul, Minn.
- Monsanto Chemical Co., St. Louis, Mo.
- Motorola, Inc., Chicago, Ill.
- National Cash Register Co., Dayton, Ohio
- National Lead Co., New York, N. Y.
- National Research Corp., Cambridge, Mass.
- National Steel Corp., Weirton, W. Va.
- North American Aviation, Inc., Rocketdyne  
Div., Canoga Park, Calif.
- Northern Electric Co., Montreal, Que.,  
Canada
- Norton Co., Worcester, Mass.
- Ovitron Corp., Long Island City, N. Y.
- Owens-Illinois Glass Co., Toledo, Ohio
- Peerless Roll Leaf Co., Inc., Union City, N. J.
- Pennsalt Chemicals Corp.,  
Philadelphia, Pa.
- Phelps Dodge Refining Corp., Maspeth, N. Y.
- Philco Corp., Research Div., Blue Bell, Pa.
- Philips Laboratories, Inc., Irvington-on-  
Hudson, N. Y.
- Pittsburgh Plate Glass Co., Chemical Div.,  
Pittsburgh, Pa.
- Potash Co. of America,  
Carlsbad, N. Mex.
- The Pure Oil Co., Research Center,  
Crystal Lake, Ill.
- Potash Corp. of America  
Tube Div., Harrison, N. J.  
RCA Victor Record Div., Indianapolis,  
Ind.
- Ray-O-Vac Co., Madison, Wis.
- Raytheon Co., Waltham, Mass.
- Remington Rand, Div. of Sperry Rand Corp.,  
New York, N. Y.
- Reynolds Metals Co., Richmond, Va.
- Rheem Semiconductor Corp.,  
Mountain View, Calif.
- Schering Corp., Bloomfield, N. J.
- Shawinigan Chemicals Ltd., Montreal, Que.,  
Canada
- Socony Mobil Oil Co., Inc.,  
Dallas, Texas
- Speer Carbon Co.  
International Graphite & Electrode  
Div., St. Marys, Pa.
- Sprague Electric Co., North Adams, Mass.
- Stackpole Carbon Co., St. Marys, Pa.
- Stauffer Chemical Co., New York, N. Y.
- Tennessee Products & Chemical Corp.,  
Nashville, Tenn.
- Texas Instruments, Inc., Dallas, Texas  
Metals and Controls Corp.,  
Attleboro, Mass.
- Three Point One Four Corp., Yonkers, N. Y.
- Titanium Metals Corp. of America,  
Henderson, Nev.
- Tung-Sol Electric Inc.,  
Newark, N. J.
- Udylite Corp., Detroit, Mich.  
(4 memberships)
- United States Borax & Chemical Corp.,  
Los Angeles, Calif.
- Universal-Cyclops Steel Corp.,  
Bridgeville, Pa.
- Upjohn Co., Kalamazoo, Mich.
- U. S. Steel Corp., Pittsburgh, Pa.
- Victor Chemical Works, Chicago, Ill.
- Western Electric Co., Inc., Chicago, Ill.
- Wyandotte Chemicals Corp.,  
Wyandotte, Mich.
- Yardney Electric Corp., New York, N. Y.